Searching for Extreme-BCG Clusters at $0.2 < z < 1.3$

by

Taweewat Somboonpanyakul

B.A., The University of Chicago (2015)

Submitted to the Department of Physics
in partial fulfillment of the requirements for the degree of

Doctor of Philosophy

at the

MASSACHUSETTS INSTITUTE OF TECHNOLOGY

September 2021

Author .....
Department of Physics
July 17, 2021

Certified by .....
Michael McDonald
Professor of Physics
Thesis Supervisor

Accepted by .....
Deepto Chakrabarty
Professor of Physics
Associate Department Head for Education

Searching for Extreme-BCG Clusters at

$0.2 < z < 1.3$

by

Taweewat Somboonpanyakul

Submitted to the Department of Physics
on July 17, 2021, in partial fulfillment of the
requirements for the degree of
Doctor of Philosophy

Abstract

Active galactic nuclei (AGN) feedback is believed to be responsible for counteracting the formation of the classical "cooling flow", predicted to be associated with most "cool core" clusters of galaxies. Several studies have shown that many phenomena found in galaxy clusters can be neatly explained by AGN feedback. Yet, the physical mechanism behind AGN feedback remains poorly understood. Careful analysis of clusters with unique characteristics, such as hosting starburst and/or active nuclei, provides an alternative path to tackle the issue of when, and how precisely, AGN feedback impacts clusters.

For my Ph.D. thesis, I show that by finding extreme-BCG clusters we can better understand the processes of cluster formation and evolution. In the first part of my thesis, I conduct an optical survey to discover new extreme-BCG clusters at low redshift. Finding clusters with distinct properties from the survey allows us to make detailed studies of the objects and better understand the formation mechanism of the feedback necessary to sustain long-lived clusters. In the second half, I study a sample of clusters over a large redshift range to find distant objects with extreme BCGs. This enables us to investigate a possible evolution of the feedback across cosmic time, and how the evolution has impacted the growth of all clusters. Thousands of galaxy clusters will be discovered in the coming decade with a certainty that a handful of them will host extreme BCGs. These peculiar objects will play an important role in understanding the complex nature of black hole feedback and galaxy evolution.

Thesis Supervisor: Michael McDonald
Title: Professor of Physics

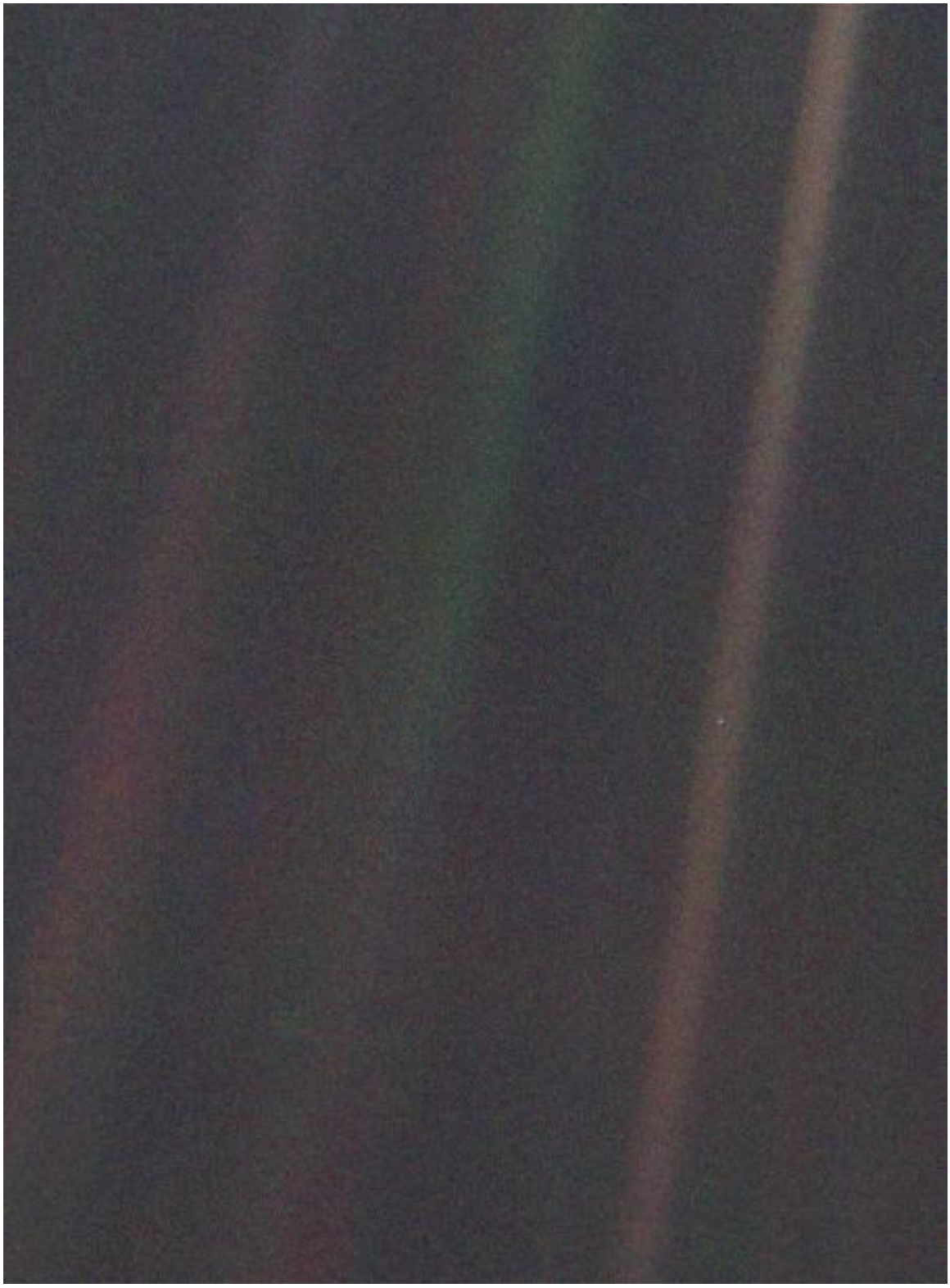

This image of Earth is one of 60 frames taken by the Voyager 1 spacecraft on February 14, 1990. In the image, the Earth is a mere point of light, a crescent only 0.12 pixel in size. *Image Credit: NASA/JPL*

Look again at that dot. That's here. That's home. That's us. On it everyone you love, everyone you know, everyone you ever heard of, every human being who ever was, lived out their lives. [...] every saint and sinner in the history of our species lived there–on a mote of dust suspended in a sunbeam.

...

It has been said that astronomy is a humbling and character-building experience. There is perhaps no better demonstration of the folly of human conceits than this distant image of our tiny world. To me, it underscores our responsibility to deal more kindly with one another, and to preserve and cherish the pale blue dot, the only home we've ever known.

Carl Sagan
Pale Blue Dot, 1994

Contents

List of Figures

List of Tables

Acknowledgments

This past year alone in my apartment often put me in a reflective mood. Six years for a PhD sounds like an extremely long time, but now that it is almost over, my years at MKI seem to pass in the blink of an eye. It has been a joyful journey for me, and I have a lot of people to thank for that.

First, I have to thank my advisor, Mike McDonald. I have learned a tremendous amount from him about various topics in astronomy and data analysis. Mike always allows me to try new solutions to tackle current problems at hands while never letting me lose sight of the big picture. Mike also made MIT feel more like home to me with his generosity to invite us to his house during summer/winter vacation. I would like to extend my gratitude to his family. But more importantly, Mike was an invaluable source of career advice from his honest responses to all my questions regarding postdoc applications. I definitely would not feel prepared to apply to most positions if not because of his encouragement. I owe my postdoc in most part to him.

Next, I'd like to thank everyone in our groups, including Matthew Bayliss, Allison Noble, Michael Calzadilla, and Florian Ruppin. I want to thank them for being a part of my PhD, and venture to wherever conferences will take us. I also benefited greatly from discussing with them and learning about their works during group meetings. I would like to thank my other two letter writers, Mark Brodwin and Eric Miller. With more than 40 postdoc applications I applied this past five months, I am extremely grateful to them for taking time to write my letters. I thank my thesis committee members, Claude Canizares and Mark Vogelsberger (and my advisor Mike), for their time to meet with me in the past three years and their useful suggestions towards the completion of this thesis. I also thank the other members of cluster groups and

stuff members from MIT and MKI, including Catherine Grant, Shuo Zhang, Fred Baganoff, Mark Bautz, Debbie Meinbresse, Thea Paneth, Cathy Modica, and Sydney Miller.

Outside of my research area, I am exceedingly grateful for the astrophysics community at MIT. I want to thank my academic advisor, John Belcher, and the rest of the astro faculty. I am especially grateful to Al Levine for his aide during the qualified exams. I also found great friends and role models among the more senior graduate students, including Aaron Ewall-Wice, Abraham Neben, Jeff Zheng, Uchupol Ruangsri, David Hernandez, Keaton Burns, Sherry Guo, Ani Chiti, Ryan McKinnon, Hang Yu, Liang Yu. Special thanks to Alex Ji and Tom Cooper for their advice on my postdoc applications. I am also honored to have overlapped with a fantastic group of younger graduate students which made the department much more fun, lively, and active. Even though there are now too many to name individually here, I am thankful for their presence in the department. I am also grateful for all friends I've made in the department, such as Huy Phan, Yunjie Yang, Miao Hu, Luke Bouma, Sameer Abraham, and many others.

It has also been a pleasure to have so many UChicago friends in the Boston area, especially Minjae Kim, Theresa Hwang, Charis Crofton, Kat Cheng, and Kristine Ma. I also would like thank all my Thai friends in the Boston area that I have met over the past six years, especially Can Naowarojna, Tee Warakkagun, Pete Kaewpanya, Natch Ruengsakulrach, and Dee Sukitpaneenit. They really showed me around Boston and made me feel at home here. I am thankful to instantly have a group of close friends when I moved here. Last but not least, I need to thank my family from Thailand. I am grateful that my family to allow me to pursue careers in science/academics. I am forever grateful.

Chapter 1

Introduction

Understanding the mechanisms that govern the evolution of matter in the universe is one of the fundamental objectives of astrophysics. And, the most massive objects, capable of significantly shaping our universe, are galaxy clusters. This implies that understanding the growth and evolution of galaxy clusters is critical to unlock the mysteries surrounding the formation and evolution of our universe.

1.1 What are Galaxy Clusters?

When we look at maps of the distribution of galaxies, such as that given by the Two Micron All Sky Survey [2MASS; 289] shown in Figure 1-1, it is immediately apparent that galaxies are not distributed randomly across the sky. Instead, they form interconnecting webs of filaments and knots which are bound together to form larger structures. These knots are galaxy clusters.

Galaxy clusters contain hundreds to thousands of galaxies, all confined to a volume of space that is not that much bigger than that occupied by a galaxy group, which usually has only tens of galaxies. The key difference lies in the high density of galaxies in galaxy clusters. Clusters are the largest gravitationally bound objects in the universe [326]. Although clusters contain many galaxies, it is important to note that not all galaxies are located in clusters. In fact, the majority of galaxies live outside of clusters, and these galaxies which are not part of clusters are called

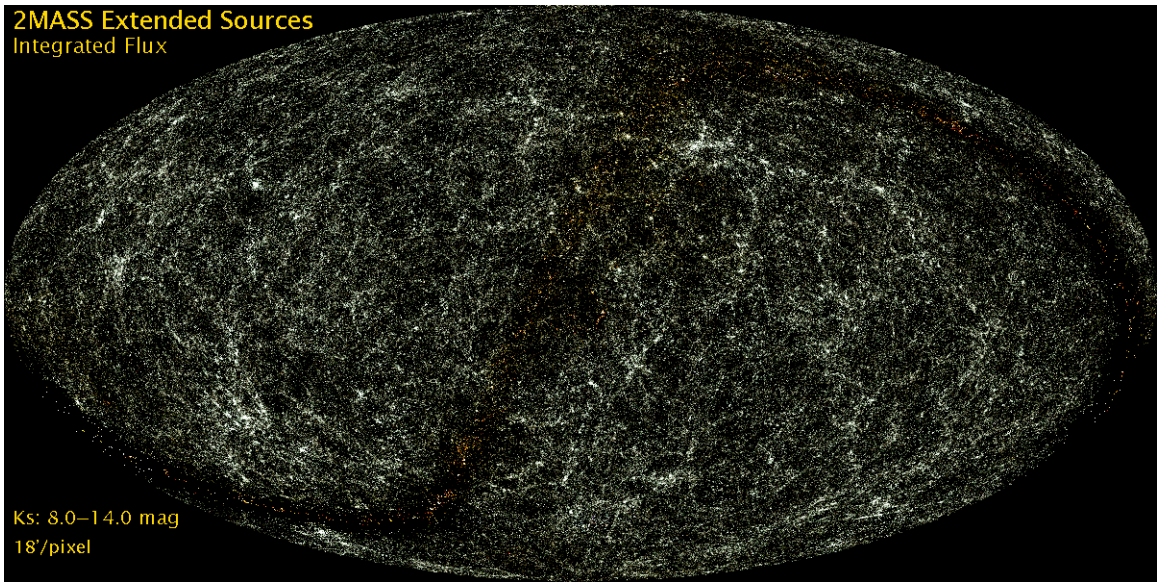

Figure 1-1 Map of the average extended source catalog integrated flux in $18' \times 18'$ bins in an equatorial Aitoff equal-area projection. *Image Credit: 2MASS/Caltech*

'field' galaxies. Galaxy clusters were first noticed from a catalog of Messier objects in the late 18^{th} century, which recorded a total of eleven extended objects within the constellation of Virgo. It is now identified as the Virgo cluster, which is the nearest galaxy cluster to the Milky Way. The Abell [1] and Zwicky et al. [344] catalogs were the first attempts to identify these clusters through the use of photographic plates. Since then, thousands of galaxy clusters have been discovered, studied, and characterized. The following sections will discuss the consequences and benefits of studying these massive objects, which includes being an important evidence for dark matter and being another crucial probe for cosmology.

1.1.1 Main Evidence for Dark Matter

One of the most important topics in astrophysics over the last century is the existence of dark matter. The hypothesis of dark matter was first introduced by Lord Kelvin in 1884 when he attempted to explain the observed velocity dispersion of the stars orbiting around the center of the Milky Way. He determined that the total mass of the galaxy is vastly different from the mass estimated from visible lights [28].

Currently, the strongest observational evidence for the presence of dark matter is the detection of the cosmic microwave background (CMB). The CMB is electromagnetic radiation from the early stage of the universe, representing the heat left over from the Big Bang. The CMB is believed to date back to about 380,000 years after the Big Bang from its extreme temperature of 273 million degrees Kelvin. Cosmological parameters, such as the density of dark matter, can be extracted from a sky map of CMB anisotropy by decomposing it to a series of acoustic peaks and fitting the cosmological models to these peaks [153]. Observationally, the CMB anisotropy was first detected by the Cosmic Background Explorer (COBE) in 1992. The COBE detection is one of the first evidence to support the Big Bang Theory although the resolution was too coarse to detect the acoustic peaks [179, 290]. A decade later, the Wilkinson Microwave Anisotropy Probe (WMAP; 2003–2012) became the first spacecraft to successfully measure the power spectrum of the acoustic peaks and demonstrate the validity of the Lambda Cold Dark Matter (ΛCDM) model, which describes a universe that contains only 5% ordinary matter, 26% dark matter and 69% dark energy [22, 23, 297]. This discovery has undoubtedly confirmed the existence of dark matter in the universe, and opened a new era of cosmology and astrophysics where we focus our efforts determining what dark matter is made of.

The most compelling early evidence for dark matter come in 1930s by Zwicky [342, 343]. Based on the motion of galaxies inside the Coma Cluster, Zwicky estimated the mass of the cluster to be too large, compared to an estimate based on the number of galaxies found in the cluster. In fact, the mass to light ratio of the cluster has to be $\sim$300 for the galaxy members to remain inside the cluster, meaning that the total

mass (including dark matter) of the cluster is 300 times larger than the visible mass. Zwicky is also the first person to coin the term "dark matter" to describe this missing mass.

Another piece of evidence for dark matter in galaxy clusters was discovered much later in 1990s when scientists detected the X-ray extended emission by hot gas in the clusters. From the X-ray energy spectrum, the gas density and temperature can be estimated. By assuming this gas is in hydrostatic equilibrium, we can estimate the mass of a cluster, which is, again, much larger than what we would expect from visible mass alone.

Lastly, galaxy clusters also support the presence of dark matter from the detection of strong gravitational lensing, which is one of the most important predictions from Einstein's general theory of relativity. This effect refers to a phenomenon when the light from a distant source is deflected as it travels toward an observer, resulting in a distorted image of the object in the sky, as shown in Figure 1-2. By measuring the distortion geometry from gravitational lensing, we can determine the mass of the intervening cluster [338], including Abell 1689 [53, 310] and SDSS J1531+3414 [282]. Additionally, weak gravitational lensing probes minuscule distortions of galaxies, using statistical analyses, to characterize the total mass of galaxy clusters [258]. The fact that both estimates of the cluster mass from strong and weak gravitational lensing are much larger than what we expect with visible matter alone suggests that dark matter indeed exists.

1.1.2 Additional Probe for Cosmology

Galaxy clusters also provide important constraints for cosmology. Because of their massive scale [$10^{14} - 10^{15}\, M_{\odot}$; 326], galaxy clusters are directly linked to the distribution of the matter in the universe. Therefore, by precisely measuring the abundance of galaxy clusters as a function of mass and redshift (the halo mass function), we obtain fairly competitive cosmological constraints for several parameters, including the density of total matter (Ω_m) and the amount of fluctuation in matter density (σ_8) [46, 138, 322]. In particular, a cosmological model with a higher Ω_m tells us

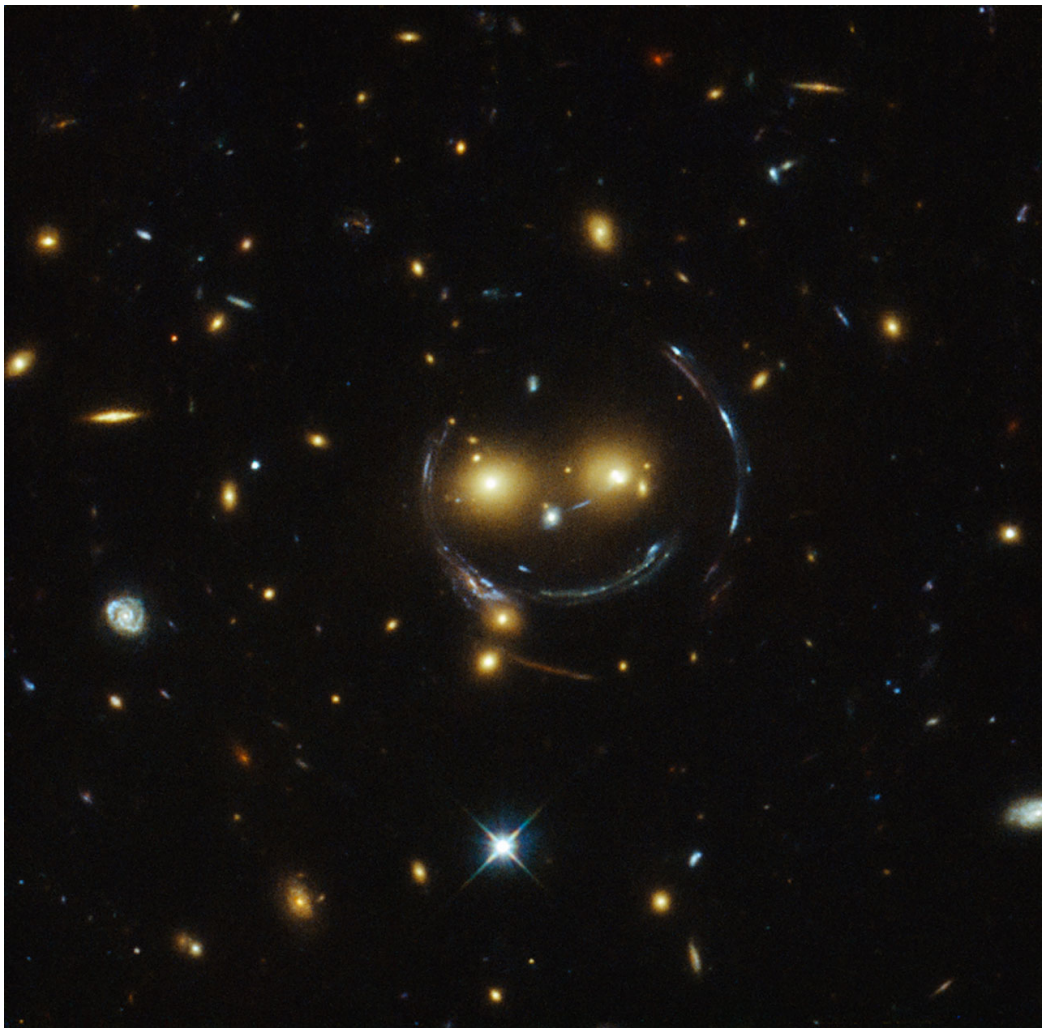

Figure 1-2 "Cheshire Cat" image of galaxy cluster [SDSS J1038+4849; 20] and gravitational lensing, imaged with the Hubble Space Telescope. *Image Credit: NASA/ESA*

that clusters will grow at a faster rate, which means that we would expect to find far fewer massive clusters at high redshift. Interestingly, the cosmological constraints found from this method perfectly complement the CMB measurement, and the combination of the two probes gives us a powerful tool to constrain cosmology [181].

The matter budget of massive galaxy clusters also provides a different probe of cosmology [4, 5, 6, 335]. The gas mass fraction (the ratio between gas mass and total mass; $f_{\rm gas}$) is expected to approximately match the baryon fraction of the universe [Ω_b/Ω_m; 45]. With the constraint on the baryon density (Ω_b) from CMB or Big Bang nucleosynthesis, this method provides a unique and robust way to constrain

Ω_m. In 1993, White et al. [335] were the first to show that $\Omega_m \sim 0.3$ from $f_{\rm gas}$ data, suggesting, for the first time, the need for "dark energy" to explain the other 70% of the entire content of the universe. Since then, there have been many studies aiming to provide better constraints using this technique. For example, Allen et al. [5] have shown that combining the $f_{\rm gas}$ measurements for 42 galaxy clusters at $0.05 < z < 1.1$ with CMB studies leads to the constraint of $\Omega_m = 0.253 \pm 0.021$, which is around eight percent accuracy. The latest cosmological constraints of Ω_m in 2021 from Corasaniti et al. [81], which include galaxy cluster sparsity, gas mass fraction, and baryon acoustic oscillation data, are at $\sim$4% level. The next generation X-ray observatories, such as Athena and Lynx, will offer the possibility to perform an even more precise study of dark energy using the $f_{\rm gas}$ technique, which is as accurate as other leading proposed procedures, such as Type Ia supernova, cluster number counts, and weak lensing studies.

In the next section, I discuss about various properties of galaxy clusters, and how they impact our understanding of galaxy clusters.

1.2 X-ray Properties of Galaxy Clusters

Even though galaxy clusters have widely been utilized in studies of dark matter and cosmology, they themselves are also fascinating objects which are worth studying. One aspect of a galaxy cluster that makes it a unique object to study, compared to an isolated galaxy and a group of galaxies, is that a cluster contains extremely hot gas ($\sim 10^7$ K) in its halo–the so called Intracluster Medium (ICM) [e.g., 274] that is readily observed in X-ray emission. Much of the baryonic mass contained in clusters is, in fact, in this hot rarefied plasma surrounding the galaxies, rather than in the galaxies themselves.

The ICM radiates X-ray emission through a process called "thermal bremsstrahlung." Bremsstrahlung is electromagnetic radiation produced by the deceleration of a charged particle, often an electron, when it is deflected by another charged particle, typically an atomic nucleus. X-ray radiation from the ICM is what

allows us to see exactly what happens to the gas inside a massive halo of a cluster. In fact, many major events in clusters are clearly imprinted in the X-ray morphology of the ICM. For example, a subcluster passing through a cluster will create a bow-shaped shock wave near the leading edge of the cluster. This effect can be easily detected in the ICM with X-ray observations, but is impossible to see in optical images. Examples of famous merging clusters include the Bullet Cluster [16, 194, 316] and El Gordo [221, 341]. Another important process which can be seen with X-ray observations is when a cluster's ICM is gravitationally disturbed by the nearby passage of other massive objects, initiating an oscillatory motion in the cluster core, called "sloshing." Examples of these objects are Abell 2052 [35] and Abell 1644 [159]. Bubbles or cavities in the ICM near the centers of clusters are also an important phenomenon found with X-ray observations. These cavities are important tracers of a jet-driven heating mechanism arising from the active galactic nuclei (AGN) in brightest cluster galaxies (BCG). Examples of strong cavity detections are the Perseus cluster [106], MS0735.6+7421 [216], and Hydra A [166].

1.2.1 Cool Cores and the Cooling Flow Problem

For galaxy clusters with strongly peaked X-ray emission, the ICM can cool via thermal bremsstrahlung on timescales much shorter than the Hubble time within a radius of $\sim$100 kpc. Simple models predict that as the ICM is rapidly losing its energy by X-ray emission, a long-lived "cooling flow" should occur in the central brightest cluster galaxies [103, 105, 243]. Such phenomenon should be possible to observed at low redshift, especially in BCGs of rapidly cooling clusters ("cool cores"; CC). CC clusters are clusters whose gas in the center of the cluster is much cooler and higher density, compared to the bulk of gas [229]. Hudson et al. [156] have shown that the best parameter for segregating cool core and non-cool core (NCC) clusters is the central cooling time $t_{\rm cool}$, where clusters with $t_{\rm cool} < 7.7h^{1/2}$ Gyr were considered CC clusters. This condition should provide necessary conditions for the cooling flows to form, and increase the number of newborn stars in the BCGs.

Nevertheless, detailed observations of these BCGs over the last two decades have

demonstrated an absence of massive cold gas repositories and extreme star formation rates in the BCGs. The results from searches were often orders of magnitude lower than predictions [91, 207, 239]. In addition, the nonexistence of expected coolant lines in high resolution X-ray spectra of large CC cluster samples shows that less than 10% of the cooling gas actually cools below $\leq$1 keV [244, 273, 309]. This is referred to as "the cooling flow problem." A balancing heating mechanism is needed to counteract cooling in the majority of cases and stop the formation of warm and cold gas associated with the cooling flow model. The heating must be, on average, approximately the same level as the X-ray luminosity. This scenario implies that the heating and cooling rates have to be tightly coupled and possibly self-regulated in the form of a feedback mechanism [e.g., 31, 73, 259].

1.2.2 Active Galactic Nuclei (AGN) Feedback

The dissipation of active galactic nucleus (AGN) power has the potential to fully replenish ICM radiative losses in regions near BCGs [e.g., 17, 262]. Compared to thermal conduction [29, 295, 296], cosmic ray heating [90, 107, 112], and mixing between cool gas and hotter material models, the AGN-driven feedback mechanism has since become the most favored candidate model to heat up cool cores.

AGN feedback occurs when the cooling ICM falls into the supermassive black hole (SMBH) of the central galaxy and triggers black hole accretion. The output energy from the accretion is massive enough to heat up an entire cluster and stop the cooling flow. There are two primary modes of AGN feedback. The first mode is known as radio-, kinetic-, or mechanical-mode feedback, which is when the associated outflowing plasmas or radio jets create cavities in the ICM, driving sound waves that ultimately dissipate into heat [106]. The energy from these cavities is theoretically enough to counter radiative losses from the ICM cooling [31, 256]. The second mode is the quasar- or radiative-mode feedback, which releases the binding energy from gas accreting onto massive black holes in the form of radiation, instead of jets. The structural difference between the two modes of feedback is thought to be governed by the specific accretion rate. When the accretion rate is high, an optically thick disk

is formed and dissipates its energy primarily in the form of radiation [114, 238, 281] while the period of moderate accretion leads to the energy being released in the form of a jetted outflow [236, 237].

There have been various studies which provide evidence supporting AGN feedback as the heating mechanism in galaxy clusters. For example, ∼70% of CC BCGs host active central radio sources [13, 224, 305], implying that radio jets are prevalent in the centers of clusters. Other works [e.g., 31, 149, 257] have shown that the power of these radio sources seems to be correlated with the X-ray luminosity. For example, Figure 1-3 illustrates the correlation between the jet power inferred from X-ray cavities and the cooling from X-ray radiation. This implies that the output energy from radio jets is enough to offset the X-ray radiative cooling and prevent cooling flows. In addition, since cool-core clusters account for ∼50% of the cluster population [8, 266], the phase must be long-lived, suggesting that the heating rates have to be regulated by a feedback loop; otherwise extreme heating would destroy the CC phase. The other feedback mechanism, which provides necessary heating, is supernova feedback. This form of feedback occurs when supernovae from massive stars inject enough energy and momentum to heat up the surrounding gas to counteract cooling. Although supernova feedback dominates the evolution of low mass galaxies, it has been shown from various works [44, 328] that it is not effective enough for galaxy clusters to be the dominant source of heating in order to stop runaway cooling.

Although we have reasonable frameworks for the two different modes of feedback (kinetic and radiative), only the kinetic mode has been thoroughly studied in galaxy clusters. In contrast, the radiative feedback on clusters is rarely investigated because of the relative lack of brightest cluster galaxies which harbor bright quasars. There are only four cases of galaxy clusters with central quasars in their BCGs, including H1821+643 [84, 267], 3C 186 [283, 284], IRAS09104+4109 [72, 241], and the Phoenix cluster [202, 212]. The small number of such objects makes it difficult to investigate the role of radiative feedback in galaxy clusters and central BCGs, such as the correlation between the nuclear power output and radiative cooling, the distinction between type I and type II quasars in clusters [165], and the duty cycle of radiative

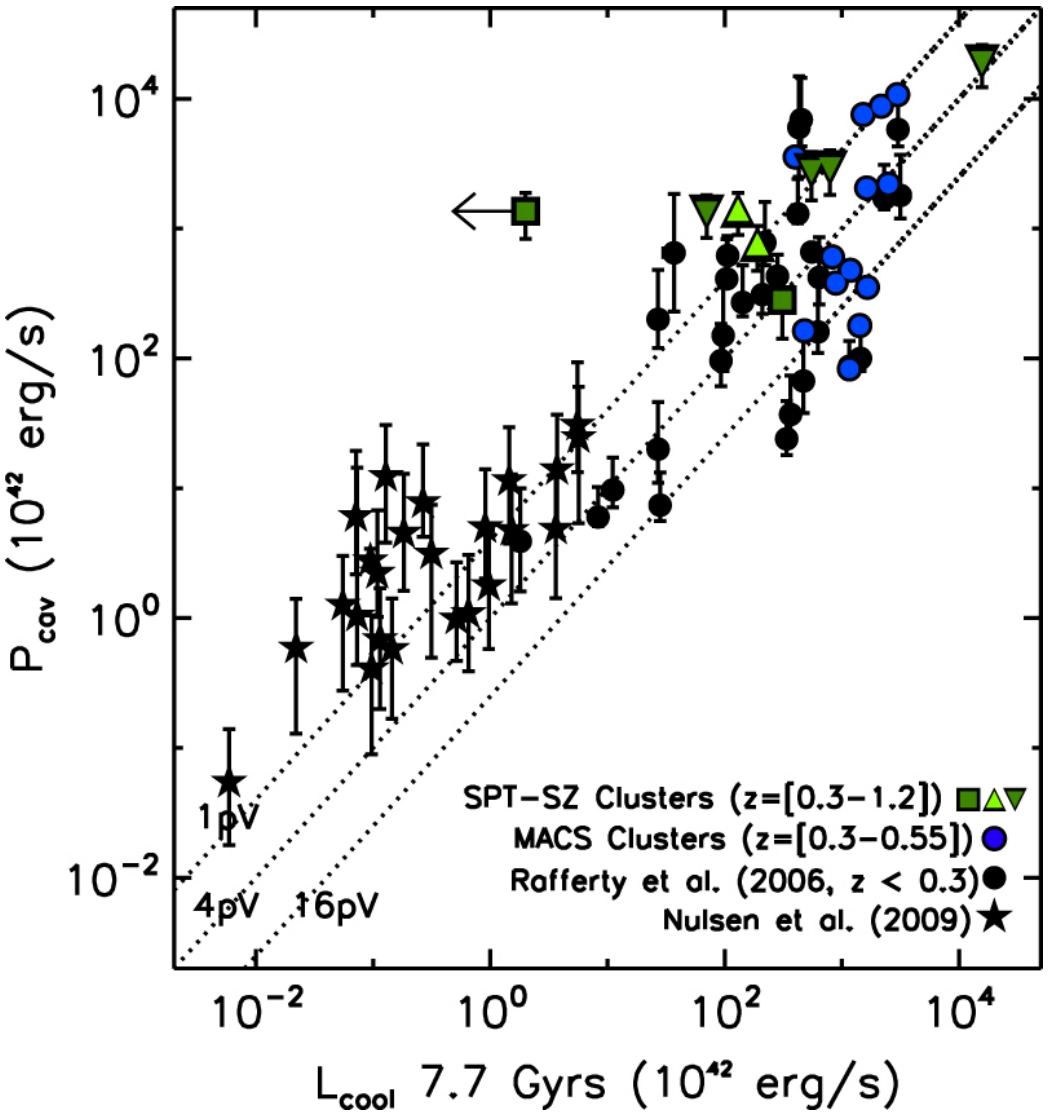

Figure 1-3 Comparison between the mechanical power being injected by the AGN in the BCG ($P_{\rm cav}$) and the cooling luminosity ($L_{\rm cool}$) of the cluster over 7.7 Gyrs. This figure clearly shows the correlation between the mechanical power from AGN and radiative cooling from X-ray emission. *Image Credit: Hlavacek-Larrondo et al. [149]*

feedback. A part of this thesis will be our attempt to address this issue by aiming to find more galaxy clusters with bright quasars in the BCGs. Finding even one or two more of these kinds of objects will drastically improve our understanding of the radiative-mode feedback of galaxy clusters.

1.2.3 The Phoenix Cluster

Out of the four galaxy clusters with bright central quasi-stellar objects (QSOs), the Phoenix cluster stands out as one of the most unique systems known. First identified by the South Pole Telescope [SPT; 63, 336] in 2012, it is the most X-ray luminous cluster discovered to date and harbors the most massive starburst in the central galaxy, with the measured star formation rate (SFR) at 500–800 $M_\odot\,\mathrm{yr}^{-1}$ [202, 210, 225]. This SFR accounts for roughly 30% of the predicted cooling flow, which is much larger than ∼1% for typical BCGs in galaxy clusters. Further studies [211, 269] also find extended, complex filamentary gas in optical and submillimeter data, suggesting that large amount of cooling is maintained all the way down to the molecular gas temperature (∼10–20 K). In addition, large X-ray cavities are found in the Phoenix cluster, pointing to extremely powerful radio jets with a power of $\sim 10^{46}\,\mathrm{erg\,s}^{-1}$, which is a signature for the kinetic-mode feedback [149, 212]. A combination of these studies hints that the cluster is experiencing runaway cooling, as predicted by the classical cooling flow model, which is extremely uncommon compared to what we know about typical clusters and the cooling flow problem. However, without any comparable systems or systematic studies of such objects, it is impossible to make any argument about how common or long-lived such a phase is.

Given the high mass ($M_{500} > 10^{15}\,M_\odot$) and extreme properties of the Phoenix cluster, it is surprising that the cluster was not discovered until recently. Interestingly, the cluster and its central BCG have been detected in many all-sky surveys at various wavelengths, but was consistently classified as a point source (either star or isolated quasar) because of the extremely bright active central galaxy and a lack of extended X-ray emission. This leads us to wonder whether there are other Phoenix-like clusters that have been misclassified as isolated point sources. The Cluster Hiding in Plain Sight (CHiPS) survey, which is the main part of this thesis, is designed specifically to address this issue by looking for galaxy clusters previously misidentified in existing surveys due to the extreme central galaxies. The number of galaxy clusters found by the survey will tell us about the duty cycle of the extreme phase of AGN feedback.

In the previous two sections, I have summarized the need to identify and characterize more samples of galaxy clusters, both for tightening our cosmology constraints and understanding AGN feedback as a heating mechanism against radiative cooling. In the next section, I discuss different methods we have employed to find new galaxy clusters by searching for overdensity of red galaxies in optical and near-infrared surveys [122], extended ICM emission in X-ray surveys [94, 95], and via Sunyaev-Zel'dovich effect [SZ; 306] in millimeter/submillimeter surveys [36, 37].

1.3 Discovery of Galaxy Clusters

1.3.1 Overdensity of Red Galaxies in Optical/Near-Infrared

As I mention in the beginning, galaxy clusters have been detected as far back as the 1800s [34] by Abell [1], Abell et al. [2], Zwicky et al. [345] via large catalogs of galaxies observed with photographic plates. Since then, various advancements in optical/near-infrared observations have been developed from single-band imaging [251], multicolor photometric data [123, 169, 168], and different cluster-finding algorithms. Specifically, these cluster finders can be divided roughly into two main classes: those based on photometric redshifts [e.g., 291, 308, 334] and those using the cluster "red sequence" [e.g., 122, 123, 124, 135, 168, 233, 311].

Photometric redshifts ($z_{\rm photo}$) of galaxies can be estimated by fitting multi-band photometry in the optical and mid-infrared to a template spectral energy distribution to estimate the galaxy's redshift. Many studies [e.g., 55, 332, 340] have shown that the most luminous member galaxies of clusters can be identified using photometric redshifts. One disadvantage of this technique is that characterizing redshifts for faint galaxies is difficult due to large uncertainties and a lack of spectroscopic training samples. In addition, $z_{\rm photo}$ estimates for cluster members might not be accurate when applying algorithms derived from the total galaxy population.

On the other hand, the red sequence method relies on the fact that almost all galaxy clusters have a well-populated "red sequence", which is a line of constant age on

the color-magnitude relation. It has been shown to have extremely small scatter and appears to be homogeneous from cluster to cluster, as shown in Figure 1-4 [48, 123]. The color of the red sequence also provides a precise redshift estimate for the detected cluster. A benefit of this technique is that it can be effective with only two filters as long as the filter pair covers the 4000 Å break. One problem with the red sequence method occurs at high redshift when the red sequence begins to disappear due to the prevalence of star-forming galaxies, making the photometric redshift method perform better in that particular case [e.g., 54, 101].

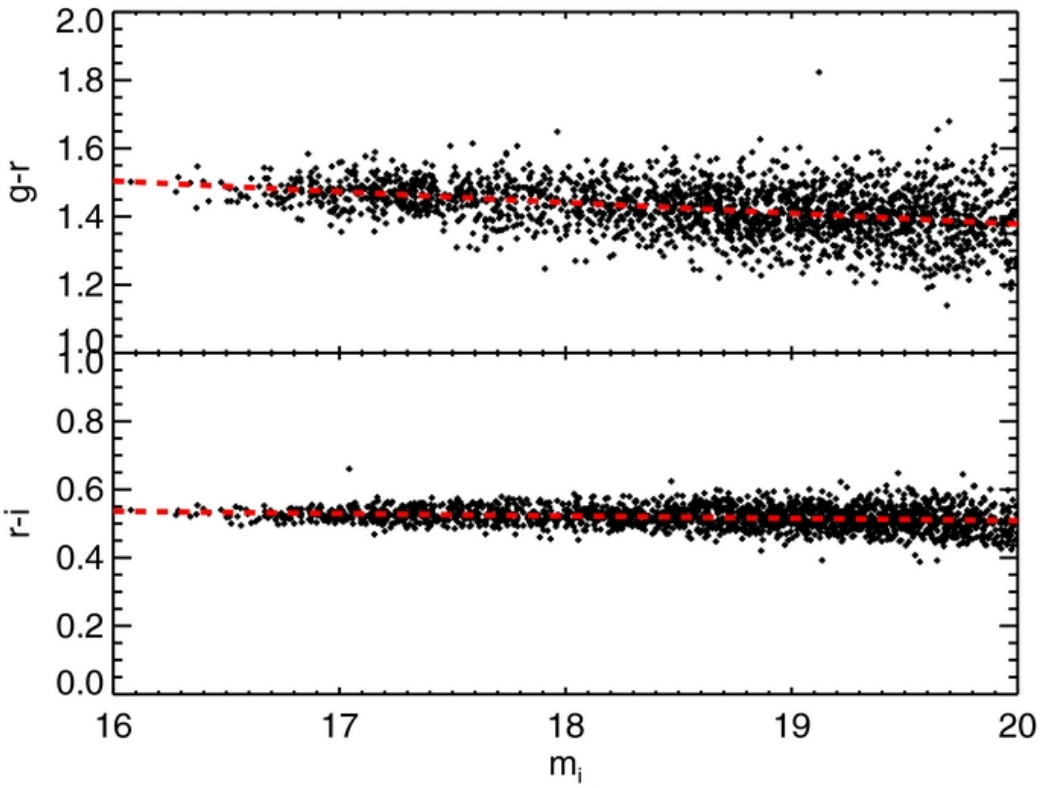

Figure 1-4 Composite red sequence at $0.25 < z < 0.26$ for color-selected galaxies with $p_{\rm mem} > 0.9$. A linear model (red dashed line) is a good representation of the red sequence in both $g-r$ and $r-i$. We note that $p_{\rm mem}$ is a probability of being a cluster member. *Image Credit: Rykoff et al. [271]*

Some notable examples of recent optical cluster-finding algorithms include redMapper [264, 270, 271], which is a red sequence cluster finder that handles an arbitrary photometric galaxy catalog with an arbitrary number of photometric bands, and the

Massive and Distant Clusters of WISE Survey [MaDCoWS; 127, 300], which is a photometric redshift method for high redshift clusters ($0.7 < z < 1.5$) based on data from the Wide-field Infrared Survey Explorer (WISE).

One important challenge for galaxy cluster identification is projection effects. By cataloguing clusters as two-dimensional objects against a clustered background, the apparent richness of the cluster could be dominated by this effect. For example, there have been debates about a significant contamination from projection effects in the well-known Abell catalog [78, 184]. van Haarlem et al. [318] estimated that about one-third of rich clusters found in optical data are misclassified from the projection of one or more clumps onto poor clusters. This issue is not an issue when we consider the other two methods of finding galaxy clusters.

1.3.2 Extended Extragalactic Emission in X-ray

With the completion of the ROSAT All-Sky Survey (RASS) in 1991 [315, 324], X-ray detected cluster samples became a promising alternative. The detection of X-ray emission from the hot ICM provides one of the best ways to compile statistically complete cluster samples. X-ray surveys are relatively unbiased because they exclusively select massive, gravitationally bound objects without uncertainties from projection effects, unlike the optical/near-infrared method [e.g., 318]. The resulting cluster samples will have a well-defined selection function based on the limiting X-ray flux, which can be used to compute the effective survey volume required for any cosmological studies.

Generally, the X-ray source extent is used to find galaxy clusters in all-sky surveys. The extent parameter is the Gaussian width of the radial source profile that is in excess of the point spread function (PSF) of the instruments. Ebeling et al. [94] demonstrated that sources with only the extent parameter will miss $\sim$25% of all clusters at all redshifts[1], nearly independent of X-ray flux limit. The misclassification of extended sources as point sources in X-ray surveys, especially in RASS, is the main focus for the first part of this thesis (see Chapter 2), which is an attempt to discover new and extreme galaxy clusters from the ROSAT Bright Source Catalog [323].

[1]This comparison was performed on Abell and Zwicky clusters.

X-ray selected galaxy clusters have proven to be excellent tracers for the large-scale structure of the universe. The distribution of these clusters in a well-selected, and statistically complete sample allows assorted studies of cosmology and large-scale evolution. Prominent examples of X-ray selected cluster samples are the ROSAT Brightest Cluster Sample [BCS; 94], extended BCS [eBCS; 95], Massive Cluster Survey [MACS; 96, 97], the ROSAT-ESO Flux Limited X-ray survey [REFLEX; 42], and many others [57, 245]. In addition, the XMM Cluster Survey [XCS; 220] is an example of an X-ray selected cluster sample in the XMM-Newton Science Archive, instead of RASS. While X-ray surveys have been more common recently, they still suffer from a strong selection bias that favors low-redshift clusters with an X-ray bright cool core [71, 98, 180, 263, 322]. This selection bias can be somewhat mitigated by excluding the cluster cores when selecting cluster candidates [98].

Almost 30 years after the launch of the ROSAT satellite, eROSITA was launched on July 13, 2019 onboard the Spectrum-Roentgen-Gamma (SRG) satellite [222, 253, 254]. eROSITA will perform an X-ray all-sky survey with the sensitivity improved by at least a factor of 20 compared to ROSAT. The new X-ray survey data from eROSITA have the potential to discover and characterize more than 100,000 galaxy clusters, drastically changing the limits of what X-ray-selected cluster samples are capable of.

1.3.3 SZ Effects in Millimeter/Submillimeter

Arguably, the least biased way to detect massive, distant galaxy clusters is through wide field millimeter/submillimeter surveys to detect the SZ effect [306]. The SZ effect, specifically the thermal SZ effect, is a characteristic spectral distortion to the CMB, arising through the inverse Compton scattering of CMB photons by energetic electrons within the hot atmospheres of galaxy clusters [see reviews by 30, 64, 231]. This results in a decrease in the intensity (relative to a blackbody at the mean CMB temperature) at frequencies below 220 GHz, and an increase in the intensity at higher frequencies. The SZ observable is the Compton y-parameter, which is related to the integration of electron pressure and the total thermal energy of the ICM. Modern

hydrodynamical simulations suggest that the thermal integrated SZ signal is one of the most robust mass proxies for galaxy clusters with a remarkably low scatter (10%–15%) [230, 234, 278, 299].

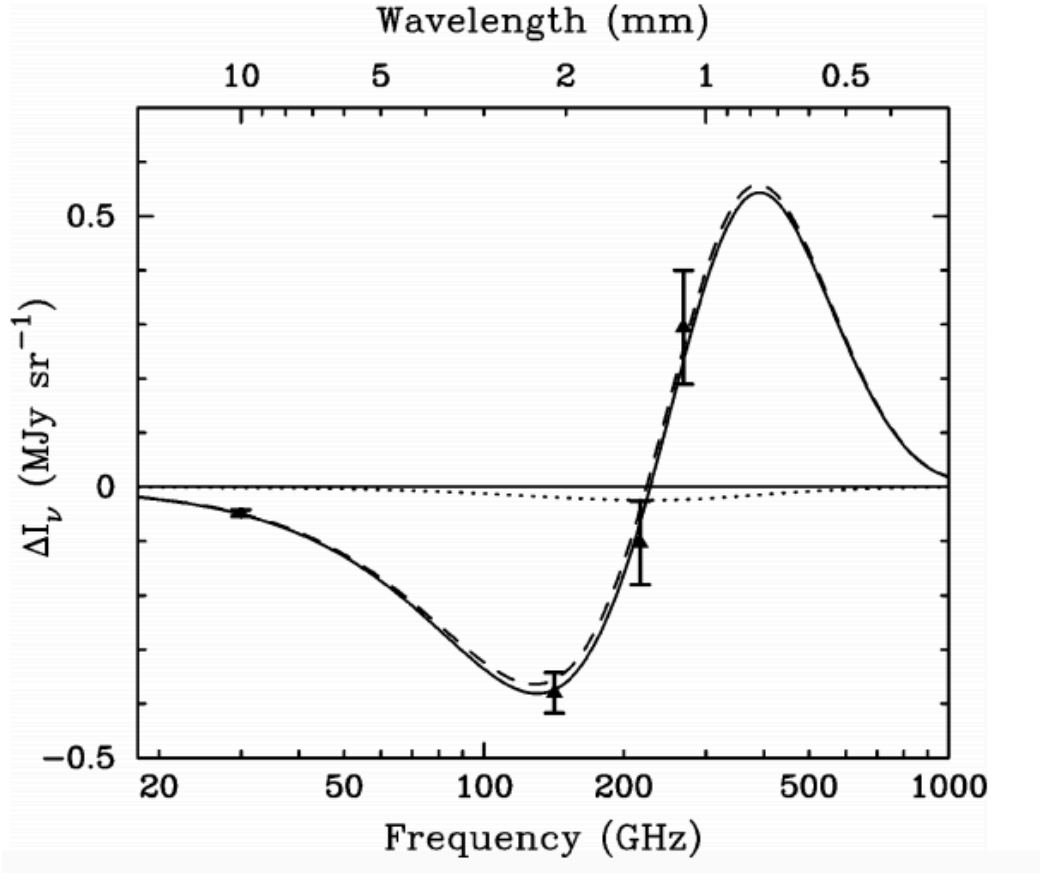

Figure 1-5 *Difference between a blackbody spectrum and the post SZ-effect CMB spectrum. The number of photons with frequencies less than 220 GHz is decreased, while the number with higher frequencies is increased. Data is from Abell 2163. Image Credit: Carlstrom et al. [64]*

A unique power of SZ selection is its ability to detect all of the massive clusters regardless of their distance to an observer. In other words, the signal from the SZ effect is independent of redshift. A flat selection function provides a nearly mass-limited census of the cluster population at all redshifts. This allows the SZ-selected cluster samples to provide strong constraints for cosmological parameters by measuring the evolution of the cluster mass function, as I described in Section 1.1.2, [39, 64, 277, 319]. It also enables many studies of the evolution of galaxy clusters over cosmic time, in-

cluding the second part of this thesis which focuses on the evolution of AGN feedback in massive clusters. The prominent SZ cluster surveys with catalogs of hundreds of massive clusters, conducted by ground- and space-based telescopes, include the South Pole Telescope [SPT; e.g., 36, 37, 336], the Planck satellite mission [247, 248], and the Atacama Cosmology Telescope [ACT; 144, 146, 196].

In this introduction, we have reviewed the basic of galaxy clusters. In particular, we discuss what galaxy clusters are and show the benefits of studying these massive objects. We also examine what we know and do not know about the physics behind galaxy clusters from X-ray radiation to cool cores to AGN feedback, and discuss the Phoenix cluster. Lastly, we describe three separate methods to find new galaxy clusters. With this background knowledge we are now ready to focus on the scientific work presented in the main part of this thesis.

1.4 A Roadmap for this Thesis

The work that constitute this thesis was originally written as four different papers. The papers appear here as Chapter 2 through Chapter 5. I played a significant role in the development, writing, and served as the first author on all four papers. Three of them have already been published in peer-review journals; Chapter 5 has been submitted and is still under review.

I have organized this thesis into two parts. In Part I, I describe my main project for my PhD, the Clusters Hiding in Plain Sight (CHiPS) survey, in three chapters.

- Chapter 2 reproduces the published paper *The Clusters Hiding in Plain Sight (CHiPS) survey: A first discovery of a massive nearby cluster around PKS1353-341* [292], written in collaboration with Michael McDonald, Henry Lin, Brian Stalder, and Antony Stark. It presents a pilot study of the CHiPS survey and a newly discovered low-redshift ($z = 0.223$) galaxy cluster, surrounding the quasar PKS1353-341. With new Chandra X-ray observations obtained for this object, we characterize the cluster to be a strong cool-core cluster from its central cooling time around 400 Myr. This chapter also serves as a proof of concept

study to demonstrate the potential of the complete version of the CHiPS survey to find massive nearby clusters hosting extreme central galaxies, which have been misidentified by previous surveys, and a great starting point for the rest of this thesis, much of which provides more details about the CHiPS survey. The work in this chapter was conducted under the supervision of Michael McDonald, but the project was lead and carried out largely by me with Brian Stalder and Antony Stark served as the principle investigators for the new instrument on the Magellan Telescope, called the Parallel Imager for Southern Cosmological Observations [PISCO; 298].

- Chapter 3 reproduces the published paper *The Clusters Hiding in Plain Sight (CHiPS) survey: Complete sample of extreme BCG clusters* [294], written in collaboration with Michael McDonald, Massimo Gaspari, Brian Stalder, and Antony Stark. It presents optical follow-up observations of cluster candidates in the CHiPS survey, which identify 11 cluster candidates, including six well-known clusters, two false associations of foreground and background clusters, and three new candidates. From that result, we compute the occurrence rate of galaxy clusters with extreme BCGs to be $2 \pm 1\%$, which is consistent with predictions from the chaotic cold accretion (CCA) model. The work in this chapter was conducted under the supervision of Michael McDonald, but was lead and carried out by me. Massimo Gaspari provided feedback on the theoretical framework of the project, and Brian Stalder and Antony Stark served as the principle investigators for PISCO.

- Chapter 4 reproduces the published paper *The Clusters Hiding in Plain Sight (CHiPS) survey: CHIPS1911+4455, a Rapidly-Cooling Core in a Merging Cluster* [293], written in collaboration with Michael McDonald, Matthew Bayliss, Mark Voit, Megan Donahue, Massimo Gaspari, Hakon Dahle, Emil Rivera-Thorsen, and Antony Stark. It presents a detailed multi-wavelength study of the other newly discovered galaxy cluster, CHIPS1911+4455, at $z = 0.485 \pm 0.005$. This cluster has a measured star formation rate SFR =140–190 $M_\odot\,\mathrm{yr}^{-1}$, which

is one of the highest rates measured in any central cluster galaxy to date. The raw optical spectra were acquired by Hakon Dahle and Emil Rivera-Thorsen, and prepared by Matthew Bayliss. Mark Voit, Megan Donahue, and Massimo Gaspari provided additional comments on the interpretation of our results. I analyzed the *Chandra* X-ray images, the *Hubble* optical images, estimated star formation rate of the optical spectra, and wrote the entire paper.

In Part II, I turn from discovering new low-redshift ($z < 0.7$) galaxy clusters to studying the properties of known galaxy clusters over a large redshift range ($0.1 < z < 1.3$) to study the evolution of AGN feedback over cosmic time.

- Chapter 5 reproduces the submitted paper *The Evolution of AGN Activity in Brightest Cluster Galaxies*, written in collaboration with Michael McDonald, Allison Noble, and several other members of the SPT-Cluster team. It presents an analysis of Wide-field Infrared Survey Explorer (WISE) observations on the full 2500 deg^2 South Pole Telescope (SPT)-SZ cluster sample in order to calculate the AGN-hosting BCG fraction over the range of $0 < z < 1.3$. We find that the fraction increases with redshift in this sample, consistent with previous studies and work on field galaxies. The work in this chapter was lead and carried out mostly by me under the supervision of Michael McDonald. The identification of BCG candidates were performed by Allison Noble as a part of the BCG-SPT cluster project (Noble in prep.). Members of the SPT-Cluster team provided additional comments and suggestion about the results.

It is my hope that this thesis presents a broad picture of how we study AGN feedback and provides a way forward for how we might eventually understand the mechanism that governs the feedback through finding and characterizing galaxy clusters with extreme central BCGs.

Part I

The Clusters Hiding in Plain Sight (CHiPS) survey

Chapter 2

A First Discovery of a Massive Nearby Cluster around PKS1353-341

The content of this chapter was submitted to The Astrophysical Journal *on January 5, 2018 and published [292] as* The Clusters Hiding in Plain Sight (CHiPS) survey: A first discovery of a massive nearby cluster around PKS1353-341 *on August 16, 2018.*

2.1 Introduction

Clusters of galaxies are the largest collapsed objects in the universe [326]. Because of the deep gravitational potential well of clusters, supernovae and active galactic nuclei (AGN) are unable to expel gas beyond the turnaround radius, allowing the study of galaxy formation in a closed system. Simulations with radiative cooling and gravity alone are not sufficient to explain the observed properties of a brightest cluster galaxy (BCG), the most luminous galaxy in a cluster [14, 52, 215]. The simulations tend to predict too much cool gas and too many newborn stars. This is referred to as *the cooling flow problem*, and the best candidate for explaining this discrepancy is kinetic feedback by the central AGN in clusters [49, 50, 85].

There are two primary modes of AGN feedback which allow the supermassive black hole (SMBH) at the center of its host galaxy to affect the final stellar mass of the galaxy. The first mode is the kinetic mode, driven by radio jets, and the sec-

ond mode is the quasar mode, or radiative mode, which relates to radiation from the accretion disk [see reviews by 104, 215]. The kinetic mode has been intensively studied, specifically in galaxy clusters, which require feedback to prevent overcooling [256, 214] via radio jets and bubbles [107]. In contrast, the impact of radiative feedback on clusters is poorly understood [285], due to the relative lack of central cluster galaxies in the quasar mode and a smaller region in the center in which the radiative feedback (compared to mechanical feedback) can be observed.

There are only four known examples of galaxy clusters hosting central quasars: H1821+643 [267], 3C 186 [283, 284], IRAS 09104+4109 [241], and the Phoenix cluster [202]. The small number of such objects is insufficient to fully exemplify the role of radiative feedback in the evolution of galaxy clusters and their central BCGs, including the duty cycle of radiative feedback, its correlation with radiative cooling, and the distinction between the effects of type I and type II quasars on clusters [165]. One possible way to uncover more of these objects comes from the surprise discovery of the Phoenix cluster, which, at $z = 0.6$, is the most X-ray luminous cluster known and the nest of a massive central starburst [202, 203, 212]. While this cluster was initially discovered with the Sunyaev Zel'dovich effect [336], further investigation reveals that it had previously been detected by several all-sky surveys at a variety of wavelengths, but had consistently been classified as an isolated AGN because of the extremely active central galaxy and a (relative) lack of extended X-ray emission due to its distance. This leads us to wonder how many nearby ($z < 0.7$) galaxy clusters with central quasars or massive starbursts are currently mislabeled in existing all-sky surveys.

In this work, we present the Clusters Hiding in Plain Sight (CHiPS) survey to look for galaxy clusters misidentified in existing surveys due to the extreme nature of their central galaxies. In this pilot study, we present a newly discovered galaxy cluster, surrounding the quasar PKS1353-341, along with new *Chandra* observation of the galaxy cluster and its central AGN. By performing a detailed study of this object, we can deduce the properties of the cluster and investigate the impact a central quasar has on the intracluster medium (ICM).

The data used in the CHiPS survey and its methodology are described in Section 2.2. In Section 2.3, we present the *Chandra* analysis. The results and discussion are presented in Sections 2.4 and 2.5. We assume $H_0 = 70\,\mathrm{km/s/Mpc}$, $\Omega_m = 0.3$ and $\Omega_\lambda = 0.7$. All errors are 1σ unless noted otherwise.

2.2 The CHiPS Survey

The CHiPS survey is designed around the idea that centrally concentrated galaxy clusters at high redshift or clusters hosting extreme central galaxies (starbursts and/or QSOs) can have been misidentified as field AGNs in the *ROSAT* All-Sky Survey (RASS).

By conducting an extensive follow-up survey of an all-sky X-ray point source catalog to look for galaxy overdensities, we will obtain a sample of such galaxy clusters. The primary question the sample will answer is whether there are other extreme-BCG clusters, similar to the Phoenix cluster, in our universe. This will tell us about the nature of highly efficient star formation in a galaxy cluster by distinguishing a short-lived phenomenon from a common occurrence in cool cores [211]. Furthermore, we will identify any clusters with central QSOs as a secondary product of the survey. These clusters are also interesting in their own right, as they will allow us to study the effect of quasar-mode feedback on the ICM [148]. This paper reports our first findings on this topic. Once the survey is complete, we will also have a better understanding of biases in X-ray surveys (i.e., the number of clusters missed due to the presence of a central point source), which is crucial for constraining cosmological parameters via cluster counts, such as the mean matter density Ω_m, the normalization of the density fluctuation power spectrum σ_8, and the dark energy equation-of-state parameter w_0, [189, 190, 322].

In order to reduce the total number of candidates to a manageable size, we require sources to be bright at X-ray, mid-IR, and radio wavelengths, relative to the optical. This requirement leads to a sample dominated by radio-loud type II QSOs and starbursts with central radio sources embedded in clusters. Subsequently, optical

follow-up is performed to confirm the existence of a galaxy cluster via an overdensity of red galaxies at the same redshift as the central bright X-ray source. Results from the survey will be available in a forthcoming paper. Here, we focus on the first stage of the survey, including cross-correlation of all-sky surveys, and the first new discovery.

2.2.1 Data Used in the Cross-correlation

We expect that clusters with central QSOs or starbursts (or both) are extremely luminous at multiple wavelengths, including X-ray, mid-IR, and radio. Compact X-ray emission may be produced by the cooling ICM of a relaxed cluster or the hot accretion disk around a central AGN. Bright mid-IR emission traces warm dust which could be heated by a starburst and/or an AGN, while bright radio emission originates primarily in AGN jets, which are found ubiquitously in cool-core clusters [305]. We use the K band as the *normalization* and select relatively bright X-ray, radio, and mid-IR sources from that. The normalization is for preventing nearby sources (i.e., stars) from dominating the sample. Below, we describe how data at each of these wavelength is acquired.

2.2.1.1 X-Ray Data: RASS

Our X-ray sample consists of 124,730 objects from the combination of the RASS Bright Source Catalog and Faint Source Catalog. RASS is the first all-sky survey in soft X-rays (0.1-2.4 keV), conducted in 1990/91 with ROSAT, a German X-ray telescope satellite [323]. However, this initial sample is dominated by sources that are not in clusters (i.e., isolated AGN, stars, etc) and requires additional cuts to reduce the total size to a manageable number for optical follow-up.

Several surveys in the past have used RASS to create X-ray flux-limited cluster catalogs. For example, the REFLEX survey has a flux limit of $3 \times 10^{-12}\,\mathrm{erg\,s^{-1}\,cm^{-2}}$ [42] while the limit of Ebeling et al. [95]'s Extended Brightest Cluster Sample was $2.8 \times 10^{-12}\,\mathrm{erg\,s^{-1}\,cm^{-2}}$ and that of Ebeling et al. [96]'s Massive Cluster Survey

(MACS) faint extension was 1–2$\times 10^{-12}$ erg s^{-1} cm^{-2}. We expect our survey to have a flux limit similar to the limites of these previous RASS-selected cluster surveys, given that we use the same data.

2.2.1.2 Radio Data: NRVO Very Large Array Sky Survey (NVSS) and Sydney University Molonglo Sky Survey (SUMSS)

Since there is no single radio all-sky survey available, the combination of two surveys, one for the northern hemisphere and one for the southern hemisphere, is necessary to achieve full-sky coverage for radio sources. For the northern hemisphere, the NVSS is a 1.4 GHz survey covering the entire sky north of a declination of $-40°$ [79]. For the southern hemisphere, the SUMSS was an 843 MHz survey covering the sky south of a declination of $-30°$ [199]. Within the 2σ positional uncertainties from the X-ray and radio catalogs, we found 13,800 X-ray sources with a 1.4 GHz radio detection in NVSS or an 843 MHz detection in SUMSS. The given positional uncertainties account for the brightness of each source, and the systematic point-spread function (PSF) of the instruments. Because the two radio surveys do not cover the same wavelength, we scaled the flux from SUMSS to NVSS assuming a power-law spectrum from synchrotron radiation ($f_{\rm NVSS}/f_{\rm SUMSS} = (1.4/0.834)^{-\alpha}$ where $\alpha = 1$ is typical of radio galaxies in clusters [150]).

2.2.1.3 Mid-infrared Data: Wide-field Infrared Survey Explorer (WISE)

WISE was an all-sky survey with imaging capabilities at 3.4, 4.6, 12, and 22 μm [337]. We matched our 13,800 X-ray and radio sources to the AllWISE Source Catalog. Despite the fact that most of our sources have counterparts in *WISE*, only $\sim 50\%$ (7380 objects) of our sample has a $W4$ (22 μm) detection with a measurable $W4$ uncertainty, implying that only half of our X-ray and radio sources are relatively bright in mid-IR. The $W4$ band is used in this analysis because of its sensitivity to warm dust, heated by either star formations or AGN [177].

2.2.1.4 Near-infrared Data: Two Micron All Sky Survey (2MASS)

The 2MASS was a near-IR all-sky survey carried out with two automated 1.3 m telescopes, one in Arizona and one in Chile [289]. The images were taken simultaneously at the J (1.25 μm), H (1.65 μm), and K (2.17 μm) bands. As with WISE, we matched our X-ray and radio samples to the 2MASS All-sky Point Source Catalog (PSC) to extract the K-band brightness of our matched objects. We use the K band because it is most sensitive to the stellar mass [19]. After cross-correlating WISE's $W4$ and 2MASS's K band, we end up with 4549 targets for further follow-up.

2.2.2 Color Cuts

By requiring candidates to be detected in all four surveys (*ROSAT*, NVSS or SUMSS, *WISE*, and 2MASS), we are guaranteed soruces that are bright at all four wavelengths, which is a specific characteristics of a few astrophysical sources, including radio-loud type II QSOs (e.g., Fanaroff-Riley type I/II radio galaxies [109]) and cooling-flow sources (e.g., the Phoenix cluster, the Perseus cluster, and Abell 1835). Since the total number of sources that exist in all four surveys remains too large (4549 objects) to perform the necessary follow-up, further cuts are required to identify the best candidates for our sample.

After combining all four surveys, we start with a catalog of 4549 candidate clusters. The first cut is to remove stars from our local neighborhood by setting a K-band brightness threshold ($m_K > 9$ mag). This reduces the number of candidates to 4,206. Subsequently, we apply a series of color-cuts at different wavelengths. In Fig. 2-1, we plot the ratios of X-ray, mid-IR, and radio flux to near-IR flux. Normalizing to the near-IR flux takes into account each sources's overall brightness, which strongly depends on the source's distance. We selected sources from the top right corner of each plot, i.e., objects that are over-luminous in X-ray, radio, and mid-IR compared to near-IR. As a result, we reduce our sample from 4206 to 735 objects. Specifically, the regions of the color cut for X-ray, radio, and mid-IR were chosen to have their minimum flux normalized to near-IR, lower than that of the Phoenix cluster by $\log_{10} 3$,

$\log_{10} 9$, and $\log_{10} 15$, respectively. These ratios were obtained by considering the expected range of color for a Phoenix-like object at an unknown redshift between 0.1 and 0.7. The 735 remaining objects define our primary sample.

For 428 out of our 735 cluster candidates, we obtain the redshift for the bright source from the *NASA/IPAC Extragalactic Database* (NED)[1]. We rejected foreground (redshift less than 0.1) and background (redshift greater than 0.7) objects. For clusters at $z < 0.1$, diffuse emission should be readily detected by eye even in the presence of a bright central point source. Thus, we do not expect many clusters to have been missed at these redshifts. At $z > 0.7$, cluster detection in the optical becomes challenging because of the limitations in detecting the red sequence from ground-based telescopes [122], and we are likely to miss them in our shallow all-sky survey data. This challenge, along with follow-up efforts, will be addressed in a forthcoming paper.

As a pilot study of the CHiPS survey, we selected 22 candidates, which were both Phoenix-like (top right corner in Fig. 2-1) and visible to observe from the 6.5-meter Magellan telescope in the spring of 2014. These candidates were initially imaged with the Inamori Magellan Areal Camera and Spectrograph [93] on the Magellan Baade telescope, and then promising candidates were further imaged using the Parallel Imager for Southern Cosmological Observations [PISCO; 298], to a depth sufficient to detect red-sequence galaxies at $z \sim 0.6$. PISCO is a photometer that produces g, r, i, and z band images simultaneously within a $9'$ field of view. Creating four band images at the same time increased our efficiency in observing these candidates by a factor of $\sim$3 (including optical losses). Further discussion about the reduction pipeline will be made in an upcoming paper. With the optical images obtained from PISCO, we searched for an overdensity of red sequence galaxies [122], selecting candidates which have a significant ($> 3\sigma$) overdensity of red galaxies at the same redshift as the cluster candidate. This led to an initial sample of four galaxy cluster candidates, which were followed up with the *Chandra* X-ray telescope. This follow-up resulted in the discovery of a new massive galaxy cluster surrounding PKS1353-341 at $z = 0.223$ with R.A. $= 13^{\rm h}56^{\rm m}05.4^{\rm s}$ and decl. $= -34^{\rm d}21^{\rm m}10.9^{\rm s}$. The red sequence of PKS1353-341,

[1] https://ned.ipac.caltech.edu

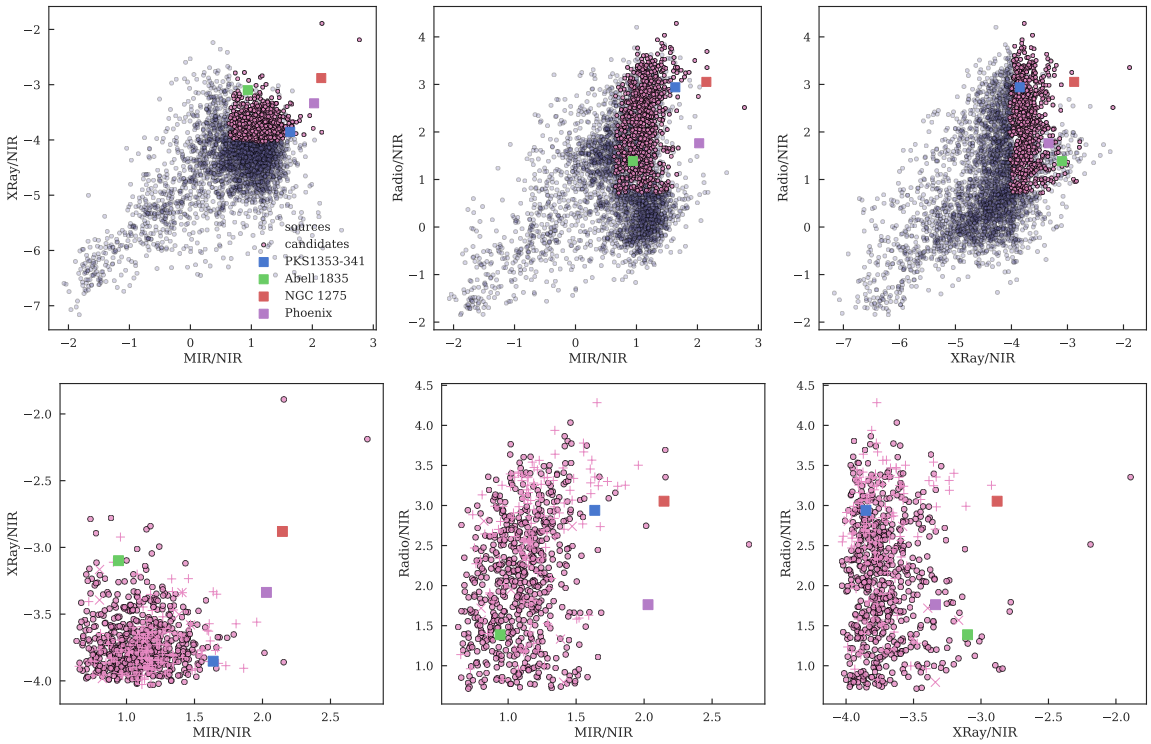

Figure 2-1 Top three panels show color-color diagrams for objects that were detected in all four all-sky surveys (4,206 objects, see Section 2.2). The axes are the logarithm of the ratio of the X-Ray, mid-IR (MIR) or radio flux to the near-IR (NIR) flux. Points in pink satisfy our three color cuts. The bottom three panels zoom in on these galaxy cluster candidates (735 objects). We remove the background ($z > 0.7$) and foreground ($z < 0.1$) sources from our sample based on redshift information from NED. The Phoenix, Perseus (NGC 1275), and A1835 clusters, which host extreme BCGs, are shown with purple, red and green squares, respectively while PKS1353-341 is shown with a blue square.

shown in the right panel of Fig. 2-2, demonstrates that the redshift of the QSO is similar redshift to that of the maximum histogram bin for the red sequence. This suggests that most of the surrounding red galaxies are located near the QSO in the physical space, and not in projection. Fig. 2-2 also demonstrates the capability of this technique to detect galaxy clusters using just optical photometry from three bands (g, r, i) up to redshift $z = 0.7$.

Two of the other three candidates turn out to be isolated X-ray point sources, implying that the galaxy overdensity exists only in projection. This led us to refine our selection algorithm which will be presented in detail in Somboonpanyakul et al.

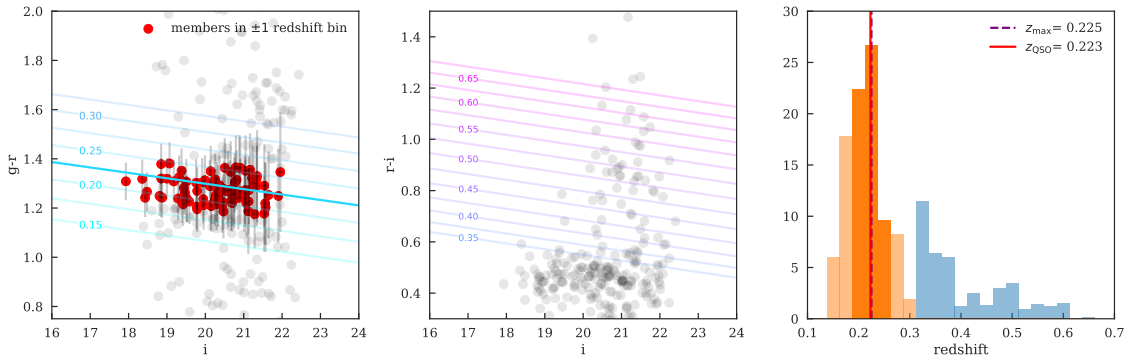

Figure 2-2 Left and Center: Color magnitude diagrams for PKS1353-341 using $g-r$ color (left) and $r-i$ color (center) to identify the red sequence at a variety of redshifts (diagonal lines). All the members within ± 1 redshift bin of the QSO's redshift are shown in red dots. Right: The number of galaxies in different redshift bins based on the red sequence templates shown in the left panels. The g-r vs i color-magnitude diagram (orange bins) is used for $z = 0.15 - 0.35$ and the r-i vs i color-magnitude diagram (blue bins) is used for $z = 0.35 - 0.70$. The redshift of the quasar, PKS1353-341, is 0.223 in red solid line while the redshift of the maximum histogram is 0.225 in purple dash line. This figure demonstrates how we can use the red sequence to find new clusters from X-ray point source catalogs up to redshift z = 0.7.

(in prep). The remaining candidate is a rich cluster (A2270) with no existing *Chandra* data. In our observations it clearly shows extended X-ray emission.

2.3 Reduction of *Chandra* Data

To confirm the existence of a massive galaxy cluster, X-ray observation is important as it provides unambiguous evidence for an extremely hot ICM, which is expected from the deep potential well of a cluster. In particular, high angular resolution X-ray images can be used to determine different properties of this hot ICM, such as the gas temperature profile, gas density profile, and total hydrostatic mass.

Fig. 2-3 shows both X-ray and optical images of PKS1353-341. The optical image from the Magellan telescope (the right panel of Fig. 2-3) shows the central BCG as an extremely bright elliptical galaxy with a bright point source in the center and a number of elliptical members nearby. The smoothed *Chandra* X-ray image clearly shows the extended hot ICM, which reveals the morphology of the cluster to be highly

relaxed without obvious perturbation in any direction, implying that this cluster has not experienced any recent mergers. The image also reveals a central concentration, apart from the central point source, reminiscent of a cool core.

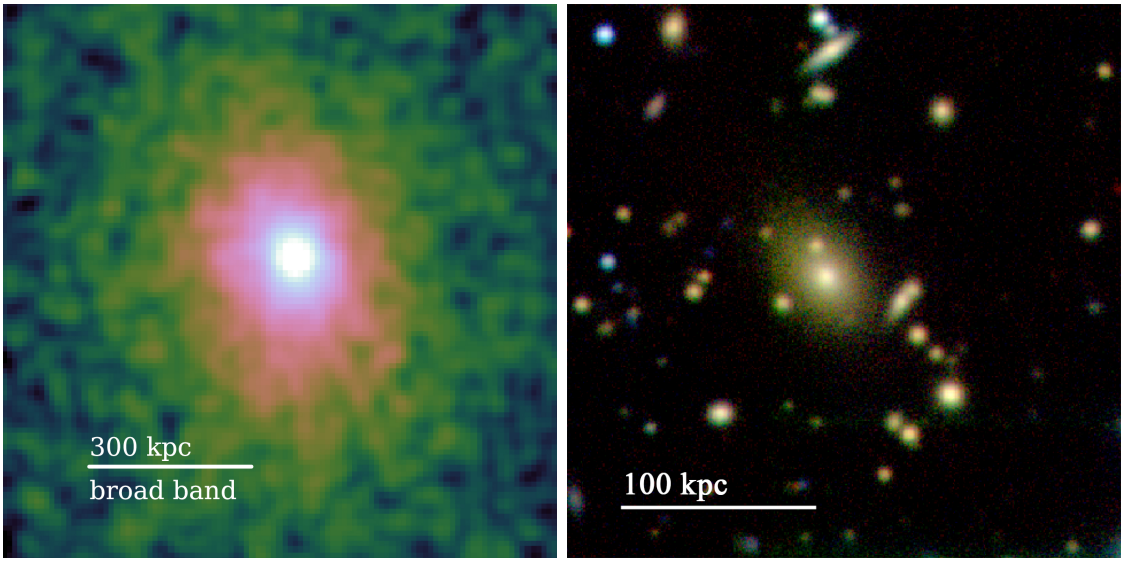

Figure 2-3 Left: *Chandra* broadband (0.5-7 keV) image for PKS1353-341 on a log-scale color bar, showing the bright central point source and the surrounding diffuse cluster emission. Right: Magellan PISCO (g , r , i) image of the inner part of the galaxy cluster, showing the central giant elliptical galaxy.

In the following sections, we describe the reduction of the *Chandra* data, followed by derivation of various ICM properties.

2.3.1 Data Preparation

PKS1353-341 (OBSID 17214) was observed with *Chandra* ACIS-I for 31 ks. The cluster has a bright point source at the center that is not piled up. Excluding the point source, the total number of counts we used for the reduction is 22,258. It was analyzed with *CIAO* version 4.8 and *CALDB* version 4.7.2, provided by the *Chandra* X-ray Center. The event data was recalibrated with VFAINT mode to improve background screening. Point sources not at the center of the cluster were identified using the *wavdetect* function and removed. A blank background was generated using the *blanksky* script, which includes combining and reprojecting the background for

the input event file. Spectra were extracted in concentric annuli (defined below), for both the cluster and background, using the *specextract* function from *CIAO*.

In order to get reliable measurements of the gas properties, such as density and cooling time, near the center of the cluster, a clear separation between the central point source and the galaxy cluster is required. The *Chandra* PSF is complicated due to smearing effects from the High-Resolution Mirror Assembly, which are produced by a combination of telescope dithering motion, the size of detector pixels, and detector effects[2]. We generate a simulation of the central point source, described below, to account for and remove the contribution of the point source to the total emission, following Russell et al. [267].

2.3.2 Simulating quasar PSF with ChaRT

ChaRT [65] is a web interface[3] to the SAOTrace ray trace code for creating a simulated point source from a given source spectrum. In order to properly use ChaRT, we must prepare ChaRT inputs, including the source spectrum, source coordinates, and pointing information for the telescope. The pointing information is acquired from the aspect solution of the *Chandra* image, while the source spectrum was obtained from *specextract* for a region dominated by the point source (central).

We use Sherpa [115] to model the X-ray emission from the inner $2''$, assuming a combination of an absorbed power-law model to represent the central AGN ($xszphabs \times xspowerlaw$) and a thermal plasma model to represent the ICM ($xspec$), with photoelectric absorption from the Milky Way ($xsphabs$) applied to both components. The hydrogen absorbing column ($n_{\rm H}$) was fixed to the average from the Leiden-Argentine-Bonn survey at 5.57×10^{20} cm^{-2} [160].

The output of ChaRT is a set of simulated rays from the point source. The MARX software (version 5.3) projects the simulated rays onto the detector plane to create pseudo-event files. Instead of using MARX directly, we utilized *CIAO*'s $simulate\_psf$ script to simplify its interface. The surface brightness profile of the

[2]http://cxc.harvard.edu/ciao/PSFs/psf_central.html
[3]http://cxc.harvard.edu/ciao/PSFs/chart2/runchart.html

simulated point source was extracted according to the procedure described in Section 2.3.3.

2.3.3 Density Profile

Radial gas density profiles were created by first obtaining the number of counts at 0.5-2 keV in concentric annuli and dividing this number by the annulus area to get the surface brightness in count per square arcsecond. The spacing for the radial bins is equally separated in the logarithmic scale for 30 bins with a minimum spacing of $1''$ and excluding the central $1''$ where the central point source dominates. We use a maximum radius of $\sim 450''$ to ensure that we have enough counts to get a good constraint on the surface brightness for each annulus. The simulated point source profile was subtracted from the surface brightness profile, as described in the previous section, to remove the surface brightness contribution from the central AGN, (see Fig. 2-4). The surface brightness was converted to units of physical density using the normalization terms from the spectral fitting (see Section 2.3.4).

The analytic expression for the 3D density profile that we use, a modified β-model, represents features of observed X-ray density profiles, including a power-law cusp, a two-component β-function with small- and large-scale slopes, and a second β-model component with a small core radius to represent the cool core [320]. The complete model for the density profile is

$$\begin{aligned} n_p n_e(r) =& n_0^2 \frac{(r/r_c)^{-\alpha}}{(1+(r/r_c)^2)^{3\beta-\alpha/2}} \frac{1}{(1+(r/r_c)^\gamma)^{\epsilon/\gamma}} \\ &+ \frac{n_{02}^2}{(1+(r/r_{c2})^2)^{3\beta}}, \end{aligned} \tag{2.1}$$

where $n_p n_e(r)$ is the product of the proton and electron densities. We fixed $\gamma = 3$ and $\epsilon \leq 5$, while all other parameters were free. Before fitting the 3D model to the 2D data, we project the model onto a 2D plane by integrating along the line of sight [320]. This projected model is fit to the model, using *emcee* [113].

2.3.4 Temperature Profile

We extract spectra in coarser annuli so that the number of counts per annulus is roughly 1500, to allow for well-constrained temperature measurements. The first annulus has an inner radius of 1.″5 (5 kpc) to avoid contamination from the AGN. We extract the cluster and blank-sky background spectra for each annulus. All spectra were fit simultaneously with APEC models for both the cluster (*xsapec*) and the Milky Way emission ($xsapec_{\rm bkg}$), photoelectric absorption from the Milky Way (*xsphabs*), and thermal bremsstrahlung from unresolved background objects (*bremss*) with a temperature of 40 keV, following McDonald et al. [204]. The temperature, metallicity, and normalization of the cluster emission model were left free and the WSTAT statistic was used. This produces a temperature profile with 7 bins over roughly the inner 700 kpc.

Instead of fitting a model with many free parameters to the poorly-constrained temperature profile, we leverage the high-S/N density profile with the fact that the pressure profile of a galaxy cluster is close to self-similar and shows little scatter at large radii [235, 9, 204]. The temperature profile is then inferred from the ideal gas law ($P = n_e kT$) and the density profile. We model the pressure profile with a modified generalized Navarro-Frenk-White (GNFW) model, as proposed by Nagai et al. [235]:

$$P(r) = \frac{P_0}{x^\gamma [1 + x^\alpha]^{(\beta-\gamma)/\alpha}}, \tag{2.2}$$

where $x = r/r_s$, and α, β, and γ are the slopes at $r \sim r_s$, $r \gg r_s$, $r \ll r_s$, respectively. Slope β was fixed at 5.4905 [9], leaving 4 free parameters (P_0, α, γ, r_s).

Dividing the model pressure profile by the model density profile yields a 3D model temperature profile which was then projected along the line of sight, using the weighting scheme for the average temperature proposed by Mazzotta et al. [200]:

$$\langle T(r) \rangle = \frac{\int_V \rho^2 (T(r))^{1/4} d^3x}{\int_V \rho^2 (T(r))^{-3/4} d^3x}, \tag{2.3}$$

where ρ is the gas density, $T(r)$ is the 3D temperature profile and $\langle T(r) \rangle$ is the

projected 2D temperature profile at a given radius. The projected temperature profile, which has three free parameters from the GNFW model, is then fit to the data, using *emcee* [113].

2.3.5 Total Mass, Gas Fraction, Entropy, and Cooling Time

Having both the density and temperature profiles allows us to calculate other thermodynamic properties of the cluster, including the enclosed total mass as a function of distance, assuming hydrostatic equilibrium [275],

$$M(r) = -\frac{kT_g(r)r}{\mu m_p G}\left(\frac{d\ln P}{d\ln r}\right) \tag{2.4}$$

where P is the gas pressure, T_g is the cluster emission temperature, μ is the chemical abundance (which is equal to 0.5954 for primordial He abundance), and m_p is the proton mass. We choose M_{500}–the total mass within R_{500}, the radius within which the average enclosed density is 500 times the critical density $\rho_c \equiv 3H_0^2/8\pi G$–as a proxy for the total cluster mass, as suggested by Vikhlinin et al. [321].

The gas mass of the cluster can be calculated by integrating the gas density over a spherical volume using $M_{gas}(r) = \int_0^r \sqrt{n_p n_e(r)} \times 1.276 \times m_p dV$, where $n_p n_e(r)$ is the product of the proton and electron densities, and 1.276 is the ratio of protons to electrons in a plasma with 0.3 $Z_\odot$ metallicity. From this, the gas fraction interior to some radius is calculated by $f_{gas}(r) = \frac{M_{gas}(r)}{M(r)}$.

With the density and temperature profile, the entropy of the ICM can be calculated using $K(r) = kT(r) \times n_e(r)^{-2/3}$, where $kT(r)$ is the temperature profile (in kiloelectronvolts) and $n_e(r)$ is the electron density profile. Entropy is a useful observable for studying the effects of feedback on a cluster because the thermal history of a cluster is influenced solely by heat gains and losses [183, 67, 242]. We expect a monotonically increasing entropy profile due to the buoyancy of high-entropy gas [326, 67].

Lastly, the cooling time represents the amount of time that the ICM needs to radiate all of the excess heat via thermal bremsstrahlung emission. This is calculated using $t_{cool} = \frac{kT(r)}{n_e(r)\Lambda(T)}$, where $T(r)$ is the temperature profile, $n_e(r)$ is the electron

density profile and $\Lambda(T)$ is the cooling function [307]. The central cooling time (the cooling time within the central $\sim$10 kpc) is often used to distinguish between cool core and non-cool core clusters [156].

2.4 Results

The fact that this galaxy cluster was not identified by *ROSAT* as a cluster suggests that there may be a hidden population of galaxy clusters hosting extreme central galaxies (i.e., starbursts and/or QSOs). The unabsorbed bolometric X-ray flux of the cluster is $4.8 \times 10^{-12}\,\mathrm{erg/cm^2/s}$ and the bolometric X-ray luminosity at $z = 0.223$ is $L_x \sim 7 \times 10^{44}\,\mathrm{erg\,s^{-1}}$. The bolometric X-ray lumnisity of the core is $L_{nuc} \sim 1.8 \times 10^{44}\,\mathrm{erg\,s^{-1}}$.

Table 2.1 shows the key properties of PKS1353-341, which are derived in this work (R_{500}, M_{500}, $M_{\mathrm{gas},500}$, T_x, $t_{\mathrm{cool},0}$, SFR), compared to other well-known clusters– namely, A1795 (a strong cool core (SCC) cluster) and H1821+643 (a quasar-hosting cluster). This table shows that PKS 1353-341 is very similar to A1795 (a typical relaxed cool-core cluster), except in terms of its central AGN.

In the following sections, we discuss in more details various derived properties of the cluster, including the gas fraction, the entropy, the total hydrostatic mass, and the cooling time.

2.4.1 Temperature and Density profile

As shown in the left panel of Fig. 2-4, the cluster has a density profile with a sharp peak in the innermost bin (the central $1''$). From the simulated PSF in Section 2.3.2, an AGN surface brightness profile is created, shown by the black solid line. This simulated profile was subtracted from the observed profile, leaving the underlying ICM density profile. The green points represent the cluster density profile after the subtraction of the simulated AGN profile. Due to PSF modeling uncertainties, the innermost bin has a large residual uncertainty. However, the overall ICM density profile fit is relatively insensitive to the first data point.

Table 2.1 Key properties for the galaxy cluster

Property of Clusters	PKS1353-341	A1795[d]	H1821+643[e]
Redshift[a](z)	0.2230	0.0622	0.299
T_x[b](keV)	$4.32^{+1.74}_{-1.92}$	6.12 ± 0.05	8.9 $(0.15 - 0.75R_{500})$
R_{500} (kpc)	1313^{+230}_{-194}	1235 ± 36	1000
M_{500} ($10^{14}\,M_\odot$)	$6.90^{+4.29}_{-2.62}$	6.03 ± 0.52	9
$M_{\rm gas,500}$ ($10^{13}\,M_\odot$)	$6.45^{+1.41}_{-1.22}$	6.27 ± 0.65	13
$f_{\rm gas,500}$	$0.094^{+0.042}_{-0.018}$	0.104 ± 0.006	0.14
$t_{\rm cool,0}$ (Myr)	299^{+92}_{-70} (at 10 kpc)	889 (at 10 kpc)	1000 (at 30 kpc)
$r_{\rm cool}$[f](kpc)	185^{+12}_{-11}	82	90
SFR[c]($M_\odot\,{\rm yr}^{-1}$)	6.2 ± 3.6	9	300^{+300}_{-200}
Cooling rate[f]($M_\odot\,{\rm yr}^{-1}$)	345^{+41}_{-37}	294	300 ± 100

[a]Redshift is obtained from *NED*. We assume that the cluster is located at the same redshift as the central AGN.

[b]T_x is measured from $0.15R_{500}$ to $1.0R_{500}$.

[c]SFR is measured from the UV luminosity of the BCG for PKS1353-341. (see Section 2.5.3)

[d]Most of the numbers for A1795 are from Vikhlinin et al. [320], except SFR is from Hicks and Mushotzky [141]. $t_{\rm cool,0}$, $r_{\rm cool}$, and cooling rate are from McDonald et al. [206]

[e]These numbers are from Russell et al. [267], Walker et al. [330], except SFR which is from Ruiz et al. [265].

[f]The cooling radius is defined to be the radius at which the cooling time is 7.7 Gyr while the cooling rate is defined within the cooling radius.

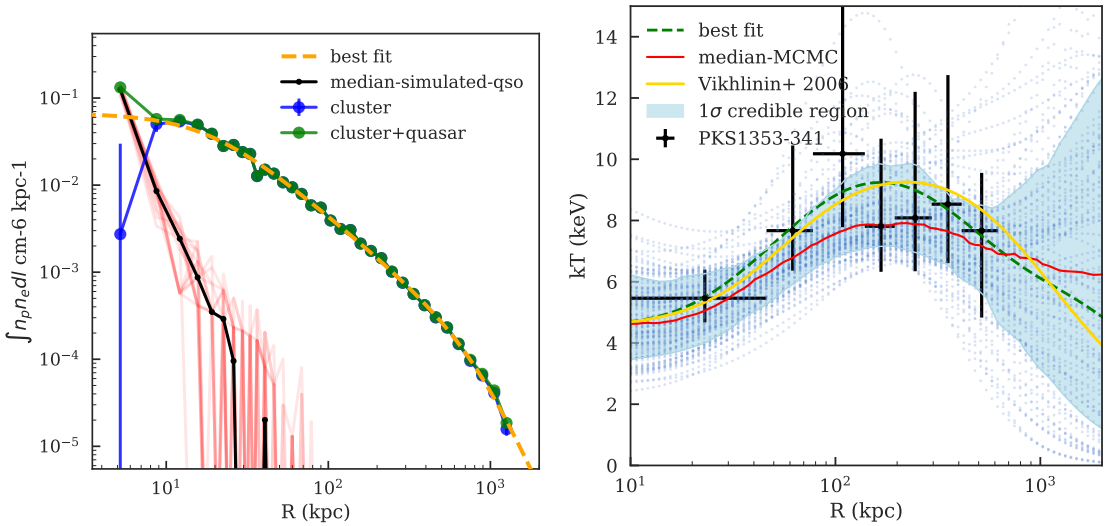

Figure 2-4 Left: the surface brightness profile with the total brightness in green and with the removed simulated point source in blue. The red lines are different realizations of the simulated point source, while the black line is their median. The orange line is the best-fit model. Right: the temperature profile of the cluster. The blue dotted lines are different Markov-chain Monte Carlo (MCMC) realizations for the fit, using *emcee*, a Python ensemble sampler [113]. The cyan-shaded region corresponds to a 1σ credible region from the MCMC simulation. The green dashed line is the best-fit model, and the red solid line is the median of the MCMC. The yellow line is the universal temperature profile from Vikhlinin et al. [320].

Based on the temperature profile in the right panel of Fig. 2-4, the cluster appears to harbor a cool core. Its temperature profile rises sharply from a minimum of 5 keV at ∼10 kpc to a maximum of 10 keV at ∼100 kpc with a core-excised $(0.15-1.0\,\mathrm{R}_{500})$ temperature of $4.32^{+1.74}_{-1.92}$ keV. The temperature profile is not well-constrained at radii greater than 700 kpc. In addition, the temperature profile has a similar shape to the universal profile (thick yellow line) derived by Vikhlinin et al. [320].

2.4.2 Total Mass, Gas Mass Fraction, Entropy, and Cooling Time

The total hydrostatic mass within R_{500} is $M_{500} = 6.90^{+4.29}_{-2.62}\times10^{14}\,M_\odot$. For comparison, the total mass within R_{500} of A1795 is $(6.03\pm0.52)\times10^{14}\,M_\odot$, while that of H1821+643 is $9\times10^{14}\,M_\odot$ [320, 267]. We measure a gas fraction of ∼0.1, consistent with what is

found within R_{500} for typical clusters [5, 126].

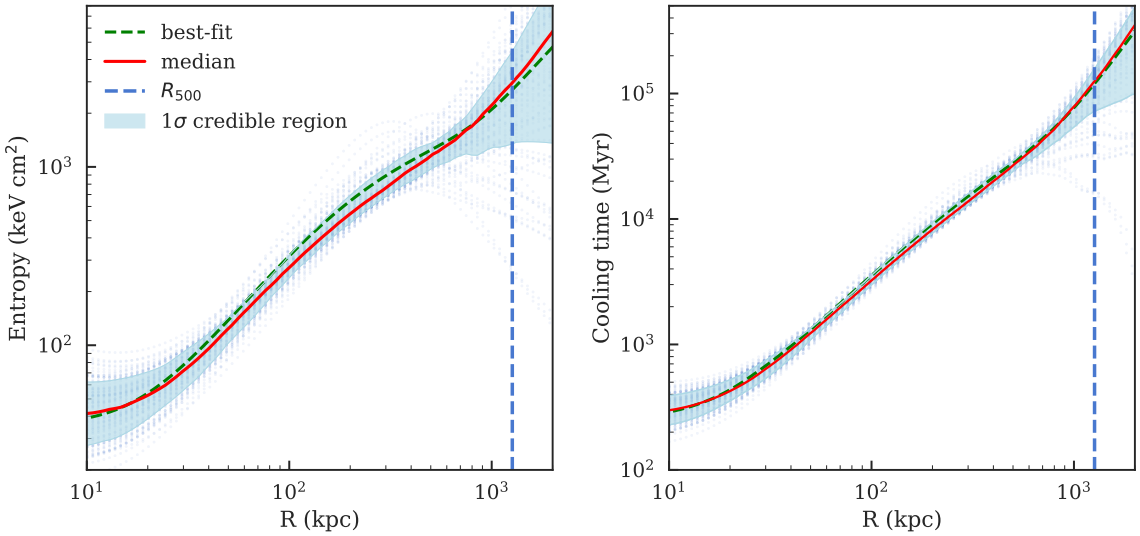

Figure 2-5 Left: entropy profile for PKS1353-341. Right: cooling time profile for PKS1353-341. The best-fit-parameter model is displayed as a green dashed line and the median model from MCMC simulation is displayed as a red solid line. The cyan-shaded region corresponds to a 1σ credible region from the MCMC simulation, the blue dotted lines are different realization of the MCMC, and the blue dashed line is an R_{500} for the cluster (1264 kpc).

The entropy profile for this cluster is shown in the left panel of Fig. 2-5. At all radii, the entropy profile is monotonically increasing. The best fit K_0, the core entropy, is $\sim 50\,\mathrm{keV\,cm^2}$, which leans toward the smaller-value mode for the bimodal distribution of K_0, found by Cavagnolo et al. [67]. A discussion of this entropy profile in the context of other galaxy clusters will be presented in Section 2.5.1.

Lastly, the right panel of Fig. 2-5 shows the cooling time profile of the cluster. The cooling time profile has a monotonically increasing profile from the center of the cluster to larger radii. The central cooling time (at 10 kpc from the center) of PKS1353-341 is $299^{+92}_{-70}\,\mathrm{Myr}$. According to Hudson et al. [156], if the central cooling time is less than 1 Gyr, then the cluster is classified as an SCC cluster. Therefore, this cluster is an SCC cluster. Both the temperature and entropy profiles also lead to the same conclusion.

The radius of the cooling region, defined as the radius at which the cooling time

is less than 7.7 Gyr, was also measured and found to be ∼200 kpc. Without any source of feedback, the ICM inside this radius should have cooled since $z \sim 1$, which suggests that some heating mechanism is required to keep the ICM hot on scales of ∼200 kpc [i.e., AGN feedback; 218].

2.5 Discussion

Close examination of PKS1353-341 reveals that it has similar physical properties to other, well-studied galaxy clusters, including its entropy profile and its total enclosed mass. In this section, we discuss the cluster in a larger context and explore other aspects of the cluster, such as the BCG star formation rate (SFR) and the AGN feedback.

2.5.1 Entropy Profile

The behavior of the entropy profile for this cluster, as described in Section 2.4.2, is consistent with what Cavagnolo et al. [67] found in his entropy profile analysis of the ICM for 239 clusters in the *Chandra* archive. The blue dotted lines in Fig. 2-6 show all 239 clusters in Cavagnolo's sample, and the red solid line is that of PKS1353-341. The two dashed lines are for a simple power law model based on Panagoulia et al. [242] and Hogan et al. [151].

The central ($r < 10$ kpc) entropy of the cluster is approximately $30 - 60\,\mathrm{keV\,cm^2}$. The large uncertainty comes from the uncertainty of the core density and temperature, due to the central AGN. The nonzero core entropy can be explained by either the AGN providing a large amount of energy to offset cooling and maintain nonzero entropy [328] or the low-entropy gas near the core having cooled and the core being refilled with higher-entropy gas. We see no significant flattening of the entropy profile near the center of the cluster, similarly to what was suggested by Panagoulia et al. [242], Hogan et al. [151] and Babyk et al. [12].

One surprising result of the entropy profile is an excess above a power law model at ∼200 kpc. Quantitatively, the entropy of PKS1353-341 in the core is lower than the

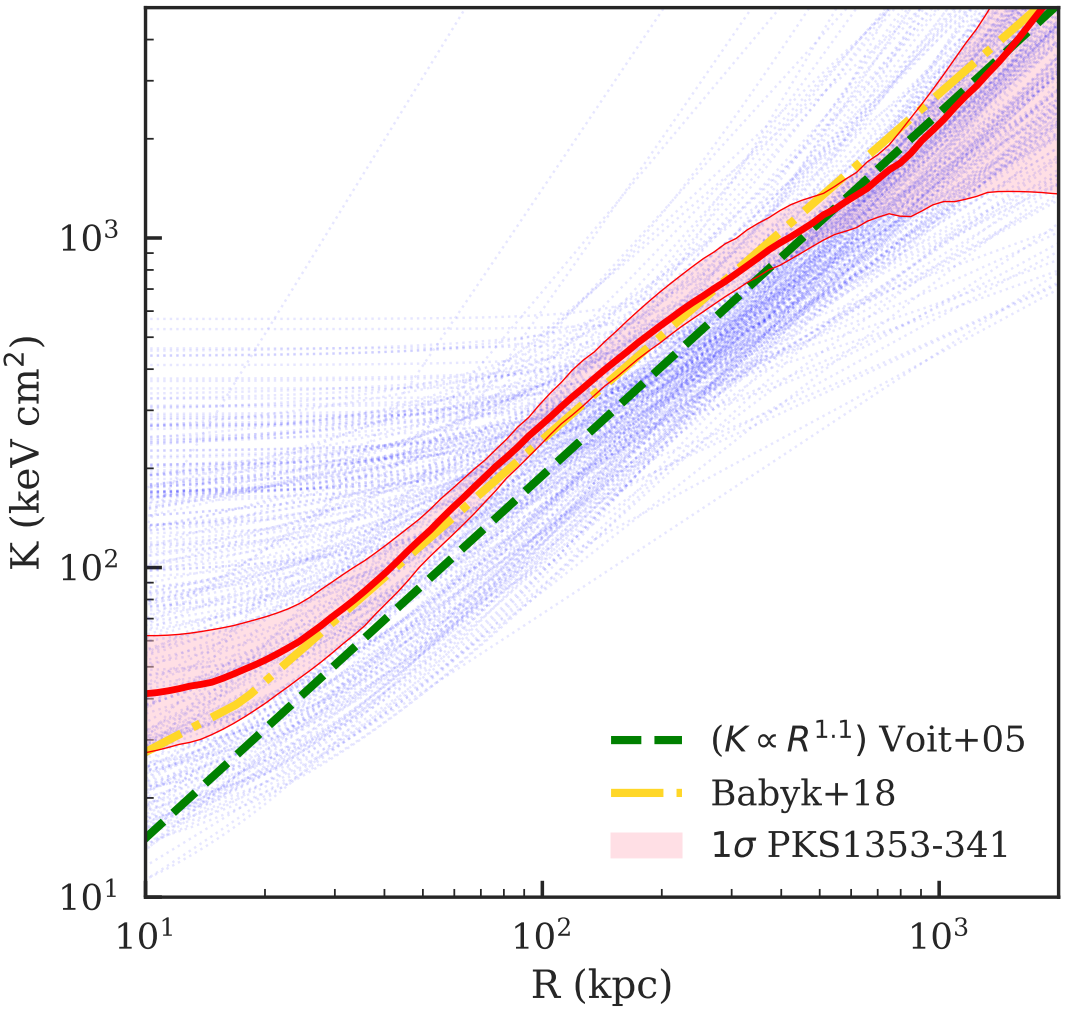

Figure 2-6 Entropy profile for PKS1353-341, compared to 239 clusters from Cavagnolo et al. [67] in blue. Best-fit entropy profiles from Voit [326] and Babyk et al. [12] are shown in green and yellow, respectively. Despite having one of the lower entropies at 10 kpc, PKS1353-341 has one of the highest entropies at 200 kpc. This bump may be due to a past energetic event at the cluster center depositing heat, which has been rising buoyantly.

median (∼35th percentile) of the 239 clusters from Cavagnolo et al. [67], consistent with being a cool-core cluster. At large radii (∼750 kpc), the measured entropy for PKS1353-341 is consistent with the median value for the 239 clusters, demonstrating the self-similar nature of clusters outside of the core. However at ∼200 kpc, the entropy for PKS1353-341 is 1σ above the median (∼84th percentile), implying that the excess is marginally significant. Given that it is only a 1σ deviation, this could very

well be simply a statistical fluctuation, or a result of model assumptions. However, if the excess is real, this behavior is unusual because any excess high-entropy gas should rise to larger radius, smoothing out any departure from a power law in relatively short timescale. Thus, any large-scale deviation from this profile is likely caused by some transient non-gravitational process in the core, such as AGN heating [326, 242]. One possible explanation for the excess at ∼200 kpc is that the AGN recently heated up the low-entropy gas at the core, which rises to a greater radius (i.e., at ∼200 kpc). As the heated gas moves outward, the high-entropy gas starts to mix with colder surrounding gas, which smooths out the excess entropy. But in this case, there is not enough time for this process to complete, leaving the excess at ∼200 kpc. Assuming that excess entropy deposited at the center rises at the sound speed, the time it takes to reach a radius of 200 kpc in PKS1353-341 is the sound crossing time $t_c = R/c_s = 180$ Myr, where $R = 200$ kpc is the position of the bubble and $c_s = \sqrt{kT/(\mu m_{\rm H})}$ ($\mu \simeq 0.62$ and $kT = 5\,{\rm keV}$) [214]. We consider that this entropy excess could also be a result of our method of using a combination of the universal pressure profile shape and the measured density profile to model the temperature profile, though we stress that this profile should have sufficient freedom to characterize the temperature at radii less than R_{500}. (see discussion in Section 2.3.4).

2.5.2 Luminosity and Cluster Cosmology

The luminosity in the *ROSAT* band (0.1−2.4 keV) for PKS1353-341 is $4.3\times10^{44}\,{\rm erg\,s^{-1}}$. Fig. 2-7 shows the luminosity of PKS1353-341 and its redshift with respect to clusters from the REFLEX all sky catalog [42]. The dotted line emphasizes the flux-limited nature of the REFLEX catalog at $3\times10^{-12}\,{\rm erg\,s^{-1}\,cm^{-2}}$. Comparison of the luminosity of PKS1353-341 with those from the REFLEX catalog suggests that PKS1353-341 should have been detected and identified as a cluster for its luminosity, if not for the extremely bright point source at its center.

The discovery of a new cluster above the RASS detection threshold suggests that the CHiPS survey will be able to identify similar galaxy clusters and improve upon the completeness of previous X-ray cluster surveys. Given that the constraint on Ω_M from

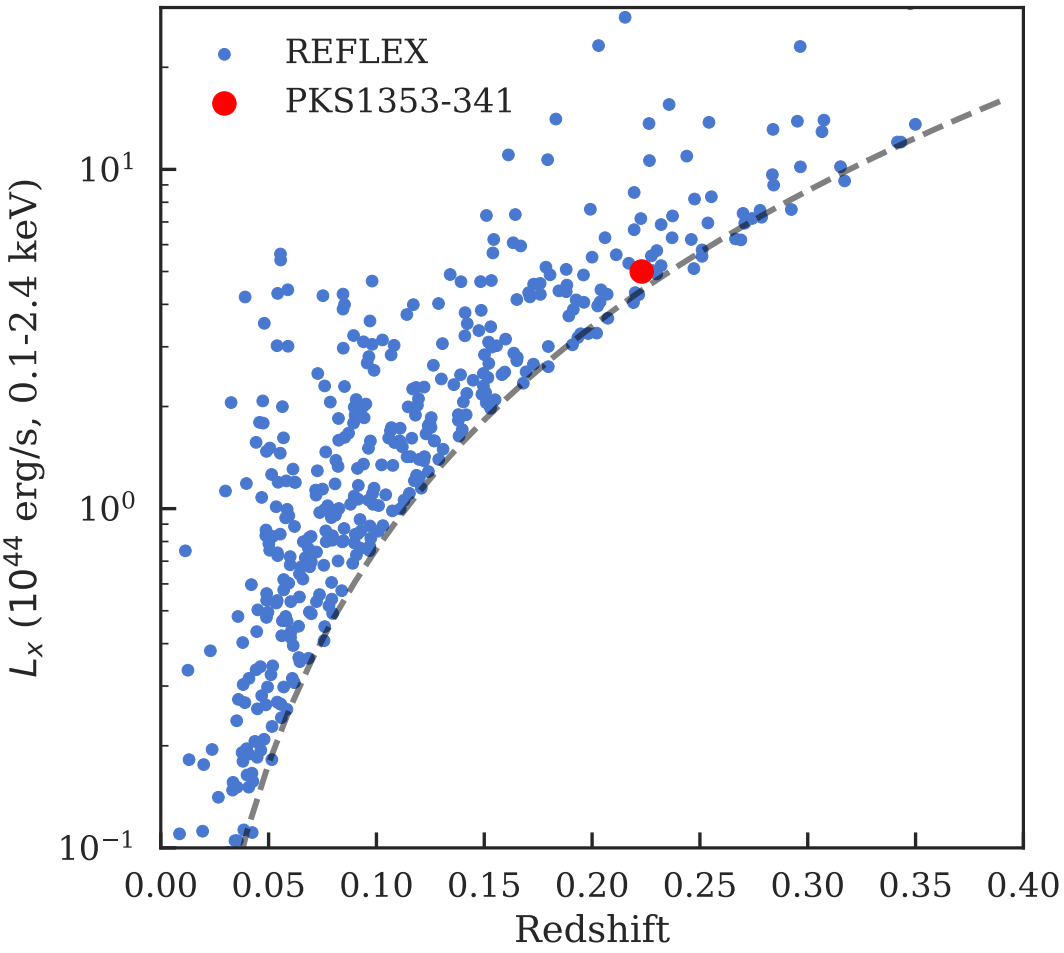

Figure 2-7 Luminosity vs. redshift for clusters from the REFLEX Cluster Survey Catalog [42], compared to PKS1353-341. The dotted line shows the cutoff introduced by Böhringer et al. [42] for X-ray flux limit at $3 \times 10^{-12}\,\mathrm{erg\,s^{-1}\,cm^{-2}}$. This figure demonstrates that PKS1353-341 should have been detected and identified as a cluster by REFLEX, and other cluster surveys based on *ROSAT* data.

cluster count cosmology is proportional to $N^{1/3}$ [134], we could have a bias of $\sim$1% in Ω_M if we are missing only a few percent of clusters due to the presence of central X-ray bright point sources. Of course, this assumes that statistics are the dominant systematic uncertainty, which is currently not the case–at present, uncertainties on Ω_M are dominated by systematic uncertainties in the cluster mass calibration. However, in the era of eROSITA (which will have a similar selection to ROSAT) and precision cluster masses, this bias may become dominant if not addressed. The CHiPS survey will provide a first estimate of how severe this bias is in the low-z universe.

2.5.3 Central Galaxy SFRs

The SFRs of the central galaxy can be used to gauge the efficiency of cooling at the core of the cluster, assuming that the hot ICM cools and forms stars [219, 239, 209, 205]. A typical central cluster galaxy has little to no star formation; on average $\sim$1% of the predicted cooling is observed in stars [239], presumably because AGN feedback prevents the ICM from cooling. However, the recently discovered Phoenix cluster has a high SFR in its central galaxy, corresponding to $\sim$30% of the predicted cooling, pointing to a different cooling mechanism or a lack of feedback at the cluster core [202]. By computing the SFR in PKS1353-341 and comparing to the cooling rate, we can get a better understanding of the heating-cooling balance in the cluster core.

The SFR for PKS1353-341 is computed using available archival UV data from the *GALEX* Mission Archive. Based on the aperture UV flux, we estimate an SFR for PKS1353-341 of $6.2 \pm 3.6\, M_\odot\, \mathrm{yr}^{-1}$, using the empirically-derived star formation rate estimators from Rosa-González et al. [261], which include intrinsic extinction corrections.

The SFR of $\sim$6 $M_\odot\, \mathrm{yr}^{-1}$ for PKS1353-341 is average, compared to those of other cool-core clusters. The SFR in this cluster should not come as a surprise since we know that cool gas is available, as evidenced by the presence of a central X-ray bright (i.e., accreting) AGN. With a larger sample size from the CHiPS survey, we could consider how the SFR depends on the two modes of AGN feedback (kinetic versus quasar).

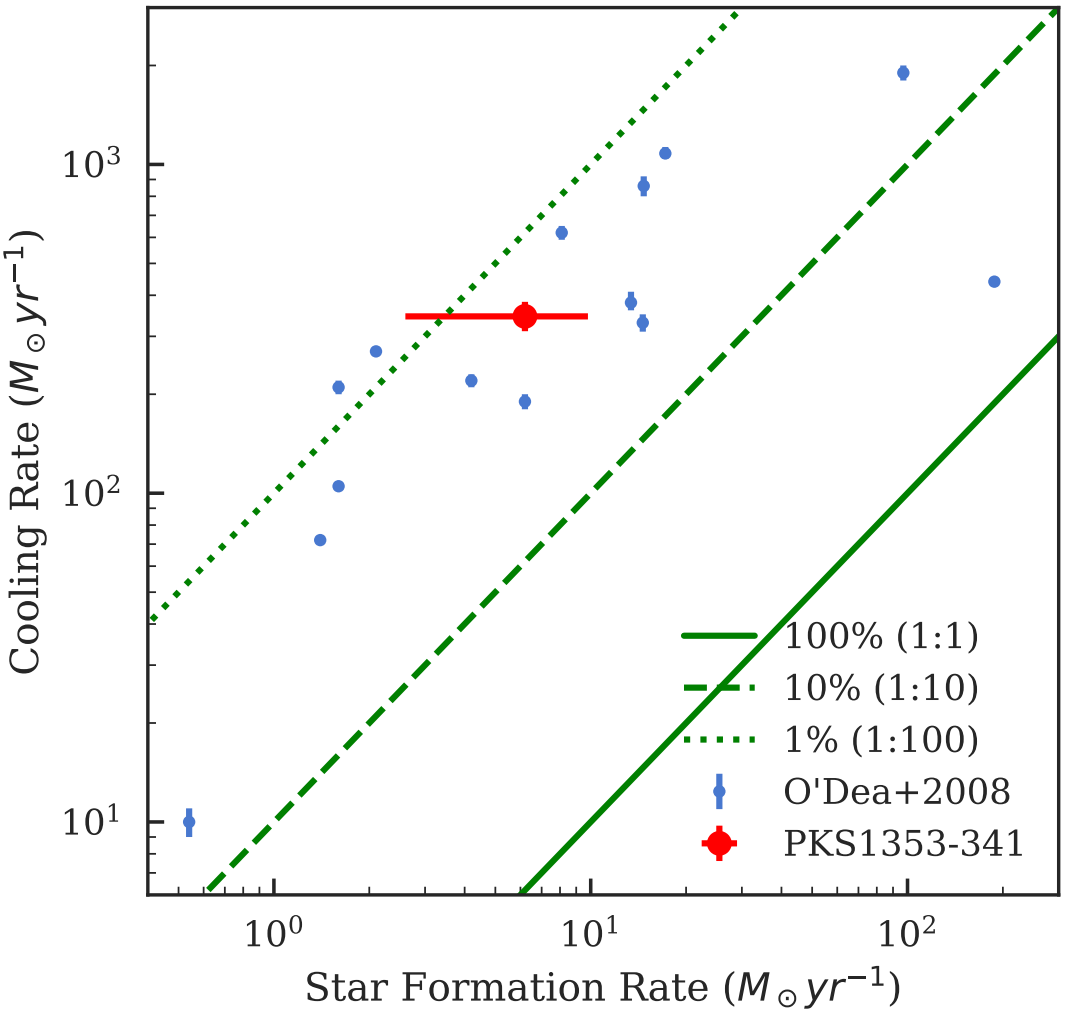

Figure 2-8 Cooling rate vs. SFR for the central galaxy in the PKS1353-341 cluster, compared to clusters from O'Dea et al. [239]. The green lines indicate star formation proceeding at 1%, 10%, and 100% efficiency with respect to the X-ray cooling rate. This figure demonstrates that cooling in PKS1353-341 is being suppressed by two orders of magnitude, presumably by AGN feedback.

This will lead us to a better understanding of the physics around the accretion disk and how accretion relates to different feedback modes in the center of clusters.

Nevertheless, this SFR is considered typical, compared to the ICM cooling rate, which is $345^{+41}_{-37}\,M_\odot\,\mathrm{yr}^{-1}$. The SFR of PKS1353-341 is about ~2% of the cooling rate, which, according to Fig. 2-8, is typical for SCCs [239]. Other SCC clusters, such as A1795 and A2597, also have SFRs at this scale. Specifically, A1795's and A2597's

SFR are 9 and $4\,M_{\odot}\,\mathrm{yr}^{-1}$, respectively [141, 88]. Thus, this system is more similar to a highly suppressed cooling flow, like A1795's, than it is to a run-away cooling flow, like the Phoenix cluster's.

2.5.4 X-ray Cavities

X-ray cavities are a result of powerful jets from central SMBHs pushing on the surrounding gas [41, 214]. Evidence for these cavities can be visible long after the outburst [107]. The detection of these cavities is evidence for the existence of a radio jet, corresponding to the kinetic feedback mode of the cluster. In addition, the location and size of the cavities tell us the timescale on which these outbursts occurred and the outburst power, respectively.

Using both 2D modeling and unsharp masking to remove the central bright point source and diffuse ICM, we see hints of negative residuals located symmetrically around the center point of the cluster, which may be a pair of cavities (as shown by the white arrows in the top left panel of Fig. 2-9). The top right panel of Fig. 2-9 shows the annuli used for constructing the azimuthal surface brightness profile, shown in the lower panel. From this profile, we see that the potential cavities are significant at roughly the 2σ level.

The northern cavity is located 8.5 kpc away from the center of the cluster with a cavity power $\mathrm{P_{cav}} = 2.3 \times 10^{44}\,\mathrm{erg\,s^{-1}}$. The cavity power was calculated from the ratio between the energy stored in the bubble and the sound crossing time. The energy stored was estimated using $E_{\mathrm{bubble}} = 4PV$ where P is the thermal pressure of the ICM and V is the volume of the cavity, whereas the sound crossing time was computed from $t_{\mathrm{cs}} = \frac{R}{c_s}$ where R is the distance from the central BCG to the middle of the cavity and c_s is the sound speed $\left(c_s = \sqrt{\frac{5}{3}kT/(0.62m_H)}\right)$ [149]. However, the resulting image depends strongly on the modeling and subtraction we used to remove the central point source, which led to large systematic uncertainties in the measured cavity power.

Fig. 2-10 shows the cavity power and the radiative power of PKS1353-341 with respect to the Eddington luminosity in the context of the clusters from Russell

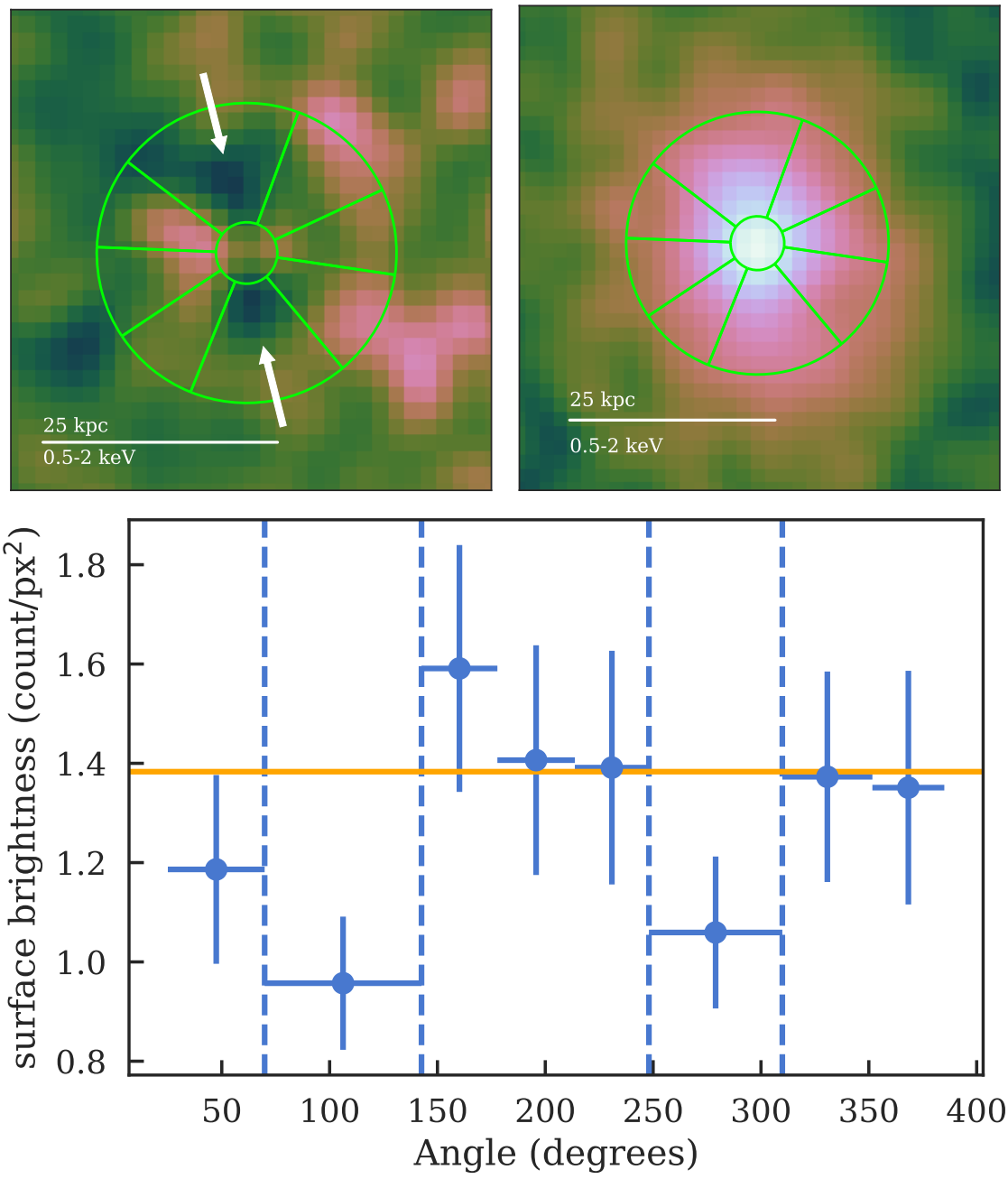

Figure 2-9 Top left: 0.5-2 keV 2D-model-subtracted X-ray image of PKS1353-341 with potential X-ray cavities (white arrows) highlighted. Top right: 0.5-2 keV X-ray image with the regions used for calculating the azimuthal surface brightness profile in green. Bottom: 0.5-2 keV azimuthal surface brightness profile for the regions shown in the upper right panel. The vertical dashed lines show the location of each cavity (adopted from Hlavacek-Larrondo et al. [149]). This figure demonstrates at $\sim 2\sigma$ depression in surface brightness at the position of the cavities.

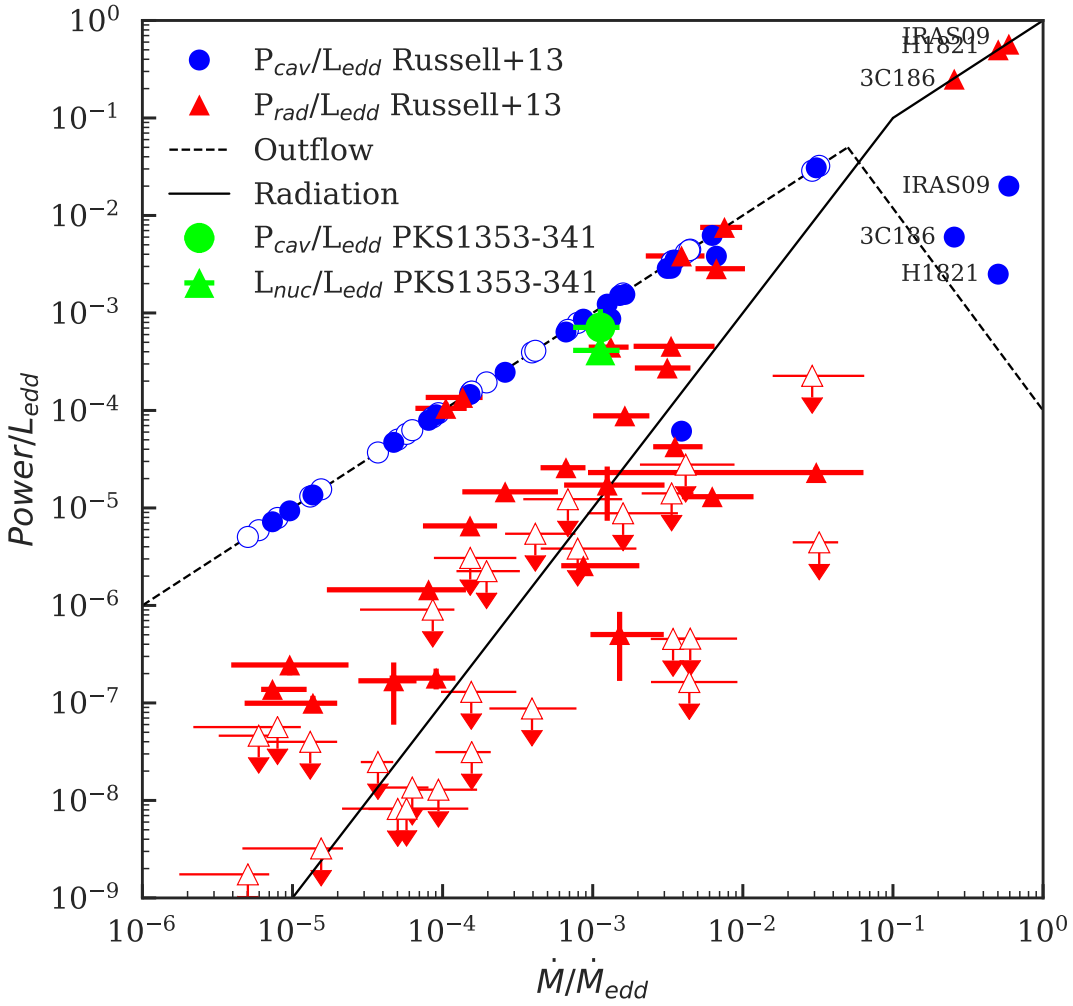

Figure 2-10 Mean black hole accretion rates ($\dot{M}/\dot{M}_{\rm edd}$), compared to the cavity power ($P_{\rm cav}/L_{\rm edd}$; circle) and the radiative power ($L_{\rm nuc}/L_{\rm edd}$) of the central AGN (triangle symbols), scaled by the Eddington luminosity. Detected X-ray sources are shown as filled symbols, and the upper limits are shown in open symbols. The radiation and outflow models are for illustrative purposes (from Russell et al. [268]'s Fig.12). This figure demonstrates that PKS1353-341 is one of a few systems with a low accretion rate and high radiative power.

et al. [268]'s sample. The sample was selected from cluster, group, and elliptical galaxy samples with evidence of AGN activity in the form of cavities in X-ray images. The nuclear luminosity ($L_{nuc} \sim 1.8 \times 10^{44}$ erg s^{-1}) was measured from the point source at the cluster center (within 8 kpc) in the 0.1–10 keV band. For fully ionized plasma, the Eddington luminosity ($L_{\rm edd}$) is $1.26 \times 10^{47} \left(\frac{M_{\rm BH}}{10^9 M_\odot}\right)$ erg s^{-1},

where $M_{\rm BH}$ is the SMBH mass. According to Graham [128], the K-band magnitude of the host galaxy from 2MASS can be used to estimate the SMBH mass, using $\log(M_{\rm BH}/M_{\odot}) = -0.037(M_K + 24) + 8.29$, where M_K is the absolute magnitude in the K band. Following Russell et al. [268], we assume that $\frac{\dot{M}}{\dot{M}_{\rm Edd}} = \frac{P_{\rm cav}+L_{\rm nuc}}{L_{\rm Edd}}$.

Note that PKS1353-341, indicated as green in Fig 2-10, has $P_{\rm cav}$ and $L_{\rm nuc}$ of similar magnitude and lies on the higher end of the mean accretion rate, where the quasars (the three highest accretion rates) tend to lie. The similar magnitude of the mechanical and radiative power suggests that this system is in the midst of transitioning between mechanically dominated and radiatively dominated modes.

In Fig 2-11, we plot the energy stored in the bubbles ($E_{\rm cav}$) for PKS1353-341 against both the total mass (M_{2500}) and the 1.4 GHz emission ($L_{1.4\rm GHz}$) compared to that of the flux-limited X-ray sample of 45 galaxy clusters from Main et al. [186]. The newly discovered cluster is located within the scatter in both relations, suggesting that for a cluster with this particular mass and radio power, our measured cavity energy is typical compared to those of the other clusters.

2.5.5 Timescale for two different modes of AGN feedback

In this work, we present a new galaxy cluster exhibiting possible quasar-mode feedback, which, combined with four other known QSO-hosting clusters [267, 284, 241, 202], leads to a sample of five such systems. In comparison, the total number of known galaxy clusters exhibiting the kinetic mode is of order $\sim$100. According to the chaotic cold accretion model proposed by Gaspari et al. [119], we can expect to see an increase in accretion rate of two orders of magnitude–which leads to X-ray bright nuclear sources–around 1% of the time. This indicates that galaxy clusters with an X-ray bright nucleus should be relatively rare, only 1% of the population. Currently, this prediction is consistent with the number of quasar-mode galaxy clusters that have been discovered, and no further mechanism is required to explain the existence of these radiatively efficient nuclei. As our survey reaches completion, we will be able to provide more evidence to either support or refute this claim.

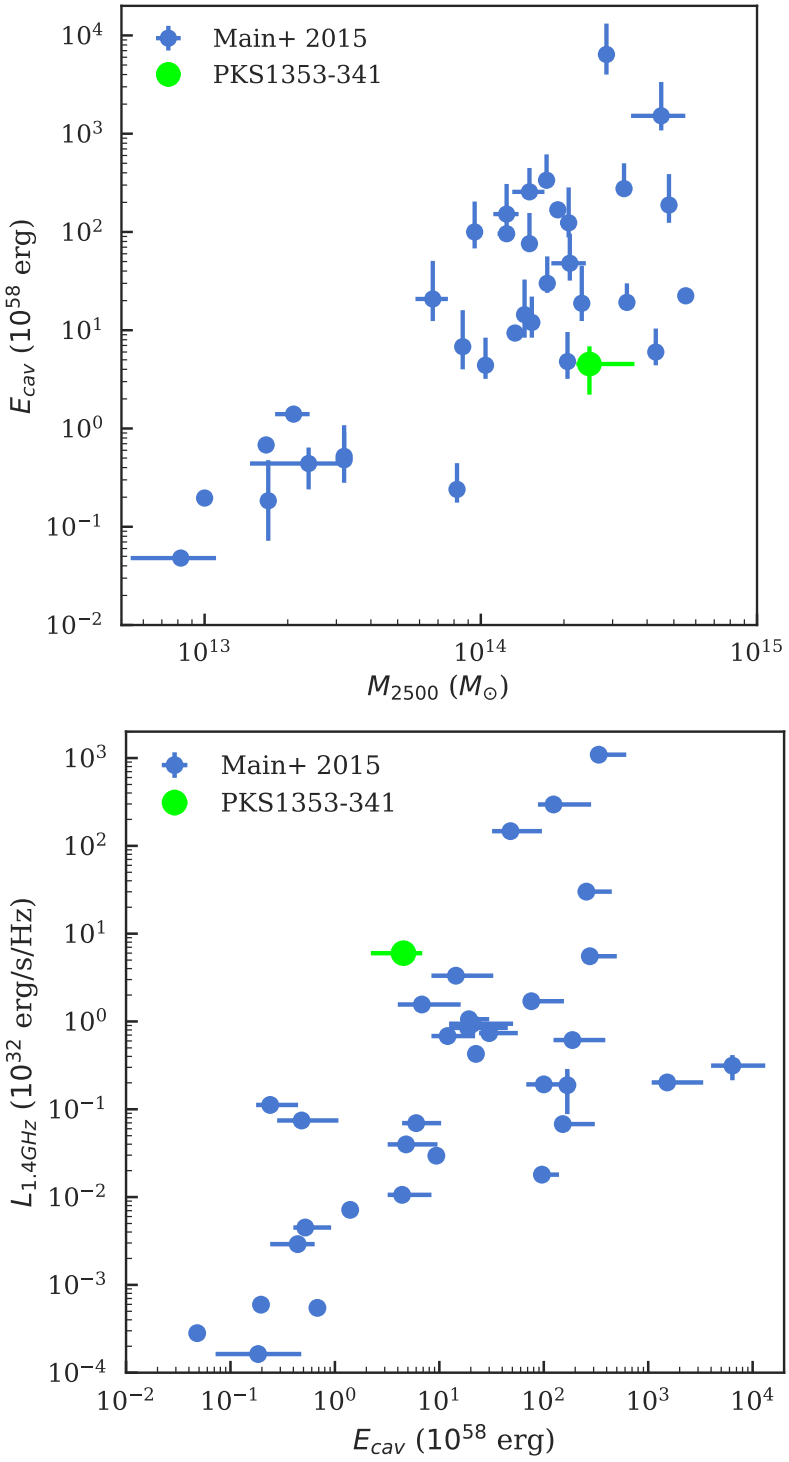

Figure 2-11 Total energy in cavities, compared to the cluster mass (left) and the central radio power (right). PKS1353-341 is shown in green and compared to clusters from Main et al. [186], shown in blue. This figure demonstrates that the amount of the mechanical feedback in PKS1353-341 is not atypical.

2.6 Summary

We have presented the properties of a newly discovered galaxy cluster hosting an extreme central galaxy as the first result of a larger survey. The cluster, discovered based on its central extreme properties, is observed with the *Chandra* X-ray telescope. The main results of the study are summarized as follows:

- We have found a new relaxed galaxy cluster with a central X-ray and radio bright AGN in its BCG, which increases the sample size of known quasar-mode feedback clusters to about five. With the exception of the X-ray bright nucleus, this cluster is similar to other well-studied clusters such as A1795.

- The luminosity of the cluster is $\sim 7 \times 10^{44}\,\mathrm{erg\,s^{-1}}$, while the average temperature is $4.3^{+1.7}_{-1.9}\,\mathrm{keV}$. The total mass, assuming hydrostatic equilibrium, is $6.90^{+4.29}_{-2.62} \times 10^{14}\,M_{\odot}$, which makes the cluster massive enough to have been discovered by former shallow all-sky surveys (e.g., RASS). This, in combination with the discovery of the Phoenix cluster, implies that all-sky X-ray surveys can miss massive nearby cluster with bright enough central point source.

- The X-ray morphology, the temperature profile, the density profile, and the central cooling time all suggest that the cluster has an SCC.

- We find weak evidence for an excess entropy at $\sim$200 kpc from the center, which indicates a possible recent ($\sim$180 Myr) heating event that occurred near the center and is heating up and buoying high-entropy gas to a larger radius.

- The central galaxy has an SFR of $6.2 \pm 3.6\,M_{\odot}\,\mathrm{yr^{-1}}$, which is consistent with typical SFRs ($\sim 1 - 10\,M_{\odot}\,\mathrm{yr^{-1}}$) for SCCs clusters and implies that cooling is suppressed by two orders of magnitude.

- We find a hint (2σ) of X-ray cavities near the cluster center. The calculated cavity power is $2.3 \times 10^{44}\,\mathrm{erg\,s^{-1}}$, which is comparable to the radiative power of the nucleus, corresponding to roughly 0.1% of the Eddington value. Deeper

observations are required to confirm the existence of the cavities. This implies that the AGN may be transitioning between radiative and mechanical modes.

We have also provided an introduction to the CHiPS survey as an all-sky survey designed to find centrally concentrated galaxy cluster or clusters hosting central QSOs misidentified in previous X-ray surveys. More details about the CHiPS survey will be available in an upcoming paper.

The discovery of a new galaxy cluster implies that the CHiPS survey has the potential to increase the number of quasar-BCG clusters. This should improve our understanding of the relation between cooling and feedback processes in the cores of clusters. In addition, the survey could discover new starburst-BCG clusters, and possibly answer the uniqueness question of the Phoenix cluster. Lastly, we will be able to use the survey to help estimate the completeness of previous X-ray survey (as most current surveys are biased against clusters with central X-ray bright point sources) and give better constraints on several cosmological parameters.

Chapter 3

Complete sample of extreme BCG clusters

The content of this chapter was submitted to The Astrophysical Journal *on August 7, 2020 and published [294] as* The Clusters Hiding in Plain Sight (CHiPS) survey: Complete sample of extreme BCG clusters *on March 25, 2021.*

3.1 Introduction

Clusters of galaxies are the largest and most massive gravitationally bound objects in the universe, with masses of roughly 10^{14}–$10^{15} M_{\odot}$ [326] and extents on scales of several megaparsecs. On this scale, the density field remains in the linear regime of density perturbation [139]. This makes the number density of clusters relatively straightforward to predict from theory [see 40, 201, 312, for the most recent calibration of halo mass function from simulations]. This number density depends strongly on several cosmological parameters, including $\Omega_{\rm m}$ (the density of total matter compare) and σ_8 (the amount of fluctuation in matter density) [322]. This forms the basis of cluster cosmology.

Now the Planck Satellite's mission has ended [249], we are living in the era of precision cosmology where cosmological parameters of the universe are routinely measured with percent-level uncertainty. To improve the precision of cluster cosmology, various

groups have been trying to increase the number of known galaxy clusters, by searching for overdensities of red galaxies in optical or near-infrared surveys [122, 127, 271], extended extragalactic emission in X-ray surveys [42, 95, 96], or via the Sunyaev-Zel'dovich (SZ) effect [36, 37, 144, 248, 306] in millimeter/submillimeter surveys. Each technique has its own unique benefits and challenges. With the invention of wide-field optical telescopes, performing optical surveys to find overdensities of galaxies is relatively cheap, although optical surveys are strongly affected by projection effects. For SZ surveys, we are capable of detecting galaxy clusters up to relatively high redshift since the SZ signature is redshift-independent. On the other hand, the SZ signature depends strongly on mass, restricting current-generation surveys to only the most massive clusters [64, 230]. Lastly, X-ray surveys have been one of the most popular techniques to discover galaxy clusters since the launch of the ROSAT X-ray satellite [e.g., the REFLEX survey, 42]. Even though X-ray surveys can only produce flux-limited samples of galaxy clusters, cosmologists can take that into account in their selection function when they estimate cosmological parameters [5, 192, 322]. However, with the continuous improvement in optical cluster finders, many of these SZ and X-ray cluster catalogs are now confirmed by the optical data, such as the recent works with SZ [37] and X-ray catalogs [167].

With the recent SZ discovery of the Phoenix cluster [202, 212, 336], the most X-ray-luminous galaxy cluster known, at $z = 0.6$, we have started to question our understanding of the X-ray-survey selection function. The Phoenix cluster was detected in several previous X-ray surveys, but was misidentified as a bright point source based on its extremely bright active galactic nucleus (AGN) and cool core in the center of the cluster. With most X-ray surveys identifying objects as either a point-like or an extended source, a galaxy cluster with a bright point source in the center could be misidentified as simply a point source. The next logical step is to ask how many of these galaxy clusters we have missed in the previous surveys, and how this translates to a correction for the selection function.

Another benefit of finding galaxy clusters hosting bright X-ray point sources is to study the cooling flow problem, which is the apparent disagreement between the X-

ray luminosity (cooling rate) of a cluster and the observed star formation rate (SFR), the latter of which is typically suppressed by a factor of ∼100. The best candidate for explaining the inconsistency is AGN feedback from the central galaxy [49, 50, 85]. There are two main modes of AGN feedback: the kinetic mode, driven mostly by jets, and the radiative mode, driven by the accretion of the AGN [104, 121, 136, 215]. With very few known galaxy clusters with extremely bright quasars, such as H1821+643 [267], 3C 186 [283, 284], 3C 254 [82, 339], IRAS 09104+4109 [241], and the Phoenix cluster [202], a larger number of such objects are required to fully understand the role of radiative-mode feedback in the evolution and formation of galaxy clusters. For example, the chaotic cold accretion (CCA) model predicts a tight coevolution between the central supermassive black hole (SMBH) and the host cluster halo [via the cooling rate or $L_{\rm x}$; 120], with flickering quasar-like peaks reached only a few percent of times [119].

In an attempt to find more galaxy clusters hosting bright central point sources, we started the Clusters Hiding in Plain Sight (CHiPS) survey. The details and the first discovery from the survey are published in Somboonpanyakul et al. [292]. In this paper, we focus on a new optical cluster-finding algorithm, developed specifically for the CHiPS survey, to look for cluster candidates after optically imaging all of the X-ray point sources with bright radio and mid-IR from the first part of the project. These candidates may have been misidentified in previous all-sky surveys due to their central galaxies' brightness. After performing the cluster-finding algorithm, we present a list of newly discovered galaxy cluster candidates along with their expected redshift and richness.

The overview of the CHiPS survey, the optical data used in the follow-up campaign, and its methodology are described in Section 3.2. In Section 3.3, we present details of the data reduction and analysis for recently obtained optical data from the Magellan telescope. Our cluster-finding algorithm is described in Section 3.4 while the X-ray data reduction is presented in Section 3.5. We discuss the results and the implications of these findings in Sections 3.6 and 3.7. Lastly, we summarize the paper in Section 3.8. We assume $H_0 = 70\,{\rm km\,s^{-1}\,Mpc^{-1}}$, $\Omega_{\rm m} = 0.3$, and $\Omega_\lambda = 0.7$. All errors

are 1σ unless noted otherwise.

3.2 The CHiPS Survey

The CHiPS survey is designed to identify new centrally concentrated galaxy clusters and clusters hosting extreme central galaxies (starbursts and/or AGNs) within the redshift range 0.1–0.7. The first part of the survey consists of identifying candidates by combining several all-sky survey catalogs to look for bright objects at multiple wavelengths. The second part of the survey, which is the focus of this paper, addresses mainly our optical follow-up program to determine the best cluster candidates by searching for an overdensity of galaxies at a given redshift centered on the location of the X-ray sources. The last part, which is also included in this paper, is to obtain Chandra data for these candidates in order to confirm the existence of these new clusters and characterize their properties, such as the gas temperature, the total mass, and the gas fraction.

3.2.1 Target Selection

Our CHiPS target selection is described in detailed in our previous publication [292]; here we outline the main steps.

To select systems similar to the Phoenix cluster, we require sources to be bright in X-ray, mid-IR, and radio, relative to near-IR. The normalization to near-IR is to prevent very nearby (e.g., Galactic) low-luminosity sources from overwhelming the sample. Starting with X-ray point-source catalogs from the ROSAT All-Sky Survey Bright Source Catalog and Faint Source Catalog [RASS-BSC and RASS-FSC; 323], we cross-correlate with radio from NVSS [79] or SUMSS [199], mid-IR with Wide-field Infrared Survey Explorer [WISE; 337], and near-IR with Two Micron All Sky Survey [2MASS; 289]. This combination leads to two types of astrophysical sources: radio-loud type II QSOs and galaxy clusters with an active core (a starburst and/or AGN-hosting brightest cluster galaxy (BCG)). This approach is similar to two other surveys from Green et al. [129] and Donahue et al. [92]. The main difference

is that Donahue et al. [92] focused on previously known, optically selected BCGs from the GMBCG catalog [135] and Green et al. [129] started with spectroscopically confirmed AGNs in the ROSAT catalog. We begin our search with a complete ROSAT point-source catalog and combine with all archival data from near-IR and mid-IR to radio.

In addition, we apply color cuts in order to select only the most extreme objects in X-ray, mid-IR, and radio, as demonstrated in Fig. 3-1. The cuts are chosen to capture the expected range of color for a Phoenix-like object at an unknown redshift between 0.1 and 0.7. The NASA/IPAC Extragalactic Database (NED)[1] was used to reject foreground ($z < 0.1$) and background ($z > 0.7$) objects. Candidates with $z < 0.1$ are close enough to be detected with past instruments even with a bright central point source. Most of these clusters were first detected by eye in various optical catalogs, including the well-known Abell and Zwicky catalogs [2, 344], meaning that we do not expect any misclassifications. On the other hand, clusters at $z > 0.7$ are exceedingly rare in the ROSAT data – not because of a bias in their selection, but because they are simply too faint. We also remove objects that have Galactic latitude less than $\pm 15^\circ$ because foreground stars and extinction from the Milky Way will obscure any clusters. After the removal, we are left with 470 objects to perform the optical follow-up, which is presented in the next section. We note that by requiring mid-IR and radio detection, we emphasize the detection of Phoenix-like clusters, at the expense of removing from the sample some BCGs with central AGN that are not radio-loud or mid-IR-bright, such as unobscured, radio-quiet AGNs. This means that the CHiPS survey will only place a lower limit on the fraction of clusters missed by the previous X-ray surveys.

Further information about our target selection and the first galaxy cluster discovered from this survey, the galaxy cluster surrounding PKS 1353-341, are presented in Somboonpanyakul et al. [292]. In the next section, we describe the data used for our optical follow-up of these 470 candidates.

[1] https://ned.ipac.caltech.edu

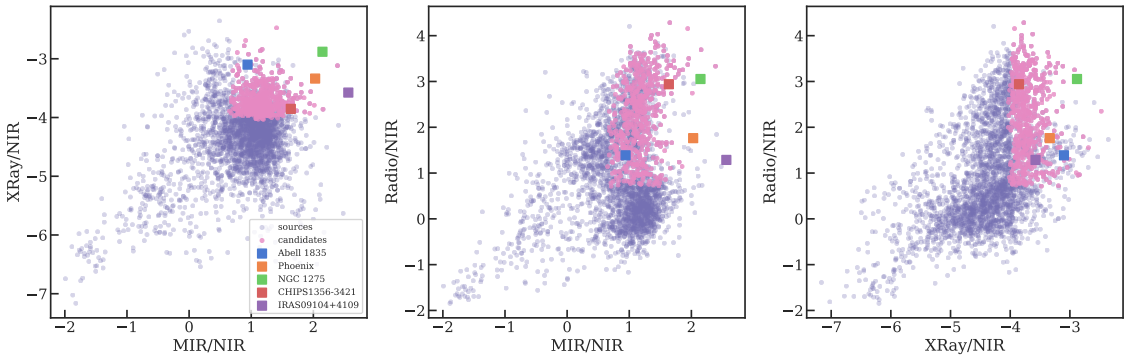

Figure 3-1 The three panels show color-color diagrams for objects that are detected in all four all-sky surveys (3450 objects). The axes are the logarithm of the ratio of the X-ray, mid-IR (MIR), or radio flux to the near-IR (NIR) flux. Points colored in pink satisfy our three color cuts. The Phoenix, Perseus (NGC 1275), A1835, and IRAS 09104+4109 clusters, which host extreme BCGs, are shown with orange, green, blue, and purple squares, respectively while CHIPS 1356-3421 is shown with a red square.

3.2.2 Optical Follow-up Observations

The optical follow-up program is separated into two parts based on the decl. of the targets. Most objects with positive decl. are followed up with the Sloan Digital Sky Survey (SDSS) because of its nearly complete coverage in the northern sky, whereas objects with negative decl. are observed with either the first data release of the Panoramic Survey Telescope and Rapid Response System [Pan-STARRS1; 70] with sky coverage of decl. greater than $-30°$ or additional pointed observations using the Parallel Imager for Southern Cosmological Observations [PISCO; 298] on the 6.5m Magellan Telescope at Las Campanas Observatory, Chile. Specifically, 256 out of our 470 candidates were observed with SDSS, 64 candidates were observed with Pan-STARRS1, and the remaining 150 candidates were individually observed with PISCO on the Magellan telescope. We note that data from the Dark Energy Survey [DES; 86] were unavailable at the onset of the project. Fig. 3-2 shows the position of all target candidates in the sky, separated by the telescope used for the follow-up.

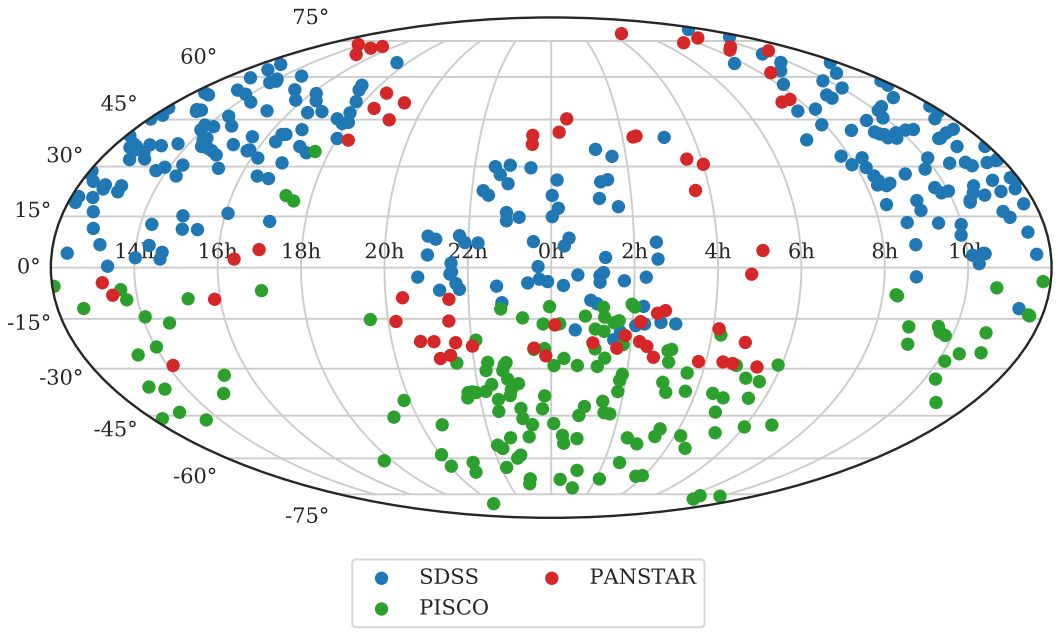

Figure 3-2 Plot of all 470 target candidates for the CHiPS survey in the sky. The blue dots represents candidates followed up with SDSS. The red dots are candidates followed up with Pan-STARRS, and the green dots are candidates from PISCO observations. The gaps at R.A. = 18–20hr and 5–7hr correspond to the Milky Way, which prevents us from finding new cluster candidates around that region.

3.2.2.1 Sloan Digital Sky Survey

The SDSS is a multispectral imaging and spectroscopic redshift survey using a 2.5 m optical telescope at Apache Point Observatory in New Mexico [131]. We utilized Data Release 14 (DR14), released in 2017, which is the second data release for SDSS-IV [3]. We retrieved the photometric data in u, g, r, i, and z bands by querying objects within a radius of $5'$ from the X-ray position, using the function `fGetNearestObjEq` with the Casjob server[2]. In Section 3.4, we apply a more stringent cut during the cluster-finding algorithm. We obtained the SDSS model magnitude (`modelMag`), which, as explained in the SDSS support documentation,[3] gives the most unbiased estimates of galaxy colors. To convert SDSS magnitude to flux units, we use the SDSS asinh magnitude formula,[3] which is also described in Lupton et al. [185].

For star/galaxy classification, "`type`" parameters, provided by SDSS, were used

[2]https://skyserver.sdss.org/CasJobs/
[3]https://www.sdss.org/dr12/algorithms/magnitudes/

to select only galaxies (`type` = 3). The classification is based on the difference between cmodel and point-spread function (PSF) magnitude. Specifically, an object is classified as extended when $\mathrm{Mag_{PSF}} - \mathrm{Mag_{cmodel}} > 0.145$. In addition, we downloaded photometric redshifts (z_{sdss}) for verification of photometric redshift estimates in Section 3.4.

3.2.2.2 Panoramic Survey Telescope and Rapid Response System

Pan-STARRS is a system for wide-field astronomical imaging in the optical g, r, i, z, and y bands, located at Haleakala Observatory, Hawaii. The survey used a 1.8 m telescope, with an imaging resolution of $0.''25\,\mathrm{pixel}^{-1}$ from its 1.4 gigapixel camera. Pan-STARRS1 (PS1), the basis for Data Release 1 (DR1), covers three-quarters of the sky (3π survey) north of a decl. of -30°.

Star/galaxy separation of PS1 is similar to that of SDSS. Specifically, the difference between model and PSF magnitude is measured to identify extended objects. However, instead of applying a simple straight line as a cut (e.g., $\mathrm{Mag_{PSF}} - \mathrm{Mag_{Kron}} > 0.05$ where $\mathrm{Mag_{Kron}}$ is Kron magnitudes as the representation for model magnitude), an exponential model is used to fit the bright part of Fig. 3-3 and then extrapolated to fainter objects, similar to [70]. Further details about this technique can be found in [110].

As shown in Fig. 3-3, the star-galaxy separation is not a horizontal cut, but an exponential curve which takes into account our inability to distinguish between stars and galaxies at the fainter end. We require the cut to be satisfied for both r and i bands. Even though this star-galaxy-separation criterion could identify more objects as galaxies, this should not create a large bias for our cluster-finding algorithm. We chose Kron magnitudes as the Pan-STARRS magnitudes for our algorithm since they capture more light from the extended parts of galaxies than PSF magnitudes.

3.2.2.3 Magellan Telescope with PISCO

Without a more robust all-sky survey in the southern sky similar to SDSS and Pan-STARRS in the north, we perform 150 individual follow-up observations for targets in

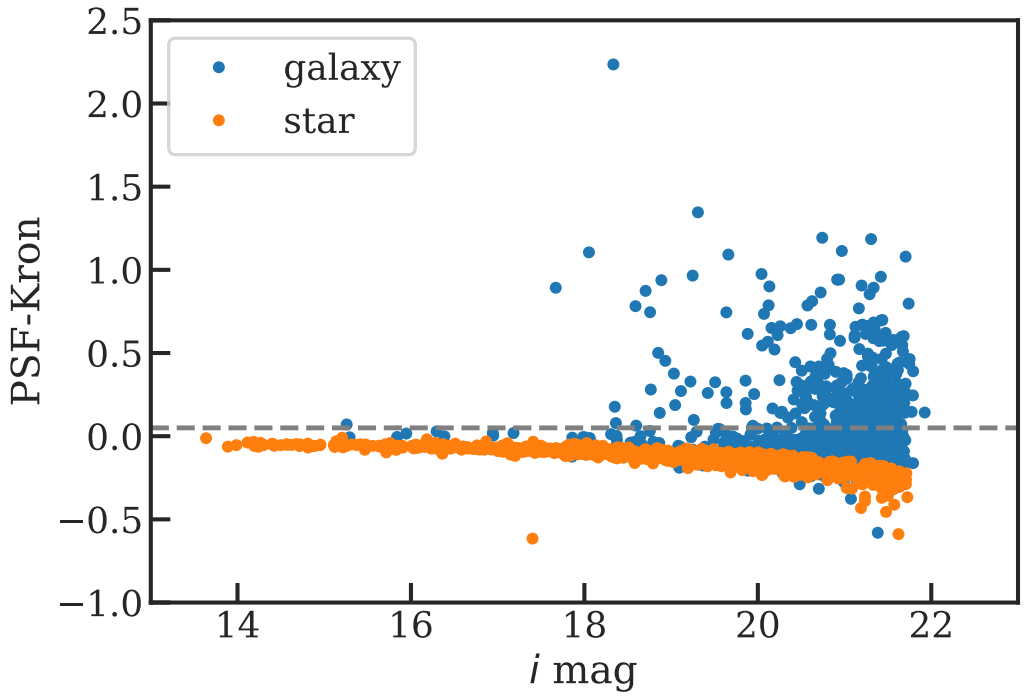

Figure 3-3 This figure demonstrates how we separate stars and galaxies in the Pan-STARRS sample catalog using the ratio of PSF and Kron magnitudes. The orange color indicates stars that pass both the r- and i-band cuts while the blue color marks galaxies.

the southern sky with the 6.5 m Magellan telescope. PISCO, a multiband photometer, is used to speed up our observations because of our large number of candidates. With the ability to produce g-, r-, i-, and z-band images simultaneously, our effective efficiency in observing these candidates increases by a factor of $\sim$3 [including optical losses; 298]. All candidates were acquired with PISCO during nine nights split over three observing runs between 2017 January and 2017 December. We observed most objects with 5 minute total exposure with two 2.5 minute exposures for dithering. To analyze the PISCO data, we have created a data processing pipeline. Further details regarding data reduction and star/galaxy separation for the CHiPS survey are presented in the next section.

3.2.3 X-Ray Follow-up Observations

To confirm the existence of a galaxy cluster, we require the detection of extended X-ray emission, indicating an extremely hot intracluster medium (ICM) that reflects the deep potential well of the cluster. The Chandra X-ray Observatory is best suited for the task, given that our targets may have bright central point sources. With an angular resolution of $0.''5$, Chandra has the capability to distinguish X-ray point sources (e.g., AGNs) from the extended emission of the ICM. We observed a total of five additional candidates from the CHiPS survey, apart from the initial sample of four candidates for the pilot study [292]. More details about the reduction process for the X-ray data can be found in Section 3.5.

3.3 PISCO Observations and Data Processing

In this section, we describe the data reduction process for the PISCO data. Since we obtain raw images from the PISCO instrument on the Magellan telescope, we developed a complete reduction pipeline to convert these images to photometric catalogs for all galaxies in the field, which are then used as an input for our cluster-finding algorithm. In contrast, SDSS and Pan-STARRS are wide-field surveys with available photometric catalogs, and as such they do not require any further data processing.

3.3.1 PISCO Image Reduction

PISCO is a photometer that produces g-, r-, i-, and z-band images simultaneously [298]. The camera is composed of four 3k×4k charge-coupled devices (CCDs), one for each of the four focal planes, with an unbinned scale of $0.''109$ per pixel, resulting in a $5' \times 9'$ field of view. Each CCD is read out with two amplifiers.

For each image, the data reduction process consists of several steps, as follows. First, the median of all bias frames for each night is subtracted from both the median of all flat frames and the science frames. We do not attempt to quantify and remove the dark current because it is negligible in these devices. The ratio between the two

subtracted frames (flat and science) is the flat-fielded image. The two flat-fielded images (one from each amplifier) of a CCD are stitched together to create a complete image for each band (g, r, i, and z) and each exposure. L.A. Cosmic is run on each image for robust cosmic-rays detection and removal [317]. Astrometric calibration is carried out via Astrometry.net,[4] which is used to find the absolute pointing, plate scale, orientation, and additional distortions in each image [174].

Multiple exposures need to be coadded to create a final, stacked image in each band. First, an initial source detection is run on all science images using `SExtractor` [26]. Objects that are corrupted or truncated are removed from the lists by requiring the `FLAGS` parameter to be less than 5. Next, `SCAMP` [27] is run over all of the images simultaneously to improve the astrometric solutions, previously obtained from Astrometry.net. The reference catalog we used for the astrometry is linked to the 2MASS catalog [289]. The individual images of each band are then resampled and coadded via `SWarp` [24]. An example of the final processed image is shown in Fig. 3-4.

3.3.2 Seeing Estimation and PSF Models

Even though each image already has an estimated seeing from the on-site seeing monitor, a more precise value is required for source extraction. We achieve this by fitting the PSF models to every object in the field and picking the most common PSF to represent the seeing of that particular field. Specifically, we create 45×45 pixel small subimage ("vignettes") for each detected object by using `SExtractor`. These small vignettes are fit using the 2D Moffat model, available in the Astropy model packages [11]. The Moffat model is a probability distribution that more accurately represents PSFs with broader wings than a simple Gaussian. We quote seeing measurements as the FWHM of the best-fit model. Fig. 3-5 shows the seeing distribution for objected observed with the PISCO camera. The median values of seeing in g, r, i, and z bands are $1.''28$, $1.''15$, $1.''14$, and $1.''03$ respectively, meaning that the PSF tends to be broader for bluer bands, as expected. For one two-night run on PISCO, the r-band data had a slightly worse (20% larger) PSF due to alignment issues within

[4] http://astrometry.net

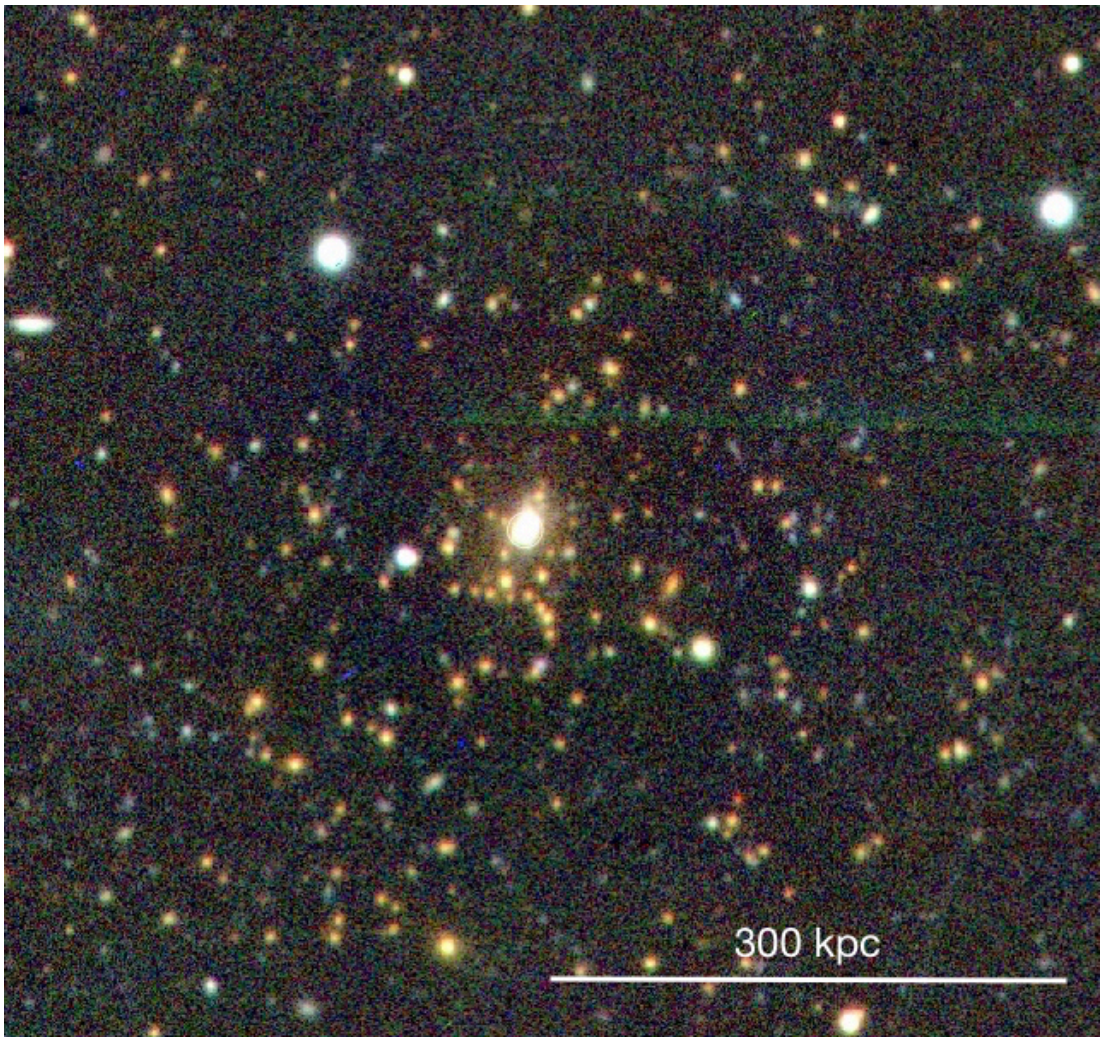

Figure 3-4 Three-color (g, r, i) image of the Phoenix cluster from PISCO. The image shows several red galaxies centrally located in the field, which is the signature of a galaxy cluster. The extremely bright point source in the center is one reason why the Phoenix cluster had been missed from previous X-ray surveys.

the instrument. Given that this enlarged PSF is still smaller than that of the SDSS or Pan-STARRS data, we do not expect this to limit our analysis. The seeing distributions are not symmetric, but highly skewed toward higher seeing, representing a variation in the weather at the time of observation.

Apart from an accurate seeing estimate, the PSF model is also required for `SExtractor` to measure MAG_PSF. We use `PSFEx` to extract the PSF models from FITS images [25], setting all parameters to default. To get a good model for the PSF,

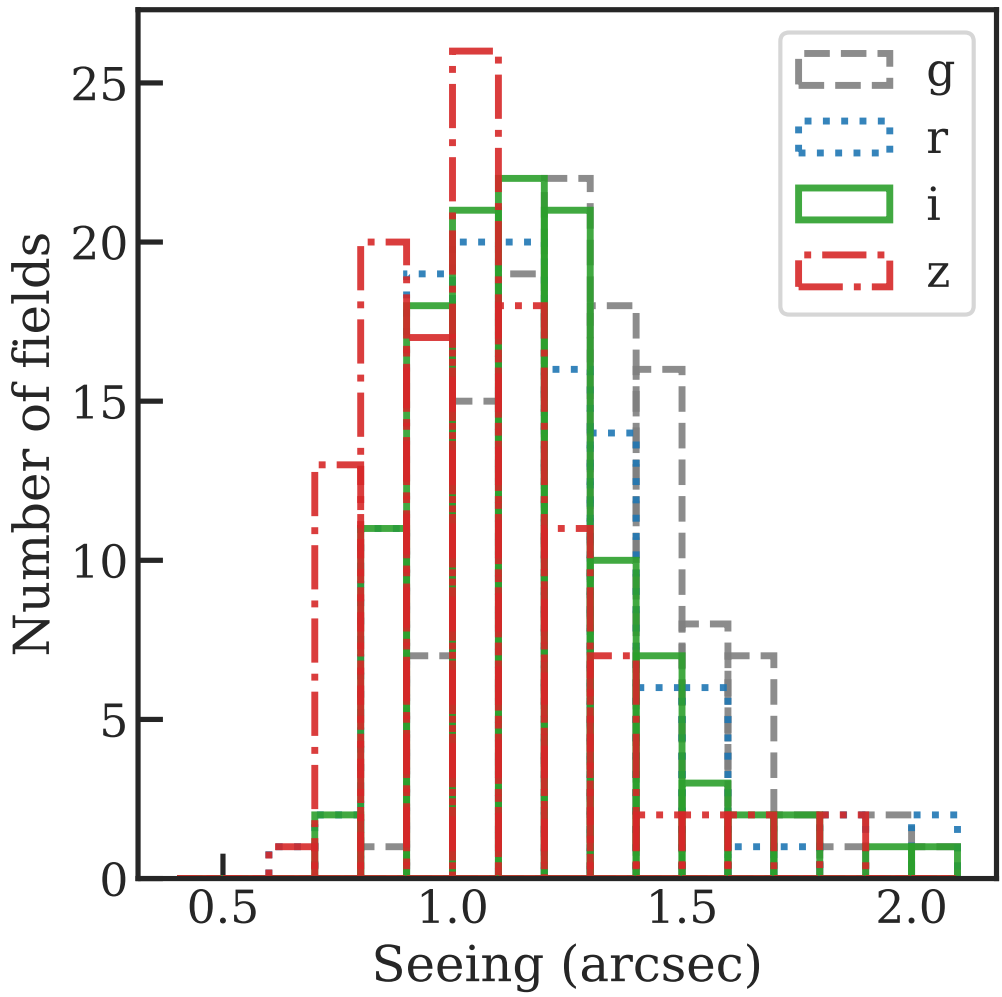

Figure 3-5 Seeing distribution for the 262 fields observed with PISCO. The g band is traced by black dashed lines, the r band is traced by blue dotted lines, the i band is traced by green solid lines, and the z band is traced by red dotted-dashed lines. The median values of the seeing in g, r, i, z bands are 1.″28, 1.″15, 1.″14, 1.″03 respectively.

we need to select only well-behaved point sources (stars) as our model. We achieve this by selecting sources that are not at the edges of the CCD, not elongated, and have an effective flux radius within 2σ of the mean for all sources in the field.

Table 3.1 `SExtractor` Source Detection Input Parameters

Parameter	Value
DETECT_MINAREA	$1.1\pi \times (i-\text{band seeing})^2$
DETECT_THRESH	1.2
GAIN	0.25
PIXEL_SCALE[a]	0.12 or 0.22
SATUR_LEVEL	61,000

[a]Depending on whether the data are binned.

3.3.3 Source Extraction

To measure an accurate color for each object, we extracted photometry via the dual-image mode of `SExtractor`, which uses the same pixel location for all photometric bands. The seeing estimates and the PSF models are used in this step with other input parameters described in Table 3.1. Next, we extract *griz* MAG_AUTO, MAG_APER, and MAG_PSF at the location of detected sources from the i-band image.

3.3.4 Star–Galaxy Separation

One of the most important steps for the reduction pipeline is to separate sources into stars and galaxies. While CLASS_STAR[5] is often used for this purpose, upon our close investigation we found non-negligible contamination in both the star and galaxy samples. Instead, we use the SPREAD_MODEL parameter (from `SExtractor`), which indicates whether the source is better fit by the PSF model or a more extended model [227]. By design, SPREAD_MODEL is close to zero for point sources and positive for extended sources. This estimator has been used in several surveys, e.g., the Blanco Cosmology Survey (BCS) [87] and the Dynamical Analysis of Nearby Clusters (DANCe) survey [47]. In particular, we separate stars and galaxies by the

[5]https : //sextractor.readthedocs.io/en/latest/ClassStar.html

following criterion:

$$\begin{aligned} galaxies &: \text{SPREAD\_MODEL\_I} > 0.005 \\ &\quad \& \, \text{MAG\_i} < 17.5 \\ stars &: \text{SPREAD\_MODEL\_I} < 0.004, \end{aligned} \tag{3.1}$$

where MAG_i is the magnitude of the object in the i band. This criterion is adapted from Sevilla-Noarbe et al. [279], providing a better separation between stars and galaxies than CLASS_STAR because we take into account the PSF variation in the calculation. The exact values of the thresholds are not extremely important since we will later estimate the photometric redshfit ($z_{\rm phot}$) for each object, as shown in Section 3.4.1. If an object is wrongly identified as a galaxy, we will not obtain a good fit for $z_{\rm phot}$ and the object will be removed from the cluster-finding algorithm. More details and different tests to quantify the performance of this star–galaxy statistic can be found in Sevilla-Noarbe et al. [279].

3.3.5 Photometric Calibration

To calibrate the color and the magnitudes of stars and galaxies, we use stellar locus regression [SLR; 143]. SLR adjusts the instrumental colors of stars and galaxies and simultaneously solves for all unknown zero-points by matching them to a universal stellar color-color locus and the known 2MASS catalog. The calibration takes into account difference in instrumental response, atmospheric transparency, and Galactic extinction. SLR has been used to calibrate photometry for various surveys including South Pole Telescope follow-up [142] and the BCS [36]. The specific implementation of the algorithm that we utilize here is described in Kelly et al. [161].

For each frame, we use the stellar sources identified in Section 3.3.4 as the starting point. We then perform the stellar locus regression, which simultaneously calibrates all optical colors onto the SDSS system. The absolute flux scaling (or zero-point) is then constrained via the optical–infrared colors from SLR, combined with the 2MASS point-source catalog [289].

3.3.6 Photometric Verification

We perform a comparison test to check the accuracy of the photometric calibration. The test is carried out by comparing between the colors ($g-r$, $r-i$, and $i-z$) we obtained from the PISCO pipeline and the SDSS colors. To enable this verification, we observed three fields in our SDSS target list with PISCO, reducing the data using the same PISCO pipeline that we have described above. Galaxies found in the SDSS catalog are matched with objects in our observed PISCO frames based on their celestial coordinates. The objects are plotted in Fig. 3-6, showing the offsets between the colors from PISCO and from SDSS. The scatter (σ) of the PISCO colors compared to the SDSS colors is around 0.08–0.14 mag for brighter objects ($16 < i_{\rm PISCO} < 20$), which is as accurate as the calibration between SDSS and Pan-STARRS [70].

3.4 Cluster-finding Algorithm

In this section, we describe the new cluster-finding algorithm. Because of the nature of our survey, which looks for cluster candidates surrounding X-ray/IR/radio sources, we already have the central location of the cluster, which we assume to be the location of the X-ray/IR/radio source. This means that unlike some optical cluster-finding surveys, we do not use a friend-of-friend algorithm [155] to search for the center of the cluster. Instead, we look for an overdensity of galaxies with similar redshifts at the location of the X-ray source.

Specifically, we search for a peak in the redshift histogram of all the galaxies within the observed fields. Members of a galaxy cluster will have similar redshifts, meaning that finding the peak in the redshift histogram will differentiate between cluster members and field galaxies. The peak location corresponds to the redshift of the galaxy cluster.

The algorithm is divided into three parts: photometric redshift measurement, aperture selection and background subtraction, and richness correction for high-redshift clusters.

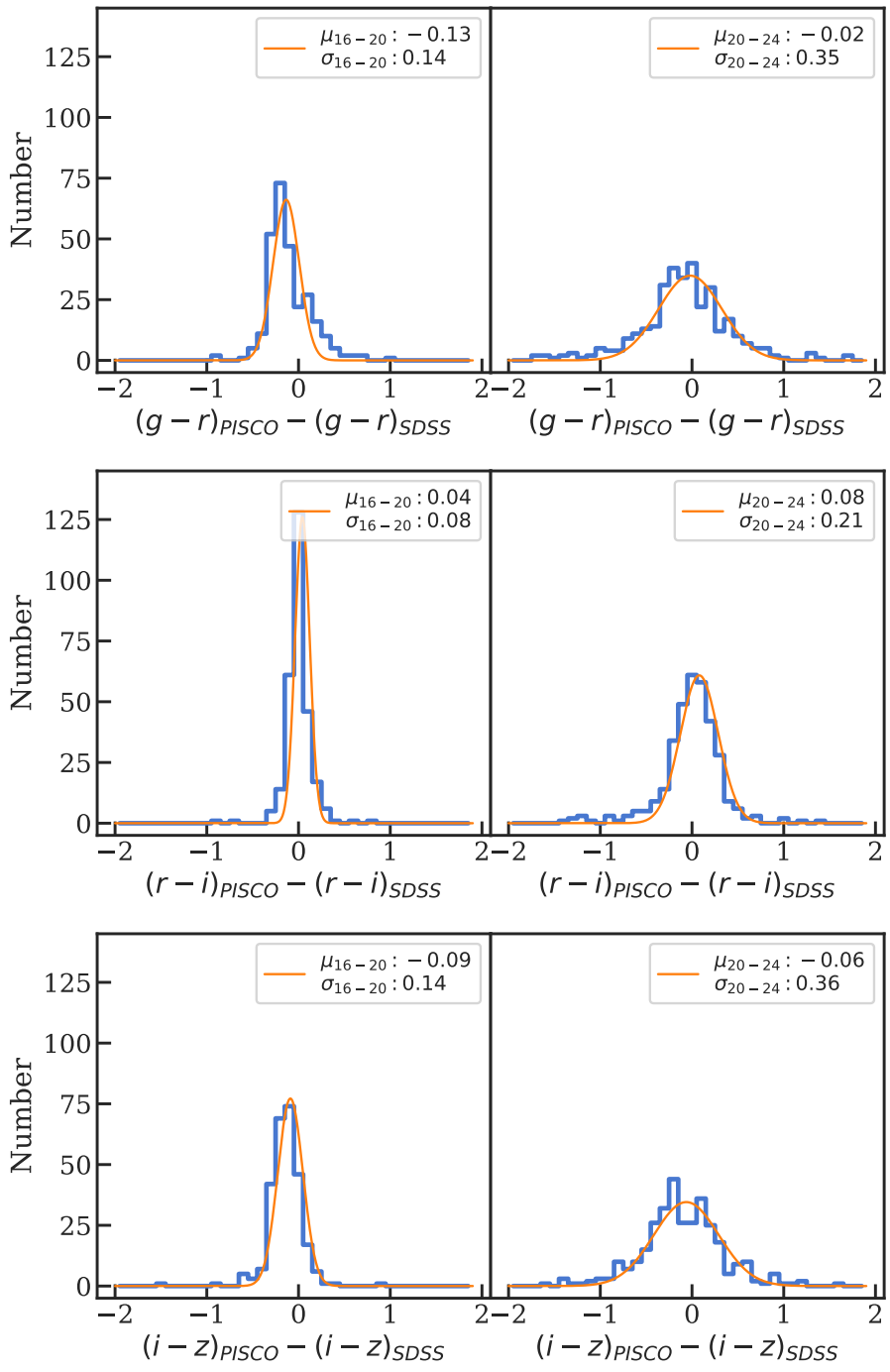

Figure 3-6 The top two panels show a comparison of $g - r$ between PISCO PSF magnitude and SDSS PSF magnitude while the middle two show a comparison of $r - i$ and the bottom two show a comparison of $i - z$. The left panels corresponds to bright objects ($16 < i_{\rm PISCO} < 20$) while the right panels corresponds to fainter ones ($20 < i_{\rm PISCO} < 24$). The orange lines are the gaussian best-fit model with its mean and its standard deviation in the legend. This demonstrates that for bright objects the scatter of the PISCO calibration from the SDSS is about 0.10–0.14 mag.

3.4.1 Photometric Redshift

The first step of the algorithm is to estimate photometric redshifts of all galaxies in the field. Mid-IR data are included in this step to improve constraints. The sections below describes data acquisition for mid-IR bands from the WISE [337], and the software used for photometric redshift estimates.

3.4.1.1 Wide-field Infrared Survey Explorer

WISE is an IR satellite with four IR filters: $W1$ (3.6 μm), $W2$ (4.3 μm), $W3$ (12 μm), and $W4$ (22 μm). We select galaxies in the AllWISE Source Catalog, using IRSA's Simple Cone Search (SCS),[6] and match them with their optical counterparts from SDSS, Pan-STARRS, or PISCO within a radius of 3". However, because the FWHM for $W1$ and $W2$ is rather large (~ 6", compared to ~ 1" for optical data[7]), we cannot separate different optical galaxies from the WISE sources, especially at the center of the cluster, where large number of objects are presented in a small region. Thus, we only use the WISE measurement from both $W1$ and $W2$ as upper limits to help constrain the photometric redshifts.

3.4.1.2 Photometric Redshift Estimate

Each galaxy's photometric redshift ($z_{\rm phot}$) is determined by fitting the photometry in optical and mid-IR bands to the template spectral energy distribution (SED) using the Bayesian Photometric Redshifts (BPZ) code [21, 76]. The BPZ code uses Bayesian inference and priors to estimate photometric redshifts using multiwavelength broad-band data. We used the default templates, consisting of one early-type, two late-type, and one irregular-type templates from Coleman et al. [77] and two starburst templates from Kinney et al. [164]. We also added WISE filters for $W1$ and $W2$ bands. Since there is no response filter for the PISCO optical bands, we convert the photometry from PISCO to SDSS bands and use SDSS response filters instead. Specifically, we

[6] https://irsa.ipac.caltech.edu/docs/vo_scs.html

[7] http://wise2.ipac.caltech.edu/docs/release/allsky/expsup/sec4_4c.html

convert the photometry to the SDSS system by fitting a linear function of the form $(g-r)_{\rm SDSS} = A + B(g-r)_{\rm PISCO}$, and likewise for $r-i$ and $i-z$ colors. This amounts to removing the offset shown in Fig. 3-6. We apply these corrections to all of the PISCO bands to shift them to the SDSS system. We do not expect the difference in the response filter to have a large impact on the final redshift since PISCO filters are designed to be as similar to the SDSS filters as possible.

3.4.1.3 Redshift Verification

To verify our photometric redshifts, we compare 612 redshifts from the BPZ algorithm to those publicly available from SDSS3 [3]. In Fig. 3-7, we show the comparison of BPZ redshifts to those from SDSS3, measuring $\sigma_z/(1+z) \sim 0.05$. The median offset between BPZ and SDSS3 redshifts is ~ 0.03, which is also less than our typical per-galaxy photometric redshift uncertainty. Utilizing six previously known clusters that were identified in our sample (see Section 3.6.1), we also find a scatter between our cluster redshifts and the published values of $\sigma_z/(1+z) \sim 0.012$. Given this overall agreement, we proceed with BPZ redshifts for the full sample.

3.4.2 Aperture Selection and Redshift Histogram

In terms of aperture selection, we choose a simple top-hat model with a radius of one arcminute. This allows us to make a more simple correction for the richness value, as discussed in Section 3.4.3. Next, we create a histogram representing the redshift distribution of all the galaxies in the selected aperture. Since the peak value includes the background level of field galaxies, we estimate the background distribution by making a redshift histogram of field galaxies in all images of each instrument (SDSS, Pan-STARRS, and PISCO). There are $\sim 22,000$ background galaxies for Pan-STARRS and PISCO, and $\sim 27,000$ galaxies for SDSS. We normalized the background histogram for each observation by scaling the total number of objects in the background histogram to be the same as in the histogram of interest and subtract from it.

Fig. 3-8 shows the limiting magnitude for each observation, which demonstrates

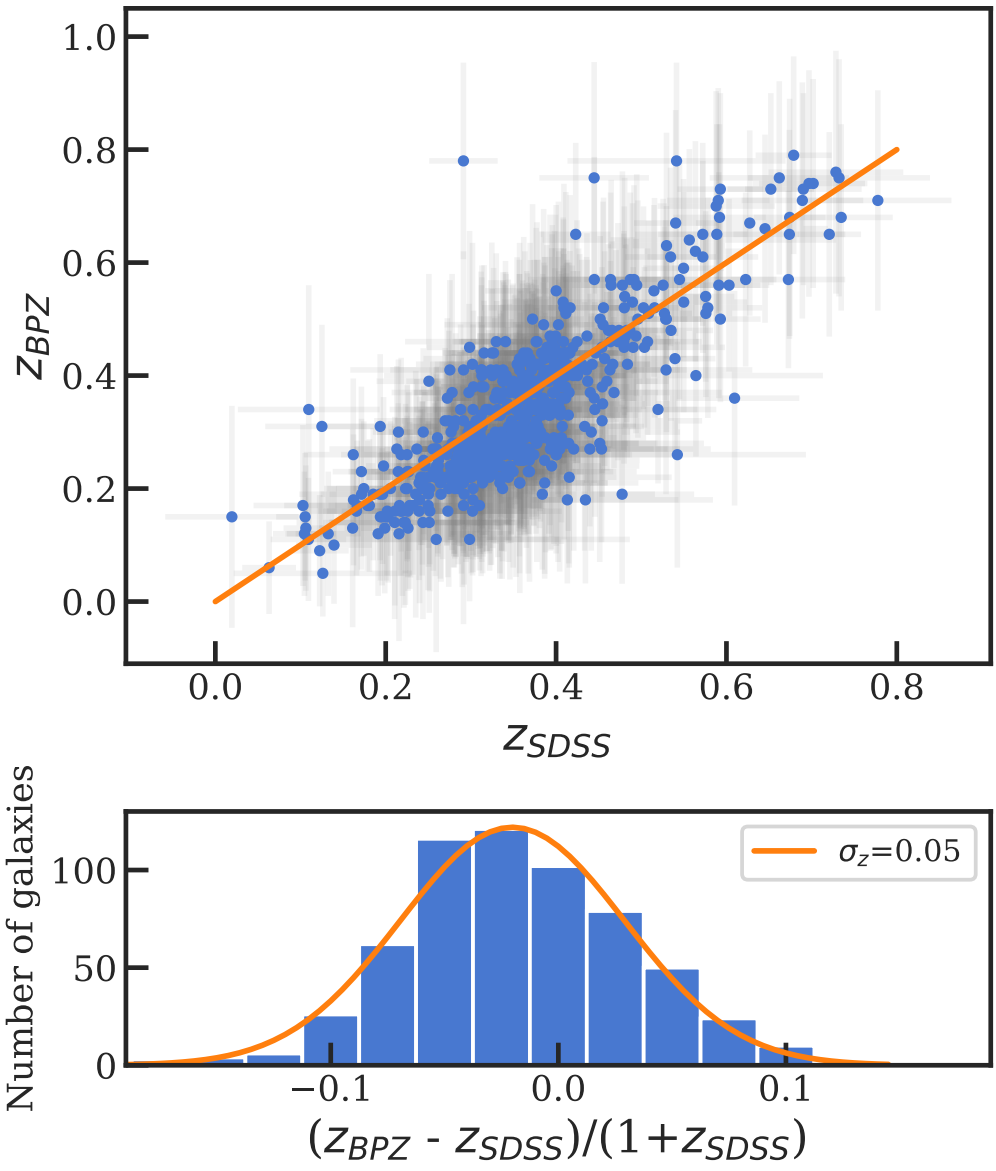

Figure 3-7 Comparison between the BPZ redshifts and published photometric redshifts from SDSS3. Most of the objects are in an agreement between the two, with a relative scatter of $\sim$5%.

that the depth of each survey is quite uniform. The detailed calculation for the limiting magnitude is presented in Section 3.4.3. For PISCO, we made sure that every observation has the same exposure time of 5 minutes. This uniformity allows us to construct the background for each instrument without large variations in limiting magnitude.

The top panel of Fig. 3-9 shows both the redshift distribution of all the galaxies (in blue) and the normalized distribution of background galaxies (in orange). The background-subtracted histogram is then used to search for a redshift peak, as shown in the bottom panel of Fig. 3-9. Since the redshifts estimated from the BPZ code have some uncertainty, we fit a fixed-width Gaussian to the peak and the two neighboring bins to get an estimate for the richness (the amplitude of the Gaussian) and the final redshift (the location of the Gaussian).

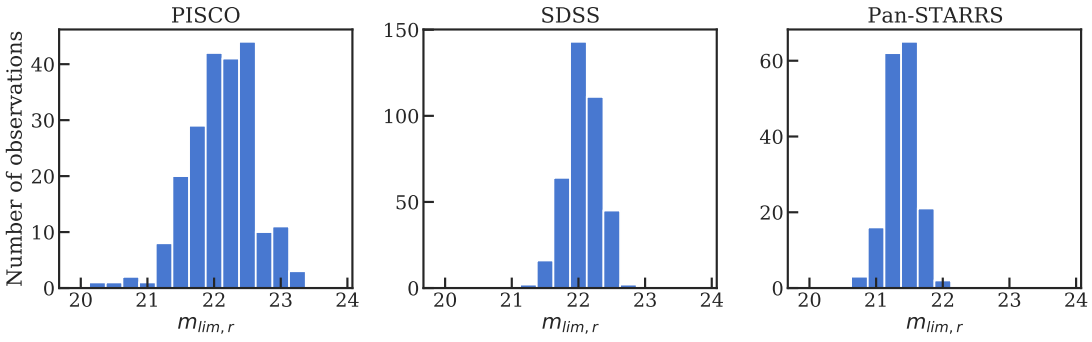

Figure 3-8 Distributions of limiting magnitude for the three telescopes (PISCO, SDSS, and Pan-STARRS, respectively). This figure shows that the magnitude limit for each telescope is fairly uniform. PISCO has significantly more scatter than SDSS and Pan-STARRS, which are wide-field surveys.

3.4.3 Richness Correction

Because observations were made from different optical telescopes, and galaxy clusters are located at different redshifts, a correction to the measured richness is necessary to have a uniform proxy for cluster mass across all fields and all redshifts. The two effects we have taken into account are the luminosity function of galaxies and the

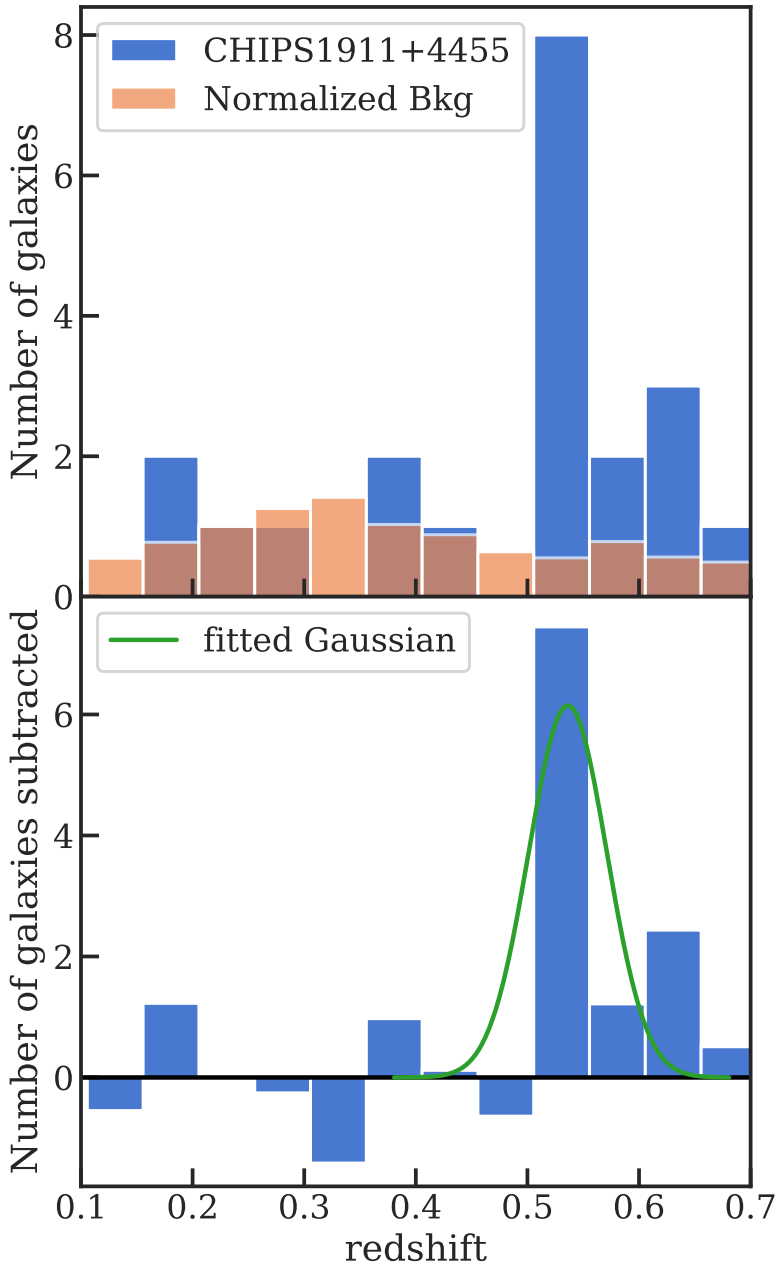

Figure 3-9 Top: the blue histogram shows the redshift distribution of all the galaxies within one arcminute of CHIPS 1911+4455. The orange histogram shows the the renormalized distribution of background galaxies. Bottom: the background-subtracted histogram is shown in blue. The green solid line shows the fixed-width Gaussian fit between the peak and the two neighboring bins to estimate the richness. The significance of the redshift peak at $z = 0.53$ strongly suggests the presence of a galaxy cluster.

evolving angular size of galaxy clusters on the sky. We check both effects and find that the correction for luminosity function is larger than that for angular diameter by a factor of ∼50–1000, depending on the redshift, so we only consider the luminosity correction.

Extremely bright objects tend to be rare, compared to fainter objects, implying that cluster candidates at higher redshift will have fewer observable members since the majority of them will be too faint to detect with our current instruments. This correction is used to remedy the galaxy counts to account for galaxies that are below detection limits. The luminosity function ($L(M)$) we used comes from Wen and Han [333] and combines the Schechter function ($\phi_s(M)$) [276] and the composite luminosity function of the BCGs ($\phi_g(M)$):

$$\begin{aligned} L(M) =& \phi_s(M) + \phi_g(M) \\ =& 0.4 \ln(10) \phi_* 10^{-0.4(M-M_*)(\alpha+1)} \\ & \exp\left[-10^{-0.4(M-M_*)}\right] \\ & + \frac{\phi_0}{\sqrt{2\pi\sigma}} \exp\left[-\frac{(M-M_0)^2}{2\sigma^2}\right] dM, \end{aligned}$$

where α is the faint-end slope, M_* and M_0 are the characteristic absolute magnitudes, and ϕ_* and ϕ_0 are the normalization factors. Another effect related to the luminosity function comes from variability in the depth of the survey in different fields/telescopes. Specifically, SDSS is deeper (fainter limiting magnitude) than Pan-STARRS, whereas, PISCO has a large variation within itself, which comes from the variation in the weather conditions when we observed these objects. We estimate the limiting magnitude for each observation by fitting two Gaussians to the brightness distribution and using the location of the fainter peak to represent the limiting magnitude. The purpose of the double Gaussian fit is to capture the skewness in the brightness distribution, which varies from field to field.

Fig. 3-10 illustrates the richness correction at different redshifts and limiting magnitudes ($M_{\rm lim}$). The correction is strongest when we consider high-redshift objects

with bright limiting magnitudes. The richness is calculated using

$$\text{Richness} = N_{\text{obs}} \frac{\int_{-\infty}^{M_{\text{deep}}} L(M)dM}{\int_{-\infty}^{M_{\text{lim}}} L(M)dM}, \tag{3.2}$$

where N_{obs} is the number of galaxies found from the survey, M_{deep} is the limiting absolute magnitude of our deepest field ($M_{\text{deep}} = -15.3$, which is equivalent to an apparent magnitude of 23 at $z = 0.1$), and M_{lim} is the absolute magnitude limit of each field based on our measured limiting apparent magnitude and redshift. The typical correction is roughly 1–5.

3.4.4 Flux-limited Nature of Previous Surveys

The CHiPS survey is designed to look for misidentified galaxy clusters in surveys based on data from the ROSAT telescope. One such survey, the ROSAT–ESO Flux-Limited X-ray (REFLEX) Galaxy Cluster Survey [42], contains 447 galaxy clusters above an X-ray flux of $\sim 3 \times 10^{37}\,\text{erg}\,\text{s}^{-1}\,\text{Mpc}^{-2}$ (0.1-2.4 keV), which are all spectroscopically confirmed. The left panel of Fig. 3-11 shows all 447 clusters in the REFLEX sample on a plot of X-ray luminosity (L_{x}) versus redshift, with the blue line showing the constant flux limit of the REFLEX sample. It is assumed that this survey has found all of the galaxy clusters with luminosities above this limit.

However, some of the X-ray-bright point sources detected by ROSAT are believed to be misidentified massive clusters with extreme central galaxies. One of our goals is to find clusters that exceed the REFLEX flux limit but that are classified as point sources. Since obtaining new optical data is more straightforward to obtain than X-ray, we convert this REFLEX flux limit to an optical richness limit, which can then be used for our richness cut, as described in Section 3.6.

In order to convert this X-ray flux limit to a richness limit, the optical richness of this sample is required. First, we cross-correlate the REFLEX clusters and SDSS survey, finding 82 clusters that are in both. By running the same cluster-finding algorithm as described in this section, we estimate the richness of all 82 REFLEX clusters. Since both the richness and X-ray luminosity are correlated with the total

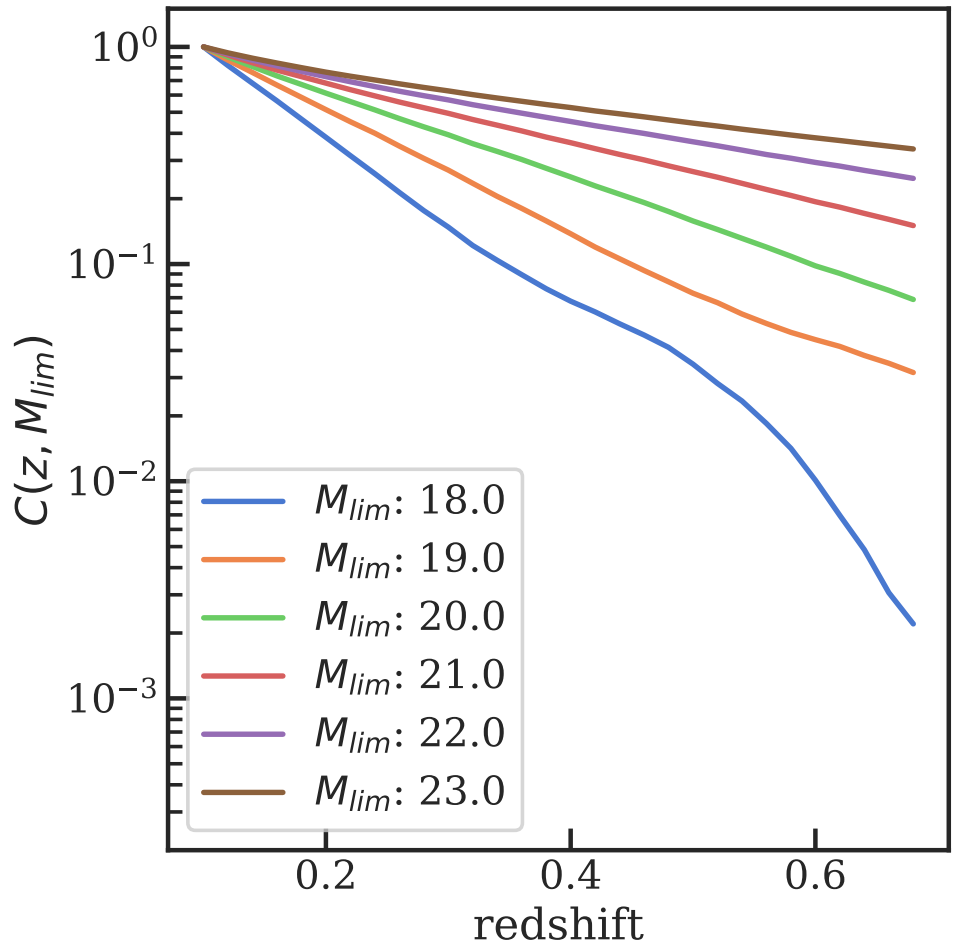

Figure 3-10 Richness correction as a function of redshift and limiting magnitude ($M_{\rm lim}$) due to the luminosity function of galaxies where there are fewer bright massive galaxies than faint smaller ones. Specifically, $R_{\rm true} = \frac{R_{\rm obs}}{C(z,M_{\rm lim})}$, where $R_{\rm true/obs}$ is the corrected/measured richness and $C(z, M_{\rm lim})$ is the richness correction.

mass of the clusters, we fit a straight line to the log–log plot, as shown in the middle panel of Fig. 3-11, to find the relation between the flux limit and the richness limit. For the small number of clusters here, and not accounting for selection effects, we measure an intrinsic scatter between richness and X-ray luminosity $\sigma_{ln\lambda|M} = 0.33 \pm 0.07$, compared to $\sigma_{ln\lambda|M} \sim 0.46$ from a sample of SDSS redMapper clusters [232]. The last panel of Fig. 3-11 shows the X-ray flux limit projected onto the richness–redshift plot, via the relationship between richness and X-ray luminosity. Assuming that all clusters

follow the same richness–luminosity relation, those systems that lie above this line should have been discovered by the REFLEX survey. In reality, there is significant scatter in the richness–luminosity relation, and those clusters that scatter high in richness at low X-ray luminosity would have been rightfully missed (for example, CHIPS 2155-3727).

3.5 X-Ray Data Reduction

In addition to the optical survey, we performed X-ray follow-up of nine promising candidates with Chandra. Three of them are shown in this work. Four candidates were followed up in Chandra Cycle 16 based on an earlier version of our selection [292], which yielded the re-observation of a lesser-known cluster, two systems that turned out to be isolated point sources, and CHIPS 1356-3421. In Cycle 20, we followed up an additional five candidates, which yielded the detection of CHIPS 1911+4455. Both of these follow-up campaigns were based on preliminary catalogs and thus had an inflated false-positive rate. In this section, we describe the X-ray data reduction process to estimate the total mass and luminosity of these clusters. A more detailed analysis with these data is described in Somboonpanyakul et al. [292].

All CHiPS candidates were observed with Chandra ACIS-I for 30–40 ks each. The data were analyzed with CIAO [116] version 4.11 and CALDB version 4.8.5, provided by Chandra X-ray Center (CXC). The event data were recalibrated with VFAINT mode, and point sources, which are not in the center, were excluded with the *wavdetect* function. The image was produced by applying *csmooth*, which adaptively smoothed an image with maximal smoothing scale of 15 pixels and signal-to-noise (S/N) ratio between 2.5 and 3.5.

High-angular-resolution X-ray images can be used to estimate different properties of the cluster, including the mass and total luminosity. We choose M_{500}, the total mass within R_{500}, the radius within which the average enclosed density is 500 times the critical density ($\rho_c = 3H_0^2/8\pi G$), to represent the total cluster mass. We use scaling relations from Vikhlinin et al. [321] iteratively to estimate R_{500}, which is then

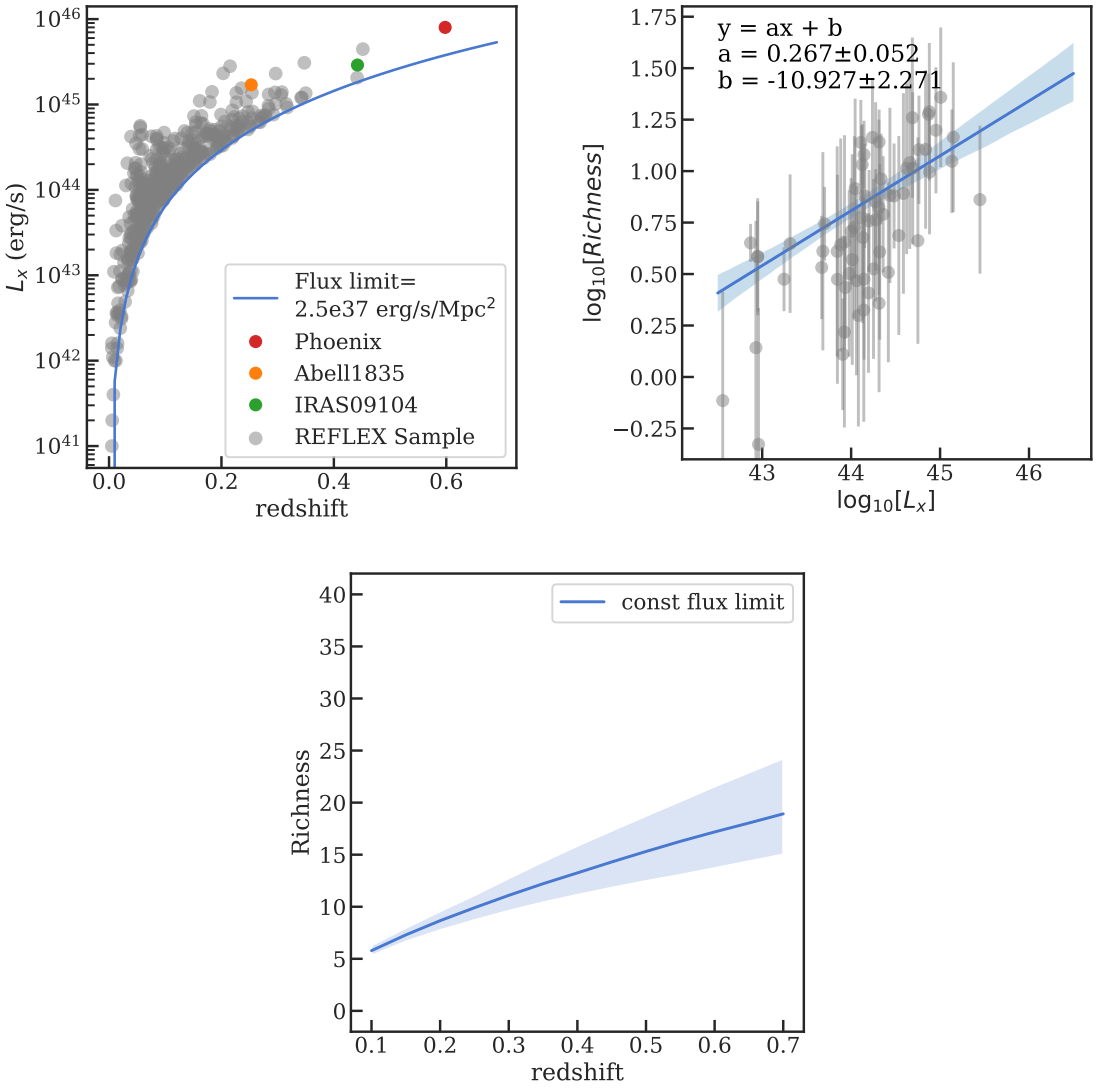

Figure 3-11 Left: the plot of luminosity v.s. redshift for all of the REFLEX clusters with SDSS data. The plot demonstrates the flux-limited nature of the REFLEX survey. The blue line shows the flux limit $= 2.5 \times 10^{37} \mathrm{erg\,s^{-1}\,Mpc^{-2}}$. The colored dots show three well-known clusters that should have been detected with the ROSAT catalog. Middle: this plot shows a power-law relationship between the luminosity from REFLEX clusters and the measured richness from this work. Right: plot of richness v.s. redshift with constant flux limit. Assuming the luminosity–richness relation from the middle panel, X-ray-selected clusters from the REFLEX catalog should have richnesses that lie above this line.

used to measure T_{x}, M_g, and M_{500}. Specifically to estimate M_{500}, we use the scaling

relation with $Y_{\rm x} = M_g \times T_{\rm x}$

$$M_{500} = (5.77 \pm 0.20) \times 10^{14} h^{0.5} M_{\odot} \times \left(\frac{Y_{\rm x}}{3 \times 10^{14} M_{\odot}} \right)^{0.57 \pm 0.03} E(z)^{-2/5}.$$

$Y_{\rm x}$ is chosen as a mass proxy because of its low scatter and insensitivity to the dynamical state of the cluster [170, 197]. More details about the method to estimate M_{500} can be found in Andersson et al. [7].

In addition to mass, we measure the total X-ray luminosity of each cluster. We first extract an X-ray spectrum of all emission within R_{500}, centered on the X-ray peak, and then we fit this spectrum using a combination of collisionally ionized plasma (`APEC`) and Galactic absorption (`PHABS`). This allows us to estimate the unabsorbed X-ray flux, which we then convert to a rest-frame luminosity given the known redshift.

3.6 Results

From Fig. 3-12, we identify 11 cluster candidates by selecting all objects above the solid blue line, which is the richness limit derived in Section 3.4.4. The objects below this line are not necessarily all isolated AGNs. They may belong to less massive clusters that fall below our selection threshold – here we only consider very massive clusters that should have been included in surveys such as REFLEX [42] and MACS [96], but were missed due to the presence of an atypical central galaxy.

Using the NASA Extragalactic Database[8] catalog, we search for known clusters within a $3'$ radius of the 11 candidates and report, when available, the redshift of known clusters. In Table 3.2, we present all 11 candidates with their celestial coordinates, richness, measured redshifts, instruments used to detect, and known clusters associated with each system.

[8] https://ned.ipac.caltech.edu

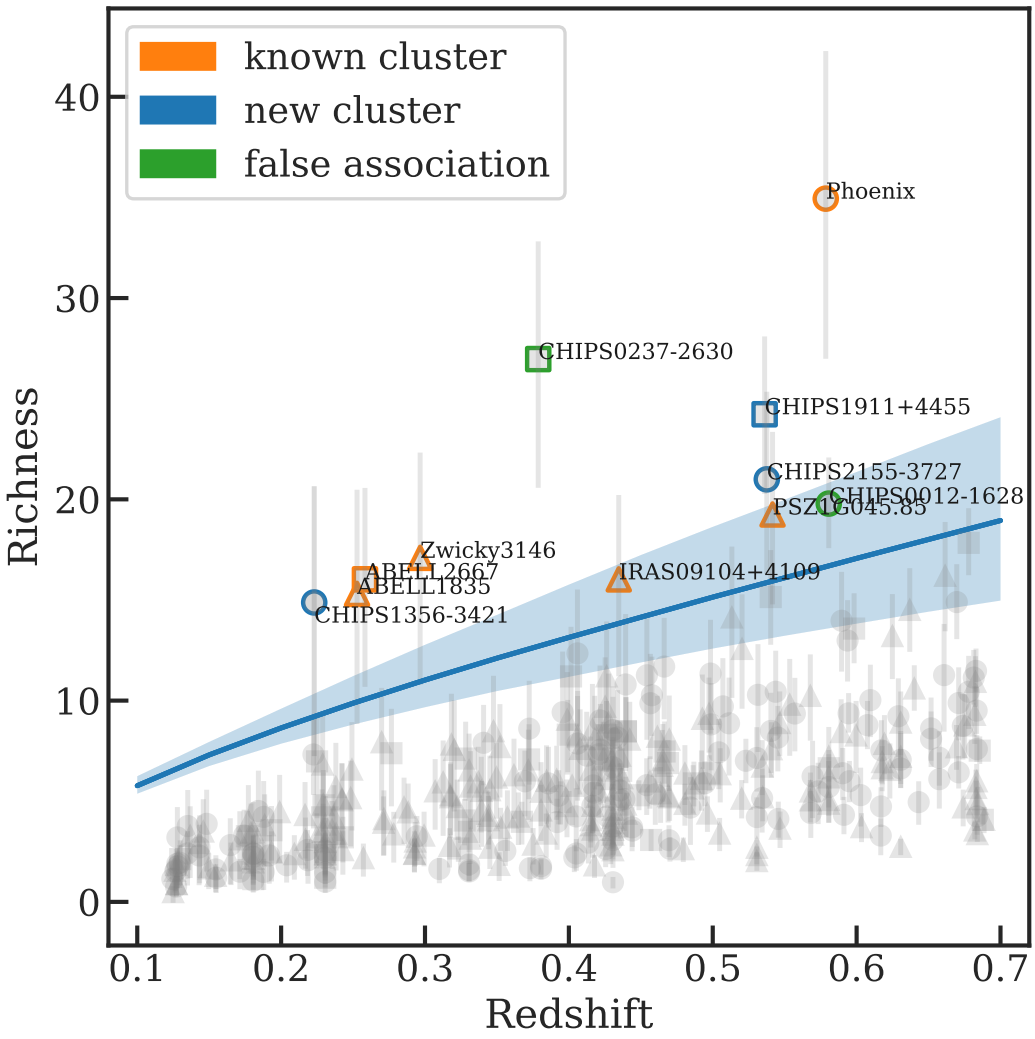

Figure 3-12 Richness v.s. redshift for all CHiPS candidates. The blue solid line shows the richness cutoff we used for the survey (see Fig. 3-11). Each object is indicated with either a circle, a square, or a triangle based on its optical follow-up telescopes, which are the Magellan telescope (PISCO), Pan-STARRS, or SDSS, respectively. The orange color indicates known clusters above the richness limit, the green color indicates a false association, and the blue color indicates a new cluster candidates. All three of the latter systems have recently obtained Chandra X-ray follow-up.

Table 3.2 Galaxy Cluster Candidates/Known above the REFLEX Flux-limit Line in the CHiPS Survey

CHiPS Name	R.A.	Decl.	Richness	z[a]	Instruments[b]	Known Cluster	$z_{\rm NED}$[c]	Sep. (arcmin)
CHIPS 2344-4243	356.18375	-42.72208	34.939	0.579	PISCO	Phoenix	0.596	0.388
CHIPS 0237-2630	39.365	-26.5075	26.968	0.379	Pan-STARRS	Abell 0368	0.22	0.395
CHIPS 1911+4455	287.75415	44.92222	24.227	0.536	Pan-STARRS	...	...	...
CHIPS 2155-3727	328.82791	-37.46361	20.993	0.538	PISCO	...	...	...
CHIPS 0012-1628	3.145	-16.46931	19.788	0.581	PISCO	Abell 0011	0.166	3.019
CHIPS 1518+2927	229.58292	29.45889	19.249	0.542	SDSS	PSZ 1G045.85	0.611	0.197
CHIPS 1023+0411	155.91374	4.18819	17.094	0.297	SDSS	Zwicky 3146	0.2805	0.145
CHIPS 2351-2605	357.91959	-26.08403	16.027	0.258	Pan-STARRS	Abell 2667	0.23	0.025
CHIPS 0913+4056	138.44167	40.93903	16.023	0.435	SDSS	IRAS 09104+4109	0.442	0.11
CHIPS 1401+0252	210.25876	2.88042	15.304	0.253	SDSS	Abell 1835	0.2532	0.055
CHIPS 1356-3421	209.023	-34.3531	14.875	0.223	PISCO	...	...	...

[a]These redshifts are photometric redshifts, estimated in Section 3.4.1. We picked a peak of the richness histogram as a cluster redshift. The uncertainty of the redshift is $\sim$0.025, which is half a histogram bin width.
[b]PISCO is the imaging instrument on the Magellan telescope in Chile while SDSS and Pan-STARRS are all-sky optical surveys.
[c]Redshift of the known cluster from the NASA Extragalactic Database.

3.6.1 Known Clusters Rediscovered

We find 6 of 11 cluster candidates to be well-known clusters via the NED catalog. In general, these clusters can be divided into two classes: starburst-hosting clusters, such as A1835 [SFR $\sim$100–180 $M_\odot\,\mathrm{yr}^{-1}$; 217] and Zwicky 3146 [SFR $\sim 70\ M_\odot\,\mathrm{yr}^{-1}$; 99], or AGN-hosting clusters, such as A2667 [260] and IRAS 09104+4109 [83]. Another notable example is the Phoenix cluster [202], which has both a starburst-hosting galaxy and a central AGN.

The list of "rediscovered" clusters includes some of the most interesting and well-known galaxy clusters in the nearby universe. It is an interesting question to ask whether they would have been misidentified by ROSAT as isolated point sources had Abell and Zwicky not performed their optical surveys first. At higher redshift and lower mass, where future surveys like the extended Roentgen Survey with an Imaging Telescope Array (eROSITA) will probe, this issue will likely be exacerbated, requiring multiwavelength surveys combining X-ray and, for example, optical or SZ to fully identify the rich variety of galaxy clusters.

3.6.2 False Associations

There are two galaxy overdensities that we identify in the background of known clusters (CHIPS 0012-1628, CHIPS 0237-2630). In both of these cases, the foreground cluster (A11, A368) harbors a BCG that is bright in the mid-IR and radio, but falls below the richness threshold defined above. At the same time, in both cases, the background overdensity corresponds to a much richer cluster that does *not* harbor an X-ray/IR/radio source at its center. Thus, in these cases, the "extreme BCG" is in the foreground, while the massive, "missed" cluster is in the background. While these systems are interesting in their own right, for a number of reasons, they do not satisfy the selection requirements of this survey.

3.6.3 New Cluster Candidates

The removal of previously known clusters and false associations leaves us with a sample of three cluster candidates, all of which are rich enough that they should have been detected by REFLEX or other similar surveys, assuming no scatter in the richness–$L_{\rm x}$ relation. Fig. 3-13 shows optical images of all three candidates–CHIPS 1356-3421, CHIPS 1911+4455, and CHIPS 2155-3727. The optical images clearly show an overdensity of red galaxies at the location of the X-ray point source, which is at the center of each field. The three candidates look similar to the Phoenix cluster in that their BCG colors are different from those of other red member galaxies, implying an active central galaxy.

We followed up all three candidates with new Chandra observations over the past two years to search for extended ICM emission, which would confirm the presence of a massive cluster. Even though optical detection of an overdensity of red galaxies alone can often be used to claim discovery of new galaxy clusters, lower-richness candidates can be the result of line-of-sight alignment from sheets and filaments of galaxies, which can coincidentally increase the numbers of red galaxies on the plane of the sky.

Fig. 3-14 shows adaptively smoothed Chandra X-ray images of all three candidates. The rightmost panel of the figure shows that CHIPS 2155-3727 has no (or extremely faint) extended X-ray emission, implying that the overdensity of red galaxies we saw in the optical image in Fig. 3-13 is likely a projection effect. The other two panels show extended emissions around bright point sources in the cores. In Table 3.3, we provide a summary of the X-ray properties (R_{500}, M_{500}, and $L_{\rm x}$) for the three cluster candidates, derived from the X-ray images. The first two objects are confirmed massive galaxy clusters, with total cluster masses greater than $3 \times 10^{14}\,M_{\odot}$. With our current dataset, we can only provide upper limits for the mass and total luminosity of a cluster for CHIPS 2155-3727. In the follow subsections, we discuss each of these three systems in further detail.

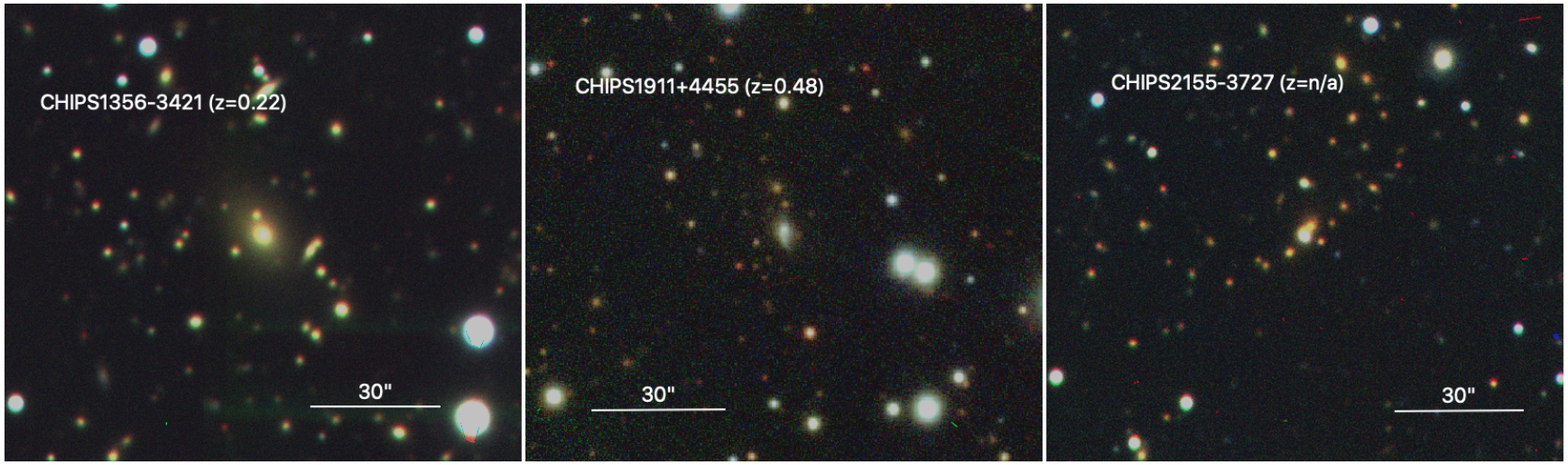

Figure 3-13 *gri* optical images of all three candidates–CHIPS 1356-3421, CHIPS 1911+4455, and CHIPS 2155-3727. These new cluster candidates are visually similar in optical to the Phoenix cluster with extremely bright objects in the center. Based on Chandra images, CHIPS 2155-3727 appears to not be a massive cluster even though the optical image suggests otherwise.

Table 3.3 CHiPS Cluster Candidates with Chandra Follow-up

CHiPS Name	z[a]	R_{500} (kpc)	M_{500} ($10^{14}\,M_\odot$)	$L_{\rm x}$[b] (10^{44} erg s^{-1})
CHIPS 1356-3421	0.22	1300 ± 200	6.4 ± 3.4	5.9
CHIPS 1911+4455	0.48	1075 ± 60	6.0 ± 0.1	19
CHIPS 2155-3727	$\sim$0.5	< 590	< 1	< 1.1

[a]The redshift is measured spectroscopically for the first two objects, while the third has only a photometric redshift estimate.
[b]$L_{\rm x}$ is measured from 0.1 to 2.4 keV with 1 Mpc aperture.

3.6.3.1 CHIPS1356-3421

The galaxy cluster surrounding PKS 1353-341, also known as CHIPS 1356-3421, was the first newly discovered and confirmed galaxy cluster from the CHiPS survey with Chandra X-ray observations [292]. It was missed from other X-ray surveys because of an extremely bright AGN in the central galaxy. Apart from the central QSO, the cluster is an ordinary cool-core cluster with $M_{500} = 6.9^{+4.3}_{-2.6} \times 10^{14} M_\odot$ and $L_{\rm x} = 7 \times 10^{44}\,{\rm erg\,s^{-1}}$ at $z = 0.223$. This cluster, with the lowest redshift of the three new CHiPS clusters, demonstrates how even massive, nearby clusters can be missed if they harbor a central X-ray-bright AGN. We measure a SFR, based on archival UV data, in the central galaxy of CHIPS 1356-3421, which is roughly a few percent of the cooling rate–typical of a well-regulated cool-core cluster. Given this low SFR, we expect that the mid-IR flux is dominated by the central AGN and not by a starburst. More details about this object can be found in our previously published paper [292].

3.6.3.2 CHIPS 1911+4455

CHIPS 1911+4455 is the second galaxy cluster we found by the CHiPS survey and confirmed with Chandra observations. The photometric redshift of the cluster is $z = 0.48$. It is our most exciting candidate so far, harboring a very blue galaxy in the center that is surrounded by many red satellite galaxies, similar to the Phoenix cluster [202]. Based on the Chandra data we obtained, the total mass and the total size

of the cluster are $M_{500} = (6.0 \pm 0.1) \times 10^{14}\, M_{\odot}$ and $R_{500} = 1075^{+54}_{-66}$ kpc, respectively, which is as massive as CHIPS 1356-3421 [292].

With our newly obtained Chandra data, we measure the core entropy at $\sim$10 kpc to be around 10-20 keV cm^2, which is as cool as in the Phoenix cluster. However, despite having a blue massive central galaxy and a strong cool core, the system shows a highly disturbed morphology on both large (>100 kpc) and small scales ($\sim$20 kpc). Possible scenarios for such a morphology include a recent major merger or a powerful AGN outburst [e.g., 60]. This finding is in opposition to most other known cool-core clusters, which are typically highly relaxed. Additional data will be obtained for this object, including high-resolution optical images from the Hubble Space Telescope and optical spectra from the Nordic Optical Telescope to look for strong emission lines, a signature of ongoing star formation. A complete analysis of this system is being published in Somboonpanyakul et al. [293], which will include a complete X-ray analysis of the cluster, optical spectroscopy of the central galaxy, and high-resolution Hubble imaging of the cluster core.

3.6.3.3 CHIPS 2155-3727

Even though the optical image of CHIPS 2155-3727 clearly shows an overdensity of red galaxies at the location of the X-ray source, as shown in Fig. 3-13, the Chandra observation of CHIPS 2155-3727 shows no extended emission around the X-ray point source. The nondetection of extended emission in Fig. 3-14 could imply that the overdensity of galaxies is either a projection of a sheet/filament along the line of sight or a smaller galaxy group below our detection threshold. Spectroscopic data are required to determine whether this is simply a projection effect. Based on the X-ray image, the estimated upper limit for the mass of the cluster, if it exists, is less than $1 \times 10^{14} M_{\odot}$.

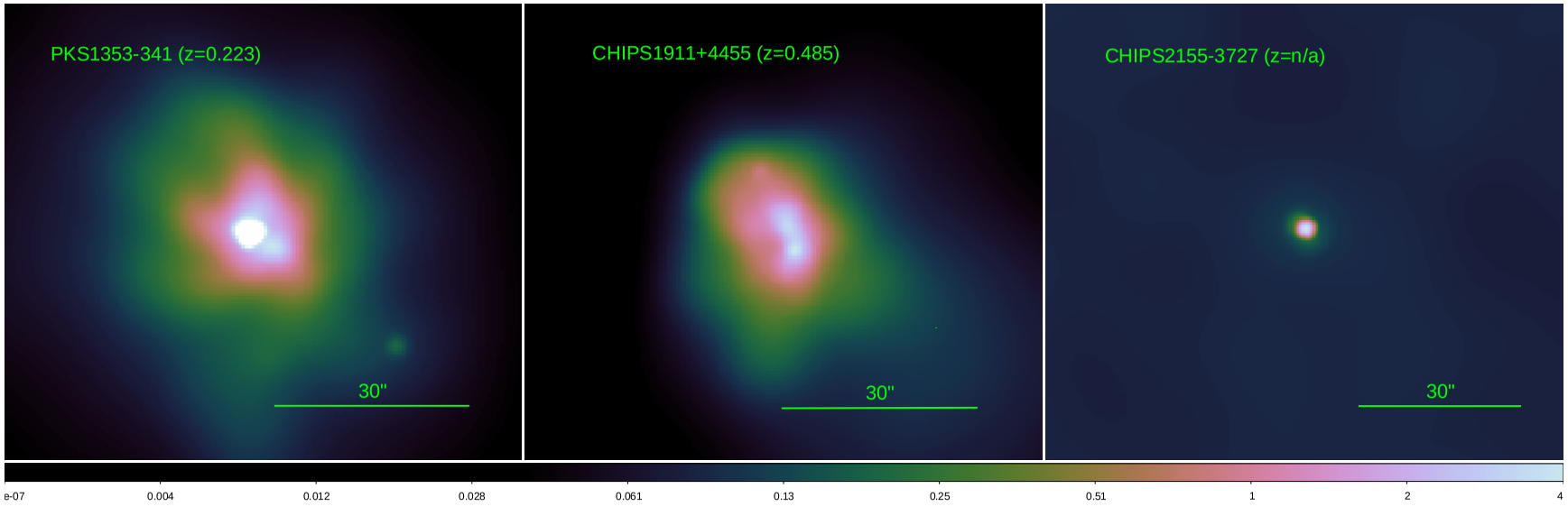

Figure 3-14 This figure shows X-ray images of the three galaxy clusters candidates–CHIPS 1356-3421, CHIPS 1911+4455, and CHIPS 2155-3727. These Chandra images confirm the discovery of two new massive galaxy clusters. These two clusters have a relatively bright core, and CHIPS 1911+4455 appears to be a recent merger. The image of CHIPS 2155-3727 shows only a bright point source without any extended emission, meaning that it is unlikely to be a massive cluster.

3.7 Discussion

3.7.1 Updating Flux-limited Surveys

We estimate the rest-frame 0.1-2.4 keV X-ray luminosity, the same as the REFLEX survey, of the new clusters within an aperture of 1 Mpc. Fig. 3-15 shows the X-ray luminosity of newly discovered galaxy clusters and their redshift with respect to clusters from the REFLEX [42], eBCS [95], and MACS [96] catalogs. These three cluster catalogs were created by first selecting X-ray-bright objects from the ROSAT All Sky Survey and then confirming via an overdensity of galaxies at a common spectroscopic redshift. The solid lines represent the flux limit of the MACS and REFLEX surveys at 1 and $3 \times 10^{-12}\,\mathrm{erg\,s^{-1}\,cm^{-2}}$, respectively. The fact that clusters from these three catalogs follow closely the aforementioned flux limits highlights the clean selection of X-ray surveys, which are biased toward high-mass systems at high z, but in a mostly predictable way. However, the figure shows that the two CHiPS clusters should have been found by these previous X-ray cluster catalogs, which are all based on the ROSAT data, but were not because of their highly concentrated X-ray profiles and nonstandard BCG colors. This is, similarly, why the Phoenix cluster was not discovered until recently even though it is the most X-ray-luminous cluster known [202].

3.7.2 Rarity of Clusters Hosting Extreme Central Galaxies

One of the main goals of the CHiPS survey is to find more galaxy clusters with extreme central galaxies (starbursts and/or AGNs) by looking for clusters around X-ray-bright point sources that are also bright in the mid-IR and radio. Given that we have only discovered two new Phoenix-like systems, only one of which has an exceptionally high star formation rate, we can conclude that such rapidly cooling systems are extremely rare. From this work, we find that the total number of galaxy clusters with extreme central galaxies to be around 10 objects above the ROSAT detection limit.

To estimate how rare such a system is, we approximate the total population of

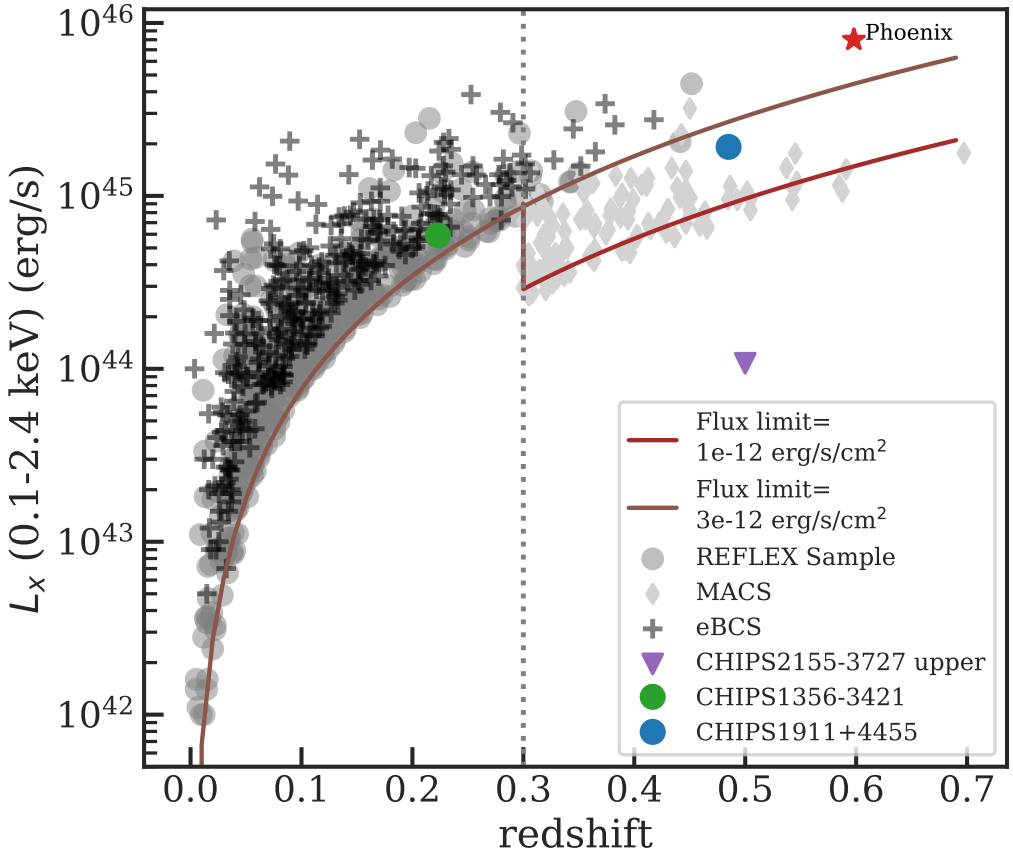

Figure 3-15 Luminosity v.s. redshift for clusters from the REFLEX Cluster Survey [42], the ROSAT All-Sky Survey Extended Brightest Cluster Sample [eBCS; 95], and the Massive Cluster Survey [MACS; 96]. The solid lines show X-ray flux limits, introduced by Böhringer et al. [42], at 1×10^{-12} erg s^{-1} cm^{-2} and 3×10^{-12} erg s^{-1} cm^{-2}. This figure shows that the Phoenix cluster, CHIPS 1356-3421, and CHIPS 1911+4455 should have been identified in the ROSAT data. The purple arrow shows an upper limit for CHIPS 2155-3727 which is not detected in our Chandra observation.

galaxy clusters found by the ROSAT satellite by combining the REFLEX, eBCS, and MACS samples. Given the total number of clusters detected with the ROSAT data to be about 460 in total ($0.1 < z < 0.7$), the occurrence rate of extreme (starbursts and/or rapidly accreting AGNs) central galaxies is $2\% \pm 1\%$. We separate the clusters into two redshift bins to see whether there is any difference. The rate is $2\% \pm 1\%$ for nearby objects ($z = 0.1$–0.3) but becomes $5\% \pm 2\%$ for higher-redshift objects ($z = 0.3$–0.7). At this stage, we do not see any significant difference between the two redshift bins. A deeper and higher-resolution X-ray all-sky survey is required to improve our estimate of the occurrence rate of extreme sources in the center of clusters.

This survey shows that the occurrence rate of clusters hosting extreme central galaxies–defined as systems with either rapidly accreting supermassive black holes or ongoing, massive starburst–is extremely low, of order a few percent. This is consistent with the temporal statistics of pink/flicker noise observed in the CCA model and related high-resolution hydrodynamical simulations [119, 120], which predict a 2 dex increase in the SMBH accretion rate $\sim 1\%$ of the time. Such a rarity of quasar-like blast events is in agreement with the tight, gentle self-regulation driven via CCA (arising from the hot halo condensation), which preserves the cool-core structure for several gigayears. Similar rarity is also consistent with the observed scatter in the SFR at fixed cooling rate [207, 228], showing $10\times$ higher SFR in less than 10% of clusters.

3.7.2.1 Uniqueness of the Phoenix Cluster

The Phoenix cluster is one of the most unusual clusters found recently [202, 208, 212]. The central galaxy of the cluster hosts an extremely X-ray-luminous AGN with bright radio jets. High-resolution optical/X-ray images also reveal a massive cooling flow extending up to hundreds of kiloparsecs, which is accompanied by a starburst-hosting BCG. The estimated SFR of its BCG is tremendous at $798 \pm 42\, M_{\odot}\, \mathrm{yr}^{-1}$ [203], which is the highest of all known clusters. It seems that the AGN feedback, which has been thought to be responsible for stopping the cooling of new stars in central galaxies [104,

215], is not effective in the Phoenix cluster, leading to an extremely high SFR in the BCG and the presence of a cooling flow. Nonetheless with only one such system, we cannot fully understand where this system fits in our overall understanding of the cooling/feedback cycle. The CHiPS survey was designed in part to find more of these systems.

In this work, we find, at most, one potential analog to the Phoenix cluster: CHIPS 1911+4455. This system has a luminous blue galaxy in the center of the cluster, similar to the Phoenix cluster, suggesting the presence of a massive starburst. We will present a detailed analysis of this system, based on ground-based optical spectroscopy and high-resolution *Hubble* imaging, in a companion paper. Further, based on in-hand Chandra data, we find evidence that the core may be cooling just as rapidly as in the Phoenix cluster [293]. Considering this, the total number of Phoenix-like clusters is, at most, two (the Phoenix cluster and CHIPS 1911+4455) out of ~ 460 systems in a complete X-ray flux-limited sample from the ROSAT All-Sky Survey. This means that the rate of occurrence for such rapidly cooling systems is less than 1% of the massive cluster population. One explanation for such a rare event is that an intense short-lived cooling of the intracluster medium or a short-lived brightening of the central AGN is a part of the AGN feedback cycle and flickering CCA [118, 252]. We can roughly estimate how short this burst of cooling would have been if we find only two such systems at $0.1 < z < 0.7$. Assuming all clusters go through the evolutionary phases in the same manner, within the past ~ 5 Gyr, the phase of rapid cooling for clusters lasts, on average, for ~ 22 Myr. Since most signatures of star formation last for roughly 20 Myr [162], this implies that almost the full cluster population could go through a short-lived phase of rapid cooling, and we would only expect to observe it (and the subsequent young stellar populations) in a few percent of clusters.

3.7.3 Planck Cluster Candidates

Two of the three clusters, CHIPS 1356-3421 and CHIPS 1911+4455, have corresponding Planck cluster candidates at S/N = 5.76 and 4.64, respectively, as shown in the first two panels of Fig. 3-16 [248]. Specifically, the Planck source at the location of

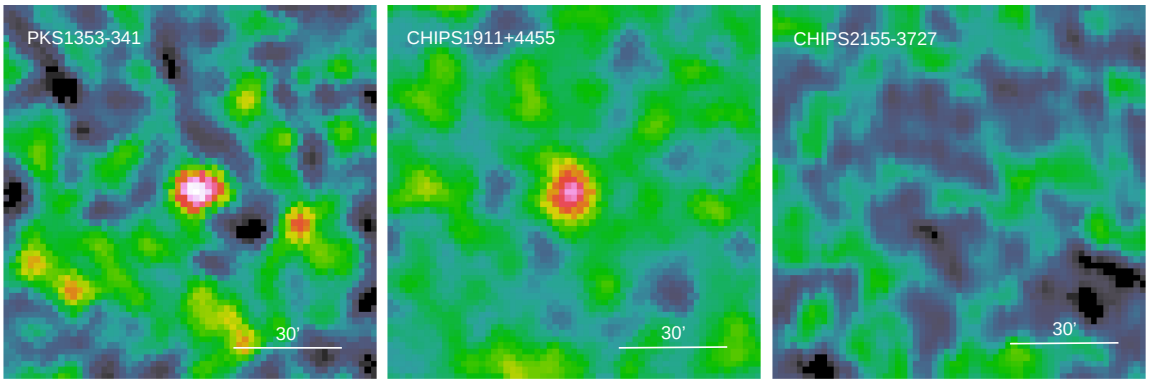

Figure 3-16 This figure shows Y-map images of three galaxy clusters candidates– CHIPS 1356-3421, CHIPS 1911+4455, and CHIPS 2155-3727 (from left to right) from the Planck satellite [248]. The two clusters in the left panels are detected with Planck and now confirmed with Chandra, as described in Section 3.6.

CHIPS 1356-3421 is among the 1653 SZ detections in the Planck catalog, but it is not one of the 1203 confirmed detections. Somboonpanyakul et al. [292] shows that it is in fact a massive cool core cluster at that location. Meanwhile, CHIPS 1911+4455 has a weaker signal with S/N = 4.64 but has an additional counterpart in an external dataset, specifically a significant galaxy overdensity in the WISE data. These two examples show that we could potentially further utilize the Planck catalog of unconfirmed SZ sources to help confirm the existence of these hidden clusters with lower richness than what we are able to achieve currently with the CHiPS survey. Even though Planck's threshold for cluster detection is higher than what we found with the CHiPS survey, the Planck catalog also includes many low-significance candidates. Works similar to the CHiPS survey [e.g., 182, 304] can confirm the existence of galaxy clusters in this lower-significance regime since it is highly unlikely that the two completely different techniques will find a cluster candidate at the same location.

3.7.4 Missing known clusters in the survey

Based on McDonald et al. [207], there are nine known clusters at $z < 1$ that host a massive star-forming galaxy (SFR $> 60\ M_{\odot}\,\mathrm{yr}^{-1}$) in the center, as shown in Table. 3.4. The CHiPS survey rediscovered four of them–A1835, Zwicky 3146, IRAS 09104+4109,

Table 3.4 List of All Known Clusters with Massive Star Formation Rate (SFR>60 $M_\odot\,yr^{-1}$)

Cluster Name	z	SFR ($M_\odot\,yr^{-1}$)[a]	CHiPS	Reason Not Found
RXJ 1504.1–0248	0.215	85 ± 9	not found	MIR is outside the range
A1835	0.2528	117 ± 24	found	
Zwicky 3146	0.2966	69 ± 24	found	
IRAS 09104+4109	0.4347	309 ± 120	found	
H1821+643	0.297	447 ± 147	not found	optical is too bright, not radio bright
Phoenix	0.579	617 ± 200	found	
Perseus	0.0179	71 ± 20	not found	redshift is too low
MACS 1931.8–2634	0.352	263 ± 53	not found	no match X-ray vs radio
RXJ 1532.9+3021	0.363	98 ± 19	not found	MIR is outside the range

[a]all SFR numbers come from McDonald et al. [207].

and the Phoenix cluster. The other five are the Perseus cluster, H1821+643, MACS 1931.8–2634, RXJ 1532.9+3021, and RXJ 1504.1–0248. In this section, we explain why these five clusters are not detected in the survey.

The Perseus cluster is the brightest cluster in the X-ray. It is not in our survey because its redshift ($z = 0.0179$) falls outside of our range of interest of $0.1 < z < 0.7$. We exclude $z < 0.1$ because there are countless optical surveys looking for massive clusters in that redshift range.

The galaxy cluster surrounding H1821+643 is the only low-redshift ($z = 0.299$) galaxy cluster that contains a highly luminous, unobscured quasar in the center [267]. However, the quasar H1821+643 is a radio-quiet quasar [38]. It is not included in the CHiPS survey because our catalog requires objects to be relatively bright in radio at 1.4 GHz. Furthermore, the *CHiPS* survey is also normalized by the optical images to remove the dependence on redshift; however, this also means that we penalize objects which have an extremely bright optical counterpart. These choices were made to reduce the number of candidates to a manageable size for optical follow-up, but will naturally exclude some interesting systems. Thus, we are unable to comment on the occurrence rate of clusters hosting extremely optically bright or radio-quiet quasars at their center.

MACS 1931.8–2634 is another example of a cluster with a powerful AGN outburst amid a major merger event [100]. However, its X-ray location from RASS-BSC and its radio location from NVSS are $36''$ apart, which is three times larger than our average distance when matching between the two surveys. 1.4 GHz radio observations from the Very Large Array (VLA) show a brighter narrow-angle tail (NAT) radio galaxy $45''$ to the south of the BCG [100]. This radio source could be a power jet from a nearby galaxy that is falling into the BCG. With the $45''$ angular resolution of the NVSS catalog, we conclude that the radio location of MACS 1931.8–2634 in NVSS is a blended point between the BCG and the radio galaxy.

The last two clusters, RXJ 1504.1–0248 and RXJ 1532.9+3021, have relatively large SFRs at $85 \pm 9\, M_\odot\, \mathrm{yr}^{-1}$ and $98 \pm 19\, M_\odot\, \mathrm{yr}^{-1}$, respectively. However, they are not within our mid-IR color-cut for our selection, which focuses our selections to the

Phoenix cluster. In fact, both of them are very close to our selection cutoff from Section 3.2. This helps to clarify the baseline type of cluster that we expect to find, specifically clusters with SFR $> 100\,M_{\odot}\,\mathrm{yr}^{-1}$ in the BCG.

Both 3C 186 and 3C 254 are also not found in the CHiPS survey. This is to be expected since their redshifts for both of them are 1.01 and 0.74, respectively, which is more than our redshift cut at 0.7, as mentioned in Section 3.2.1.

3.7.5 eROSITA

With the recent launch of the eROSITA [255] mission in July 2019, an X-ray instrument performing the first imaging all-sky survey in the energy range up to 10 keV, thousands of new galaxy clusters and AGNs will be discovered.

The CHiPS survey helps to predict the potential biases in the eROSITA survey, if selection is made based solely on the presence of extended X-ray emission. Some massive groups and clusters with extreme BCGs will appear pointlike in the X-ray, similar to what we found with the ROSAT All-Sky Survey and the CHiPS survey. Specifically, the types of system that will be missed include systems where the point source dominates the extended emission (e.g., QSO-central clusters) and systems whose cool core appears pointlike (e.g., distant, strongly cooling systems). With the predicted 10^5 clusters found with *eROSITA* [246], 2% of clusters with extreme central galaxies, as described in Section 3.7.2, is equal to $\sim$2000 clusters that eROSITA will miss if the survey only characterizes extended X-ray emissions as cluster candidates. Pillepich et al. [246] also estimated that with eROSITA cluster counts and cosmology priors from the Planck mission, the uncertainty of Ω_{m} will be less than 2%. Thus, it is crucial to take into account these missing clusters, which appear pointlike.

One proposed solution for eROSITA is to allow new X-ray detections to be classified as both a point source and an extended source if there is any faint extended emission surrounding a point source. This could potentially help identify even more clusters with extreme central properties. Additionally, the upcoming Vera C. Rubin Observatory, a wide-field telescope with 8.4 m primary mirror, is expected to be operating by 2021/2022 [157]. The telescope will provide an enormous amount of

optical data suitable for following up new cluster candidates. An important note for the optical follow-up is the need to allow the presence of nontypical (i.e., blue) BCGs, which is a current problem in many BCG-identifying codes.

3.8 Summary

In this work, we present a complete optical description of the CHiPS survey, a new galaxy cluster survey using both archival data (SDSS and Pan-STARRS) and newly acquired data from the Magellan telescope to find new clusters that harbor extreme central galaxies. Our findings are summarized below.

- By looking at the photometric redshifts of galaxies around X-ray, radio, and mid-IR-bright point sources, we have identified 11 cluster candidates. Of these, we rediscovered six well-known galaxy clusters with both starburst-hosting and QSO-hosting central galaxies. Two of these candidates were false associations of foreground and background clusters, while the remaining three are previously unknown.

- With additional follow-up data from the Chandra X-ray telescope for the three new candidates, we confirmed two newly discovered galaxy clusters. We do not detect extended X-ray emission around the other cluster candidate, finding an upper limit on the total mass of $\sim 10^{14}\ M_{\odot}$. Details for the first one, CHIPS 1356-3421, or the cluster surrounding PKS 1353-341, are already published in our pilot paper [292].

- We estimate the total mass and the total luminosity of the other new cluster, CHIPS 1911+4455. The total mass (M_{500}), using the $Y_{\rm x}$–M_{500} relation, is $(6.0 \pm 1.0) \times 10^{14}\ M_{\odot}$, whereas, the X-ray luminosity (0.1–2.4 keV) for this cluster is $1.9 \times 10^{45}\,{\rm erg\,s^{-1}}$. This implies that CHIPS 1911+4455 is massive enough to be found by previous X-ray clusters surveys, such as the REFLEX and MACS surveys.

- We find a massive blue central galaxy in CHIPS 1911+4455, pointing to an extreme central galaxy similar to the Phoenix cluster. With the Chandra data, we find the core entropy at $\sim$10 kpc to be as low as in Phoenix, but it has a morphology unlike Phoenix and any known strong cool-core cluster. More details about CHIPS 1911+4455 is published in Somboonpanyakul et al. [293].

- With the CHiPS survey, we find the occurrence rate of clusters that appear as X-ray point sources with bright mid-IR and radio flux to be $2\% \pm 1\%$, and the occurrence rate of clusters with rapidly cooling cores similar to the Phoenix cluster to be less than 1%. Such rarity is consistent with the flicker-noise statistics expected during the CCA cycles and with its driven average gentle self-regulation.

- One of the primary goals of this survey was to determine whether the Phoenix cluster is unique. It looks like it is: there is no cluster at $z < 0.7$ that has a more massive central starburst within a factor of ~ 3 in magnitude. If there were, we would have found it in this survey.

In general, the discovery of these CHiPS clusters emphasizes a need for X-ray point source/cluster-finding algorithms to allow the possibility of finding both pointlike and extended objects at the same time. By limiting the algorithm to picking out only X-ray-bright point sources, many clusters hosting extreme objects (starbursts/AGNs) were missed in the past. Objects of this type are critical in our quest to understand the relation between cooling flow and feedback from the central BCGs. Lastly, by only finding one new galaxy cluster with a massive starburst galaxy in the center (CHIPS 1911+4455), we conclude that the Phoenix cluster is in fact a rare occurrence (less than 1% of the whole cluster population). This finding will be important in helping us understand the mechanism of forming a Phoenix-like cluster in the future.

Chapter 4

CHIPS1911+4455, a Rapidly-Cooling Core in a Merging Cluster

The content of this chapter was submitted to The Astrophysical Journal Letters *on November 9, 2020 and published [293] as* The Clusters Hiding in Plain Sight (CHiPS) survey: CHIPS1911+4455, a Rapidly-Cooling Core in a Merging Cluster *on January 12, 2021.*

4.1 Introduction

Early X-ray observations of the intracluster medium (ICM) in the center of galaxy clusters revealed cooling times much shorter than the Hubble time, leading to the development of the cooling flow model [e.g., 103]. In this model, hot gas in dense cores should radiatively cool and fuel 100–1000 $M_\odot\,\mathrm{yr}^{-1}$ starbursts in the central brightest cluster galaxy (BCG). However, many studies have shown that BCGs are only forming stars at $\sim$1% of this rate [e.g., 207]. A promising mechanism proposed for preventing cooling of the ICM is active galactic nucleus (AGN) heating by jets and bubble-induced weak shocks [see reviews by 104, 215, 121]. Evidence supporting these theories includes the ubiquitous presence of radio galaxies at the center of clusters [305] and the similarity between the mechanical energy released by AGN-driven bubbles and the energy needed to quench cooling [e.g., 32, 257, 149].

Galaxy clusters with signatures of cooling in their centers are often called “cool-core" (CC) clusters, with their counterparts being referred to as “non cool-core" (NCC) clusters. Hudson et al. [156] found that the best way to segregate the two is to consider their central cooling time (t_{cool}). Specifically, CC clusters have $t_{cool} < 7.7$ Gyr, while clusters with $t_{cool} < 1.0$ Gyr are referred to as “strong CCs”. A number of observational studies have found that CCs are mostly found in relaxed clusters while NCCs reside in dynamically active clusters. Indeed, all of the strongest CCs known (based on cooling rate) are found in the most relaxed clusters (e.g., Phoenix [202], Abell 1835 [217], Zw3146 [99]). This is also consistent with a variety of other studies that found star-forming BCGs in the most relaxed CC clusters [84, 89, 228, 68]. On the other hand, morphologically disturbed clusters (which are likely to be recent mergers) generally have no evidence for ongoing cooling, suggesting that major mergers may have the potential to destroy cool cores [59, 250] through shock-heating [58] and mixing [125].

The discovery of CHIPS1911+4455 (Somboonpanyakul et al., in press) runs counter to these established norms, since it not only harbors a very blue (star-forming) galaxy in the center, but also shows a highly disturbed morphology on both large (∼200 kpc) and small (∼20 kpc) scales. There are no known nearby clusters that have properties similar to CHIP1911+4455, though McDonald et al. [205] report a higher fraction of star-forming BCGs in merging clusters at $z > 1$. This implies that CHIPS1911+4455 may provide an avenue for studying a high-redshift phenomenon in a low-redshift cluster. To fully understand this system we have obtained new observations in the core of CHIPS1911+4455, which we will discuss below.

Throughout this Letter, we assume $H_0 = 70\,\mathrm{km\,s^{-1}Mpc^{-1}}$, $\Omega_m = 0.3$, and $\Omega_\Lambda = 0.7$. All errors are $1\,\sigma$ unless noted otherwise.

4.2 Observations

In this section, we summarize the acquisition and reduction of data obtained from the Chandra X-ray telescope, the Hubble Space Telescope, and the Nordic Optical

Telescope (NOT).

4.2.1 X-Ray: Chandra

CHIPS1911+4455 (OBSID: 21544) was observed in 2019 with Chandra ACIS-I for a total of 30.5 ks. The data were analyzed with `CIAO` v4.11 and `CALDB` v4.8.5 and recalibrated with VFAINT mode for improved background screening. To look for small-scale structures near the center of the cluster, images were smoothed adaptively, using `CSMOOTH`[1] to achieve a uniform signal-to-noise ratio over the full image, as shown in the left panel of Fig. 4-1.

The temperature profile was extracted from coarse annuli so that the number of counts per annulus was around 800, which is enough to get well-constrained temperature measurements ($\Delta kT/kT$ ~20%). All spectra were fit simultaneously with the `APEC` model for the cluster emission, a second `APEC` model for the Milky Way ($kT = 0.18\,\mathrm{keV}$), the `PHABS` model for Galactic absorption, and the `BREMSS` model to represent a hard background ($kT = 0.40\,\mathrm{keV}$) from unresolved point sources, following [203]. The WSTAT statistic was used.

The gas density profile was created by first computing the 0.7-2.0 keV surface brightness profile. The conversion from the X-ray surface brightness profile to the emission-measure profile ($\mathrm{EM}(r) = \int n_p n_e dl$) was calculated as a function of radius based on the best-fit temperature profile and assuming a collisionally ionized plasma `APEC` model with metallicity $0.3\mathrm{Z}_\odot$. For more details of the X-ray analysis, see [292].

4.2.2 Optical: Hubble

CHIPS1911+4455 was observed for two orbits with the Hubble Space Telescope (HST) during Cycle 27. The data include mediumband F550M data from the Advance Camera for Surveys (ACS) and broadband F110W data from the Wide Field Camera infrared channel (WFC3-IR). The F550M filter contains both the blue continuum and the bright [O II] doublet at the redshift of the cluster, which should both be

[1] https://cxc.harvard.edu/ciao/ahelp/csmooth.html

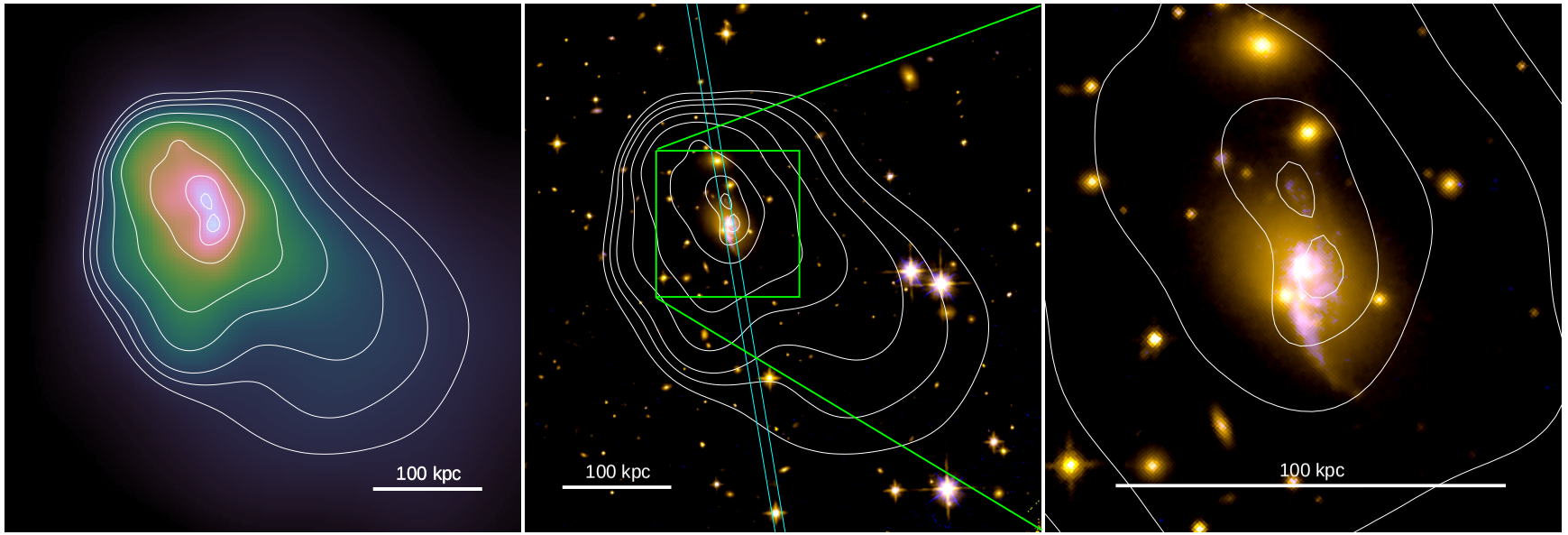

Figure 4-1 Left: Chandra 0.5–7.0 keV image of CHIPS1911+4455, highlighting the asymmetric morphology on both small and large scales. The image is oriented such that north is up and east is to the left. Middle: Hubble images with X-ray contours overlaid. The contour lines were chosen arbitrarily to guide the eye. The cyan box shows the orientation of the long slit (see also Fig. 4-5). Right: the Hubble images of the central galaxy, showing the blue star-forming filaments, extending on scales of $\sim$ 30 kpc. These images show that the cool, star-forming gas is centered on the X-ray peak, with a faint set of filaments extending north to the secondary peak and a brighter filament extending to the south.

elevated in star-forming regions. The F110W filter, on the other hand, is sensitive to the red continuum, probing the old stellar populations of the BCG and other cluster members.

4.2.3 Optical Spectra: Nordic Telescope

Two optical spectra of the BCG of CHIPS1911+4455 were obtained with the Alhambra Faint Object Spectrograph and Camera (ALFOSC) at the 2.56m Nordic Optical Telescope (NOT) on 2019 May 9. One of the spectra was obtained from Grism#4 (R=360, 3200–9600 Å) with 1.″3 slit for 1500-second exposure. The other spectrum was a stack of two 1100 s spectra from Grism#5 (R=415, 5000–10700 Å) with 1.″3slit at 90° from the first spectrum. Wavelength solutions for the two spectra were calibrated with HeNe and ThAr arc lamps, respectively, with an absolute calibration uncertainty of 2 Å. Masks were applied to remove cosmic rays before the 1D spectra were extracted from the 2D spectral images. The 1D spectra were then flat-fielded, and background-subtracted from off-source regions surrounding the 1D extraction region.

4.3 Results

4.3.1 CHIPS1911+4455: A Strong Cool Core

The thermodynamic profiles of CHIPS1911+4455 are shown in Fig. 4-2. The electron density at 10 kpc is $0.0884\,\mathrm{cm}^{-3}$, which is among the highest measured to date [156, 206], while the temperature profile drops from a maximum of ∼8 keV at ∼300 kpc to 4 keV at ∼10 kpc.

The entropy of the ICM ($K \equiv kTn_e^{-2/3}$) reflects the thermal history of a cluster, which is solely affected by heat gains and losses [67, 242], while the cooling time ($t_{cool} \equiv \frac{3}{2}\frac{(n_e+n_p)kT}{n_e n_p \Lambda(T)}$) represents the amount of time required for the ICM to radiate

all the excess heat, where $\Lambda(T)$ is the cooling function [307]. For CHIPS1911+4455, the central ($r = 10\,\mathrm{kpc}$) cooling time is $98^{+7}_{-32}\,\mathrm{Myr}$, which is classified as a strong cool core [156]. The deprojected entropy profiles for CHIPS1911+4455, the Phoenix cluster, and hundreds of clusters from the ACCEPT survey [67] are shown in Fig. 4-3. Both CHIPS1911+4455 and the Phoenix cluster have entropy profiles that are among the lowest known. The core ($r = 10\,\mathrm{kpc}$) entropy for CHIPS1911+4455 is $17^{+2}_{-9}\,\mathrm{keVcm}^2$, which is in the 5th percentile of all clusters in the ACCEPT survey.

4.3.2 CHIPS1911+4455: A Major Merger

There are various ways to quantify the dynamical state of a cluster, with some of the best combining X-ray data with information on the galaxy velocities. Lacking the latter, we restrict ourselves to X-ray-only indicators. The two particular quantities we consider are the "peakiness" of the surface brightness profile and the distance between the center of symmetry on small and large scales ("symmetry"), following Mantz et al. [191]. The peakiness measure is a proxy for the presence of a cool core, which is typically found in relaxed clusters. A cluster with high symmetry appears similar on small and large scales, suggesting that it is dynamically relaxed. Given that both of these proxies probe the dynamical state of the cluster, albeit in different ways, it is unsurprising that they are correlated [191]. The green points in Fig. 4-4 show the population of relaxed clusters in this morphology plane. For CHIPS1911+4455, the peakiness is measured to be -0.501, which is in the 96th percentile of all clusters, while the symmetry is estimated to be 0.425, which is in the 7th percentile. The fact that CHIPS1911+4455 is simultaneously one of the strongest cool cores *and* least symmetric clusters known is highly unusual.

4.3.3 CHIPS1911+4455: A Starburst BCG

In Fig. 4-1, we compare optical and X-ray images of CHIPS1911+4455. The Hubble images show that the red emission from old stellar populations is relatively smooth and symmetric, while the blue emission from the young stellar populations and cool

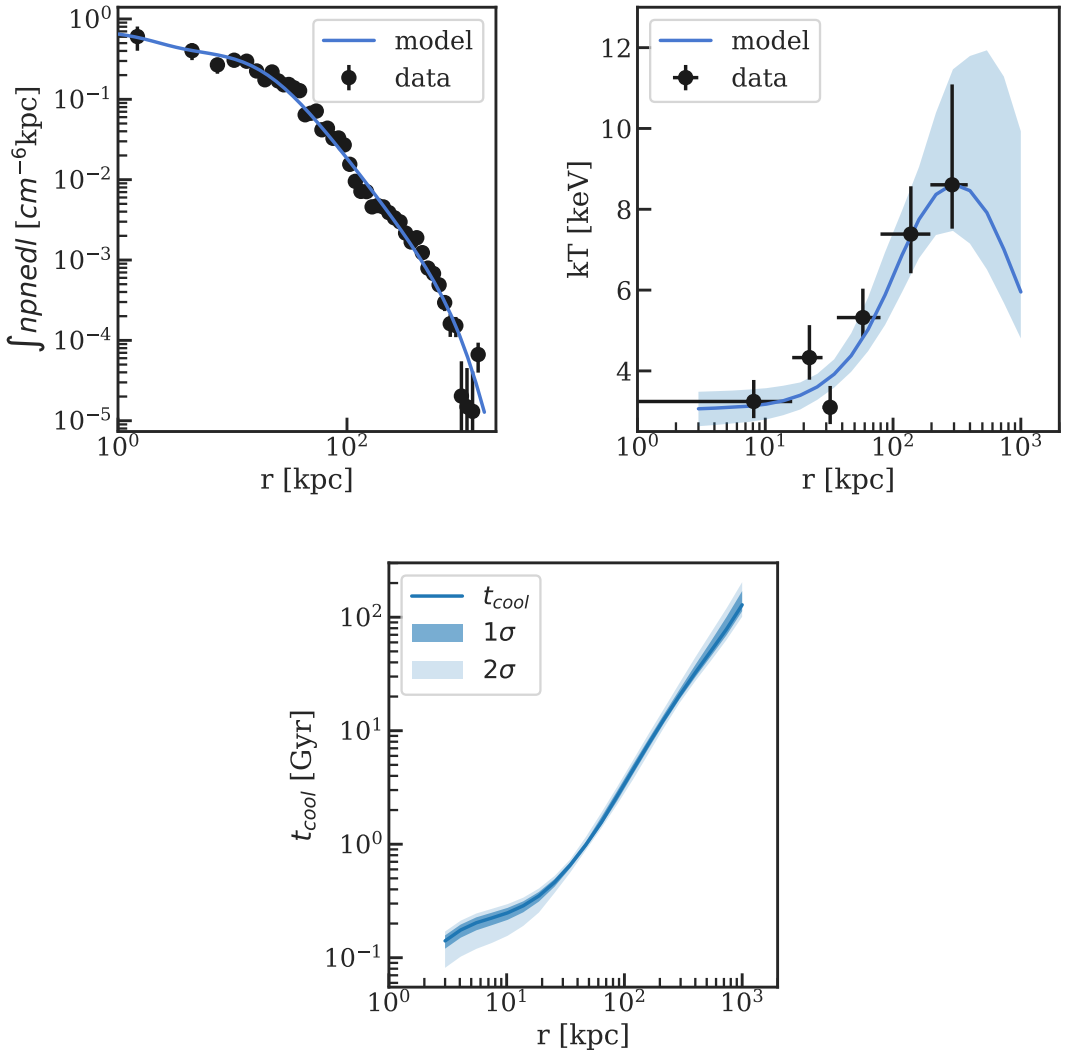

Figure 4-2 Left: the surface brightness profile of CHIPS1911+4455. The black dots are data points, and the blue line is the best-fit model [see 292, for a further description of this modeling]. Middle: the projected 2D temperature profile of the cluster. The black dots are data extracted from modeling of the X-ray spectra. The blue line is the best-fit model following [320]. Right: the cooling time profile of the cluster. The cyan shaded region corresponds to 1σ credible region from the models in the left and middle panels, while the light blue shaded region corresponds to the 2σ credible region. This cluster is classified as a strong cool core, based on a large drop in the core temperature and a central cooling time less than 1 Gyr [156].

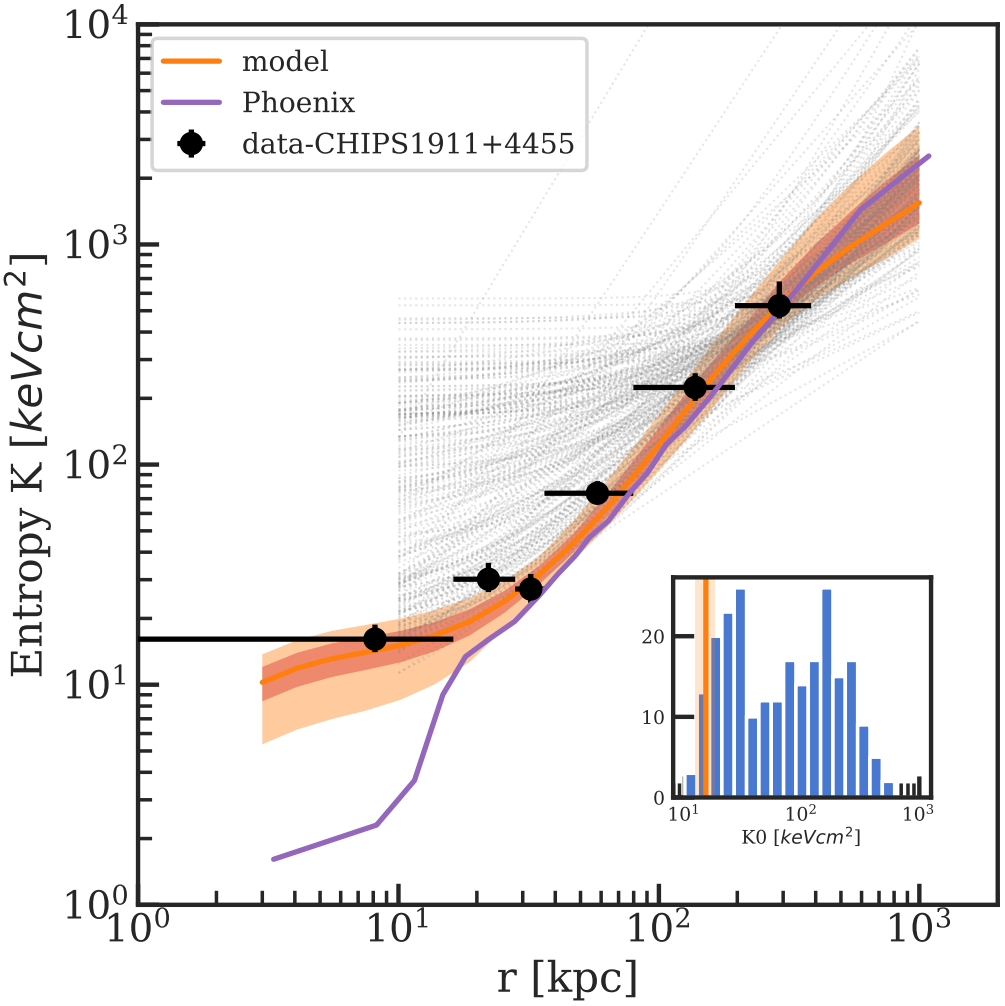

Figure 4-3 Entropy profile for CHIPS1911+4455 (orange), compared to 239 clusters from the ACCEPT survey [gray; 67] and the Phoenix cluster [purple; 208]. The shaded region corresponds to 1σ and 2σ credible regions (see Fig. 4-2). The black dots are data points, estimated from the projected 2D temperature data and the 3D density model. The inset shows the histogram of the core entropy ($r < 10\,\mathrm{kpc}$) of all the ACCEPT clusters and CHIPS1911+4455 (orange). CHIPS1911+4455's core entropy is in the lowest 10% of all ACCEPT clusters.

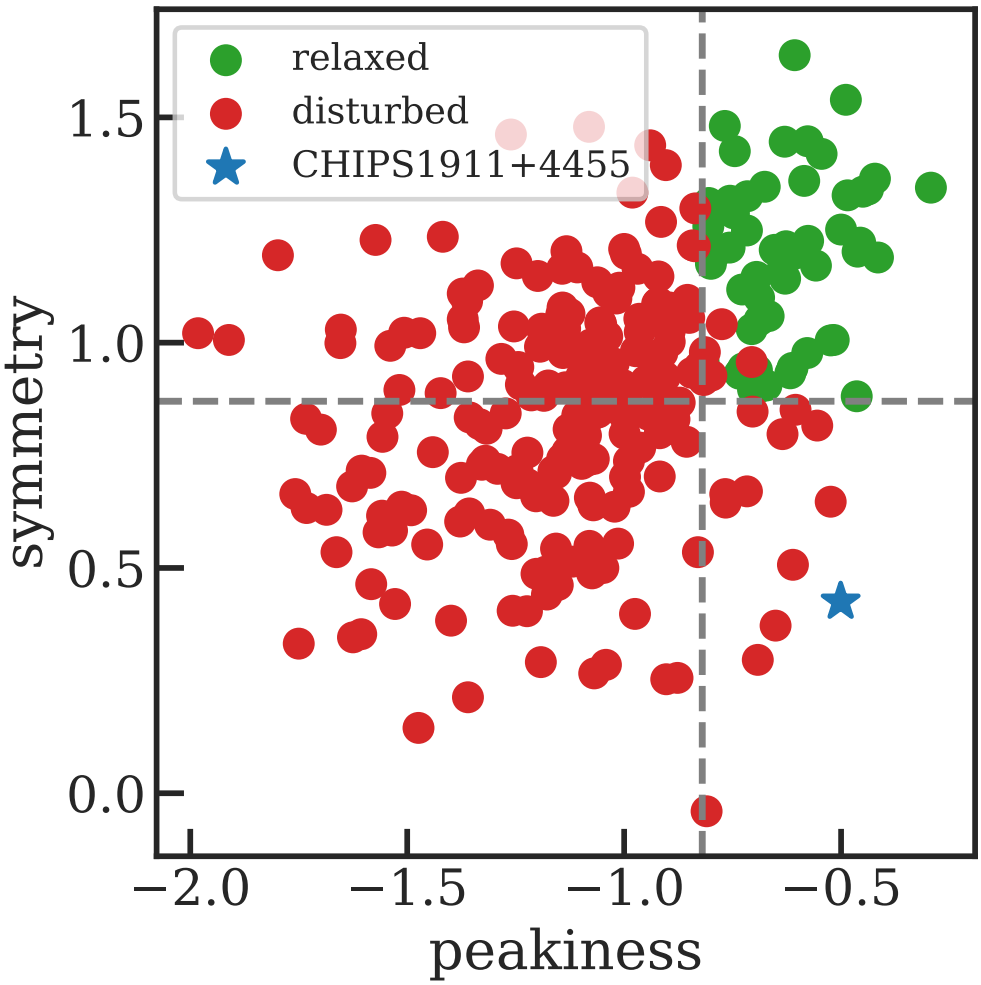

Figure 4-4 Distribution of X-ray symmetry and peakiness for clusters presented in Mantz et al. [191]. Dashed lines show the cuts used to define the relaxed sample, which were chosen to broadly agree with "by-eye" assessments of relaxedness. Clusters satisfying this criterion are shown in green, while red points show the non-relaxed clusters. The blue star represents the location of CHIPS1911+4455, which is the peakiest cluster with large-scale asymmetry.

gas is clumpy, asymmetric, and extended on >30 kpc scales. In particular, the red emission shows no elongation toward the galaxies to the north, suggesting that there has not been a recent interaction between these galaxies. Given this, and the fact that the central entropy is amongst the ∼2–3 lowest ever measured, we propose that the young stars are forming directly from the cooling ICM. The filamentary complex structures in the blue emission are similar to the emission nebula in the Phoenix cluster [208] and other nearby cool-core clusters [e.g., 209, 314, 240].

From the optical spectrum in Fig. 4-5, we identify several bright emission lines, including Hβ and [O II]. The relative lack of bright [O III] compared to [O II] indicates that the central galaxy in CHIPS1911+4455 is a massive starburst and not a bright AGN. We use these emission lines to estimate the redshift of the central galaxy, finding $z = 0.485 \pm 0.005$. From the two slit orientations, we measure [O II] equivalent widths of 40.9 ± 1.0 Å and 43.8 ± 1.0 Å, which are consistent with one another. To convert to flux, we model the spectral energy distribution (SED) of the galaxy, based on data from Pan-STARRS [g, i, r, z, and y; 313] and WISE [$w1$ and $w2$; 337], with a linear combination of "young" and "old" stellar populations, along with dust reddening [61]. The best-fit SED model is shown in Fig. 4-5. We estimate a dereddened continuum flux at the location of [O II] of $3.5 \pm 0.5 \times 10^{-16}\,\mathrm{erg\,s^{-1}\,cm^{-2}\AA^{-1}}$, which we combine with the EW to estimate the star formation rate (SFR) of the central galaxy, arriving at $189^{+25}_{-22}\,\mathrm{M_\odot\,yr^{-1}}$ [162].

Another way to measure SFR is to use the $24\mu m$ emission since mid-IR fluxes are unaffected by dust extinction, unlike UV and optical tracers. Instead, mid-IR emission comes from the reprocessed light by dust, produced from recently formed stars. Based on the WISE4 flux ($\sim 4 \times 10^{-18}\,\mathrm{erg\,s^{-1}\,cm^{-2}\AA^{-1}}$), we estimate the SFR for the central galaxy to be $143^{+31}_{-26}, \mathrm{M_\odot\,yr^{-1}}$, based on Cluver et al. [75].

Considering both the [O II] emission line luminosity and the mid-IR continuum, we obtain consistent SFRs of ∼140–190 $M_\odot\,\mathrm{yr^{-1}}$, making the BCG in CHIPS1911+4455 one of the most star-forming BCGs in the $z < 1$ universe [see, e.g., 207]

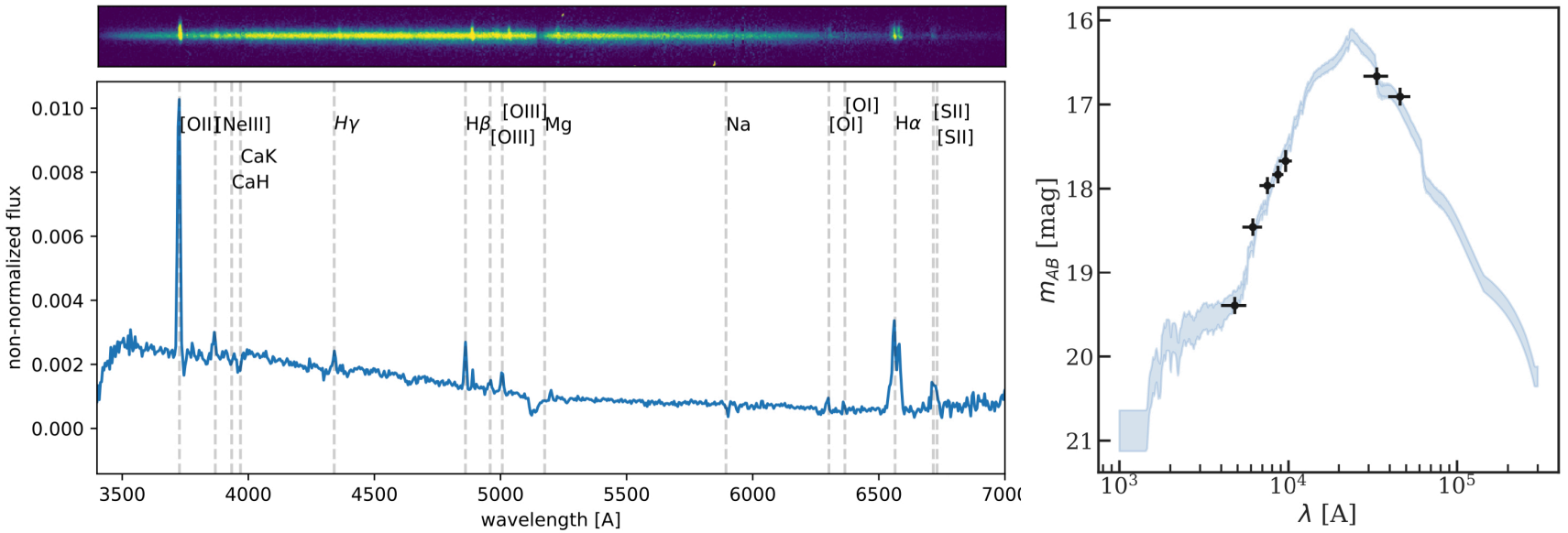

Figure 4-5 Top left: the 2D spectral image of the BCG of CHIPS1911+4455 from the Nordic Optical Telescope showing that the line-emitting gas is extended along the slit (vertical) direction. This confirms that the [O II] emission is not coming (exclusively) from a central AGN, and that the extended emission in Fig. 4-1 is indicating the presence of cool gas, rather than purely blue continuum from young stars. Bottom left: the 1D spectrum in the rest frame from the 2D spectral image above. Grey dashed lines show the location of well-known emission lines. The spectrum clearly shows the strong [O II] doublet at 3727 Å and the Hα emission line at 6562.8 Å. Right: the fitted spectral energy distribution (SED) model with broadband optical data (g, r, i, z, and y) from Pan-STARRS and mid-IR from WISE.

4.4 Discussion

It is clear, based on Sections 4.3.1–4.3.3, that CHIPS1911+4455 is a unique system in the nearby universe ($z < 0.5$) with an extremely high central SFR, a strong cool core, and large-scale morphology consistent with a recent merger. It is common knowledge that, at low redshift, the most star-forming BCGs tend to be located in the most relaxed, cool-core clusters [66, 89]. Whereas, the SFR in high-redshift BCGs tend to be higher in dynamically active, non-cool-core clusters [205, 43]. CHIPS1911+4455 may represent a low-redshift analog of these high-redshift systems, allowing us to study physical processes that may have been much more common at early times. Below, we speculate on possible explanations for the observed starburst.

In the precipitation scenario [325] for AGN feeding and feedback, cool clouds condense and can form stars or fuel AGN feedback when the cooling time ($t_{\rm cool}$) is significantly shorter than the timescale for the cloud to fall to the center of the cluster potential ($t_{\rm ff}$). The latter timescale is a proxy for the mixing time of the cooling gas. The threshold for thermal instability is usually taken to be $t_{\rm cool}/t_{\rm ff} < 10$ [e.g., 325, 121], but this depends on the medium's susceptibility to condensation, the slope of the entropy profile, the amount of turbulence, and the amplitude of entropy perturbation [329, 327]. If a dense, low-entropy core is perturbed from the center of the gravitational potential, the timescale for mixing is increased while the cooling time remains constant, leading to an enhancement in thermal instabilities. Further, the separation of the low-entropy gas from the direct influence of the central AGN could prevent $\rm t_{cool}$ from increasing. This displacement of low-entropy gas from the central massive galaxy would happen naturally during a merger (i.e., in CHIPS1911+4455). The X-ray data in Fig. 4-1 support this scenario, depicting a disturbed cool core elongated in the north-south direction. While the bulk of the cool, star-forming gas extends along a southern-pointing filament, there is a fainter blue filament that connects the central BCG to the more northern X-ray peak. This suggests that the northern X-ray peak might contain low-entropy gas that is dislodged from the location of the BCG. The existence of this system – a dynamically active but rapidly

cooling core – provides evidence that mergers may stimulate star formation and enhance cooling. This process would be especially relevant in the distant universe when mergers were more common compared to the present time [108].

Closely related to this, in the chaotic cold accretion scenario [CCA; e.g., 120] turbulence is a key ingredient to drive direct nonlinear thermal instability and extended condensation. During CCA the global driver can be tied not only to AGN feedback, but to mergers too, which can stimulate a significant amount of turbulence [e.g., 176] and density fluctuations at large injection scales, enabling enhanced condensation.

In summary, there are multiple ways that a recent cluster-cluster merger could enhance cooling: by increasing the fallback time of a low-entropy cloud (lowering $t_{\rm cool}/t_{\rm ff}$), by physically separating the cool gas and the heat source (AGN), and by increasing the local turbulence, leading to larger density fluctuations. The inclusion of dynamically active clusters in the suite of high-resolution, zoom-in simulations that study the detailed interplay between radio-loud AGN and the cooling, multiphase ICM [e.g., 120], is a necessary next step toward understanding the relative importance of these phenomena.

4.5 Conclusion

In this work, we present new data from Hubble, Chandra, and the Nordic Optical Telescope. Our findings are summarized as follows:

1. We measure the ICM density in the core ($r < 10\,$kpc) of CHIPS1911+4455 to be 0.09 cm^{-3}, which is typical for a cool-core cluster. The core entropy is 17^{+2}_{-9} keV cm^2, which is within the lowest 10% for cluster cores from the ACCEPT samples [67]. The low-entropy core is a clear signature of strong cooling in the center of the cluster.

2. The X-ray morphology of CHIPS1911+4455 is highly peaked in the center (96th percentile for "peakiness") and very asymmetric (7th percentile for "symmetry") compared to a large sample of X-ray-selected clusters. This contradiction in

its morphology between a relaxed (peaky) cluster and a dynamically active (asymmetric) cluster is highly unusual, and is rarely observed.

3. Based on the [O II] emission line luminosity, we measure an SFR in the BCG of $189^{+25}_{-22}\,M_\odot\,yr^{-1}$. This is consistent with an estimate based on the mid-IR continuum of $143^{+31}_{-26}\,M_\odot\,yr^{-1}$. This BCG is among the five most star-forming BCGs in the low-z universe. Data from Hubble confirm that this emission is extended in complex blue filaments near the BCG, with no evidence for an ongoing merger.

4. Based on the highly asymmetric X-ray morphology on small ($\sim$20 kpc) scales, coupled with the exceptionally low core entropy, we propose that rapid cooling in this system may have been triggered by a dynamical interaction between two similar-mass clusters. In this scenario, some of the low-entropy gas from the more massive cluster is dislodged from the central AGN-hosting galaxy. For the low-entropy gas separated from the central galaxy, cooling is more favorable due to the longer mixing times, enhanced large-scale turbulence and CCA rain, and lack of a direct heat source (AGN). This system may provide a link to high-redshift clusters, where previous studies have found an abundance of star-forming BCGs in dynamically active clusters.

CHIPS1911+4455 is the first low-redshift ($z < 1$) galaxy cluster with this distinctive characteristic (hosting a high star-forming BCG and a strong cool-core but having a disturbed morphology). The cluster was discovered by the Clusters Hiding in Plain Sight (CHiPS) survey because of its exceptionally bright cool core that appears to be pointlike in previous X-ray cluster catalogs [292]. CHIPS1911+4455 represents a unique opportunity to understand the relationship between a merging galaxy cluster and star formation in its BCG, which, in turn, unravels an alternative method to form cooling flows and massive starbursts apart from a simple accretion model. This mechanism will become much more important at high redshift ($z > 1$) when the cluster merger rate is significantly higher [108, 205].

Part II

The Evolution of AGN Activity in Brightest Cluster Galaxies

Chapter 5

The Evolution of AGN Activity in Brightest Cluster Galaxies

The content of this chapter was submitted to The Astrophysical Journal *on June 30, 2021 as* The Evolution of AGN Activity in Brightest Cluster Galaxies

5.1 Introduction

Galaxy clusters are the most massive gravitationally bound objects in the universe [326]. Because of their extremely deep potential wells, the temperature of the intracluster medium (ICM) is high enough to radiate X-rays. The central parts of clusters, which have the densest X-ray-emitting gas, often have their cooling times shorter than the Hubble time, implying that the hot X-ray gas should have had enough time to cool and form large inward flows of cooling material, known as cooling flows [103, 274]. However, multi-wavelength observations have only seen a fraction of these massive cooling flows which are expected from standard cooling models [e.g., 91, 207, 239]. This is referred to as “the cooling-flow problem", and active galactic nuclei (AGN) feedback is thought to be responsible for preventing the hot gas from cooling by propagating energy from the supermassive black hole (SMBH) to the ICM. The two primary modes of AGN feedback are the kinetic mode, with relativistic jets pushing aside the hot gas and creating cavities, and the quasar mode, with the radiation

coming from the accretion disk [see reviews by 104, 215].

With the recent development of galaxy cluster surveys which utilize the Sunyaev-Zel'dovich (SZ) effect [306], such as the South Pole Telescope [SPT; 36, 37, 63, 154] and the Atacama Cosmology Telescope [ACT; 146, 145], the number of known high-z ($z > 1$) clusters with good mass estimates has increased dramatically. This has enabled many studies of the evolution of AGN feedback in clusters over cosmic time [132, 203, 206]. However, the evolution of AGN feedback in galaxy clusters with redshift remains poorly understood. In particular, Hlavacek-Larrondo et al. [149] found no evidence for evolution in jetted power generated by AGN feedback from X-ray cavities over the past 7 Gyr ($z = 0.8$). An earlier study by Hlavacek-Larrondo et al. [148] suggested that the fraction of brightest cluster galaxies (BCGs) with X-ray bright nuclei is decreasing with time (or increasing with redshift), suggesting a strong evolution in radiative mode feedback. In contrast, a recent study looking for nuclear BCG X-ray emission in Chandra archival data instead found no evidence for evolution between two redshift bins ($\langle z \rangle \sim 0.25$ and $\langle z \rangle \sim 0.65$) [339]. The disagreement between various studies about the evolution of AGN feedback restricts our ability to fully understand this issue.

In this work, we calculate the AGN-hosting BCG fraction by identifying BCGs in the 2500 deg^2 SPT-SZ cluster samples [36] and classifying whether they are AGNs, based on mid-infrared data. The fraction of BCGs hosting luminous AGNs is an important indicator for AGN fueling processes, availability of cold clumpy gas in the centers of clusters, the duration and duty cycle of the AGNs, and how BCGs and the host clusters grow and evolve together. This is because additional physical mechanisms are often required to explain the transport of the cold gas, which serves as the primary fuel source for the central black holes. The fact that we find a relative absence of AGNs in the centers of clusters has led us to study many physical processes, including ram-pressure stripping [130], tidal effects from the cluster gravitational potential [223], and the lack of new infall of cold gas [175]. Similarly, understanding the evolution of AGN activities in BCGs will help us understand the evolution mechanism of galaxy clusters, and how the feedback might play a role in that.

Our goal for this paper is to study the redshift evolution of the AGN-hosting BCG fraction up to $z = 1.3$ to understand the fueling processes in the centers of clusters, determine when AGN feedback is fully established, and identify whether there is any more extreme AGN-hosting BCGs in the sample, similar to the Phoenix cluster. The paper is organized as follows. In Section 5.2 and Section 5.3 we summarize the data and additional information used in this paper. The results and their implications are presented in Section 5.4 and Section 5.5, respectively. We conclude our work in Section 5.6. We assume $H_0 = 70\,\mathrm{km\,s^{-1}\,Mpc^{-1}}$, $\Omega_\mathrm{m} = 0.3$ and $\Omega_\lambda = 0.7$. All errors are 1σ unless noted otherwise.

5.2 Data

5.2.1 The SPT-SZ 2500 deg^2 Cluster Sample

We use the full 2500 deg^2 SPT-SZ cluster sample from Bleem et al. [36] with the improvement in the cluster redshift estimates from Bocquet et al. [39] by incorporating new spectroscopic and improved photometric measurements [18, 163]. The survey spans a contiguous 2500 deg^2 area within a boundary of RA = 20h–7h, and Dec. = -65°–-40°. Once we limit the redshift range to $0 < z < 1.3$, the total number of clusters in our sample is 475.

5.2.2 Position of BCGs

Given the diversity of BCG colors, morphologies, and assembly state as a function of redshift, typical identification algorithms may be biased when they select BCGs based on single-band fluxes. We have instead developed a novel BCG identification pipeline that utilizes the full probability distribution of redshift and stellar mass for every object within 500 projected kiloparsec of the SZ cluster center to assign BCG likelihoods. Photometry is provided by the Dark Energy Survey (Year 3) catalogs [158, 280], cross-correlated with unWISE [173], which is a combination of WISE and NEOWISE images. Various cuts and flags are utilized to avoid stars, and objects

with poor photometric measurements. Probability distributions of photometric redshift and stellar mass for each source are estimated with EAZY [51] and FAST [171], respectively. We then randomly sample from each distribution to find the most massive cluster galaxy at the cluster redshift within each field, iterating this process 10^5 times to build up a BCG likelihood for each galaxy. In this way, all galaxies are assigned a value between 0 to 100% probability of being the BCG within each cluster. Full details on the pipeline, along with the BCG catalog, will be provided in Noble et al. (in preparation). The top three panels of Fig. 5-1 show optical images of example SPT galaxy clusters with identified BCGs in white squares. This demonstrates that the algorithm selects likely BCGs that match the galaxies that typical/traditional visual BCG identification methods would select cover a wide range of redshift.

5.2.3 Data for AGN Selection

Most photometric techniques for identifying AGNs are severely biased toward unobscured (type 1) AGNs since their nuclear emissions dominate over host galaxies, making these AGNs easily identifiable. This implies that most obscured (type 2) AGNs are often underrepresented in most studies. The most promising techniques for identifying both obscured and unobscured AGNs include radio, hard X-ray, and mid-infrared selections. However, not all AGNs are radio loud [e.g., 301] and the current hard X-ray satellites remain limited in their sensitivity and field of view. This leaves mid-infrared selection as a popular technique to quickly identify large AGN populations (obscured and unobscured). The idea of mid-infrared selection is to separate between the power-law AGN spectrum and the blackbody stellar spectrum of galaxies, which peaks at rest frame $1.6\,\mu m$. The power-law spectra of the AGNs is due to the thermal emission from the warm-hot dust in the torus, which is heated by absorbing shorter wavelength photons from the accretion disk [140, 303]. This implies that the emission is not strongly suppressed by the dusty torus, unlike UV to near-IR wavelength, allowing this technique to detect more obscured AGNs. Additionally, with the first all-sky data release of Wide-field Infrared Survey Explorer [WISE; 337] in 2012, mid-infrared selection became one of the top methods of probing the AGN

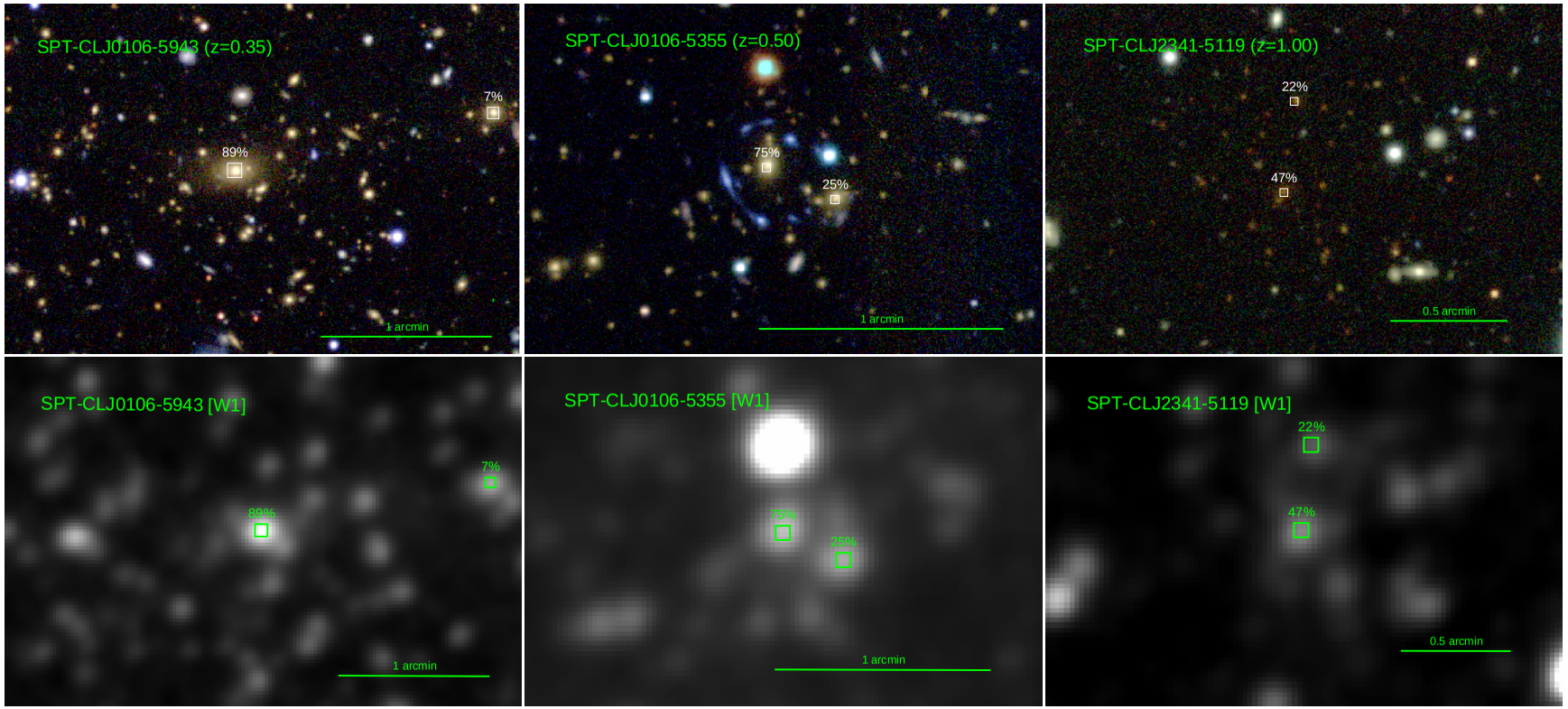

Figure 5-1 The top three panels show *gri* optical images of three SPT galaxy clusters, including SPT-CLJ0106-5943, SPT-CLJ0106-5355, and SPT-CLJ2341-5119. The white boxes show the location of the two highest-probability BCG candidates for each cluster while the white numbers show the probability (in percentage) for each object to be a true BCG. The three examples are ranging from $z = 0.35$ to $z = 1.00$, demonstrating the ability for this method to find BCG candidates up to high redshift. The bottom three panels show the corresponding W1 images from WISE for the three SPT clusters. The green boxes show the same location of the two highest-probability BCG candidates, suggesting that the BCG candidates are detectable in mid-IR.

population over the entire sky without additional observations.

One drawback of the mid-IR technique is that the dilution from the host galaxies limits the mid-IR color from selecting low-luminosity AGNs [303]. This means that AGNs selected by the mid-IR color tend to be brighter relative to the host galaxies than those selected by other techniques. For example, Assef et al. [10] found that in the sample of relatively luminous AGNs ($L_{\rm AGN}/L_{\rm host} > 0.5$), the luminosity of mid-IR AGNs tends to be greater than $\sim 5 \times 10^{44}\,{\rm erg\,s^{-1}}$, taking into account the bolometric correction [288]. Assuming the efficiency of turning accreting matter into energy $\epsilon_{acc} = 0.1$ and a typical mass of the supermassive black hole $M_{\rm BH} \sim 10^8$–$10^9\,M_\odot$ [268], the black hole mean accretion rate ($\dot{M}_{BH} = L_{\rm bol,nuc}/\epsilon_{acc}c^2$) of mid-IR selected AGNs should be greater than 4×10^{-3}–$4 \times 10^{-2}\,\dot{M}_{\rm Edd}$, where $\dot{M}_{\rm Edd}$ is the limiting Eddington accretion rate. This level of accretion is relatively high, compared to typical optical/radio AGNs, which have an accretion rate at around 10^{-6}–$10^{-2}\,\dot{M}_{\rm Edd}$ [213]. This implies that the mid-IR technique will identify mainly a brighter and more massive AGN population. From now on, AGNs mentioned in this paper mean the mid-IR-selected AGN population.

5.2.3.1 Mid-IR Data from WISE

WISE is an infrared-wavelength space satellite with four IR filters, including $W1$ ($\lambda_{cen} = 3.6\ \mu m$), $W2$ (4.3 μm), $W3$ (12 μm), and $W4$ (22 μm) [337]. The satellite operated for two years with cryogen until 2011, before reactivated and resumed operation as NEOWISE in 2013, and has continued to observe ever since [187]. Instead of using the main source catalog from WISE (AllWISE) that only includes the data obtained from 2010 to 2011, we make use of CatWISE to get the best photometry with available data. CatWISE is an updated all-sky infrared source catalog, which combines the 2010 and 2011 data from WISE with the 2013 through 2016 NEOWISE data [102]. The caveat is that the CatWISE catalog only includes 3.6 ($W1$) and 4.3 ($W2$) μm data. In this work, we use the Preliminary CatWISE catalog to obtain the WISE color for each BCG, which has an advantage of including four times as many exposures as that used for the AllWISE catalog while using the same AllWISE

software, making it more straightforward to make a comparison with previous works.

For every BCG identified (with probability $> 5\%$) from Section 5.2.2, we search for mid-IR counterparts in the CatWISE catalog within a radius of $3''$ from the identified BCG, since the typical FWHM for $W1$ and $W2$ are $6.08''$ and $6.84''$, respectively. Both $W1$ and $W2$ are converted from Vega to AB magnitudes using the correction from the Explanatory Supplement to the WISE Products[1]. The bottom three panels of Fig. 5-1 shows $W1$ images of the three SPT clusters, showing that their BCG candidates can be detected with WISE data.

5.2.3.2 CatWISE Color Correction

We perform a comparison test between the AllWISE and CatWISE catalogs. The test is carried out by comparing the $(W1 - W2)_{\rm AB}$ color of bright objects ($16.5 < W1_{\rm AB} < 18$) between the two catalogs within 10 arcmins of one field. The objects are plotted in Fig. 5-2, showing the offset between the color from AllWISE and CatWISE to be around 0.042. Further investigation reveals that this is due to the gradual diminishing of the $W2$ throughput with time, leading to a bluer $(W1-W2)_{\rm AB}$ color, compared to AllWISE. We apply this correction of 0.042 mag to CatWISE $W1-W2$ colors.

5.3 Method

5.3.1 AGN Selection

With the *WISE* satellite, Stern et al. [303] developed a well-known formula to quickly identify AGN candidates with a simple color criterion, $(W1 - W2)_{\rm Vega} \geq 0.8$ or $(W1-W2)_{\rm AB} \geq 0.16$. One benefit of mid-IR selected samples is that both unobscured (type 1) and obscured (type 2) AGN can be identified [172, 302, 303]. However, since the colors of galaxies drastically change over a large redshift range, this simple criterion is not accurate enough to characterize a large population of AGNs. To

[1] wise2.ipac.caltech.edu/docs/release/allsky/expsup/sec4_4h.html

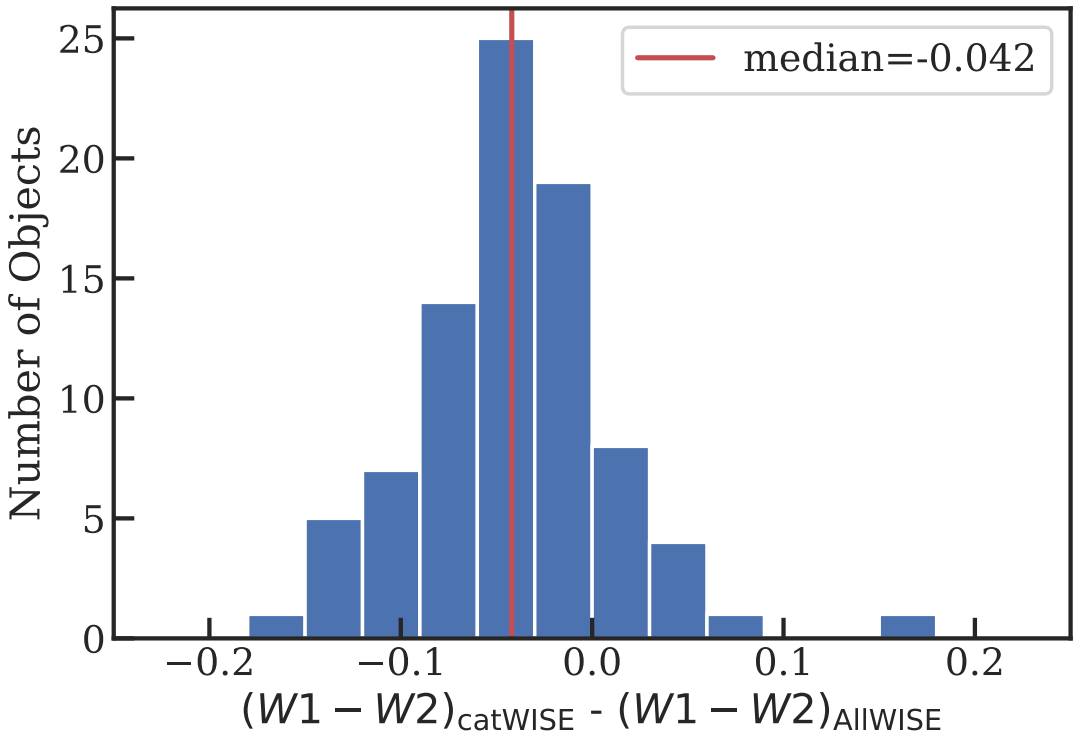

Figure 5-2 This figure shows a comparison of $W1-W2$ between AllWISE and CatWISE. The red line is the median of the difference at 0.042 mag.

increase the number of AGNs we can identify, we develop a new color criterion which depends on redshifts of galaxies.

5.3.1.1 EzGal Galaxy Color Model

To determine whether each BCG harbors an AGN, we calculate the expected color for typical elliptical galaxies using EzGal[2]. EzGal calculates the magnitude evolution as a function of redshift from evolving the spectral energy distribution (SED) models of a stellar population with time and projecting them through filters [188]. This calculation takes into account both the stellar evolution of a galaxy as young stars evolve as well as the wavelength shift due to the distance of a galaxy. To find the model that best describes our overall sample, we perform a grid search between three stellar population model sets [i.e., 56, 80, 193], various formation redshifts, two different initial mass functions (IMF) [i.e., 69, 272], star formation history as a single exponential decaying burst of star formation with an e-folding time parameter (τ) between 0.1 and 10 Gyr, and the representative metallicity (Z) for our galaxy sample from 0.001 to 0.03. Ultimately, the best-fit model (based on the Chi-square test) is the Bruzual and Charlot [56] stellar model with a formation redshift of (z_f) 3.5, the Salpeter [272] IMF, $\tau = 0.1$ Gyr for star formation history, and the metallicity of 0.016. The orange line in the top panel of Fig. 5-3 shows the expected $W1 - W2$ color evolution, generated from the EzGal model with this particular set of parameters. The bottom panel shows the residual from the expected value of $W1$-$W2$ for each BCG. It demonstrates that the scatter is distributed around zero with extremely small trend, implying that we have successfully removed the continuum contribution. In this work, galaxies which are redder (the residual greater than 0.2) than typical elliptical galaxies based on the EzGal model are considered AGN candidates. For a range of threshold values from 0.2 to 0.6, the highest redshift bin has more AGN-hosting BCGs, compared to the lowest redshift bin, implying that an increase in the fraction of AGN-hosting BCGs is independent of this choice.

One assumption we apply in this section is that we only consider a single-burst

[2]www.baryons.org/ezgal/

stellar population model with a single formation redshift, star formation history, and metallicity. Even though this simple model is likely not sufficient to describe our data, it is currently not possible to use multiple stellar population models since they would require a much larger sample of BCGs and more multiwavelength data to get a good constraint on the models. With a single-burst model, we find that the slope of the expected $W1$-$W2$ at high redshift could not be steeper than our fitted model, implying that there is no other steeper-slope model that could explain the evolution trend at high redshift. This means that the redder mid-IR color that we observe could mean either that there are in fact more AGN at high redshift or our single-burst population model is not adequate to describe the data. We should keep this caveat in mind when we discuss the implication of our results.

As a test to see how a starburst can affect the mid-IR color, we consider Abell 1835 [100] and MACS J1931.8-2634 [147], which are the most star forming BCGs known [SFR $\sim 100\,M_{\odot}\,\mathrm{yr}^{-1}$ 207] that also lack evidence of a strong AGN. The two colored stars in Fig. 5-3 demonstrate that even though a star-forming BCG would have boosted mid-IR emission due to dust, polycyclic aromatic hydrocarbon molecules (PAH), and molecular gas, the emission is not as strong as the power-law spectra of AGNs, and our selection does not include these two BCGs. On the other hand, the two clusters with the most luminous AGNs (H 1821+643 and IRAS 09104+4109) are easily detected with our criterion.

5.3.1.2 Spitzer Color Verification

Because the point-spread function (PSF) of the two WISE bands are not small ($\mathrm{PSF}_{W1} = 6.''08$ and $\mathrm{PSF}_{W2} = 6.''84$), we compare the results from *WISE* mid-IR color with those from the *Spitzer* Space Telescope. *Spitzer* is an infrared telescope with the Infrared Array Camera [IRAC; 111] as one of its main science instruments. IRAC is a four-channel imaging camera capable of taking simultaneous images at wavelengths of 3.6, 4.5, 5.8, and 8.0 μm. Thus, the channel 1 and 2 ([3.6] and [4.5]) on IRAC are roughly equivalent with $W1$ and $W2$ from *WISE*, but with a benefit of having a much better PSF at $1.''95$ and $2.''02$, respectively [111].

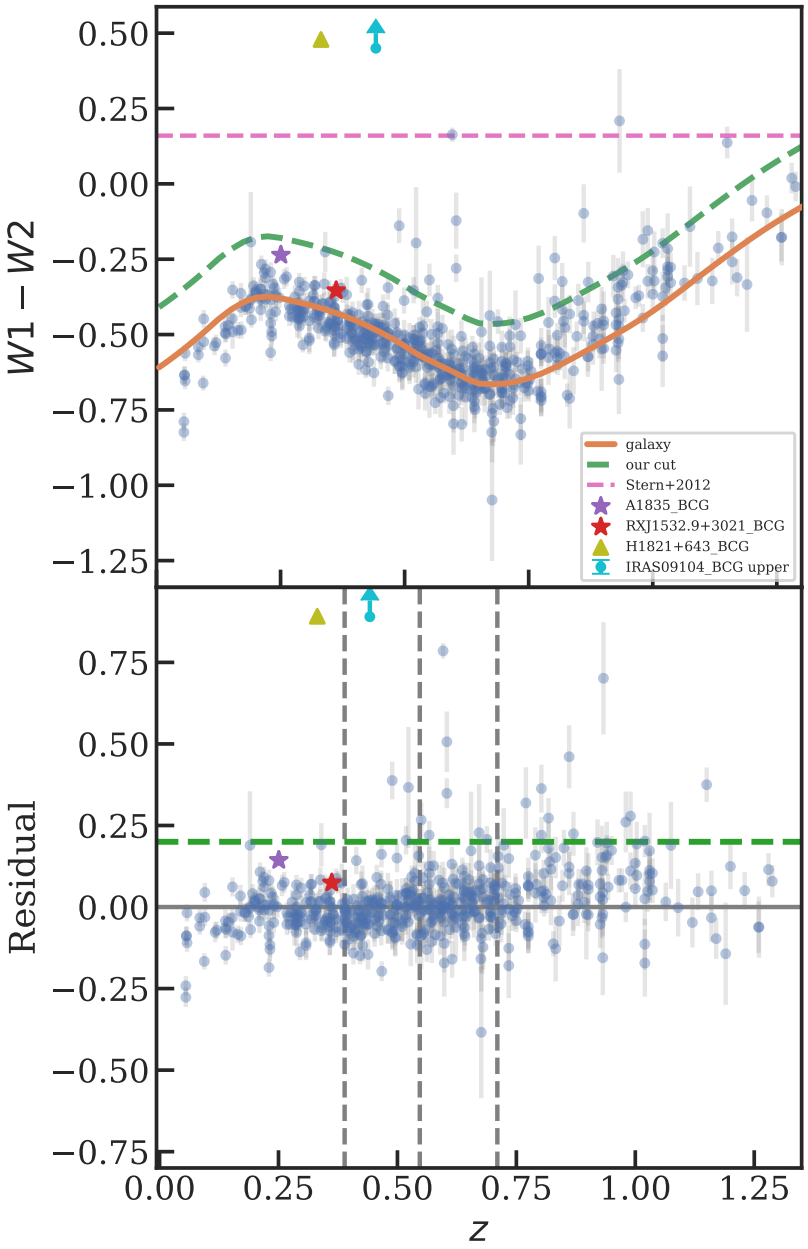

Figure 5-3 Top: $W1$-$W2$ color for each BCG candidate as a function of cluster redshift. The orange line shows the expected color as a function of redshift for our elliptical galaxy model using EzGal, as described in Section 5.3.1.1. The green line shows our criterion for selecting AGNs, which is derived from the orange line, and the pink line shows the cut from the previous work by Stern et al. [303]. Bottom: the $W1$-$W2$ color difference between each BCG candidate and the expected color. Every object with the residual greater than 0.2 is likely to be an AGN. The vertical gray dashed lines show the binning for the results in Fig. 5-5. The two colored stars are known galaxy clusters with large SFR, showing that our selection criterion does not select these starburst BCGs, while the two clusters with luminous AGNs (H 1821+643 and IRAS 09104+4109) are clearly above our criterion.

A certain fraction of the SPT cluster sample has been observed with IRAC. For verification, we compare the [3.6]-[4.5] colors of our AGN-hosting BCG candidates with their $W1-W2$ colors. If the Spitzer color, which has a higher angular resolution, is bluer (smaller) than the WISE color, it shows that there is a contamination from nearby galaxies within the WISE aperture. On the other hand, if the Spitzer color is redder (larger), it implies that the object is even more likely to be an AGN. Fig. 5-4 shows the comparison between WISE's $W1-W2$ (in gray squares) and Spitzer's [3.6]-[4.5] color (in circles) for our AGN candidates. We find that most AGN candidates have IRAC infrared color difference either compatible or larger than the WISE ones. This suggests that most of our AGN candidates are likely to be real quasars. One clear exception is SPT-CL J2146-4633, which has a WISE color much redder than Spitzer. Further investigation shows that there is a point-like source near the location of the object, but not at the BCG location, meaning that the WISE color is probably contaminated by a nearby AGN while the Spitzer color is not.

5.3.2 Calculating the AGN fraction

We compute the fraction of galaxy clusters with AGN-hosting BCGs based on the number of BCGs whose mid-IR colors are redder than expected, as described in Section 5.3.1.1, in four redshift bins to study the redshift evolution. With the probability estimated in Section 5.2.2, we first include in Fig. 5-3 all the BCGs which are identified with a probability that is higher than 20%, meaning that some clusters will have more than one BCG candidate. The fraction of AGN-hosting BCGs are calculated over the total number of BCG candidates, instead of the total number of clusters in each bin. The bins are defined from $z = 0$–1.3 in such a way that each bin contains roughly the same number of BCG candidates ($\sim$140 BCGs). We will discuss these particular choices of calculating AGN-hosting BCG fraction in Section 5.4. The uncertainties associated with the AGN fractions are estimated by combining the measurement errors associated and the corresponding binomial uncertainty derived from Cameron

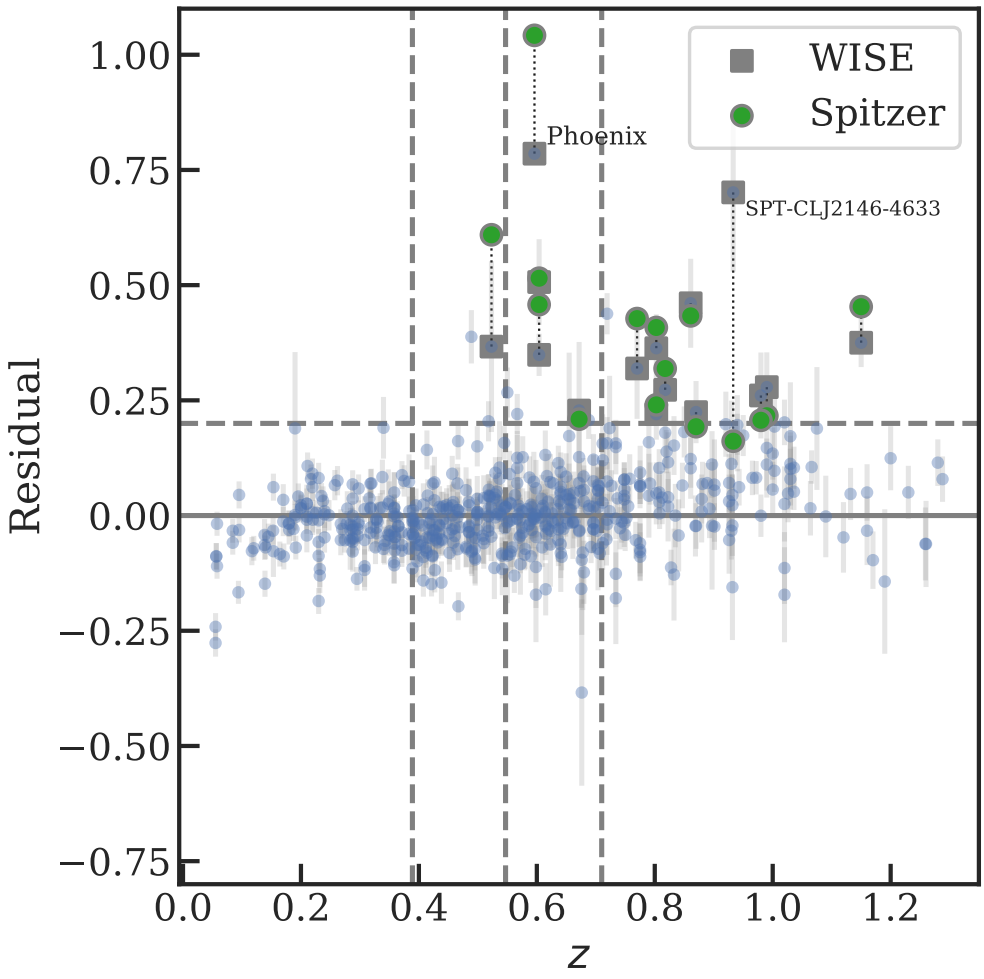

Figure 5-4 The residual plot similar to the bottom panel of Fig. 5-3. The blue points are the $W1$-$W2$ color difference between each BCG candidate and the expected color. The gray squares emphasize the $W1$-$W2$ color from WISE for the sample which has been observed by Spitzer while the colored circles show the color from Spitzer, demonstrating that most of the objects we classify as AGNs have a difference of Spitzer and WISE color to be either compatible (60% of the sources have a difference to be within ± 0.07 mag) or Spitzer is slightly redder (33% of the sources have the Spitzer color larger than the WISE one by $\sim$0.2 mag). This means the color and our results are not strongly impacted by WISE's larger PSF.

[62]. In particular, we use a beta probability distribution:

$$B(a,b) = \frac{(a+b-1)!}{(a-1)!(b-1)!} p^{a-1} q^{b-1}, \tag{5.1}$$

where k is a number of successes in a series of n independent trials, $a = k+1$, $b = n-k+1$, p is the probability of success, and $q = 1-p$, respectively, which is a normalized version of a 'binomial distribution,' as a likelihood function. By assuming the Bayes-Laplace uniform prior, for which $P_{prior}(p) = 1$ for $0 < p < 1$, we treat this beta distribution for p as a posterior probability distribution, which can then be used to estimate the Bayesian confident intervals directly Cameron [62].

5.4 Results and Verification

The blue points in Fig. 5-5 show the fraction of AGN-hosting BCGs in the four redshift bins with their corresponding 68% confidence intervals. We observe 3.4σ evidence that the fraction is increasing with redshift in the SPT sample, given the size of the bins in this work. The gray points show the fraction of points that have residuals less than -0.2. If the scatter is truly random, there should be a similar number of points below -0.2, compared to those above +0.2, which are classified as AGNs. This result implies that the increasing trend of the AGN-hosting BCGs fraction is not a result of the data quality. Such a trend has been suggested and shown in previous works [e.g., 33, 148, 205, 226]. In particular, we show that the fraction is $\sim$2% at $z \approx 0.5$ which is consistent with what Somboonpanyakul et al. [294] found from looking at extreme central BCGs in clusters. We note that since some AGN-dominated galaxies will have poor photometric redshift constraints as they are estimated from the stellar spectrum and not AGN's power-law spectrum, we might misidentify these galaxies in our BCG finding algorithm. This implies that the number of BCGs with central AGNs found in this work gives a lower limit on the AGN-hosting BCG fraction, and the actual evolution could be even stronger.

The two main assumptions applied for this work are 1.) we include all BCG

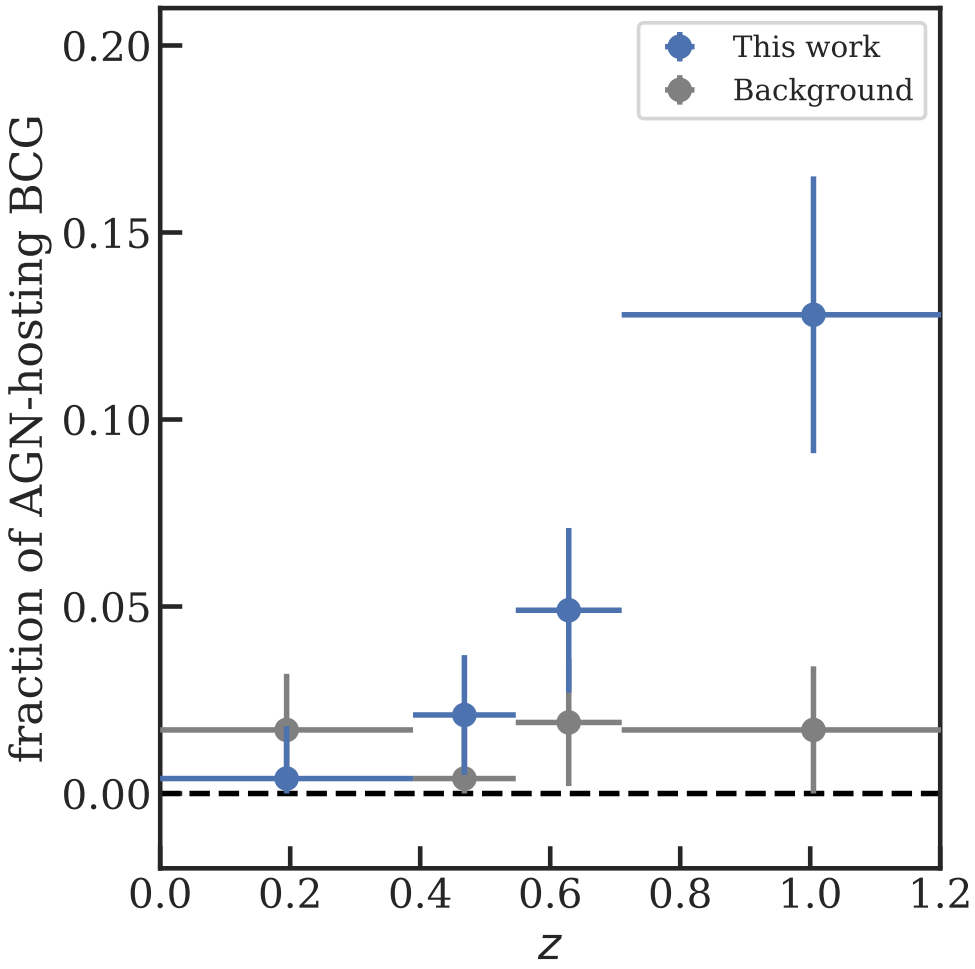

Figure 5-5 The fractions of clusters with AGN-hosting BCGs as a function of redshift. Blue points show the fractions from this work, which comes from the $W1-W2$ color residual in the SPT sample. The size of the error bar takes the binomial uncertainty into account. Gray points show the fraction of points that have residual less than -0.2, which we consider a “background". This figure demonstrates that the fraction of AGN-hosting BCG increases with redshift.

candidates with probability higher than 20% in our sample, instead of picking only one BCG per cluster, and 2.) we calculate the fraction of BCGs with AGNs over the total number of BCG candidates, and not the fraction of clusters with AGN-hosting BCGs over the total number of clusters. The reason for these two assumptions is that we want to include AGN-hosting BCGs from systems with more than one obvious BCG, which are typical for merging systems such as the Coma cluster [342], and the Bullet cluster [195]. We perform consistency checks to address both of these assumptions. Fig. 5-6 shows the fraction of AGN-hosting BCGs when we consider the most likely BCG candidates, every BCG candidate with the probability higher than 20%, and every BCG candidate with the probability higher than 10%, respectively. This figure shows that the increasing trend of the fraction of AGN-hosting BCGs over redshift remains consistent in all three scenarios, regardless of how we select BCGs.

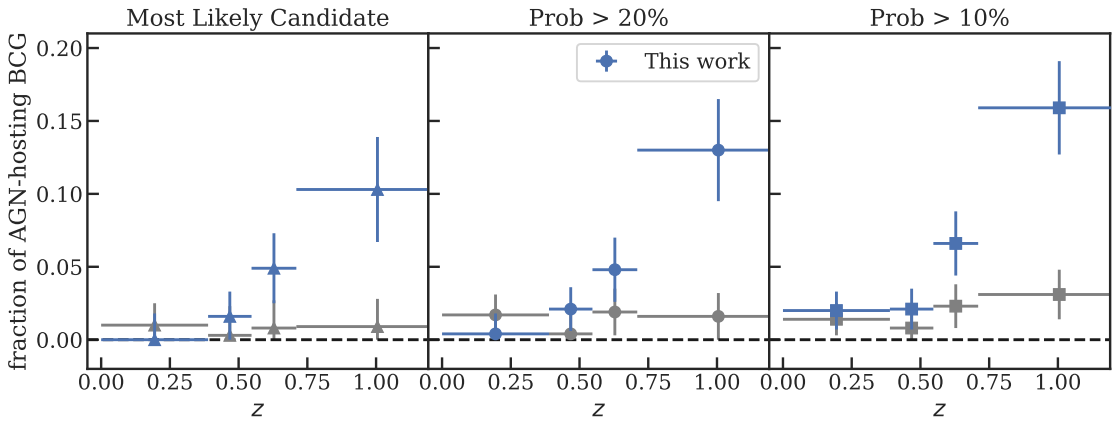

Figure 5-6 All three panels show the fractions of clusters with AGN-hosting BCGs, similar to Fig. 5-5. The left panel (triangles) shows the fraction when we consider only the most likely BCG for each cluster. The middle panel (dots) includes all possible BCGs with probability higher than 20% while the right panel (squares) includes those with probability higher than 10%. With all scenarios, the fraction remains increasing as a function of redshift.

On the other hand, Fig. 5-7 shows the results when we use different definitions of AGN fractions. The gray and blue points in Fig. 5-7 are calculated with the total number of clusters as a denominator, instead of the number of BCG candidates. For the blue points, we consider one BCG per cluster and include both the probability of

being BCGs, as calculated in Section 5.2.2 and the uncertainty of the mid-IR color for each BCG to emphasize the fact that the uncertainties of identifying BCGs and BCG colors are higher at high redshift. The empty gray dots are the largest possible fractions, which are calculated from clusters that have any of their potential BCGs to be considered as AGNs, while the empty gray squares are the smallest possible fractions by counting only clusters which have all of their BCG candidates to be classified as AGNs. This figure illustrates that all of these definitions qualitatively give the same conclusion to our initial results.

We compare our results with the AGN fraction in field galaxies to determine whether there is a difference in the fractions between the two environments. The green and pink squares in the left panel of Fig. 5-8 show the field X-ray AGN fractions from the zCOSMOS survey [287] and the *Chandra* Multiwavelength Project results [ChaMP; 133], respectively. The results from our work are consistent with these two results, suggesting that the source of fuel required for AGN accretion in field galaxies could be similar to that in the center of galaxy clusters. Additional evidence for the AGN fraction evolution in field galaxies has been seen in other works. For example, Lehmer et al. [178] finds an evolution in early type galaxies ($z \sim 0.7$) consistent with the $(1+z)^3$ pure luminosity evolution model. The gray dotted line in Fig. 5-8 shows the curve for $(1+z)^3$ although it is only intended to be illustrative since it is arbitrarily normalized. The dashed line instead shows the curve for $(1+z)^{5.3}$, which seems to better fit with our results. This line is first suggested by Martini et al. [198] who show the AGN fraction of cluster members to increase as $\sim (1+z)^{5.3}$ for AGN above an X-ray luminosity $L_x > 10^{43}\,\mathrm{erg\,s^{-1}}$, hosted by luminous galaxies. We also fit the power law model ($\propto (1+z)^{\alpha}$) to the blue points in Fig. 5-8 and find a power law exponent $\alpha = 5.4 \pm 0.5$, which is consistent with the results from Martini et al. [198]. Nevertheless, there are caveats regarding the relationship between cluster BCGs and field galaxies. One concern is that the AGN selection criteria for both BCGs and field galaxies are different, making it difficult to make a direct comparison between the two. In addition, according to the work about the evolution of AGN luminosity [137, 286] which shows that AGNs in galaxies tend to be brighter at high

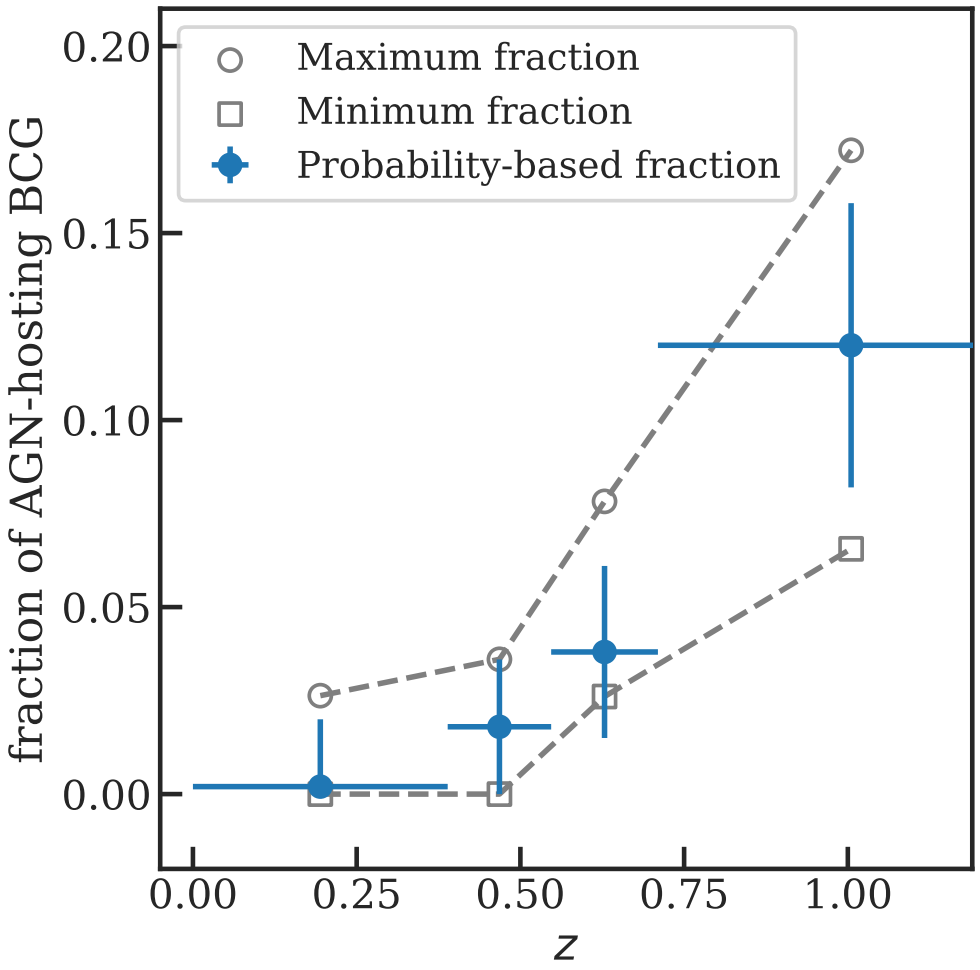

Figure 5-7 The fractions of clusters with AGN-hosting BCGs, similar to Fig. 5-5. The blue points assume one BCG per cluster and incorporate the probability of being a BCG, estimated from Section 5.2.2. The empty gray dots are for clusters which have any of their potential BCGs to be considered as AGNs, which is equivalent to the maximum fraction. The empty gray squares only include clusters whose BCG candidates are all considered AGNs, which is the minimum fraction. This figure shows that all of these definitions qualitatively give the same conclusion to our initial results.

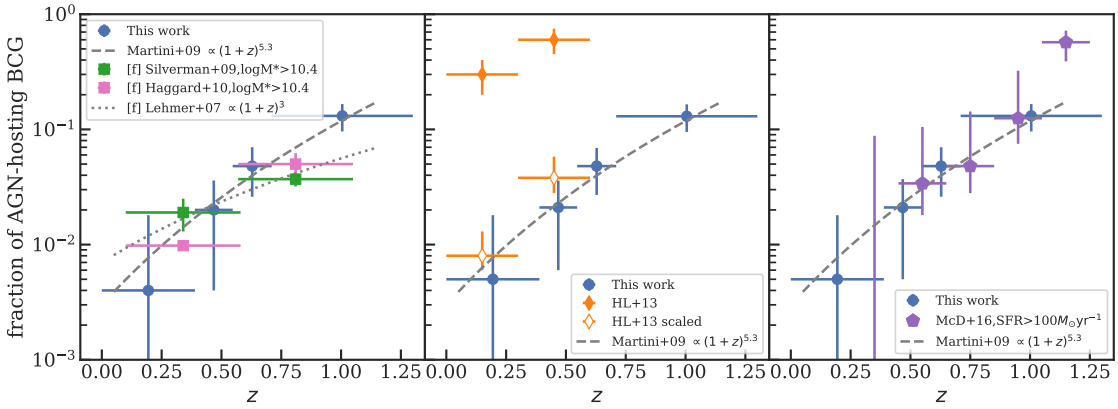

Figure 5-8 Comparison of the fraction of clusters with AGN-hosting BCGs to other published works. Left: Green and pink squares are the field AGN fraction from Silverman et al. [287] and Haggard et al. [133], respectively. The gray dotted line indicates pure luminosity evolution $\propto (1+z)^3$, suggested by Lehmer et al. [178], while the gray dashed line shows the $(1+z)^{5.3}$ line, suggested by Martini et al. [198]. Middle: Orange diamonds show the estimated fractions of BCGs with bright AGNs ($\log_{10}(\mathrm{L_{X,nuc}}\,[\mathrm{erg\,s^{-1}}]) > 42.2$) from Hlavacek-Larrondo et al. [148] with orange open diamonds showing the scaled version by changing the total number of clusters to a larger parent sample which Hlavacek-Larrondo et al. [148] had drawn from since this work only focuses on highly X-ray-luminous clusters ($L_X > 3 \times 10^{44}\,\mathrm{erg/s}$). Right: Purple points show the fraction of BCGs with SFR $> 100\,M_\odot\,\mathrm{yr}^{-1}$ from McDonald et al. [205].

redshift, we would naturally expect to find a higher AGN fraction at high redshift since we usually selected AGNs based on a certain luminosity threshold. [198].

5.5 Discussion

The results obtained in Section 5.4 demonstrate that there is an increase in the fraction of AGN-hosting BCGs with redshift. This finding is consistent with previously published studies [e.g., 33, 148], which focus on different samples with distinct selection effects. In particular, the results from Hlavacek-Larrondo et al. [148] and ours, as shown in the middle panel of Figure 5-8, show the same trend of increasing fraction of AGN-hosting BCGs with redshift. However, the normalizations are vastly different. Hlavacek-Larrondo et al. [148] claimed that the fraction of active BCGs is

30% at $z \approx 0.1$ and 60% at $z \approx 0.5$. On the other hand, we show that the fraction is less than 20% at all redshift bins. A possible explanation is the very different samples that these works consider. While this study is based on an effectively mass-selected sample of clusters, with no consideration of X-ray properties, the sample used by Hlavacek-Larrondo et al. [148] focuses solely on highly X-ray-luminous clusters ($L_{X,\mathrm{cluster}} > 3 \times 10^{44}\,\mathrm{erg\,s^{-1}}$), which show clear X-ray cavities. To put these two studies on the same scale, we modify the denominator used by Hlavacek-Larrondo et al. [148] in calculating the AGN fraction to account for the full parent population of clusters from which their sample of 32 clusters was drawn. Given that this previous work included a subsample of clusters drawn from the REFLEX [42], eBCS [95], MACS [96], and SPT-XVP [203] surveys, we consider these surveys in their entirety as the total population (the denominator) when calculating the AGN fraction. With this rescaling, we find that the fraction of BCGs hosting bright AGN is consistent between this work and Hlavacek-Larrondo et al. [148], and that the observed evolution is consistent between both studies. This suggests that the X-ray-selected sample has a higher fraction of clusters with AGN-hosting BCGs simply because that particular sample includes exclusively X-ray bright clusters (biased to cool cores) and active galaxies (i.e., high jet power). We note that even though the scaled version of Hlavacek-Larrondo et al. [148]'s work is still biased compared to our sample of AGNs because of different selection techniques (X-ray versus mid-IR), at least the X-ray sample no longer includes only powerful AGNs in the sample, making it more reasonable for a comparison.

An increase of the fraction of BCGs hosting central AGNs with redshift suggests that the accretion rates of the supermassive black holes in the BCGs are higher at high redshift since AGN luminosity is proportional to accretion rate. Several works about the relation between the mean black hole accretion rates and the cavity (kinetic)/quasar (radiative) power of the central AGN [74, 268] have shown that as black hole accretion increases in the BCGs, the cavity power of the AGN also increases to counteract the cooling from the accretion in a form of a negative feedback cycle. However, as the black hole accretion rates rise to near the Eddington limit, the

cavity/jet power seems to be saturated and the radiative power tends to dominate at this level of accretion. The fact that the radiative power from AGNs usually promotes more cooling in the ICM, instead of preventing it, suggests that a well-regulated feedback system between a central black hole and its host cluster is no longer possible at high accretion, implying that some galaxies might not have a fully established AGN feedback loop at this redshift range.

A similar conclusion has been reached from the work related to star forming galaxies [43, 205, 331], which have shown that the fraction of starburst BCGs is higher at high redshift ($z > 1$). Specifically, McDonald et al. [205] found the fraction of BCGs with SFR over $10\,M_{\odot}\,\mathrm{yr}^{-1}$ to be $34 \pm 5\%$ at $0.25 < z < 1.25$, compared to $\sim$1–5% at $z \sim 0$. The right panel of Figure 5-8 compares the fraction of AGN-hosting BCGs in this work with the fraction of starburst BCGs ($\mathrm{SFR_{BCG}} > 100\,M_{\odot}\,\mathrm{yr}^{-1}$) from McDonald et al. [205], demonstrating that in the center of cluster environments both massive starburst galaxies and bright AGNs behave similarly. These two results strongly hint that AGN feedback might not be as effective to prevent overcooling at high redshift as we have previously thought.

All of these results lead us to suspect that the reason for the observed redshift trend and the breakdown of AGN feedback at high redshift comes from the fact that there is an abundance of cold gas at that redshift. Typically in the local universe, BCGs grows by merging with gas-poor satellites without triggering any AGN activity. However, BCGs at high redshift could grow by merging, instead, with gas-rich members. Cold gas from the mergers could be a source of fuel for increasing AGN activities in the center of clusters. This is consistent with the picture we get from the studies of starburst BCGs [205, 331] since cold dense clouds from gas-rich mergers could provide enough matter required for creating new stars. This scenario can also explain recent studies about the cool core (CC) fraction which show no sign of evolution over the same redshift range [206, 266]. If AGN feedback breaks down at high redshift, one would expect that the CC fractions of clusters would be higher since more gas should have been cooled near the center. However, if black hole accretion and star formation in high-redshift BCGs are fueled by something other than cooling of the hot gas,

such as gas-rich mergers [15, 152], it would be reasonable to think that the trends of AGN- and starburst-hosting BCG fractions would be different from the trend of CC fraction. If this observed increase in AGN activity is linked to gas-rich mergers, rather than ICM cooling, we would expect to see an increase in scatter in the P_{cav} vs L_{cool} relation [256] at $z > 1$.

Another possible scenario to explain the trend of high AGN-hosting BCG fraction at high redshift has to do with cluster mergers. It has been shown both in simulations [108] and observations [206] that the cluster merger rate is significantly higher at high redshift. Major mergers between two clusters have the potential to disrupt a tightly-regulated AGN feedback loop and promote black hole accretion and star formation by potentially increasing the local turbulence of the system. This is consistent with the turbulent picture in the precipitation model for AGN feedback, called "chaotic cold accretion (CCA)", which states that turbulence is a key component to drive nonlinear thermal instability and extended condensation [121, 325]. Turbulent forcing can help stimulate precipitation and condensation by raising the velocity dispersion of the ambient medium, resulting in more black hole accretion and star formation [327]. With a more energetic environment in the early universe, it is reasonable to assume that the turbulence will be higher at high redshift, resulting in higher black hole accretion rates. The recent discovery of CHIPS 1911+4455, a merging galaxy cluster with a massive starburst in the center, provides strong evidence that mergers can indeed increase star formation [293, 294]. With the development of the next generation X-ray observatories, such as Athena and Lynx, we will be able to directly measure motions in the hot gas and determine whether mergers of groups/clusters can boost cooling via an increase in turbulence.

Lastly, Fig. 5-4 shows that the BCG of the Phoenix cluster remains the most extreme AGN in the entire SPT-SZ sample, which is over a 2500 deg^2 area and spans all redshifts. In combination of the recent work from the CHiPS survey [294], which have confirmed that the Phoenix cluster hosts the most extreme BCG with the strongest cool core at $z < 0.7$, the runaway cooling phase, as we have seen in the Phoenix cluster, is indeed extremely rare.

5.6 Conclusion

In this work, we present results on the mid-IR colors of BCGs in SPT-selected galaxy clusters at $0 < z < 1.3$. This study allows us to track the evolution of BCG properties over $\sim$9 Gyr of cluster growth. In particular, we focus our work on black hole accretion in BCGs, which turns these central galaxies into bright AGNs. Our findings are summarized as follows:

1. Given a single-burst stellar population model, we find a 3.4σ evidence for an increase with redshift of the fraction of AGN-hosting BCGs in galaxy clusters over $0 < z < 1.3$. For the lower redshift bins ($z < 0.6$), an increase is not statistically significant, and the results are compatible with the background. On the other hand, we see an increase in the fraction of BCGs with AGNs at high redshift bins ($z > 0.6$), similar to what others have found in previous works [33, 148, 205].

2. We show that our results are consistent with both the evolution of the fraction of AGNs in field galaxies [133, 287] and the fraction of starburst BCGs [205, 331], suggesting that the reason for the evolution of both AGN and starburst fraction could come from the fact that more cold gas is available in the early universe. This should lead to a higher level of gas-rich mergers in BCGs, which could fuel both AGN activity and star formation in the center of clusters. There remain some caveats about the direct comparison between cluster and field galaxies ranging from selection criteria to the evolution of AGN luminosity.

3. Another possible explanations for the increase in the fraction of AGN-hosting BCGs with redshift could be a higher level of local turbulence from dynamically active galaxy clusters at high redshift, leading to elevated cooling and subsequent black hole accretion. However, this scenario has a difficult time explaining the similarity to the trend in field galaxies.

4. We do not see any additional cluster with a BCG that is as extreme in the mid-IR color as the Phoenix cluster. In other words, the Phoenix cluster likely

hosts the most extreme central AGN in the SPT sample.

An enhancement of the AGN activities inside the BCGs at high redshift suggests that a triggering mechanism of these AGNs may come from the state of clusters which do not yet have a fully established AGN feedback. Further studies with deeper and higher angular resolution mid-IR imaging, such as the upcoming *James Webb Space Telescope* [JWST; 117], will be required to better understand the evolution of AGN feedback and its impact on galaxy clusters.

Chapter 6

Conclusion

This thesis has focused on the discovery of galaxy clusters hosting extreme BCGs over a large redshift range, follow-up studies on individual objects, and the investigation of the evolution of AGN feedback over time. Focusing on these extreme central galaxies, which are distinct from typical BCGs in most galaxy clusters, has opened up a unique opportunity to carefully examine our current astrophysical models of galaxy cluster formation and evolution.

The main part of the thesis was split into two parts. In Part I, *the Clusters Hiding in Plain Sight survey*, I described all the details about the CHiPS surveys and the two newly discovered galaxy clusters found with the survey. Specifically, in Chapter 2 of this thesis, I introduced the initial selection process of the CHiPS survey to include bright X-ray-, radio-, and mid-IR-bright objects that were then followed up with optical data. In addition, I presented a comprehensive analysis of the X-ray Chandra data for CHIPS 1356-3421, or the galaxy cluster surrounding PKS 1353-341. The total mass M_{500} of the cluster is $6.9^{+4.3}_{-2.6} \times 10^{14}\,M_{\odot}$, and the bolometric X-ray luminosity $L_{\rm x}$ is $\sim 7 \times 10^{44}\,{\rm erg\,s^{-1}}$. With the cluster's bulk properties being similar to other known clusters, this cluster is massive enough to be identifiable as a cluster in the ROSAT All-sky Survey, if not because of its bright AGN in the BCG.

In Chapter 3 of this thesis, I described a new optical cluster finding algorithm, developed specifically for the CHiPS survey, to identify cluster candidates with optical data. The top candidates were later observed with the Chandra X-ray telescope to

confirm that they are, in fact, clusters with extended X-ray emission. As a result, I rediscovered six well-known clusters and two newly discovered galaxy clusters–CHIPS 1356-3421 and CHIPS 1911+4455. The main result for this chapter is that I found the occurrence rate for galaxy clusters hosting extreme BCGs (starbursts and/or AGNs) over the redshift range 0.1–0.7 to be $2 \pm 1\%$, consistent with predictions from several theoretical calculations. By looking for clusters with extreme BCGs over the entire sky and not finding more exceptional objects, I also demonstrated that the Phoenix cluster hosts the strongest starburst BCGs at $z < 0.7$.

In Chapter 4 of this thesis, I reported on the newly discovered galaxy cluster, CHIPS 1911+4455. The cluster has an exceptionally low core entropy, but a highly asymmetric morphology. This suggests a strong cool core inside a dynamically active cluster, which is uncommon among all known clusters. The measured star formation rate of $140 - 190\, M_{\odot}\, \mathrm{yr}^{-1}$ is considered one of the highest rates measured in a central galaxy to date. The uniqueness of this cluster creates more questions than answers. Further studies of such objects will give us important insight into the relation between cluster-cluster mergers, star formation, and cooling in the BCGs, and how these processes fit in the bigger picture of AGN feedback.

Given the fact that I have successfully found two new galaxy clusters with remarkable properties from a point source catalog, there could potentially be many more unique objects that have been misclassified as something else in previous catalogs, waiting to be found. The issue of misclassification will become even more prominent as we enter the era of Big Data, with more large survey telescopes coming online and generating terabytes of data. Examples of the next generation telescopes include the recently launched eROSITA in X-ray and the Vera C. Rubin Observatory in optical/infrared. One possible solution to combat this issue is by reducing the number of assumptions we put in our classification algorithms. These assumptions allow us to quickly find objects that fit the mould, but they often prevent us from discovering new types of objects that are even more intriguing to study.

On the other hand, in Part II of the thesis, titled *The Evolution of AGN Activity in Brightest Cluster Galaxies*, I analyzed Wide-field Infrared Survey Explorer (WISE)

observations on the full 2500 deg^2 South Pole Telescope (SPT)-SZ cluster sample in order to calculate the AGN-hosting BCG fraction over the range of $0 < z < 1.3$. I found that the fraction increases with redshift. Instead of studying specific objects that have unique properties like what I did with the CHiPS survey, this work allows us to study the evolution of AGN feedback since the change in the fraction of AGN-hosting BCG can tell us about AGN fueling process, availability of cold gas in the centers of clusters, and the duration/duty cycle of the AGNs. One way to explain the result is that member galaxies at high redshift tend to have more cold gas. BCGs at high redshift could primarily merge with gas-rich satellites, providing fuel needed for feeding AGNs. If this observed increase in AGN activity is linked to gas-rich mergers, rather than ICM cooling, we would expect to see an increase in scatter in the $P_{\rm cav}$ vs $L_{\rm cool}$ relation at $z > 1$. More detailed observations of galaxy clusters with luminous AGN-hosting BCGs at high-redshift are required to verify this prediction.

Altogether, this thesis represents six years of work toward understanding the mechanism behind AGN feedback of galaxy clusters. My work cover a wide range of topics from finding unique galaxy clusters with optical imaging to characterizing the clusters with X-ray and optical data to studying the redshift evolution of AGN feedback from the SPT-SZ sample. This work has made significant contributions to the galaxy cluster community by shining a spotlight on galaxy clusters hosting extreme BCGs and showing how they are a crucial part of our quests to understand AGN feedback mechanism. And yet, many questions regarding such systems and how they impact our knowledge of galaxy cluster formation and evolution remain to be answered. As several next-generation telescopes are being planned and developed, considerably more galaxy clusters, some with extreme central galaxies, will be discovered in the near future. I am excited to continue investigating these clusters in an attempt to learn the processes responsible for the complex nature of cluster evolution.

Bibliography

[1] George O. Abell. The Distribution of Rich Clusters of Galaxies. ApJS, 3:211, May 1958. doi: 10.1086/190036.

[2] George O. Abell, Jr. Corwin, Harold G., and Ronald P. Olowin. A Catalog of Rich Clusters of Galaxies. ApJS, 70:1, May 1989. doi: 10.1086/191333.

[3] Bela Abolfathi and et al. The Fourteenth Data Release of the Sloan Digital Sky Survey: First Spectroscopic Data from the Extended Baryon Oscillation Spectroscopic Survey and from the Second Phase of the Apache Point Observatory Galactic Evolution Experiment. ApJS, 235(2):42, April 2018. doi: 10.3847/1538-4365/aa9e8a.

[4] S. W. Allen, R. W. Schmidt, H. Ebeling, A. C. Fabian, and L. van Speybroeck. Constraints on dark energy from Chandra observations of the largest relaxed galaxy clusters. MNRAS, 353(2):457–467, September 2004. doi: 10.1111/j.1365-2966.2004.08080.x.

[5] S. W. Allen, D. A. Rapetti, R. W. Schmidt, H. Ebeling, R. G. Morris, and A. C. Fabian. Improved constraints on dark energy from Chandra X-ray observations of the largest relaxed galaxy clusters. MNRAS, 383(3):879–896, January 2008. doi: 10.1111/j.1365-2966.2007.12610.x.

[6] Steven W. Allen, August E. Evrard, and Adam B. Mantz. Cosmological Parameters from Observations of Galaxy Clusters. ARA&A, 49(1):409–470, September 2011. doi: 10.1146/annurev-astro-081710-102514.

[7] K. Andersson, B. A. Benson, P. A. R. Ade, K. A. Aird, B. Armstrong, M. Bautz, L. E. Bleem, M. Brodwin, J. E. Carlstrom, C. L. Chang, T. M. Crawford, A. T. Crites, T. de Haan, S. Desai, M. A. Dobbs, J. P. Dudley, R. J. Foley, W. R. Forman, G. Garmire, E. M. George, M. D. Gladders, N. W. Halverson, F. W. High, G. P. Holder, W. L. Holzapfel, J. D. Hrubes, C. Jones, M. Joy, R. Keisler, L. Knox, A. T. Lee, E. M. Leitch, M. Lueker, D. P. Marrone, J. J. McMahon, J. Mehl, S. S. Meyer, J. J. Mohr, T. E. Montroy, S. S. Murray, S. Padin, T. Plagge, C. Pryke, C. L. Reichardt, A. Rest, J. Ruel, J. E. Ruhl, K. K. Schaffer, L. Shaw, E. Shirokoff, J. Song, H. G. Spieler, B. Stalder, Z. Staniszewski, A. A. Stark, C. W. Stubbs, K. Vanderlinde, J. D. Vieira, A. Vikhlinin, R. Williamson, Y. Yang, O. Zahn, and A. Zenteno. X-Ray Properties of the First Sunyaev-Zel'dovich Effect Selected Galaxy Cluster

Sample from the South Pole Telescope. ApJ, 738(1):48, September 2011. doi: 10.1088/0004-637X/738/1/48.

[8] Felipe Andrade-Santos, Christine Jones, William R. Forman, Lorenzo Lovisari, Alexey Vikhlinin, Reinout J. van Weeren, Stephen S. Murray, Monique Arnaud, Gabriel W. Pratt, Jessica Démoclès, Ralph Kraft, Pasquale Mazzotta, Hans Böhringer, Gayoung Chon, Simona Giacintucci, Tracy E. Clarke, Stefano Borgani, Larry David, Marian Douspis, Etienne Pointecouteau, Hakon Dahle, Shea Brown, Nabila Aghanim, and Elena Rasia. The Fraction of Cool-core Clusters in X-Ray versus SZ Samples Using Chandra Observations. ApJ, 843 (1):76, July 2017. doi: 10.3847/1538-4357/aa7461.

[9] M. Arnaud, G. W. Pratt, R. Piffaretti, H. Böhringer, J. H. Croston, and E. Pointecouteau. The universal galaxy cluster pressure profile from a representative sample of nearby systems (REXCESS) and the Y_{SZ} - M_{500} relation. A&A, 517:A92, July 2010. doi: 10.1051/0004-6361/200913416.

[10] R. J. Assef, D. Stern, C. S. Kochanek, A. W. Blain, M. Brodwin, M. J. I. Brown, E. Donoso, P. R. M. Eisenhardt, B. T. Jannuzi, T. H. Jarrett, S. A. Stanford, C. W. Tsai, J. Wu, and L. Yan. Mid-infrared Selection of Active Galactic Nuclei with the Wide-field Infrared Survey Explorer. II. Properties of WISE-selected Active Galactic Nuclei in the NDWFS Boötes Field. ApJ, 772(1):26, July 2013. doi: 10.1088/0004-637X/772/1/26.

[11] Astropy Collaboration, A. M. Price-Whelan, B. M. Sipőcz, H. M. Günther, P. L. Lim, S. M. Crawford, S. Conseil, D. L. Shupe, M. W. Craig, N. Dencheva, A. Ginsburg, J. T. Vand erPlas, L. D. Bradley, D. Pérez-Suárez, M. de Val-Borro, T. L. Aldcroft, K. L. Cruz, T. P. Robitaille, E. J. Tollerud, C. Ardelean, T. Babej, Y. P. Bach, M. Bachetti, A. V. Bakanov, S. P. Bamford, G. Barentsen, P. Barmby, A. Baumbach, K. L. Berry, F. Biscani, M. Boquien, K. A. Bostroem, L. G. Bouma, G. B. Brammer, E. M. Bray, H. Breytenbach, H. Buddelmeijer, D. J. Burke, G. Calderone, J. L. Cano Rodríguez, M. Cara, J. V. M. Cardoso, S. Cheedella, Y. Copin, L. Corrales, D. Crichton, D. D'Avella, C. Deil, É. Depagne, J. P. Dietrich, A. Donath, M. Droettboom, N. Earl, T. Erben, S. Fabbro, L. A. Ferreira, T. Finethy, R. T. Fox, L. H. Garrison, S. L. J. Gibbons, D. A. Goldstein, R. Gommers, J. P. Greco, P. Greenfield, A. M. Groener, F. Grollier, A. Hagen, P. Hirst, D. Homeier, A. J. Horton, G. Hosseinzadeh, L. Hu, J. S. Hunkeler, Ž. Ivezić, A. Jain, T. Jenness, G. Kanarek, S. Kendrew, N. S. Kern, W. E. Kerzendorf, A. Khvalko, J. King, D. Kirkby, A. M. Kulkarni, A. Kumar, A. Lee, D. Lenz, S. P. Littlefair, Z. Ma, D. M. Macleod, M. Mastropietro, C. McCully, S. Montagnac, B. M. Morris, M. Mueller, S. J. Mumford, D. Muna, N. A. Murphy, S. Nelson, G. H. Nguyen, J. P. Ninan, M. Nöthe, S. Ogaz, S. Oh, J. K. Parejko, N. Parley, S. Pascual, R. Patil, A. A. Patil, A. L. Plunkett, J. X. Prochaska, T. Rastogi, V. Reddy Janga, J. Sabater, P. Sakurikar, M. Seifert, L. E. Sherbert, H. Sherwood-Taylor, A. Y. Shih, J. Sick, M. T. Silbiger, S. Singanamalla, L. P. Singer, P. H. Sladen, K. A. Sooley, S. Sornarajah, O. Streicher,

P. Teuben, S. W. Thomas, G. R. Tremblay, J. E. H. Turner, V. Terrón, M. H. van Kerkwijk, A. de la Vega, L. L. Watkins, B. A. Weaver, J. B. Whitmore, J. Woillez, V. Zabalza, and Astropy Contributors. The Astropy Project: Building an Open-science Project and Status of the v2.0 Core Package. AJ, 156(3): 123, Sep 2018. doi: 10.3847/1538-3881/aabc4f.

[12] Iu. V. Babyk, B. R. McNamara, P. E. J. Nulsen, H. R. Russell, A. N. Vantyghem, M. T. Hogan, and F. A. Pulido. A Universal Entropy Profile for the Hot Atmospheres of Galaxies and Clusters within R $_{2500}$. ApJ, 862(1):39, July 2018. doi: 10.3847/1538-4357/aacce5.

[13] Rayford Ball, Jack O. Burns, and Chris Loken. The Radio Properties of CD Galaxies in Abell Clusters. II. The VLA Sample. AJ, 105:53, January 1993. doi: 10.1086/116409.

[14] Michael L. Balogh, Frazer R. Pearce, Richard G. Bower, and Scott T. Kay. Revisiting the cosmic cooling crisis. MNRAS, 326(4):1228–1234, October 2001. doi: 10.1111/j.1365-2966.2001.04667.x.

[15] Joshua E. Barnes and Lars E. Hernquist. Fueling Starburst Galaxies with Gas-rich Mergers. ApJ, 370:L65, April 1991. doi: 10.1086/185978.

[16] R. Barrena, A. Biviano, M. Ramella, E. E. Falco, and S. Seitz. The dynamical status of the cluster of galaxies 1E0657-56. A&A, 386:816–828, May 2002. doi: 10.1051/0004-6361:20020244.

[17] S. A. Baum and C. P. O'Dea. Multifrequency VLA observations of PKS 0745-191: the archetypal "cooling flow" radio source? MNRAS, 250:737, June 1991. doi: 10.1093/mnras/250.4.737.

[18] M. B. Bayliss, J. Ruel, C. W. Stubbs, S. W. Allen, D. E. Applegate, M. L. N. Ashby, M. Bautz, B. A. Benson, L. E. Bleem, S. Bocquet, M. Brodwin, R. Capasso, J. E. Carlstrom, C. L. Chang, I. Chiu, H. M. Cho, A. Clocchiatti, T. M. Crawford, A. T. Crites, T. de Haan, S. Desai, J. P. Dietrich, M. A. Dobbs, A. N. Doucouliagos, R. J. Foley, W. R. Forman, G. P. Garmire, E. M. George, M. D. Gladders, A. H. Gonzalez, N. Gupta, N. W. Halverson, J. Hlavacek-Larrondo, H. Hoekstra, G. P. Holder, W. L. Holzapfel, Z. Hou, J. D. Hrubes, N. Huang, C. Jones, R. Keisler, L. Knox, A. T. Lee, E. M. Leitch, A. von der Linden, D. Luong-Van, A. Mantz, D. P. Marrone, M. McDonald, J. J. McMahon, S. S. Meyer, L. M. Mocanu, J. J. Mohr, S. S. Murray, S. Padin, C. Pryke, D. Rapetti, C. L. Reichardt, A. Rest, J. E. Ruhl, B. R. Saliwanchik, A. Saro, J. T. Sayre, K. K. Schaffer, T. Schrabback, E. Shirokoff, J. Song, H. G. Spieler, B. Stalder, S. A. Stanford, Z. Staniszewski, A. A. Stark, K. T. Story, K. Vanderlinde, J. D. Vieira, A. Vikhlinin, R. Williamson, and A. Zenteno. SPT-GMOS: A Gemini/GMOS-South Spectroscopic Survey of Galaxy Clusters in the SPT-SZ Survey. ApJS, 227(1):3, November 2016. doi: 10.3847/0067-0049/227/1/3.

[19] Eric F. Bell, Richard G. Bower, Roelof S. de Jong, Mark Hereld, and Bernard J. Rauscher. The stellar populations of low surface brightness galaxies. MNRAS, 302(4):L55–L59, February 1999. doi: 10.1046/j.1365-8711.1999.02282.x.

[20] V. Belokurov, N. W. Evans, P. C. Hewett, A. Moiseev, R. G. McMahon, S. F. Sanchez, and L. J. King. Two new large-separation gravitational lenses from SDSS. MNRAS, 392(1):104–112, January 2009. doi: 10.1111/j.1365-2966.2008.14075.x.

[21] Narciso Benítez. Bayesian Photometric Redshift Estimation. ApJ, 536(2):571–583, June 2000. doi: 10.1086/308947.

[22] C. L. Bennett, M. Halpern, G. Hinshaw, N. Jarosik, A. Kogut, M. Limon, S. S. Meyer, L. Page, D. N. Spergel, G. S. Tucker, E. Wollack, E. L. Wright, C. Barnes, M. R. Greason, R. S. Hill, E. Komatsu, M. R. Nolta, N. Odegard, H. V. Peiris, L. Verde, and J. L. Weiland. First-Year Wilkinson Microwave Anisotropy Probe (WMAP) Observations: Preliminary Maps and Basic Results. ApJS, 148(1):1–27, September 2003. doi: 10.1086/377253.

[23] C. L. Bennett, R. S. Hill, G. Hinshaw, M. R. Nolta, N. Odegard, L. Page, D. N. Spergel, J. L. Weiland, E. L. Wright, M. Halpern, N. Jarosik, A. Kogut, M. Limon, S. S. Meyer, G. S. Tucker, and E. Wollack. First-Year Wilkinson Microwave Anisotropy Probe (WMAP) Observations: Foreground Emission. ApJS, 148(1):97–117, September 2003. doi: 10.1086/377252.

[24] E. Bertin. Automatic Astrometric and Photometric Calibration with SCAMP. In C. Gabriel, C. Arviset, D. Ponz, and S. Enrique, editors, *Astronomical Data Analysis Software and Systems XV*, volume 351 of *Astronomical Society of the Pacific Conference Series*, page 112, July 2006.

[25] E. Bertin. Automated Morphometry with SExtractor and PSFEx. In I. N. Evans, A. Accomazzi, D. J. Mink, and A. H. Rots, editors, *Astronomical Data Analysis Software and Systems XX*, volume 442 of *Astronomical Society of the Pacific Conference Series*, page 435, July 2011.

[26] E. Bertin and S. Arnouts. SExtractor: Software for source extraction. A&AS, 117:393–404, June 1996. doi: 10.1051/aas:1996164.

[27] Emmanuel Bertin, Yannick Mellier, Mario Radovich, Gilles Missonnier, Pierre Didelon, and Bertrand Morin. The TERAPIX Pipeline. In David A. Bohlender, Daniel Durand, and Thomas H. Handley, editors, *Astronomical Data Analysis Software and Systems XI*, volume 281 of *Astronomical Society of the Pacific Conference Series*, page 228, January 2002.

[28] Gianfranco Bertone and Dan Hooper. History of dark matter. *Reviews of Modern Physics*, 90(4):045002, October 2018. doi: 10.1103/RevModPhys.90.045002.

[29] E. Bertschinger and A. Meiksin. The Role of Heat Conduction in the Cooling Flows of Galaxy Clusters. ApJ, 306:L1, July 1986. doi: 10.1086/184692.

[30] M. Birkinshaw. The Sunyaev-Zel'dovich effect. Phys. Rep., 310(2-3):97–195, March 1999. doi: 10.1016/S0370-1573(98)00080-5.

[31] L. Bîrzan, D. A. Rafferty, B. R. McNamara, M. W. Wise, and P. E. J. Nulsen. A Systematic Study of Radio-induced X-Ray Cavities in Clusters, Groups, and Galaxies. ApJ, 607(2):800–809, June 2004. doi: 10.1086/383519.

[32] L. Bîrzan, B. R. McNamara, P. E. J. Nulsen, C. L. Carilli, and M. W. Wise. Radiative Efficiency and Content of Extragalactic Radio Sources: Toward a Universal Scaling Relation between Jet Power and Radio Power. ApJ, 686(2): 859–880, October 2008. doi: 10.1086/591416.

[33] L. Bîrzan, D. A. Rafferty, M. Brüggen, and H. T. Intema. A study of high-redshift AGN feedback in SZ cluster samples. MNRAS, 471(2):1766–1787, October 2017. doi: 10.1093/mnras/stx1505.

[34] Andrea Biviano. From Messier to Abell: 200 Years of Science with Galaxy Clusters. In Florence Durret and Daniel Gerbal, editors, *Constructing the Universe with Clusters of Galaxies*, page 1, January 2000.

[35] E. L. Blanton, S. W. Randall, E. M. Douglass, C. L. Sarazin, T. E. Clarke, and B. R. McNamara. Shocks and Bubbles in a Deep Chandra Observation of the Cooling Flow Cluster Abell 2052. ApJ, 697(2):L95–L98, June 2009. doi: 10.1088/0004-637X/697/2/L95.

[36] L. E. Bleem, B. Stalder, T. de Haan, K. A. Aird, S. W. Allen, D. E. Applegate, M. L. N. Ashby, M. Bautz, M. Bayliss, B. A. Benson, S. Bocquet, M. Brodwin, J. E. Carlstrom, C. L. Chang, I. Chiu, H. M. Cho, A. Clocchiatti, T. M. Crawford, A. T. Crites, S. Desai, J. P. Dietrich, M. A. Dobbs, R. J. Foley, W. R. Forman, E. M. George, M. D. Gladders, A. H. Gonzalez, N. W. Halverson, C. Hennig, H. Hoekstra, G. P. Holder, W. L. Holzapfel, J. D. Hrubes, C. Jones, R. Keisler, L. Knox, A. T. Lee, E. M. Leitch, J. Liu, M. Lueker, D. Luong-Van, A. Mantz, D. P. Marrone, M. McDonald, J. J. McMahon, S. S. Meyer, L. Mocanu, J. J. Mohr, S. S. Murray, S. Padin, C. Pryke, C. L. Reichardt, A. Rest, J. Ruel, J. E. Ruhl, B. R. Saliwanchik, A. Saro, J. T. Sayre, K. K. Schaffer, T. Schrabback, E. Shirokoff, J. Song, H. G. Spieler, S. A. Stanford, Z. Staniszewski, A. A. Stark, K. T. Story, C. W. Stubbs, K. Vanderlinde, J. D. Vieira, A. Vikhlinin, R. Williamson, O. Zahn, and A. Zenteno. Galaxy Clusters Discovered via the Sunyaev-Zel'dovich Effect in the 2500-Square-Degree SPT-SZ Survey. ApJS, 216(2):27, February 2015. doi: 10.1088/0067-0049/216/2/27.

[37] L. E. Bleem, S. Bocquet, B. Stalder, M. D. Gladders, P. A. R. Ade, S. W. Allen, A. J. Anderson, J. Annis, M. L. N. Ashby, J. E. Austermann, S. Avila, J. S. Avva, M. Bayliss, J. A. Beall, K. Bechtol, A. N. Bender, B. A. Benson,

E. Bertin, F. Bianchini, C. Blake, M. Brodwin, D. Brooks, E. Buckley-Geer, D. L. Burke, J. E. Carlstrom, A. Carnero Rosell, M. Carrasco Kind, J. Carretero, C. L. Chang, H. C. Chiang, R. Citron, C. Corbett Moran, M. Costanzi, T. M. Crawford, A. T. Crites, L. N. da Costa, T. de Haan, J. De Vicente, S. Desai, H. T. Diehl, J. P. Dietrich, M. A. Dobbs, T. F. Eifler, W. Everett, B. Flaugher, B. Floyd, J. Frieman, J. Gallicchio, J. García-Bellido, E. M. George, D. W. Gerdes, A. Gilbert, D. Gruen, R. A. Gruendl, J. Gschwend, N. Gupta, G. Gutierrez, N. W. Halverson, N. Harrington, J. W. Henning, C. Heymans, G. P. Holder, D. L. Hollowood, W. L. Holzapfel, K. Honscheid, J. D. Hrubes, N. Huang, J. Hubmayr, K. D. Irwin, D. J. James, T. Jeltema, S. Joudaki, G. Khullar, M. Klein, L. Knox, N. Kuropatkin, A. T. Lee, D. Li, C. Lidman, A. Lowitz, N. MacCrann, G. Mahler, M. A. G. Maia, J. L. Marshall, M. McDonald, J. J. McMahon, P. Melchior, F. Menanteau, S. S. Meyer, R. Miquel, L. M. Mocanu, J. J. Mohr, J. Montgomery, A. Nadolski, T. Natoli, J. P. Nibarger, G. Noble, V. Novosad, S. Padin, A. Palmese, D. Parkinson, S. Patil, F. Paz-Chinchón, A. A. Plazas, C. Pryke, N. S. Ramachandra, C. L. Reichardt, J. D. Remolina González, A. K. Romer, A. Roodman, J. E. Ruhl, E. S. Rykoff, B. R. Saliwanchik, E. Sanchez, A. Saro, J. T. Sayre, K. K. Schaffer, T. Schrabback, S. Serrano, K. Sharon, C. Sievers, G. Smecher, M. Smith, M. Soares-Santos, A. A. Stark, K. T. Story, E. Suchyta, G. Tarle, C. Tucker, K. Vanderlinde, T. Veach, J. D. Vieira, G. Wang, J. Weller, N. Whitehorn, W. L. K. Wu, V. Yefremenko, and Y. Zhang. The SPTpol Extended Cluster Survey. ApJS, 247(1):25, March 2020. doi: 10.3847/1538-4365/ab6993.

[38] Katherine M. Blundell and Steve Rawlings. The Optically Powerful Quasar E1821+643 is Associated with a 300 Kiloparsec-Scale FR I Radio Structure. ApJ, 562(1):L5–L8, November 2001. doi: 10.1086/337970.

[39] S. Bocquet, J. P. Dietrich, T. Schrabback, L. E. Bleem, M. Klein, S. W. Allen, D. E. Applegate, M. L. N. Ashby, M. Bautz, M. Bayliss, B. A. Benson, M. Brodwin, E. Bulbul, R. E. A. Canning, R. Capasso, J. E. Carlstrom, C. L. Chang, I. Chiu, H. M. Cho, A. Clocchiatti, T. M. Crawford, A. T. Crites, T. de Haan, S. Desai, M. A. Dobbs, R. J. Foley, W. R. Forman, G. P. Garmire, E. M. George, M. D. Gladders, A. H. Gonzalez, S. Grandis, N. Gupta, N. W. Halverson, J. Hlavacek-Larrondo, H. Hoekstra, G. P. Holder, W. L. Holzapfel, Z. Hou, J. D. Hrubes, N. Huang, C. Jones, G. Khullar, L. Knox, R. Kraft, A. T. Lee, A. von der Linden, D. Luong-Van, A. Mantz, D. P. Marrone, M. McDonald, J. J. McMahon, S. S. Meyer, L. M. Mocanu, J. J. Mohr, R. G. Morris, S. Padin, S. Patil, C. Pryke, D. Rapetti, C. L. Reichardt, A. Rest, J. E. Ruhl, B. R. Saliwanchik, A. Saro, J. T. Sayre, K. K. Schaffer, E. Shirokoff, B. Stalder, S. A. Stanford, Z. Staniszewski, A. A. Stark, K. T. Story, V. Strazzullo, C. W. Stubbs, K. Vanderlinde, J. D. Vieira, A. Vikhlinin, R. Williamson, and A. Zenteno. Cluster Cosmology Constraints from the 2500 deg^2 SPT-SZ Survey: Inclusion of Weak Gravitational Lensing Data from Magellan and the Hubble Space Telescope. ApJ, 878(1):55, June 2019. doi: 10.3847/1538-4357/ab1f10.

[40] Sebastian Bocquet, Katrin Heitmann, Salman Habib, Earl Lawrence, Thomas Uram, Nicholas Frontiere, Adrian Pope, and Hal Finkel. The Mira-Titan Universe. III. Emulation of the Halo Mass Function. ApJ, 901(1):5, September 2020. doi: 10.3847/1538-4357/abac5c.

[41] H. Boehringer, W. Voges, A. C. Fabian, A. C. Edge, and D. M. Neumann. A ROSAT HRI study of the interaction of the X-ray emitting gas and radio lobes of NGC 1275. MNRAS, 264:L25–L28, October 1993. doi: 10.1093/mnras/264.1.L25.

[42] H. Böhringer, P. Schuecker, L. Guzzo, C. A. Collins, W. Voges, R. G. Cruddace, A. Ortiz-Gil, G. Chincarini, S. De Grandi, A. C. Edge, H. T. MacGillivray, D. M. Neumann, S. Schindler, and P. Shaver. The ROSAT-ESO Flux Limited X-ray (REFLEX) Galaxy cluster survey. V. The cluster catalogue. A&A, 425: 367–383, October 2004. doi: 10.1051/0004-6361:20034484.

[43] N. R. Bonaventura, T. M. A. Webb, A. Muzzin, A. Noble, C. Lidman, G. Wilson, H. K. C. Yee, J. Geach, Y. Hezaveh, D. Shupe, and J. Surace. Red but not dead: unveiling the star-forming far-infrared spectral energy distribution of SpARCS brightest cluster galaxies at $0 < z < 1.8$. MNRAS, 469(2):1259–1281, August 2017. doi: 10.1093/mnras/stx722.

[44] S. Borgani, F. Governato, J. Wadsley, N. Menci, P. Tozzi, T. Quinn, J. Stadel, and G. Lake. The effect of non-gravitational gas heating in groups and clusters of galaxies. MNRAS, 336(2):409–424, October 2002. doi: 10.1046/j.1365-8711.2002.05746.x.

[45] Stefano Borgani and Andrey Kravtsov. Cosmological Simulations of Galaxy Clusters. *Advanced Science Letters*, 4(2):204–227, February 2011. doi: 10.1166/asl.2011.1209.

[46] Stefano Borgani, Piero Rosati, Paolo Tozzi, S. A. Stanford, Peter R. Eisenhardt, Chris Lidman, Bradford Holden, Roberto Della Ceca, Colin Norman, and Gordon Squires. Measuring Ω_m with the ROSAT Deep Cluster Survey. ApJ, 561 (1):13–21, November 2001. doi: 10.1086/323214.

[47] H. Bouy, E. Bertin, E. Moraux, J. C. Cuillandre, J. Bouvier, D. Barrado, E. Solano, and A. Bayo. Dynamical analysis of nearby clusters. Automated astrometry from the ground: precision proper motions over a wide field. A&A, 554:A101, June 2013. doi: 10.1051/0004-6361/201220748.

[48] R. G. Bower, J. R. Lucey, and R. S. Ellis. Precision photometry of early-type galaxies in the Coma and Virgo clusters : a test of the universality of the colour-magnitude relation - II. Analysis. MNRAS, 254:601, February 1992. doi: 10.1093/mnras/254.4.601.

[49] R. G. Bower, A. J. Benson, R. Malbon, J. C. Helly, C. S. Frenk, C. M. Baugh, S. Cole, and C. G. Lacey. Breaking the hierarchy of galaxy formation. MNRAS, 370(2):645–655, August 2006. doi: 10.1111/j.1365-2966.2006.10519.x.

[50] R. G. Bower, I. G. McCarthy, and A. J. Benson. The flip side of galaxy formation: a combined model of galaxy formation and cluster heating. MNRAS, 390 (4):1399–1410, November 2008. doi: 10.1111/j.1365-2966.2008.13869.x.

[51] Gabriel B. Brammer, Pieter G. van Dokkum, and Paolo Coppi. EAZY: A Fast, Public Photometric Redshift Code. ApJ, 686(2):1503–1513, October 2008. doi: 10.1086/591786.

[52] Joel N. Bregman. The Search for the Missing Baryons at Low Redshift. ARA&A, 45(1):221–259, September 2007. doi: 10.1146/annurev.astro.45.051806.110619.

[53] Tom Broadhurst, Narciso Benítez, Dan Coe, Keren Sharon, Kerry Zekser, Rick White, Holland Ford, Rychard Bouwens, John Blakeslee, Marc Clampin, Nick Cross, Marijn Franx, Brenda Frye, George Hartig, Garth Illingworth, Leopoldo Infante, Felipe Menanteau, Gerhardt Meurer, Marc Postman, D. R. Ardila, F. Bartko, R. A. Brown, C. J. Burrows, E. S. Cheng, P. D. Feldman, D. A. Golimowski, T. Goto, C. Gronwall, D. Herranz, B. Holden, N. Homeier, J. E. Krist, M. P. Lesser, A. R. Martel, G. K. Miley, P. Rosati, M. Sirianni, W. B. Sparks, S. Steindling, H. D. Tran, Z. I. Tsvetanov, and W. Zheng. Strong-Lensing Analysis of A1689 from Deep Advanced Camera Images. ApJ, 621(1): 53–88, March 2005. doi: 10.1086/426494.

[54] M. Brodwin, D. Stern, A. Vikhlinin, S. A. Stanford, A. H. Gonzalez, P. R. Eisenhardt, M. L. N. Ashby, M. Bautz, A. Dey, W. R. Forman, D. Gettings, R. C. Hickox, B. T. Jannuzi, C. Jones, C. Mancone, E. D. Miller, L. A. Moustakas, J. Ruel, G. Snyder, and G. Zeimann. X-ray Emission from Two Infrared-selected Galaxy Clusters at z $>$ 1.4 in the IRAC Shallow Cluster Survey. ApJ, 732(1): 33, May 2011. doi: 10.1088/0004-637X/732/1/33.

[55] R. J. Brunner and L. M. Lubin. A Probabilistic Quantification of Galaxy Cluster Membership. AJ, 120(6):2851–2858, December 2000. doi: 10.1086/316849.

[56] G. Bruzual and S. Charlot. Stellar population synthesis at the resolution of 2003. MNRAS, 344(4):1000–1028, October 2003. doi: 10.1046/j.1365-8711.2003.06897.x.

[57] R. A. Burenin, A. Vikhlinin, A. Hornstrup, H. Ebeling, H. Quintana, and A. Mescheryakov. The 400 Square Degree ROSAT PSPC Galaxy Cluster Survey: Catalog and Statistical Calibration. ApJS, 172(2):561–582, October 2007. doi: 10.1086/519457.

[58] Jack O. Burns, Chris Loken, Percy Gomez, Elizabeth Rizza, Mark Bliton, and Michael Ledlow. "Listening" To Cluster Cooling Flows: Radio Emission and

The Cluster Environment. In Noam Soker, editor, *Galactic Cluster Cooling Flows*, volume 115 of *Astronomical Society of the Pacific Conference Series*, page 21, January 1997.

[59] Jack O. Burns, Eric J. Hallman, Brennan Gantner, Patrick M. Motl, and Michael L. Norman. Why Do Only Some Galaxy Clusters Have Cool Cores? ApJ, 675(2):1125–1140, March 2008. doi: 10.1086/526514.

[60] Michael S. Calzadilla, Michael McDonald, Matthew Bayliss, Bradford A. Benson, Lindsey E. Bleem, Mark Brodwin, Alastair C. Edge, Benjamin Floyd, Nikhel Gupta, Julie Hlavacek-Larrondo, Brian R. McNamara, Christian L. Reichardt, and SPT Collaboration. Discovery of a Powerful $>10^{61}$ erg AGN Outburst in the Distant Galaxy Cluster SPT-CLJ0528-5300. ApJ, 887(1):L17, December 2019. doi: 10.3847/2041-8213/ab5b07.

[61] Daniela Calzetti, Lee Armus, Ralph C. Bohlin, Anne L. Kinney, Jan Koornneef, and Thaisa Storchi-Bergmann. The Dust Content and Opacity of Actively Star-forming Galaxies. ApJ, 533(2):682–695, April 2000. doi: 10.1086/308692.

[62] Ewan Cameron. On the Estimation of Confidence Intervals for Binomial Population Proportions in Astronomy: The Simplicity and Superiority of the Bayesian Approach. PASA, 28(2):128–139, June 2011. doi: 10.1071/AS10046.

[63] J. E. Carlstrom, P. A. R. Ade, K. A. Aird, B. A. Benson, L. E. Bleem, S. Busetti, C. L. Chang, E. Chauvin, H. M. Cho, T. M. Crawford, A. T. Crites, M. A. Dobbs, N. W. Halverson, S. Heimsath, W. L. Holzapfel, J. D. Hrubes, M. Joy, R. Keisler, T. M. Lanting, A. T. Lee, E. M. Leitch, J. Leong, W. Lu, M. Lueker, D. Luong-Van, J. J. McMahon, J. Mehl, S. S. Meyer, J. J. Mohr, T. E. Montroy, S. Padin, T. Plagge, C. Pryke, J. E. Ruhl, K. K. Schaffer, D. Schwan, E. Shirokoff, H. G. Spieler, Z. Staniszewski, A. A. Stark, C. Tucker, K. Vanderlinde, J. D. Vieira, and R. Williamson. The 10 Meter South Pole Telescope. PASP, 123(903):568, May 2011. doi: 10.1086/659879.

[64] John E. Carlstrom, Gilbert P. Holder, and Erik D. Reese. Cosmology with the Sunyaev-Zel'dovich Effect. ARA&A, 40:643–680, January 2002. doi: 10.1146/annurev.astro.40.060401.093803.

[65] C. Carter, M. Karovska, D. Jerius, K. Glotfelty, and S. Beikman. ChaRT: The Chandra Ray Tracer. In H. E. Payne, R. I. Jedrzejewski, and R. N. Hook, editors, *Astronomical Data Analysis Software and Systems XII*, volume 295 of *Astronomical Society of the Pacific Conference Series*, page 477, January 2003.

[66] Kenneth W. Cavagnolo, Megan Donahue, G. Mark Voit, and Ming Sun. An Entropy Threshold for Strong Hα and Radio Emission in the Cores of Galaxy Clusters. ApJ, 683(2):L107, August 2008. doi: 10.1086/591665.

[67] Kenneth W. Cavagnolo, Megan Donahue, G. Mark Voit, and Ming Sun. Intracluster Medium Entropy Profiles for a Chandra Archival Sample of Galaxy Clusters. ApJS, 182(1):12–32, May 2009. doi: 10.1088/0067-0049/182/1/12.

[68] P. Cerulo, G. A. Orellana, and G. Covone. The evolution of brightest cluster galaxies in the nearby Universe - I. Colours and stellar masses from the Sloan Digital Sky Survey and Wide Infrared Survey Explorer. MNRAS, 487(3):3759–3775, August 2019. doi: 10.1093/mnras/stz1495.

[69] Gilles Chabrier. Galactic Stellar and Substellar Initial Mass Function. PASP, 115(809):763–795, July 2003. doi: 10.1086/376392.

[70] K. C. Chambers, E. A. Magnier, N. Metcalfe, H. A. Flewelling, M. E. Huber, C. Z. Waters, L. Denneau, P. W. Draper, D. Farrow, D. P. Finkbeiner, C. Holmberg, J. Koppenhoefer, P. A. Price, A. Rest, R. P. Saglia, E. F. Schlafly, S. J. Smartt, W. Sweeney, R. J. Wainscoat, W. S. Burgett, S. Chastel, T. Grav, J. N. Heasley, K. W. Hodapp, R. Jedicke, N. Kaiser, R. P. Kudritzki, G. A. Luppino, R. H. Lupton, D. G. Monet, J. S. Morgan, P. M. Onaka, B. Shiao, C. W. Stubbs, J. L. Tonry, R. White, E. Bañados, E. F. Bell, R. Bender, E. J. Bernard, M. Boegner, F. Boffi, M. T. Botticella, A. Calamida, S. Casertano, W. P. Chen, X. Chen, S. Cole, N. Deacon, C. Frenk, A. Fitzsimmons, S. Gezari, V. Gibbs, C. Goessl, T. Goggia, R. Gourgue, B. Goldman, P. Grant, E. K. Grebel, N. C. Hambly, G. Hasinger, A. F. Heavens, T. M. Heckman, R. Henderson, T. Henning, M. Holman, U. Hopp, W. H. Ip, S. Isani, M. Jackson, C. D. Keyes, A. M. Koekemoer, R. Kotak, D. Le, D. Liska, K. S. Long, J. R. Lucey, M. Liu, N. F. Martin, G. Masci, B. McLean, E. Mindel, P. Misra, E. Morganson, D. N. A. Murphy, A. Obaika, G. Narayan, M. A. Nieto-Santisteban, P. Norberg, J. A. Peacock, E. A. Pier, M. Postman, N. Primak, C. Rae, A. Rai, A. Riess, A. Riffeser, H. W. Rix, S. Röser, R. Russel, L. Rutz, E. Schilbach, A. S. B. Schultz, D. Scolnic, L. Strolger, A. Szalay, S. Seitz, E. Small, K. W. Smith, D. R. Soderblom, P. Taylor, R. Thomson, A. N. Taylor, A. R. Thakar, J. Thiel, D. Thilker, D. Unger, Y. Urata, J. Valenti, J. Wagner, T. Walder, F. Walter, S. P. Watters, S. Werner, W. M. Wood-Vasey, and R. Wyse. The Pan-STARRS1 Surveys. *arXiv e-prints*, art. arXiv:1612.05560, December 2016.

[71] Y. Chen, T. H. Reiprich, H. Böhringer, Y. Ikebe, and Y. Y. Zhang. Statistics of X-ray observables for the cooling-core and non-cooling core galaxy clusters. A&A, 466(3):805–812, May 2007. doi: 10.1051/0004-6361:20066471.

[72] Chia-Ying Chiang, E. M. Cackett, P. Gandhi, and A. C. Fabian. Confirmation of the nature of the absorber in IRAS 09104+4109. MNRAS, 430(4):2943–2950, April 2013. doi: 10.1093/mnras/stt097.

[73] E. Churazov, R. Sunyaev, W. Forman, and H. Böhringer. Cooling flows as a calorimeter of active galactic nucleus mechanical power. MNRAS, 332(3): 729–734, May 2002. doi: 10.1046/j.1365-8711.2002.05332.x.

[74] E. Churazov, S. Sazonov, R. Sunyaev, W. Forman, C. Jones, and H. Böhringer. Supermassive black holes in elliptical galaxies: switching from very bright to very dim. MNRAS, 363(1):L91–L95, October 2005. doi: 10.1111/j.1745-3933.2005.00093.x.

[75] M. E. Cluver, T. H. Jarrett, D. A. Dale, J. D. T. Smith, Tamlyn August, and M. J. I. Brown. Calibrating Star Formation in WISE Using Total Infrared Luminosity. ApJ, 850(1):68, November 2017. doi: 10.3847/1538-4357/aa92c7.

[76] Dan Coe, Narciso Benítez, Sebastián F. Sánchez, Myungkook Jee, Rychard Bouwens, and Holland Ford. Galaxies in the Hubble Ultra Deep Field. I. Detection, Multiband Photometry, Photometric Redshifts, and Morphology. AJ, 132(2):926–959, August 2006. doi: 10.1086/505530.

[77] G. D. Coleman, C. C. Wu, and D. W. Weedman. Colors and magnitudes predicted for high redshift galaxies. ApJS, 43:393–416, July 1980. doi: 10.1086/190674.

[78] C. A. Collins, L. Guzzo, R. C. Nichol, and S. L. Lumsden. The Edinburgh-Durham Southern Galaxy Catalogue - VII. The Edinburgh-Milano cluster redshift survey. MNRAS, 274(4):1071–1092, June 1995. doi: 10.1093/mnras/274.4.1071.

[79] J. J. Condon, W. D. Cotton, E. W. Greisen, Q. F. Yin, R. A. Perley, G. B. Taylor, and J. J. Broderick. The NRAO VLA Sky Survey. AJ, 115(5):1693–1716, May 1998. doi: 10.1086/300337.

[80] Charlie Conroy, James E. Gunn, and Martin White. The Propagation of Uncertainties in Stellar Population Synthesis Modeling. I. The Relevance of Uncertain Aspects of Stellar Evolution and the Initial Mass Function to the Derived Physical Properties of Galaxies. ApJ, 699(1):486–506, July 2009. doi: 10.1088/0004-637X/699/1/486.

[81] P. S. Corasaniti, M. Sereno, and S. Ettori. Cosmological Constraints from Galaxy Cluster Sparsity, Cluster Gas Mass Fraction and Baryon Acoustic Oscillations Data. *arXiv e-prints*, art. arXiv:2103.03283, March 2021.

[82] C. S. Crawford and A. C. Fabian. Extended X-ray emission around four 3C quasars at $0.55 < z < 0.75$ observed with Chandra. MNRAS, 339(4):1163–1169, March 2003. doi: 10.1046/j.1365-8711.2003.06268.x.

[83] C. S. Crawford and C. Vanderriest. Optical integral field spectroscopy and ROSAT X-ray imaging of IRAS 09104+4109. MNRAS, 283(3):1003–1014, December 1996. doi: 10.1093/mnras/283.3.1003.

[84] C. S. Crawford, S. W. Allen, H. Ebeling, A. C. Edge, and A. C. Fabian. The ROSAT Brightest Cluster Sample - III. Optical spectra of the central cluster galaxies. MNRAS, 306(4):857–896, July 1999. doi: 10.1046/j.1365-8711.1999.02583.x.

[85] Darren J. Croton, Volker Springel, Simon D. M. White, G. De Lucia, C. S. Frenk, L. Gao, A. Jenkins, G. Kauffmann, J. F. Navarro, and N. Yoshida. The many lives of active galactic nuclei: cooling flows, black holes and the luminosities and colours of galaxies. MNRAS, 365(1):11–28, January 2006. doi: 10.1111/j.1365-2966.2005.09675.x.

[86] Dark Energy Survey Collaboration, T. Abbott, F. B. Abdalla, J. Aleksić, S. Allam, A. Amara, D. Bacon, E. Balbinot, M. Banerji, K. Bechtol, A. Benoit-Lévy, G. M. Bernstein, E. Bertin, J. Blazek, C. Bonnett, S. Bridle, D. Brooks, R. J. Brunner, E. Buckley-Geer, D. L. Burke, G. B. Caminha, D. Capozzi, J. Carlsen, A. Carnero-Rosell, M. Carollo, M. Carrasco-Kind, J. Carretero, F. J. Castander, L. Clerkin, T. Collett, C. Conselice, M. Crocce, C. E. Cunha, C. B. D'Andrea, L. N. da Costa, T. M. Davis, S. Desai, H. T. Diehl, J. P. Dietrich, S. Dodelson, P. Doel, A. Drlica-Wagner, J. Estrada, J. Etherington, A. E. Evrard, J. Fabbri, D. A. Finley, B. Flaugher, R. J. Foley, P. Fosalba, J. Frieman, J. García-Bellido, E. Gaztanaga, D. W. Gerdes, T. Giannantonio, D. A. Goldstein, D. Gruen, R. A. Gruendl, P. Guarnieri, G. Gutierrez, W. Hartley, K. Honscheid, B. Jain, D. J. James, T. Jeltema, S. Jouvel, R. Kessler, A. King, D. Kirk, R. Kron, K. Kuehn, N. Kuropatkin, O. Lahav, T. S. Li, M. Lima, H. Lin, M. A. G. Maia, M. Makler, M. Manera, C. Maraston, J. L. Marshall, P. Martini, R. G. McMahon, P. Melchior, A. Merson, C. J. Miller, R. Miquel, J. J. Mohr, X. Morice-Atkinson, K. Naidoo, E. Neilsen, R. C. Nichol, B. Nord, R. Ogando, F. Ostrovski, A. Palmese, A. Papadopoulos, H. V. Peiris, J. Peoples, W. J. Percival, A. A. Plazas, S. L. Reed, A. Refregier, A. K. Romer, A. Roodman, A. Ross, E. Rozo, E. S. Rykoff, I. Sadeh, M. Sako, C. Sánchez, E. Sanchez, B. Santiago, V. Scarpine, M. Schubnell, I. Sevilla-Noarbe, E. Sheldon, M. Smith, R. C. Smith, M. Soares-Santos, F. Sobreira, M. Soumagnac, E. Suchyta, M. Sullivan, M. Swanson, G. Tarle, J. Thaler, D. Thomas, R. C. Thomas, D. Tucker, J. D. Vieira, V. Vikram, A. R. Walker, R. H. Wechsler, J. Weller, W. Wester, L. Whiteway, H. Wilcox, B. Yanny, Y. Zhang, and J. Zuntz. The Dark Energy Survey: more than dark energy - an overview. MNRAS, 460(2):1270–1299, August 2016. doi: 10.1093/mnras/stw641.

[87] S. Desai, R. Armstrong, J. J. Mohr, D. R. Semler, J. Liu, E. Bertin, S. S. Allam, W. A. Barkhouse, G. Bazin, E. J. Buckley-Geer, M. C. Cooper, S. M. Hansen, F. W. High, H. Lin, Y. T. Lin, C. C. Ngeow, A. Rest, J. Song, D. Tucker, and A. Zenteno. The Blanco Cosmology Survey: Data Acquisition, Processing, Calibration, Quality Diagnostics, and Data Release. ApJ, 757(1):83, September 2012. doi: 10.1088/0004-637X/757/1/83.

[88] Megan Donahue, Andrés Jordán, Stefi A. Baum, Patrick Côté, Laura Ferrarese, Paul Goudfrooij, Duccio Macchetto, Sangeeta Malhotra, Christopher P. O'Dea, James E. Pringle, James E. Rhoads, William B. Sparks, and G. Mark Voit. Infrared Emission from the Nearby Cool Core Cluster Abell 2597. ApJ, 670(1): 231–236, November 2007. doi: 10.1086/522575.

[89] Megan Donahue, Seth Bruch, Emily Wang, G. Mark Voit, Amalia K. Hicks, Deborah B. Haarsma, Judith H. Croston, Gabriel W. Pratt, Daniele Pierini, Robert W. O'Connell, and Hans Böhringer. Star Formation and UV colors of the Brightest Cluster Galaxies in the Representative XMM-Newton Cluster Structure Survey. ApJ, 715(2):881–896, June 2010. doi: 10.1088/0004-637X/715/2/881.

[90] Megan Donahue, Geneviève E. de Messières, Robert W. O'Connell, G. Mark Voit, Aaron Hoffer, Brian R. McNamara, and Paul E. J. Nulsen. Polycyclic Aromatic Hydrocarbons, Ionized Gas, and Molecular Hydrogen in Brightest Cluster Galaxies of Cool-core Clusters of Galaxies. ApJ, 732(1):40, May 2011. doi: 10.1088/0004-637X/732/1/40.

[91] Megan Donahue, Thomas Connor, Kevin Fogarty, Yuan Li, G. Mark Voit, Marc Postman, Anton Koekemoer, John Moustakas, Larry Bradley, and Holland Ford. Ultraviolet Morphology and Unobscured UV Star Formation Rates of CLASH Brightest Cluster Galaxies. ApJ, 805(2):177, June 2015. doi: 10.1088/0004-637X/805/2/177.

[92] Megan Donahue, Kelsey Funkhouser, Dana Koeppe, Rachel L. S. Frisbie, and G. Mark Voit. Clusters of Galaxies Masquerading as X-Ray Quasars. ApJ, 889 (2):121, February 2020. doi: 10.3847/1538-4357/ab64da.

[93] Alan Dressler, Bruce Bigelow, Tyson Hare, Brian Sutin, Ian Thompson, Greg Burley, Harland Epps, Jr. Oemler, Augustus, Alan Bagish, Christoph Birk, Ken Clardy, Steve Gunnels, Daniel Kelson, Stephen Shectman, and David Osip. IMACS: The Inamori-Magellan Areal Camera and Spectrograph on Magellan-Baade. PASP, 123(901):288, March 2011. doi: 10.1086/658908.

[94] H. Ebeling, A. C. Edge, H. Bohringer, S. W. Allen, C. S. Crawford, A. C. Fabian, W. Voges, and J. P. Huchra. The ROSAT Brightest Cluster Sample - I. The compilation of the sample and the cluster log N-log S distribution. MNRAS, 301(4):881–914, December 1998. doi: 10.1046/j.1365-8711.1998.01949.x.

[95] H. Ebeling, A. C. Edge, S. W. Allen, C. S. Crawford, A. C. Fabian, and J. P. Huchra. The ROSAT Brightest Cluster Sample - IV. The extended sample. MNRAS, 318(2):333–340, October 2000. doi: 10.1046/j.1365-8711.2000.03549.x.

[96] H. Ebeling, A. C. Edge, and J. P. Henry. MACS: A Quest for the Most Massive Galaxy Clusters in the Universe. ApJ, 553(2):668–676, June 2001. doi: 10.1086/320958.

[97] H. Ebeling, A. C. Edge, A. Mantz, E. Barrett, J. Patrick Henry, C. J. Ma, and L. van Speybroeck. The X-ray brightest clusters of galaxies from the Massive Cluster Survey. MNRAS, 407(1):83–93, September 2010. doi: 10.1111/j.1365-2966.2010.16920.x.

[98] D. Eckert, S. Molendi, and S. Paltani. The cool-core bias in X-ray galaxy cluster samples. I. Method and application to HIFLUGCS. A&A, 526:A79, February 2011. doi: 10.1051/0004-6361/201015856.

[99] A. C. Edge, A. C. Fabian, S. W. Allen, C. S. Crawford, D. A. White, H. Bohringer, and W. Voges. Zwicky 3146 : the most massive cooling flow ? MNRAS, 270:L1–L5, September 1994. doi: 10.1093/mnras/270.1.L1.

[100] S. Ehlert, S. W. Allen, A. von der Linden, A. Simionescu, N. Werner, G. B. Taylor, G. Gentile, H. Ebeling, M. T. Allen, D. Applegate, R. J. H. Dunn, A. C. Fabian, P. Kelly, E. T. Million, R. G. Morris, J. S. Sanders, and R. W. Schmidt. Extreme active galactic nucleus feedback and cool-core destruction in the X-ray luminous galaxy cluster MACS J1931.8-2634. MNRAS, 411(3): 1641–1658, March 2011. doi: 10.1111/j.1365-2966.2010.17801.x.

[101] Peter R. M. Eisenhardt, Mark Brodwin, Anthony H. Gonzalez, S. Adam Stanford, Daniel Stern, Pauline Barmby, Michael J. I. Brown, Kyle Dawson, Arjun Dey, Mamoru Doi, Audrey Galametz, B. T. Jannuzi, C. S. Kochanek, Joshua Meyers, Tomoki Morokuma, and Leonidas A. Moustakas. Clusters of Galaxies in the First Half of the Universe from the IRAC Shallow Survey. ApJ, 684(2): 905–932, September 2008. doi: 10.1086/590105.

[102] Peter R. M. Eisenhardt, Federico Marocco, John W. Fowler, Aaron M. Meisner, J. Davy Kirkpatrick, Nelson Garcia, Thomas H. Jarrett, Renata Koontz, Elijah J. Marchese, S. Adam Stanford, Dan Caselden, Michael C. Cushing, Roc M. Cutri, Jacqueline K. Faherty, Christopher R. Gelino, Anthony H. Gonzalez, Amanda Mainzer, Bahram Mobasher, David J. Schlegel, Daniel Stern, Harry I. Teplitz, and Edward L. Wright. The CatWISE Preliminary Catalog: Motions from WISE and NEOWISE Data. ApJS, 247(2):69, April 2020. doi: 10.3847/1538-4365/ab7f2a.

[103] A. C. Fabian. Cooling Flows in Clusters of Galaxies. ARA&A, 32:277–318, January 1994. doi: 10.1146/annurev.aa.32.090194.001425.

[104] A. C. Fabian. Observational Evidence of Active Galactic Nuclei Feedback. ARA&A, 50:455–489, September 2012. doi: 10.1146/annurev-astro-081811-125521.

[105] A. C. Fabian and P. E. J. Nulsen. Subsonic accretion of cooling gas in clusters of galaxies. MNRAS, 180:479–484, August 1977. doi: 10.1093/mnras/180.3.479.

[106] A. C. Fabian, J. S. Sanders, S. W. Allen, C. S. Crawford, K. Iwasawa, R. M. Johnstone, R. W. Schmidt, and G. B. Taylor. A deep Chandra observation of the Perseus cluster: shocks and ripples. MNRAS, 344(3):L43–L47, September 2003. doi: 10.1046/j.1365-8711.2003.06902.x.

[107] A. C. Fabian, J. S. Sanders, S. W. Allen, R. E. A. Canning, E. Churazov, C. S. Crawford, W. Forman, J. Gabany, J. Hlavacek-Larrondo, R. M. Johnstone,

H. R. Russell, C. S. Reynolds, P. Salomé, G. B. Taylor, and A. J. Young. A wide Chandra view of the core of the Perseus cluster. MNRAS, 418(4):2154–2164, December 2011. doi: 10.1111/j.1365-2966.2011.19402.x.

[108] Onsi Fakhouri, Chung-Pei Ma, and Michael Boylan-Kolchin. The merger rates and mass assembly histories of dark matter haloes in the two Millennium simulations. MNRAS, 406(4):2267–2278, August 2010. doi: 10.1111/j.1365-2966.2010.16859.x.

[109] B. L. Fanaroff and J. M. Riley. The morphology of extragalactic radio sources of high and low luminosity. MNRAS, 167:31P–36P, May 1974. doi: 10.1093/mnras/167.1.31P.

[110] Daniel J. Farrow, Shaun Cole, N. Metcalfe, P. W. Draper, Peder Norberg, Sébastien Foucaud, W. S. Burgett, K. C. Chambers, N. Kaiser, R. P. Kudritzki, E. A. Magnier, P. A. Price, J. L. Tonry, and C. Waters. Pan-STARRS1: Galaxy clustering in the Small Area Survey 2. MNRAS, 437(1):748–770, January 2014. doi: 10.1093/mnras/stt1933.

[111] G. G. Fazio, J. L. Hora, L. E. Allen, M. L. N. Ashby, P. Barmby, L. K. Deutsch, J. S. Huang, S. Kleiner, M. Marengo, S. T. Megeath, G. J. Melnick, M. A. Pahre, B. M. Patten, J. Polizotti, H. A. Smith, R. S. Taylor, Z. Wang, S. P. Willner, W. F. Hoffmann, J. L. Pipher, W. J. Forrest, C. W. McMurty, C. R. McCreight, M. E. McKelvey, R. E. McMurray, D. G. Koch, S. H. Moseley, R. G. Arendt, J. E. Mentzell, C. T. Marx, P. Losch, P. Mayman, W. Eichhorn, D. Krebs, M. Jhabvala, D. Y. Gezari, D. J. Fixsen, J. Flores, K. Shakoorzadeh, R. Jungo, C. Hakun, L. Workman, G. Karpati, R. Kichak, R. Whitley, S. Mann, E. V. Tollestrup, P. Eisenhardt, D. Stern, V. Gorjian, B. Bhattacharya, S. Carey, B. O. Nelson, W. J. Glaccum, M. Lacy, P. J. Lowrance, S. Laine, W. T. Reach, J. A. Stauffer, J. A. Surace, G. Wilson, E. L. Wright, A. Hoffman, G. Domingo, and M. Cohen. The Infrared Array Camera (IRAC) for the Spitzer Space Telescope. ApJS, 154(1):10–17, September 2004. doi: 10.1086/422843.

[112] G. J. Ferland, A. C. Fabian, N. A. Hatch, R. M. Johnstone, R. L. Porter, P. A. M. van Hoof, and R. J. R. Williams. Collisional heating as the origin of filament emission in galaxy clusters. MNRAS, 392(4):1475–1502, February 2009. doi: 10.1111/j.1365-2966.2008.14153.x.

[113] Daniel Foreman-Mackey, David W. Hogg, Dustin Lang, and Jonathan Goodman. emcee: The MCMC Hammer. PASP, 125(925):306, March 2013. doi: 10.1086/670067.

[114] Juhan Frank, Andrew King, and Derek J. Raine. *Accretion Power in Astrophysics: Third Edition*. Cambridge University Press, 3rd edition, 2002.

[115] Peter Freeman, Stephen Doe, and Aneta Siemiginowska. Sherpa: a mission-independent data analysis application. In Jean-Luc Starck and Fionn D.

Murtagh, editors, *Astronomical Data Analysis*, volume 4477 of *Society of Photo-Optical Instrumentation Engineers (SPIE) Conference Series*, pages 76–87, November 2001. doi: 10.1117/12.447161.

[116] Antonella Fruscione, Jonathan C. McDowell, Glenn E. Allen, Nancy S. Brickhouse, Douglas J. Burke, John E. Davis, Nick Durham, Martin Elvis, Elizabeth C. Galle, Daniel E. Harris, David P. Huenemoerder, John C. Houck, Bish Ishibashi, Margarita Karovska, Fabrizio Nicastro, Michael S. Noble, Michael A. Nowak, Frank A. Primini, Aneta Siemiginowska, Randall K. Smith, and Michael Wise. CIAO: Chandra's data analysis system. In David R. Silva and Rodger E. Doxsey, editors, *Observatory Operations: Strategies, Processes, and Systems*, volume 6270, pages 586 – 597. International Society for Optics and Photonics, SPIE, 2006. doi: 10.1117/12.671760. URL `https://doi.org/10.1117/12.671760`.

[117] Jonathan P. Gardner, John C. Mather, Mark Clampin, Rene Doyon, Matthew A. Greenhouse, Heidi B. Hammel, John B. Hutchings, Peter Jakobsen, Simon J. Lilly, Knox S. Long, Jonathan I. Lunine, Mark J. McCaughrean, Matt Mountain, John Nella, George H. Rieke, Marcia J. Rieke, Hans-Walter Rix, Eric P. Smith, George Sonneborn, Massimo Stiavelli, H. S. Stockman, Rogier A. Windhorst, and Gillian S. Wright. The James Webb Space Telescope. Space Sci. Rev., 123(4):485–606, April 2006. doi: 10.1007/s11214-006-8315-7.

[118] M. Gaspari, C. Melioli, F. Brighenti, and A. D'Ercole. The dance of heating and cooling in galaxy clusters: three-dimensional simulations of self-regulated active galactic nuclei outflows. MNRAS, 411(1):349–372, February 2011. doi: 10.1111/j.1365-2966.2010.17688.x.

[119] M. Gaspari, P. Temi, and F. Brighenti. Raining on black holes and massive galaxies: the top-down multiphase condensation model. MNRAS, 466(1):677–704, April 2017. doi: 10.1093/mnras/stw3108.

[120] M. Gaspari, D. Eckert, S. Ettori, P. Tozzi, L. Bassini, E. Rasia, F. Brighenti, M. Sun, S. Borgani, S. D. Johnson, G. R. Tremblay, J. M. Stone, P. Temi, H. Y. K. Yang, F. Tombesi, and M. Cappi. The X-Ray Halo Scaling Relations of Supermassive Black Holes. ApJ, 884(2):169, October 2019. doi: 10.3847/1538-4357/ab3c5d.

[121] Massimo Gaspari, Francesco Tombesi, and Massimo Cappi. Linking macro-, meso- and microscales in multiphase AGN feeding and feedback. *Nature Astronomy*, 4:10–13, January 2020. doi: 10.1038/s41550-019-0970-1.

[122] Michael D. Gladders and H. K. C. Yee. A New Method For Galaxy Cluster Detection. I. The Algorithm. AJ, 120(4):2148–2162, October 2000. doi: 10.1086/301557.

[123] Michael D. Gladders and H. K. C. Yee. The Red-Sequence Cluster Survey. I. The Survey and Cluster Catalogs for Patches RCS 0926+37 and RCS 1327+29. ApJS, 157(1):1–29, March 2005. doi: 10.1086/427327.

[124] Michael D. Gladders, H. K. C. Yee, Subhabrata Majumdar, L. Felipe Barrientos, Henk Hoekstra, Patrick B. Hall, and Leopoldo Infante. Cosmological Constraints from the Red-Sequence Cluster Survey. ApJ, 655(1):128–134, January 2007. doi: 10.1086/509909.

[125] P. L. Gómez, C. Loken, K. Roettiger, and J. O. Burns. Do Cooling Flows Survive Cluster Mergers? ApJ, 569(1):122–133, April 2002. doi: 10.1086/339280.

[126] Anthony H. Gonzalez, Suresh Sivanandam, Ann I. Zabludoff, and Dennis Zaritsky. Galaxy Cluster Baryon Fractions Revisited. ApJ, 778(1):14, November 2013. doi: 10.1088/0004-637X/778/1/14.

[127] Anthony H. Gonzalez, Daniel P. Gettings, Mark Brodwin, Peter R. M. Eisenhardt, S. A. Stanford, Dominika Wylezalek, Bandon Decker, Daniel P. Marrone, Emily Moravec, Christine O'Donnell, Brian Stalder, Daniel Stern, Zubair Abdulla, Gillen Brown, John Carlstrom, Kenneth C. Chambers, Brian Hayden, Yen-ting Lin, Eugene Magnier, Frank J. Masci, Adam B. Mantz, Michael McDonald, Wenli Mo, Saul Perlmutter, Edward L. Wright, and Gregory R. Zeimann. The Massive and Distant Clusters of WISE Survey. I. Survey Overview and a Catalog of >2000 Galaxy Clusters at z = 1. ApJS, 240(2): 33, February 2019. doi: 10.3847/1538-4365/aafad2.

[128] Alister W. Graham. The black hole mass - spheroid luminosity relation. MNRAS, 379(2):711–722, August 2007. doi: 10.1111/j.1365-2966.2007.11950.x.

[129] T. S. Green, A. C. Edge, H. Ebeling, W. S. Burgett, P. W. Draper, N. Kaiser, R. P. Kudritzki, E. A. Magnier, N. Metcalfe, R. J. Wainscoat, and C. Waters. Hiding in plain sight - recovering clusters of galaxies with the strongest AGN in their cores. MNRAS, 465(4):4872–4885, March 2017. doi: 10.1093/mnras/stw3059.

[130] James E. Gunn and III Gott, J. Richard. On the Infall of Matter Into Clusters of Galaxies and Some Effects on Their Evolution. ApJ, 176:1, August 1972. doi: 10.1086/151605.

[131] James E. Gunn, Walter A. Siegmund, Edward J. Mannery, Russell E. Owen, Charles L. Hull, R. French Leger, Larry N. Carey, Gillian R. Knapp, Donald G. York, William N. Boroski, Stephen M. Kent, Robert H. Lupton, Constance M. Rockosi, Michael L. Evans, Patrick Waddell, John E. Anderson, James Annis, John C. Barentine, Larry M. Bartoszek, Steven Bastian, Stephen B. Bracker, Howard J. Brewington, Charles I. Briegel, Jon Brinkmann, Yorke J. Brown, Michael A. Carr, Paul C. Czarapata, Craig C. Drennan, Thomas Dombeck, Glenn R. Federwitz, Bruce A. Gillespie, Carlos Gonzales, Sten U. Hansen,

Michael Harvanek, Jeffrey Hayes, Wendell Jordan, Ellyne Kinney, Mark Klaene, S. J. Kleinman, Richard G. Kron, Jurek Kresinski, Glenn Lee, Siriluk Limmongkol, Carl W. Lindenmeyer, Daniel C. Long, Craig L. Loomis, Peregrine M. McGehee, Paul M. Mantsch, Jr. Neilsen, Eric H., Richard M. Neswold, Peter R. Newman, Atsuko Nitta, Jr. Peoples, John, Jeffrey R. Pier, Peter S. Prieto, Angela Prosapio, Claudio Rivetta, Donald P. Schneider, Stephanie Snedden, and Shu-i. Wang. The 2.5 m Telescope of the Sloan Digital Sky Survey. AJ, 131(4): 2332–2359, April 2006. doi: 10.1086/500975.

[132] N. Gupta, M. Pannella, J. J. Mohr, M. Klein, E. S. Rykoff, J. Annis, S. Avila, F. Bianchini, D. Brooks, E. Buckley-Geer, E. Bulbul, A. Carnero Rosell, M. Carrasco Kind, J. Carretero, I. Chiu, M. Costanzi, L. N. da Costa, J. De Vicente, S. Desai, J. P. Dietrich, P. Doel, S. Everett, A. E. Evrard, J. García-Bellido, E. Gaztanaga, D. Gruen, R. A. Gruendl, J. Gschwend, G. Gutierrez, D. L. Hollowood, K. Honscheid, D. J. James, T. Jeltema, K. Kuehn, C. Lidman, M. Lima, M. A. G. Maia, J. L. Marshall, M. McDonald, F. Menanteau, R. Miquel, R. L. C. Ogando, A. Palmese, F. Paz-Chinchón, A. A. Plazas, C. L. Reichardt, E. Sanchez, B. Santiago, A. Saro, V. Scarpine, R. Schindler, M. Schubnell, S. Serrano, I. Sevilla-Noarbe, X. Shao, M. Smith, J. P. Stott, V. Strazzullo, E. Suchyta, M. E. C. Swanson, V. Vikram, and A. Zenteno. Constraining radio mode feedback in galaxy clusters with the cluster radio AGNs properties to z $\sim$ 1. MNRAS, 494(2):1705–1723, May 2020. doi: 10.1093/mnras/staa832.

[133] Daryl Haggard, Paul J. Green, Scott F. Anderson, Anca Constantin, Tom L. Aldcroft, Dong-Woo Kim, and Wayne A. Barkhouse. The Field X-ray AGN Fraction to z = 0.7 from the Chandra Multiwavelength Project and the Sloan Digital Sky Survey. ApJ, 723(2):1447–1468, November 2010. doi: 10.1088/0004-637X/723/2/1447.

[134] Zoltán Haiman, David N. Spergel, and Edwin L. Turner. Predictions for the Counts of Faint, High-Redshift Galaxies in the Mid-Infrared. ApJ, 585(2):630–637, March 2003. doi: 10.1086/346201.

[135] Jiangang Hao, Timothy A. McKay, Benjamin P. Koester, Eli S. Rykoff, Eduardo Rozo, James Annis, Risa H. Wechsler, August Evrard, Seth R. Siegel, Matthew Becker, Michael Busha, David Gerdes, David E. Johnston, and Erin Sheldon. A GMBCG Galaxy Cluster Catalog of 55,424 Rich Clusters from SDSS DR7. ApJS, 191(2):254–274, December 2010. doi: 10.1088/0067-0049/191/2/254.

[136] C. M. Harrison. Impact of supermassive black hole growth on star formation. *Nature Astronomy*, 1:0165, July 2017. doi: 10.1038/s41550-017-0165.

[137] G. Hasinger, T. Miyaji, and M. Schmidt. Luminosity-dependent evolution of soft X-ray selected AGN. New Chandra and XMM-Newton surveys. A&A, 441 (2):417–434, October 2005. doi: 10.1051/0004-6361:20042134.

[138] J. Patrick Henry. X-Ray Temperatures for the Extended Medium-Sensitivity Survey High-Redshift Cluster Sample: Constraints on Cosmology and the Dark Energy Equation of State. ApJ, 609(2):603–616, July 2004. doi: 10.1086/421336.

[139] J. Patrick Henry and Keith A. Arnaud. A Measurement of the Mass Fluctuation Spectrum from the Cluster X-Ray Temperature Function. ApJ, 372:410, May 1991. doi: 10.1086/169987.

[140] Ryan C. Hickox and David M. Alexander. Obscured Active Galactic Nuclei. ARA&A, 56:625–671, September 2018. doi: 10.1146/annurev-astro-081817-051803.

[141] A. K. Hicks and R. Mushotzky. Star Formation Rates in Cooling Flow Clusters: A UV Pilot Study with Archival XMM-Newton Optical Monitor Data. ApJ, 635(1):L9–L12, December 2005. doi: 10.1086/499123.

[142] F. W. High, B. Stalder, J. Song, P. A. R. Ade, K. A. Aird, S. S. Allam, R. Armstrong, W. A. Barkhouse, B. A. Benson, E. Bertin, S. Bhattacharya, L. E. Bleem, M. Brodwin, E. J. Buckley-Geer, J. E. Carlstrom, P. Challis, C. L. Chang, T. M. Crawford, A. T. Crites, T. de Haan, S. Desai, M. A. Dobbs, J. P. Dudley, R. J. Foley, E. M. George, M. Gladders, N. W. Halverson, M. Hamuy, S. M. Hansen, G. P. Holder, W. L. Holzapfel, J. D. Hrubes, M. Joy, R. Keisler, A. T. Lee, E. M. Leitch, H. Lin, Y. T. Lin, A. Loehr, M. Lueker, D. Marrone, J. J. McMahon, J. Mehl, S. S. Meyer, J. J. Mohr, T. E. Montroy, N. Morell, C. C. Ngeow, S. Padin, T. Plagge, C. Pryke, C. L. Reichardt, A. Rest, J. Ruel, J. E. Ruhl, K. K. Schaffer, L. Shaw, E. Shirokoff, R. C. Smith, H. G. Spieler, Z. Staniszewski, A. A. Stark, C. W. Stubbs, D. L. Tucker, K. Vanderlinde, J. D. Vieira, R. Williamson, W. M. Wood-Vasey, Y. Yang, O. Zahn, and A. Zenteno. Optical Redshift and Richness Estimates for Galaxy Clusters Selected with the Sunyaev-Zel'dovich Effect from 2008 South Pole Telescope Observations. ApJ, 723(2):1736–1747, November 2010. doi: 10.1088/0004-637X/723/2/1736.

[143] F. William High, Christopher W. Stubbs, Armin Rest, Brian Stalder, and Peter Challis. Stellar Locus Regression: Accurate Color Calibration and the Real-Time Determination of Galaxy Cluster Photometric Redshifts. AJ, 138(1):110–129, July 2009. doi: 10.1088/0004-6256/138/1/110.

[144] M. Hilton, C. Sifón, S. Naess, M. Madhavacheril, M. Oguri, E. Rozo, E. Rykoff, T. M. C. Abbott, S. Adhikari, M. Aguena, S. Aiola, S. Allam, S. Amodeo, A. Amon, J. Annis, B. Ansarinejad, C. Aros-Bunster, J. E. Austermann, S. Avila, D. Bacon, N. Battaglia, J. A. Beall, D. T. Becker, G. M. Bernstein, E. Bertin, T. Bhandarkar, S. Bhargava, J. R. Bond, D. Brooks, D. L. Burke, E. Calabrese, J. Carretero, S. K. Choi, A. Choi, C. Conselice, L. N. da Costa, M. Costanzi, D. Crichton, K. T. Crowley, R. Dünner, E. V. Denison, M. J. Devlin, S. R. Dicker, H. T. Diehl, J. P. Dietrich, P. Doel, S. M. Duff, A. J. Duivenvoorden, J. Dunkley, S. Everett, S. Ferraro, I. Ferrero, A. Ferté,

B. Flaugher, J. Frieman, P. A. Gallardo, J. García-Bellido, E. Gaztanaga, D. W. Gerdes, P. Giles, J. E. Golec, M. B. Gralla, S. Grandis, D. Gruen, R. A. Gruendl, J. Gschwend, G. Gutierrez, D. Han, W. G. Hartley, M. Hasselfield, J. C. Hill, G. C. Hilton, A. D. Hincks, S. R. Hinton, S-P. P. Ho, K. Honscheid, B. Hoyle, J. Hubmayr, K. M. Huffenberger, J. P. Hughes, A. T. Jaelani, B. Jain, D. J. James, T. Jeltema, S. Kent, M. Carrasco Kind, K. Knowles, B. J. Koopman, K. Kuehn, O. Lahav, M. Lima, Y-T. Lin, M. Lokken, S. I. Loubser, N. MacCrann, M. A. G. Maia, T. A. Marriage, J. Martin, J. McMahon, P. Melchior, F. Menanteau, R. Miquel, H. Miyatake, K. Moodley, R. Morgan, T. Mroczkowski, F. Nati, L. B. Newburgh, M. D. Niemack, A. J. Nishizawa, R. L. C. Ogando, J. Orlowski-Scherer, L. A. Page, A. Palmese, B. Partridge, F. Paz-Chinchón, P. Phakathi, A. A. Plazas, N. C. Robertson, A. K. Romer, A. Carnero Rosell, M. Salatino, E. Sanchez, E. Schaan, A. Schillaci, N. Sehgal, S. Serrano, T. Shin, S. M. Simon, M. Smith, M. Soares-Santos, D. N. Spergel, S. T. Staggs, E. R. Storer, E. Suchyta, M. E. C. Swanson, G. Tarle, D. Thomas, C. To, H. Trac, J. N. Ullom, L. R. Vale, J. Van Lanen, E. M. Vavagiakis, J. De Vicente, R. D. Wilkinson, E. J. Wollack, Z. Xu, and Y. Zhang. The Atacama Cosmology Telescope: A Catalog of $>$ 4000 Sunyaev-Zel'dovich Galaxy Clusters. *arXiv e-prints*, art. arXiv:2009.11043, September 2020.

[145] M. Hilton, C. Sifón, S. Naess, M. Madhavacheril, M. Oguri, E. Rozo, E. Rykoff, T. M. C. Abbott, S. Adhikari, M. Aguena, S. Aiola, S. Allam, S. Amodeo, A. Amon, J. Annis, B. Ansarinejad, C. Aros-Bunster, J. E. Austermann, S. Avila, D. Bacon, N. Battaglia, J. A. Beall, D. T. Becker, G. M. Bernstein, E. Bertin, T. Bhandarkar, S. Bhargava, J. R. Bond, D. Brooks, D. L. Burke, E. Calabrese, M. Carrasco Kind, J. Carretero, S. K. Choi, A. Choi, C. Conselice, L. N. da Costa, M. Costanzi, D. Crichton, K. T. Crowley, R. Dünner, E. V. Denison, M. J. Devlin, S. R. Dicker, H. T. Diehl, J. P. Dietrich, P. Doel, S. M. Duff, A. J. Duivenvoorden, J. Dunkley, S. Everett, S. Ferraro, I. Ferrero, A. Ferté, B. Flaugher, J. Frieman, P. A. Gallardo, J. García-Bellido, E. Gaztanaga, D. W. Gerdes, P. Giles, J. E. Golec, M. B. Gralla, S. Grandis, D. Gruen, R. A. Gruendl, J. Gschwend, G. Gutierrez, D. Han, W. G. Hartley, M. Hasselfield, J. C. Hill, G. C. Hilton, A. D. Hincks, S. R. Hinton, S. P. P. Ho, K. Honscheid, B. Hoyle, J. Hubmayr, K. M. Huffenberger, J. P. Hughes, A. T. Jaelani, B. Jain, D. J. James, T. Jeltema, S. Kent, K. Knowles, B. J. Koopman, K. Kuehn, O. Lahav, M. Lima, Y. T. Lin, M. Lokken, S. I. Loubser, N. MacCrann, M. A. G. Maia, T. A. Marriage, J. Martin, J. McMahon, P. Melchior, F. Menanteau, R. Miquel, H. Miyatake, K. Moodley, R. Morgan, T. Mroczkowski, F. Nati, L. B. Newburgh, M. D. Niemack, A. J. Nishizawa, R. L. C. Ogando, J. Orlowski-Scherer, L. A. Page, A. Palmese, B. Partridge, F. Paz-Chinchón, P. Phakathi, A. A. Plazas, N. C. Robertson, A. K. Romer, A. Carnero Rosell, M. Salatino, E. Sanchez, E. Schaan, A. Schillaci, N. Sehgal, S. Serrano, T. Shin, S. M. Simon, M. Smith, M. Soares-Santos, D. N. Spergel, S. T. Staggs, E. R. Storer, E. Suchyta, M. E. C. Swanson, G. Tarle, D. Thomas, C. To, H. Trac, J. N. Ullom, L. R. Vale, J. Van Lanen, E. M. Vavagiakis, J. De

Vicente, R. D. Wilkinson, E. J. Wollack, Z. Xu, and Y. Zhang. The Atacama Cosmology Telescope: A Catalog of >4000 Sunyaev–Zel'dovich Galaxy Clusters. ApJS, 253(1):3, March 2021. doi: 10.3847/1538-4365/abd023.

[146] Matt Hilton, Matthew Hasselfield, Cristóbal Sifón, Nicholas Battaglia, Simone Aiola, V. Bharadwaj, J. Richard Bond, Steve K. Choi, Devin Crichton, Rahul Datta, Mark J. Devlin, Joanna Dunkley, Rolando Dünner, Patricio A. Gallardo, Megan Gralla, Adam D. Hincks, Shuay-Pwu P. Ho, Johannes Hubmayr, Kevin M. Huffenberger, John P. Hughes, Brian J. Koopman, Arthur Kosowsky, Thibaut Louis, Mathew S. Madhavacheril, Tobias A. Marriage, Loïc Maurin, Jeff McMahon, Hironao Miyatake, Kavilan Moodley, Sigurd Næss, Federico Nati, Laura Newburgh, Michael D. Niemack, Masamune Oguri, Lyman A. Page, Bruce Partridge, Benjamin L. Schmitt, Jon Sievers, David N. Spergel, Suzanne T. Staggs, Hy Trac, Alexander van Engelen, Eve M. Vavagiakis, and Edward J. Wollack. The Atacama Cosmology Telescope: The Two-season ACTPol Sunyaev-Zel'dovich Effect Selected Cluster Catalog. ApJS, 235(1):20, March 2018. doi: 10.3847/1538-4365/aaa6cb.

[147] J. Hlavacek-Larrondo, S. W. Allen, G. B. Taylor, A. C. Fabian, R. E. A. Canning, N. Werner, J. S. Sanders, C. K. Grimes, S. Ehlert, and A. von der Linden. Probing the Extreme Realm of Active Galactic Nucleus Feedback in the Massive Galaxy Cluster, RX J1532.9+3021. ApJ, 777(2):163, November 2013. doi: 10.1088/0004-637X/777/2/163.

[148] J. Hlavacek-Larrondo, A. C. Fabian, A. C. Edge, H. Ebeling, S. W. Allen, J. S. Sanders, and G. B. Taylor. The rapid evolution of AGN feedback in brightest cluster galaxies: switching from quasar-mode to radio-mode feedback. MNRAS, 431(2):1638–1658, May 2013. doi: 10.1093/mnras/stt283.

[149] J. Hlavacek-Larrondo, M. McDonald, B. A. Benson, W. R. Forman, S. W. Allen, L. E. Bleem, M. L. N. Ashby, S. Bocquet, M. Brodwin, J. P. Dietrich, C. Jones, J. Liu, C. L. Reichardt, B. R. Saliwanchik, A. Saro, T. Schrabback, J. Song, B. Stalder, A. Vikhlinin, and A. Zenteno. X-Ray Cavities in a Sample of 83 SPT-selected Clusters of Galaxies: Tracing the Evolution of AGN Feedback in Clusters of Galaxies out to z=1.2. ApJ, 805(1):35, May 2015. doi: 10.1088/0004-637X/805/1/35.

[150] M. T. Hogan, A. C. Edge, J. Hlavacek-Larrondo, K. J. B. Grainge, S. L. Hamer, E. K. Mahony, H. R. Russell, A. C. Fabian, B. R. McNamara, and R. J. Wilman. A comprehensive study of the radio properties of brightest cluster galaxies. MNRAS, 453(2):1201–1222, October 2015. doi: 10.1093/mnras/stv1517.

[151] M. T. Hogan, B. R. McNamara, F. A. Pulido, P. E. J. Nulsen, A. N. Vantyghem, H. R. Russell, A. C. Edge, Iu. Babyk, R. A. Main, and M. McDonald. The Onset of Thermally Unstable Cooling from the Hot Atmospheres of Giant Galaxies in Clusters: Constraints on Feedback Models. ApJ, 851(1):66, December 2017. doi: 10.3847/1538-4357/aa9af3.

[152] Philip F. Hopkins, Lars Hernquist, Thomas J. Cox, Tiziana Di Matteo, Brant Robertson, and Volker Springel. A Unified, Merger-driven Model of the Origin of Starbursts, Quasars, the Cosmic X-Ray Background, Supermassive Black Holes, and Galaxy Spheroids. ApJS, 163(1):1–49, March 2006. doi: 10.1086/499298.

[153] Wayne Hu, Masataka Fukugita, Matias Zaldarriaga, and Max Tegmark. Cosmic Microwave Background Observables and Their Cosmological Implications. ApJ, 549(2):669–680, March 2001. doi: 10.1086/319449.

[154] N. Huang, L. E. Bleem, B. Stalder, P. A. R. Ade, S. W. Allen, A. J. Anderson, J. E. Austermann, J. S. Avva, J. A. Beall, A. N. Bender, B. A. Benson, F. Bianchini, S. Bocquet, M. Brodwin, J. E. Carlstrom, C. L. Chang, H. C. Chiang, R. Citron, C. Corbett Moran, T. M. Crawford, A. T. Crites, T. de Haan, M. A. Dobbs, W. Everett, B. Floyd, J. Gallicchio, E. M. George, A. Gilbert, M. D. Gladders, S. Guns, N. Gupta, N. W. Halverson, N. Harrington, J. W. Henning, G. C. Hilton, G. P. Holder, W. L. Holzapfel, J. D. Hrubes, J. Hubmayr, K. D. Irwin, G. Khullar, L. Knox, A. T. Lee, D. Li, A. Lowitz, M. McDonald, J. J. McMahon, S. S. Meyer, L. M. Mocanu, J. Montgomery, A. Nadolski, T. Natoli, J. P. Nibarger, G. Noble, V. Novosad, S. Padin, S. Patil, C. Pryke, C. L. Reichardt, J. E. Ruhl, B. R. Saliwanchik, A. Saro, J. T. Sayre, K. K. Schaffer, K. Sharon, C. Sievers, G. Smecher, A. A. Stark, K. T. Story, C. Tucker, K. Vanderlinde, T. Veach, J. D. Vieira, G. Wang, N. Whitehorn, W. L. K. Wu, and V. Yefremenko. Galaxy Clusters Selected via the Sunyaev-Zel'dovich Effect in the SPTpol 100-square-degree Survey. AJ, 159(3):110, March 2020. doi: 10.3847/1538-3881/ab6a96.

[155] J. P. Huchra and M. J. Geller. Groups of Galaxies. I. Nearby groups. ApJ, 257: 423–437, June 1982. doi: 10.1086/160000.

[156] D. S. Hudson, R. Mittal, T. H. Reiprich, P. E. J. Nulsen, H. Andernach, and C. L. Sarazin. What is a cool-core cluster? a detailed analysis of the cores of the X-ray flux-limited HIFLUGCS cluster sample. A&A, 513:A37, April 2010. doi: 10.1051/0004-6361/200912377.

[157] Željko Ivezić and et al. LSST: From Science Drivers to Reference Design and Anticipated Data Products. ApJ, 873(2):111, March 2019. doi: 10.3847/1538-4357/ab042c.

[158] M. Jarvis, G. M. Bernstein, A. Amon, C. Davis, P. F. Léget, K. Bechtol, I. Harrison, M. Gatti, A. Roodman, C. Chang, R. Chen, A. Choi, S. Desai, A. Drlica-Wagner, D. Gruen, R. A. Gruendl, A. Hernandez, N. MacCrann, J. Meyers, A. Navarro-Alsina, S. Pandey, A. A. Plazas, L. F. Secco, E. Sheldon, M. A. Troxel, S. Vorperian, K. Wei, J. Zuntz, T. M. C. Abbott, M. Aguena, S. Allam, S. Avila, S. Bhargava, S. L. Bridle, D. Brooks, A. Carnero Rosell, M. Carrasco Kind, J. Carretero, M. Costanzi, L. N. da Costa, J. De Vicente, H. T. Diehl, P. Doel, S. Everett, B. Flaugher, P. Fosalba, J. Frieman, J. García-Bellido, E. Gaztanaga, D. W. Gerdes, G. Gutierrez, S. R. Hinton, D. L.

Hollowood, K. Honscheid, D. J. James, S. Kent, K. Kuehn, N. Kuropatkin, O. Lahav, M. A. G. Maia, M. March, J. L. Marshall, P. Melchior, F. Menanteau, R. Miquel, R. L. C. Ogando, F. Paz-Chinchón, E. S. Rykoff, E. Sanchez, V. Scarpine, M. Schubnell, S. Serrano, I. Sevilla-Noarbe, M. Smith, E. Suchyta, M. E. C. Swanson, G. Tarle, T. N. Varga, A. R. Walker, W. Wester, R. D. Wilkinson, and DES Collaboration. Dark Energy Survey year 3 results: point spread function modelling. MNRAS, 501(1):1282–1299, February 2021. doi: 10.1093/mnras/staa3679.

[159] Ryan E. Johnson, Maxim Markevitch, Gary A. Wegner, Christine Jones, and William R. Forman. Core Gas Sloshing in Abell 1644. ApJ, 710(2):1776–1785, February 2010. doi: 10.1088/0004-637X/710/2/1776.

[160] P. M. W. Kalberla, W. B. Burton, Dap Hartmann, E. M. Arnal, E. Bajaja, R. Morras, and W. G. L. Pöppel. The Leiden/Argentine/Bonn (LAB) Survey of Galactic HI. Final data release of the combined LDS and IAR surveys with improved stray-radiation corrections. A&A, 440(2):775–782, September 2005. doi: 10.1051/0004-6361:20041864.

[161] Patrick L. Kelly, Anja von der Linden, Douglas E. Applegate, Mark T. Allen, Steven W. Allen, Patricia R. Burchat, David L. Burke, Harald Ebeling, Peter Capak, Oliver Czoske, David Donovan, Adam Mantz, and R. Glenn Morris. Weighing the Giants - II. Improved calibration of photometry from stellar colours and accurate photometric redshifts. MNRAS, 439(1):28–47, March 2014. doi: 10.1093/mnras/stt1946.

[162] Jr. Kennicutt, Robert C. Star Formation in Galaxies Along the Hubble Sequence. ARA&A, 36:189–232, January 1998. doi: 10.1146/annurev.astro.36.1.189.

[163] G. Khullar, L. E. Bleem, M. B. Bayliss, M. D. Gladders, B. A. Benson, M. McDonald, S. W. Allen, D. E. Applegate, M. L. N. Ashby, S. Bocquet, M. Brodwin, E. Bulbul, R. E. A. Canning, R. Capasso, I. Chiu, T. M. Crawford, T. de Haan, J. P. Dietrich, A. H. Gonzalez, J. Hlavacek-Larrondo, H. Hoekstra, W. L. Holzapfel, A. von der Linden, A. B. Mantz, S. Patil, C. L. Reichardt, A. Saro, K. Sharon, B. Stalder, S. A. Stanford, A. A. Stark, and V. Strazzullo. Spectroscopic Confirmation of Five Galaxy Clusters at $z > 1.25$ in the 2500 deg^2 SPT-SZ Survey. ApJ, 870(1):7, January 2019. doi: 10.3847/1538-4357/aaeed0.

[164] Anne L. Kinney, Daniela Calzetti, Ralph C. Bohlin, Kerry McQuade, Thaisa Storchi-Bergmann, and Henrique R. Schmitt. Template Ultraviolet to Near-Infrared Spectra of Star-forming Galaxies and Their Application to K-Corrections. ApJ, 467:38, August 1996. doi: 10.1086/177583.

[165] Brian Kirk, Matt Hilton, Catherine Cress, Steven M. Crawford, John P. Hughes, Nicholas Battaglia, J. Richard Bond, Claire Burke, Megan B. Gralla, Amir Hajian, Matthew Hasselfield, Adam D. Hincks, Leopoldo Infante, Arthur

Kosowsky, Tobias A. Marriage, Felipe Menanteau, Kavilan Moodley, Michael D. Niemack, Jonathan L. Sievers, Cristóbal Sifón, Susan Wilson, Edward J. Wollack, and Caroline Zunckel. SALT spectroscopic observations of galaxy clusters detected by ACT and a type II quasar hosted by a brightest cluster galaxy. MNRAS, 449(4):4010–4026, June 2015. doi: 10.1093/mnras/stv595.

[166] C. C. Kirkpatrick, M. Gitti, K. W. Cavagnolo, B. R. McNamara, L. P. David, P. E. J. Nulsen, and M. W. Wise. Direct Evidence for Outflow of Metal-Enriched Gas Along the Radio Jets of Hydra A. ApJ, 707(1):L69–L72, December 2009. doi: 10.1088/0004-637X/707/1/L69.

[167] M. Klein, S. Grandis, J. J. Mohr, M. Paulus, T. M. C. Abbott, J. Annis, S. Avila, E. Bertin, D. Brooks, E. Buckley-Geer, A. Carnero Rosell, M. Carrasco Kind, J. Carretero, F. J. Castander, C. E. Cunha, C. B. D'Andrea, L. N. da Costa, J. De Vicente, S. Desai, H. T. Diehl, J. P. Dietrich, P. Doel, A. E. Evrard, B. Flaugher, P. Fosalba, J. Frieman, J. García-Bellido, E. Gaztanaga, P. A. Giles, D. Gruen, R. A. Gruendl, J. Gschwend, G. Gutierrez, W. G. Hartley, D. L. Hollowood, K. Honscheid, B. Hoyle, D. J. James, T. Jeltema, K. Kuehn, N. Kuropatkin, M. Lima, M. A. G. Maia, M. March, J. L. Marshall, F. Menanteau, R. Miquel, R. L. C. Ogando, A. A. Plazas, A. K. Romer, A. Roodman, E. Sanchez, V. Scarpine, R. Schindler, S. Serrano, I. Sevilla-Noarbe, M. Smith, R. C. Smith, M. Soares-Santos, F. Sobreira, E. Suchyta, M. E. C. Swanson, G. Tarle, D. Thomas, V. Vikram, and DES Collaboration. A new RASS galaxy cluster catalogue with low contamination extending to z $\sim$ 1 in the DES overlap region. MNRAS, 488(1):739–769, September 2019. doi: 10.1093/mnras/stz1463.

[168] B. P. Koester, T. A. McKay, J. Annis, R. H. Wechsler, A. Evrard, L. Bleem, M. Becker, D. Johnston, E. Sheldon, R. Nichol, C. Miller, R. Scranton, N. Bahcall, J. Barentine, H. Brewington, J. Brinkmann, M. Harvanek, S. Kleinman, J. Krzesinski, D. Long, A. Nitta, D. P. Schneider, S. Sneddin, W. Voges, and D. York. A MaxBCG Catalog of 13,823 Galaxy Clusters from the Sloan Digital Sky Survey. ApJ, 660(1):239–255, May 2007. doi: 10.1086/509599.

[169] Benjamin P. Koester, Timothy A. McKay, James Annis, Risa H. Wechsler, August E. Evrard, Eduardo Rozo, Lindsey Bleem, Erin S. Sheldon, and David Johnston. MaxBCG: A Red-Sequence Galaxy Cluster Finder. ApJ, 660(1): 221–238, May 2007. doi: 10.1086/512092.

[170] Andrey V. Kravtsov, Alexey Vikhlinin, and Daisuke Nagai. A New Robust Low-Scatter X-Ray Mass Indicator for Clusters of Galaxies. ApJ, 650(1):128–136, October 2006. doi: 10.1086/506319.

[171] Mariska Kriek, Pieter G. van Dokkum, Ivo Labbé, Marijn Franx, Garth D. Illingworth, Danilo Marchesini, and Ryan F. Quadri. An Ultra-Deep Near-Infrared Spectrum of a Compact Quiescent Galaxy at z = 2.2. ApJ, 700(1): 221–231, July 2009. doi: 10.1088/0004-637X/700/1/221.

[172] M. Lacy, L. J. Storrie-Lombardi, A. Sajina, P. N. Appleton, L. Armus, S. C. Chapman, P. I. Choi, D. Fadda, F. Fang, D. T. Frayer, I. Heinrichsen, G. Helou, M. Im, F. R. Marleau, F. Masci, D. L. Shupe, B. T. Soifer, J. Surace, H. I. Teplitz, G. Wilson, and L. Yan. Obscured and Unobscured Active Galactic Nuclei in the Spitzer Space Telescope First Look Survey. ApJS, 154(1):166–169, September 2004. doi: 10.1086/422816.

[173] Dustin Lang. unWISE: Unblurred Coadds of the WISE Imaging. AJ, 147(5): 108, May 2014. doi: 10.1088/0004-6256/147/5/108.

[174] Dustin Lang, David W. Hogg, Keir Mierle, Michael Blanton, and Sam Roweis. Astrometry.net: Blind Astrometric Calibration of Arbitrary Astronomical Images. AJ, 139(5):1782–1800, May 2010. doi: 10.1088/0004-6256/139/5/1782.

[175] R. B. Larson, B. M. Tinsley, and C. N. Caldwell. The evolution of disk galaxies and the origin of S0 galaxies. ApJ, 237:692–707, May 1980. doi: 10.1086/157917.

[176] Erwin T. Lau, Massimo Gaspari, Daisuke Nagai, and Paolo Coppi. Physical Origins of Gas Motions in Galaxy Cluster Cores: Interpreting Hitomi Observations of the Perseus Cluster. ApJ, 849(1):54, November 2017. doi: 10.3847/1538-4357/aa8c00.

[177] Jong Chul Lee, Ho Seong Hwang, and Jongwan Ko. The Calibration of Star Formation Rate Indicators for WISE 22 μm-Selected Galaxies in the Sloan Digital Sky Survey. ApJ, 774(1):62, September 2013. doi: 10.1088/0004-637X/774/1/62.

[178] B. D. Lehmer, W. N. Brandt, D. M. Alexander, E. F. Bell, D. H. McIntosh, F. E. Bauer, G. Hasinger, V. Mainieri, T. Miyaji, D. P. Schneider, and A. T. Steffen. The X-Ray Evolution of Early-Type Galaxies in the Extended Chandra Deep Field-South. ApJ, 657(2):681–699, March 2007. doi: 10.1086/511297.

[179] Andrew R. Liddle and David H. Lyth. The cold dark matter density perturbation. Phys. Rep., 231(1-2):1–105, August 1993. doi: 10.1016/0370-1573(93)90114-S.

[180] Henry W. Lin, Michael McDonald, Bradford Benson, and Eric Miller. Cool Core Bias in Sunyaev-Zel'dovich Galaxy Cluster Surveys. ApJ, 802(1):34, March 2015. doi: 10.1088/0004-637X/802/1/34.

[181] E. V. Linder and A. Jenkins. Cosmic structure growth and dark energy. MNRAS, 346(2):573–583, December 2003. doi: 10.1046/j.1365-2966.2003.07112.x.

[182] J. Liu, C. Hennig, S. Desai, B. Hoyle, J. Koppenhoefer, J. J. Mohr, K. Paech, W. S. Burgett, K. C. Chambers, S. Cole, P. W. Draper, N. Kaiser, N. Metcalfe, J. S. Morgan, P. A. Price, C. W. Stubbs, J. L. Tonry, R. J. Wainscoat, and C. Waters. Optical confirmation and redshift estimation of the Planck cluster candidates overlapping the Pan-STARRS Survey. MNRAS, 449(4):3370–3380, June 2015. doi: 10.1093/mnras/stv458.

[183] E. J. Lloyd-Davies, T. J. Ponman, and D. B. Cannon. The entropy and energy of intergalactic gas in galaxy clusters. MNRAS, 315(4):689–702, July 2000. doi: 10.1046/j.1365-8711.2000.03380.x.

[184] J. R. Lucey. An assessment of the completeness and correctness of the Abell catalogue. MNRAS, 204:33–43, July 1983. doi: 10.1093/mnras/204.1.33.

[185] Robert H. Lupton, James E. Gunn, and Alexander S. Szalay. A Modified Magnitude System that Produces Well-Behaved Magnitudes, Colors, and Errors Even for Low Signal-to-Noise Ratio Measurements. AJ, 118(3):1406–1410, September 1999. doi: 10.1086/301004.

[186] R. A. Main, B. R. McNamara, P. E. J. Nulsen, H. R. Russell, and A. N. Vantyghem. A relationship between halo mass, cooling, active galactic nuclei heating and the co-evolution of massive black holes. MNRAS, 464(4):4360–4382, February 2017. doi: 10.1093/mnras/stw2644.

[187] A. Mainzer, J. Bauer, R. M. Cutri, T. Grav, J. Masiero, R. Beck, P. Clarkson, T. Conrow, J. Dailey, P. Eisenhardt, B. Fabinsky, S. Fajardo-Acosta, J. Fowler, C. Gelino, C. Grillmair, I. Heinrichsen, M. Kendall, J. Davy Kirkpatrick, F. Liu, F. Masci, H. McCallon, C. R. Nugent, M. Papin, E. Rice, D. Royer, T. Ryan, P. Sevilla, S. Sonnett, R. Stevenson, D. B. Thompson, S. Wheelock, D. Wiemer, M. Wittman, E. Wright, and L. Yan. Initial Performance of the NEOWISE Reactivation Mission. ApJ, 792(1):30, September 2014. doi: 10.1088/0004-637X/792/1/30.

[188] Conor L. Mancone and Anthony H. Gonzalez. EzGal: A Flexible Interface for Stellar Population Synthesis Models. PASP, 124(916):606, June 2012. doi: 10.1086/666502.

[189] A. Mantz, S. W. Allen, H. Ebeling, and D. Rapetti. New constraints on dark energy from the observed growth of the most X-ray luminous galaxy clusters. MNRAS, 387(3):1179–1192, July 2008. doi: 10.1111/j.1365-2966.2008.13311.x.

[190] A. B. Mantz, S. W. Allen, R. G. Morris, D. A. Rapetti, D. E. Applegate, P. L. Kelly, A. von der Linden, and R. W. Schmidt. Cosmology and astrophysics from relaxed galaxy clusters - II. Cosmological constraints. MNRAS, 440(3): 2077–2098, May 2014. doi: 10.1093/mnras/stu368.

[191] Adam B. Mantz, Steven W. Allen, R. Glenn Morris, Robert W. Schmidt, Anja von der Linden, and Ondrej Urban. Cosmology and astrophysics from relaxed galaxy clusters - I. Sample selection. MNRAS, 449(1):199–219, May 2015. doi: 10.1093/mnras/stv219.

[192] Adam B. Mantz, Anja von der Linden, Steven W. Allen, Douglas E. Applegate, Patrick L. Kelly, R. Glenn Morris, David A. Rapetti, Robert W. Schmidt, Saroj Adhikari, Mark T. Allen, Patricia R. Burchat, David L. Burke, Matteo Cataneo, David Donovan, Harald Ebeling, Sarah Shandera, and Adam Wright. Weighing

the giants - IV. Cosmology and neutrino mass. MNRAS, 446(3):2205–2225, January 2015. doi: 10.1093/mnras/stu2096.

[193] Claudia Maraston. Evolutionary population synthesis: models, analysis of the ingredients and application to high-z galaxies. MNRAS, 362(3):799–825, September 2005. doi: 10.1111/j.1365-2966.2005.09270.x.

[194] M. Markevitch, A. H. Gonzalez, L. David, A. Vikhlinin, S. Murray, W. Forman, C. Jones, and W. Tucker. A Textbook Example of a Bow Shock in the Merging Galaxy Cluster 1E 0657-56. ApJ, 567(1):L27–L31, March 2002. doi: 10.1086/339619.

[195] M. Markevitch, A. H. Gonzalez, D. Clowe, A. Vikhlinin, W. Forman, C. Jones, S. Murray, and W. Tucker. Direct Constraints on the Dark Matter Self-Interaction Cross Section from the Merging Galaxy Cluster 1E 0657-56. ApJ, 606(2):819–824, May 2004. doi: 10.1086/383178.

[196] Tobias A. Marriage, Viviana Acquaviva, Peter A. R. Ade, Paula Aguirre, Mandana Amiri, John William Appel, L. Felipe Barrientos, Elia S. Battistelli, J. Richard Bond, Ben Brown, Bryce Burger, Jay Chervenak, Sudeep Das, Mark J. Devlin, Simon R. Dicker, W. Bertrand Doriese, Joanna Dunkley, Rolando Dünner, Thomas Essinger-Hileman, Ryan P. Fisher, Joseph W. Fowler, Amir Hajian, Mark Halpern, Matthew Hasselfield, Carlos Hernández-Monteagudo, Gene C. Hilton, Matt Hilton, Adam D. Hincks, Renée Hlozek, Kevin M. Huffenberger, David Handel Hughes, John P. Hughes, Leopoldo Infante, Kent D. Irwin, Jean Baptiste Juin, Madhuri Kaul, Jeff Klein, Arthur Kosowsky, Judy M. Lau, Michele Limon, Yen-Ting Lin, Robert H. Lupton, Danica Marsden, Krista Martocci, Phil Mauskopf, Felipe Menanteau, Kavilan Moodley, Harvey Moseley, Calvin B. Netterfield, Michael D. Niemack, Michael R. Nolta, Lyman A. Page, Lucas Parker, Bruce Partridge, Hernan Quintana, Erik D. Reese, Beth Reid, Neelima Sehgal, Blake D. Sherwin, Jon Sievers, David N. Spergel, Suzanne T. Staggs, Daniel S. Swetz, Eric R. Switzer, Robert Thornton, Hy Trac, Carole Tucker, Ryan Warne, Grant Wilson, Ed Wollack, and Yue Zhao. The Atacama Cosmology Telescope: Sunyaev-Zel'dovich-Selected Galaxy Clusters at 148 GHz in the 2008 Survey. ApJ, 737(2):61, August 2011. doi: 10.1088/0004-637X/737/2/61.

[197] Daniel P. Marrone, Graham P. Smith, Johan Richard, Marshall Joy, Massimiliano Bonamente, Nicole Hasler, Victoria Hamilton-Morris, Jean-Paul Kneib, Thomas Culverhouse, John E. Carlstrom, Christopher Greer, David Hawkins, Ryan Hennessy, James W. Lamb, Erik M. Leitch, Michael Loh, Amber Miller, Tony Mroczkowski, Stephen Muchovej, Clem Pryke, Matthew K. Sharp, and David Woody. LoCuSS: A Comparison of Sunyaev-Zel'dovich Effect and Gravitational-Lensing Measurements of Galaxy Clusters. ApJ, 701(2):L114–L118, August 2009. doi: 10.1088/0004-637X/701/2/L114.

[198] Paul Martini, Gregory R. Sivakoff, and John S. Mulchaey. The Evolution of Active Galactic Nuclei in Clusters of Galaxies to Redshift 1.3. ApJ, 701(1): 66–85, August 2009. doi: 10.1088/0004-637X/701/1/66.

[199] T. Mauch, T. Murphy, H. J. Buttery, J. Curran, R. W. Hunstead, B. Piestrzynski, J. G. Robertson, and E. M. Sadler. SUMSS: a wide-field radio imaging survey of the southern sky - II. The source catalogue. MNRAS, 342(4):1117–1130, July 2003. doi: 10.1046/j.1365-8711.2003.06605.x.

[200] P. Mazzotta, E. Rasia, L. Moscardini, and G. Tormen. Comparing the temperatures of galaxy clusters from hydrodynamical N-body simulations to Chandra and XMM-Newton observations. MNRAS, 354(1):10–24, October 2004. doi: 10.1111/j.1365-2966.2004.08167.x.

[201] Thomas McClintock, Eduardo Rozo, Matthew R. Becker, Joseph DeRose, Yao-Yuan Mao, Sean McLaughlin, Jeremy L. Tinker, Risa H. Wechsler, and Zhongxu Zhai. The Aemulus Project. II. Emulating the Halo Mass Function. ApJ, 872 (1):53, February 2019. doi: 10.3847/1538-4357/aaf568.

[202] M. McDonald, M. Bayliss, B. A. Benson, R. J. Foley, J. Ruel, P. Sullivan, S. Veilleux, K. A. Aird, M. L. N. Ashby, M. Bautz, G. Bazin, L. E. Bleem, M. Brodwin, J. E. Carlstrom, C. L. Chang, H. M. Cho, A. Clocchiatti, T. M. Crawford, A. T. Crites, T. de Haan, S. Desai, M. A. Dobbs, J. P. Dudley, E. Egami, W. R. Forman, G. P. Garmire, E. M. George, M. D. Gladders, A. H. Gonzalez, N. W. Halverson, N. L. Harrington, F. W. High, G. P. Holder, W. L. Holzapfel, S. Hoover, J. D. Hrubes, C. Jones, M. Joy, R. Keisler, L. Knox, A. T. Lee, E. M. Leitch, J. Liu, M. Lueker, D. Luong-van, A. Mantz, D. P. Marrone, J. J. McMahon, J. Mehl, S. S. Meyer, E. D. Miller, L. Mocanu, J. J. Mohr, T. E. Montroy, S. S. Murray, T. Natoli, S. Padin, T. Plagge, C. Pryke, T. D. Rawle, C. L. Reichardt, A. Rest, M. Rex, J. E. Ruhl, B. R. Saliwanchik, A. Saro, J. T. Sayre, K. K. Schaffer, L. Shaw, E. Shirokoff, R. Simcoe, J. Song, H. G. Spieler, B. Stalder, Z. Staniszewski, A. A. Stark, K. Story, C. W. Stubbs, R. Šuhada, A. van Engelen, K. Vanderlinde, J. D. Vieira, A. Vikhlinin, R. Williamson, O. Zahn, and A. Zenteno. A massive, cooling-flow-induced starburst in the core of a luminous cluster of galaxies. Nature, 488(7411):349–352, August 2012. doi: 10.1038/nature11379.

[203] M. McDonald, B. A. Benson, A. Vikhlinin, B. Stalder, L. E. Bleem, T. de Haan, H. W. Lin, K. A. Aird, M. L. N. Ashby, M. W. Bautz, M. Bayliss, S. Bocquet, M. Brodwin, J. E. Carlstrom, C. L. Chang, H. M. Cho, A. Clocchiatti, T. M. Crawford, A. T. Crites, S. Desai, M. A. Dobbs, J. P. Dudley, R. J. Foley, W. R. Forman, E. M. George, D. Gettings, M. D. Gladders, A. H. Gonzalez, N. W. Halverson, F. W. High, G. P. Holder, W. L. Holzapfel, S. Hoover, J. D. Hrubes, C. Jones, M. Joy, R. Keisler, L. Knox, A. T. Lee, E. M. Leitch, J. Liu, M. Lueker, D. Luong-Van, A. Mantz, D. P. Marrone, J. J. McMahon, J. Mehl, S. S. Meyer, E. D. Miller, L. Mocanu, J. J. Mohr, T. E. Montroy, S. S. Murray,

D. Nurgaliev, S. Padin, T. Plagge, C. Pryke, C. L. Reichardt, A. Rest, J. Ruel, J. E. Ruhl, B. R. Saliwanchik, A. Saro, J. T. Sayre, K. K. Schaffer, E. Shirokoff, J. Song, R. Šuhada, H. G. Spieler, S. A. Stanford, Z. Staniszewski, A. A. Stark, K. Story, A. van Engelen, K. Vanderlinde, J. D. Vieira, R. Williamson, O. Zahn, and A. Zenteno. The Growth of Cool Cores and Evolution of Cooling Properties in a Sample of 83 Galaxy Clusters at $0.3 < z < 1.2$ Selected from the SPT-SZ Survey. ApJ, 774(1):23, September 2013. doi: 10.1088/0004-637X/774/1/23.

[204] M. McDonald, B. A. Benson, A. Vikhlinin, K. A. Aird, S. W. Allen, M. Bautz, M. Bayliss, L. E. Bleem, S. Bocquet, M. Brodwin, J. E. Carlstrom, C. L. Chang, H. M. Cho, A. Clocchiatti, T. M. Crawford, A. T. Crites, T. de Haan, M. A. Dobbs, R. J. Foley, W. R. Forman, E. M. George, M. D. Gladders, A. H. Gonzalez, N. W. Halverson, J. Hlavacek-Larrondo, G. P. Holder, W. L. Holzapfel, J. D. Hrubes, C. Jones, R. Keisler, L. Knox, A. T. Lee, E. M. Leitch, J. Liu, M. Lueker, D. Luong-Van, A. Mantz, D. P. Marrone, J. J. McMahon, S. S. Meyer, E. D. Miller, L. Mocanu, J. J. Mohr, S. S. Murray, S. Padin, C. Pryke, C. L. Reichardt, A. Rest, J. E. Ruhl, B. R. Saliwanchik, A. Saro, J. T. Sayre, K. K. Schaffer, E. Shirokoff, H. G. Spieler, B. Stalder, S. A. Stanford, Z. Staniszewski, A. A. Stark, K. T. Story, C. W. Stubbs, K. Vanderlinde, J. D. Vieira, R. Williamson, O. Zahn, and A. Zenteno. The Redshift Evolution of the Mean Temperature, Pressure, and Entropy Profiles in 80 SPT-Selected Galaxy Clusters. ApJ, 794(1):67, October 2014. doi: 10.1088/0004-637X/794/1/67.

[205] M. McDonald, B. Stalder, M. Bayliss, S. W. Allen, D. E. Applegate, M. L. N. Ashby, M. Bautz, B. A. Benson, L. E. Bleem, M. Brodwin, J. E. Carlstrom, I. Chiu, S. Desai, A. H. Gonzalez, J. Hlavacek-Larrondo, W. L. Holzapfel, D. P. Marrone, E. D. Miller, C. L. Reichardt, B. R. Saliwanchik, A. Saro, T. Schrabback, S. A. Stanford, A. A. Stark, J. D. Vieira, and A. Zenteno. Star-forming Brightest Cluster Galaxies at $0.25 < z < 1.25$: A Transitioning Fuel Supply. ApJ, 817(2):86, February 2016. doi: 10.3847/0004-637X/817/2/86.

[206] M. McDonald, S. W. Allen, M. Bayliss, B. A. Benson, L. E. Bleem, M. Brodwin, E. Bulbul, J. E. Carlstrom, W. R. Forman, J. Hlavacek-Larrondo, G. P. Garmire, M. Gaspari, M. D. Gladders, A. B. Mantz, and S. S. Murray. The Remarkable Similarity of Massive Galaxy Clusters from $z \sim 0$ to $z \sim 1.9$. ApJ, 843(1):28, July 2017. doi: 10.3847/1538-4357/aa7740.

[207] M. McDonald, M. Gaspari, B. R. McNamara, and G. R. Tremblay. Revisiting the Cooling Flow Problem in Galaxies, Groups, and Clusters of Galaxies. ApJ, 858(1):45, May 2018. doi: 10.3847/1538-4357/aabace.

[208] M. McDonald, B. R. McNamara, G. M. Voit, M. Bayliss, B. A. Benson, M. Brodwin, R. E. A. Canning, M. K. Florian, G. P. Garmire, M. Gaspari, M. D. Gladders, J. Hlavacek-Larrondo, E. Kara, C. L. Reichardt, H. R. Russell, A. Saro, K. Sharon, T. Somboonpanyakul, G. R. Tremblay, and R. J. van

Weeren. Anatomy of a Cooling Flow: The Feedback Response to Pure Cooling in the Core of the Phoenix Cluster. ApJ, 885(1):63, November 2019. doi: 10.3847/1538-4357/ab464c.

[209] Michael McDonald, Sylvain Veilleux, David S. N. Rupke, Richard Mushotzky, and Christopher Reynolds. Star Formation Efficiency in the Cool Cores of Galaxy Clusters. ApJ, 734(2):95, June 2011. doi: 10.1088/0004-637X/734/2/95.

[210] Michael McDonald, Bradford Benson, Sylvain Veilleux, Marshall W. Bautz, and Christian L. Reichardt. An HST/WFC3-UVIS View of the Starburst in the Cool Core of the Phoenix Cluster. ApJ, 765(2):L37, March 2013. doi: 10.1088/2041-8205/765/2/L37.

[211] Michael McDonald, Mark Swinbank, Alastair C. Edge, David J. Wilner, Sylvain Veilleux, Bradford A. Benson, Michael T. Hogan, Daniel P. Marrone, Brian R. McNamara, Lisa H. Wei, Matthew B. Bayliss, and Marshall W. Bautz. The State of the Warm and Cold Gas in the Extreme Starburst at the Core of the Phoenix Galaxy Cluster (SPT-CLJ2344-4243). ApJ, 784(1):18, March 2014. doi: 10.1088/0004-637X/784/1/18.

[212] Michael McDonald, Brian R. McNamara, Reinout J. van Weeren, Douglas E. Applegate, Matthew Bayliss, Marshall W. Bautz, Bradford A. Benson, John E. Carlstrom, Lindsey E. Bleem, Marios Chatzikos, Alastair C. Edge, Andrew C. Fabian, Gordon P. Garmire, Julie Hlavacek-Larrondo, Christine Jones-Forman, Adam B. Mantz, Eric D. Miller, Brian Stalder, Sylvain Veilleux, and John A. ZuHone. Deep Chandra, HST-COS, and Megacam Observations of the Phoenix Cluster: Extreme Star Formation and AGN Feedback on Hundred Kiloparsec Scales. ApJ, 811(2):111, October 2015. doi: 10.1088/0004-637X/811/2/111.

[213] Michael McDonald, Brian R. McNamara, Michael S. Calzadilla, Chien-Ting Chen, Massimo Gaspari, Ryan C. Hickox, Erin Kara, and Ilia Korchagin. Observational Evidence for Enhanced Black Hole Accretion in Giant Elliptical Galaxies. ApJ, 908(1):85, February 2021. doi: 10.3847/1538-4357/abd47f.

[214] B. R. McNamara and P. E. J. Nulsen. Heating Hot Atmospheres with Active Galactic Nuclei. ARA&A, 45(1):117–175, September 2007. doi: 10.1146/annurev.astro.45.051806.110625.

[215] B. R. McNamara and P. E. J. Nulsen. Mechanical feedback from active galactic nuclei in galaxies, groups and clusters. *New Journal of Physics*, 14(5):055023, May 2012. doi: 10.1088/1367-2630/14/5/055023.

[216] B. R. McNamara, P. E. J. Nulsen, M. W. Wise, D. A. Rafferty, C. Carilli, C. L. Sarazin, and E. L. Blanton. The heating of gas in a galaxy cluster by X-ray cavities and large-scale shock fronts. Nature, 433(7021):45–47, January 2005. doi: 10.1038/nature03202.

[217] B. R. McNamara, D. A. Rafferty, L. Bîrzan, J. Steiner, M. W. Wise, P. E. J. Nulsen, C. L. Carilli, R. Ryan, and M. Sharma. The Starburst in the Abell 1835 Cluster Central Galaxy: A Case Study of Galaxy Formation Regulated by an Outburst from a Supermassive Black Hole. ApJ, 648(1):164–175, September 2006. doi: 10.1086/505859.

[218] B. R. McNamara, H. R. Russell, P. E. J. Nulsen, A. C. Edge, N. W. Murray, R. A. Main, A. N. Vantyghem, F. Combes, A. C. Fabian, P. Salome, C. C. Kirkpatrick, S. A. Baum, J. N. Bregman, M. Donahue, E. Egami, S. Hamer, C. P. O'Dea, J. B. R. Oonk, G. Tremblay, and G. M. Voit. A 10^{10} Solar Mass Flow of Molecular Gas in the A1835 Brightest Cluster Galaxy. ApJ, 785(1):44, April 2014. doi: 10.1088/0004-637X/785/1/44.

[219] Brian R. McNamara and Robert W. O'Connell. Star formation in cooling flows in clusters of galaxies. AJ, 98:2018–2043, December 1989. doi: 10.1086/115275.

[220] Nicola Mehrtens, A. Kathy Romer, Matt Hilton, E. J. Lloyd-Davies, Christopher J. Miller, S. A. Stanford, Mark Hosmer, Ben Hoyle, Chris A. Collins, Andrew R. Liddle, Pedro T. P. Viana, Robert C. Nichol, John P. Stott, E. Naomi Dubois, Scott T. Kay, Martin Sahlén, Owain Young, C. J. Short, L. Christodoulou, William A. Watson, Michael Davidson, Craig D. Harrison, Leon Baruah, Mathew Smith, Claire Burke, Julian A. Mayers, Paul-James Deadman, Philip J. Rooney, Edward M. Edmondson, Michael West, Heather C. Campbell, Alastair C. Edge, Robert G. Mann, Kivanc Sabirli, David Wake, Christophe Benoist, Luiz da Costa, Marcio A. G. Maia, and Ricardo Ogando. The XMM Cluster Survey: optical analysis methodology and the first data release. MNRAS, 423(2):1024–1052, June 2012. doi: 10.1111/j.1365-2966.2012.20931.x.

[221] Felipe Menanteau, John P. Hughes, Cristóbal Sifón, Matt Hilton, Jorge González, Leopoldo Infante, L. Felipe Barrientos, Andrew J. Baker, John R. Bond, Sudeep Das, Mark J. Devlin, Joanna Dunkley, Amir Hajian, Adam D. Hincks, Arthur Kosowsky, Danica Marsden, Tobias A. Marriage, Kavilan Moodley, Michael D. Niemack, Michael R. Nolta, Lyman A. Page, Erik D. Reese, Neelima Sehgal, Jon Sievers, David N. Spergel, Suzanne T. Staggs, and Edward Wollack. The Atacama Cosmology Telescope: ACT-CL J0102-4915 "El Gordo," a Massive Merging Cluster at Redshift 0.87. ApJ, 748(1):7, March 2012. doi: 10.1088/0004-637X/748/1/7.

[222] A. Merloni, P. Predehl, W. Becker, H. Böhringer, T. Boller, H. Brunner, M. Brusa, K. Dennerl, M. Freyberg, P. Friedrich, A. Georgakakis, F. Haberl, G. Hasinger, N. Meidinger, J. Mohr, K. Nandra, A. Rau, T. H. Reiprich, J. Robrade, M. Salvato, A. Santangelo, M. Sasaki, A. Schwope, J. Wilms, and the German eROSITA Consortium. eROSITA Science Book: Mapping the Structure of the Energetic Universe. *arXiv e-prints*, art. arXiv:1209.3114, September 2012.

[223] D. Merritt. Relaxation and tidal stripping in rich clusters of galaxies. I. Evolution of the mass distribution. ApJ, 264:24–48, January 1983. doi: 10.1086/160571.

[224] R. Mittal, D. S. Hudson, T. H. Reiprich, and T. Clarke. AGN heating and ICM cooling in the HIFLUGCS sample of galaxy clusters. A&A, 501(3):835–850, July 2009. doi: 10.1051/0004-6361/200810836.

[225] Rupal Mittal, M. McDonald, John T. Whelan, and Gustavo Bruzual. The challenging task of determining star formation rates: the case of a massive stellar burst in the brightest cluster galaxy of Phoenix galaxy cluster. MNRAS, 465(3):3143–3153, March 2017. doi: 10.1093/mnras/stw2915.

[226] Wenli Mo, Anthony Gonzalez, Mark Brodwin, Bandon Decker, Peter Eisenhardt, Emily Moravec, S. A. Stanford, Daniel Stern, and Dominika Wylezalek. The Massive and Distant Clusters of WISE Survey. VIII. Radio Activity in Massive Galaxy Clusters. ApJ, 901(2):131, October 2020. doi: 10.3847/1538-4357/abb08d.

[227] Joseph J. Mohr, Robert Armstrong, Emmanuel Bertin, Greg Daues, Shantanu Desai, Michelle Gower, Robert Gruendl, William Hanlon, Nikolay Kuropatkin, Huan Lin, John Marriner, Donald Petravic, Ignacio Sevilla, Molly Swanson, Todd Tomashek, Douglas Tucker, and Brian Yanny. The Dark Energy Survey data processing and calibration system. In Nicole M. Radziwill and Gianluca Chiozzi, editors, *Software and Cyberinfrastructure for Astronomy II*, volume 8451 of *Society of Photo-Optical Instrumentation Engineers (SPIE) Conference Series*, page 84510D, September 2012. doi: 10.1117/12.926785.

[228] S. Molendi, P. Tozzi, M. Gaspari, S. De Grandi, F. Gastaldello, S. Ghizzardi, and M. Rossetti. Where does the gas fueling star formation in brightest cluster galaxies originate? A&A, 595:A123, November 2016. doi: 10.1051/0004-6361/201628338.

[229] Silvano Molendi and Fabio Pizzolato. Is the Gas in Cooling Flows Multiphase? ApJ, 560(1):194–200, October 2001. doi: 10.1086/322387.

[230] Patrick M. Motl, Eric J. Hallman, Jack O. Burns, and Michael L. Norman. The Integrated Sunyaev-Zeldovich Effect as a Superior Method for Measuring the Mass of Clusters of Galaxies. ApJ, 623(2):L63–L66, April 2005. doi: 10.1086/430144.

[231] Tony Mroczkowski, Daisuke Nagai, Kaustuv Basu, Jens Chluba, Jack Sayers, Rémi Adam, Eugene Churazov, Abigail Crites, Luca Di Mascolo, Dominique Eckert, Juan Macias-Perez, Frédéric Mayet, Laurence Perotto, Etienne Pointecouteau, Charles Romero, Florian Ruppin, Evan Scannapieco, and John ZuHone. Astrophysics with the Spatially and Spectrally Resolved Sunyaev-Zeldovich Effects. A Millimetre/Submillimetre Probe of the Warm

and Hot Universe. Space Sci. Rev., 215(1):17, February 2019. doi: 10.1007/s11214-019-0581-2.

[232] Ryoma Murata, Takahiro Nishimichi, Masahiro Takada, Hironao Miyatake, Masato Shirasaki, Surhud More, Ryuichi Takahashi, and Ken Osato. Constraints on the Mass-Richness Relation from the Abundance and Weak Lensing of SDSS Clusters. ApJ, 854(2):120, February 2018. doi: 10.3847/1538-4357/aaaab8.

[233] D. N. A. Murphy, J. E. Geach, and R. G. Bower. ORCA: The Overdense Red-sequence Cluster Algorithm. MNRAS, 420(3):1861–1881, March 2012. doi: 10.1111/j.1365-2966.2011.19782.x.

[234] Daisuke Nagai. The Impact of Galaxy Formation on the Sunyaev-Zel'dovich Effect of Galaxy Clusters. ApJ, 650(2):538–549, October 2006. doi: 10.1086/506467.

[235] Daisuke Nagai, Andrey V. Kravtsov, and Alexey Vikhlinin. Effects of Galaxy Formation on Thermodynamics of the Intracluster Medium. ApJ, 668(1):1–14, October 2007. doi: 10.1086/521328.

[236] Ramesh Narayan and Jeffrey E. McClintock. Advection-dominated accretion and the black hole event horizon. New A Rev., 51(10-12):733–751, May 2008. doi: 10.1016/j.newar.2008.03.002.

[237] Ramesh Narayan and Insu Yi. Advection-dominated Accretion: A Self-similar Solution. ApJ, 428:L13, June 1994. doi: 10.1086/187381.

[238] I. D. Novikov and K. S. Thorne. Astrophysics of black holes. In *Black Holes (Les Astres Occlus)*, pages 343–450, January 1973.

[239] Christopher P. O'Dea, Stefi A. Baum, George Privon, Jacob Noel-Storr, Alice C. Quillen, Nicholas Zufelt, Jaehong Park, Alastair Edge, Helen Russell, Andrew C. Fabian, Megan Donahue, Craig L. Sarazin, Brian McNamara, Joel N. Bregman, and Eiichi Egami. An Infrared Survey of Brightest Cluster Galaxies. II. Why are Some Brightest Cluster Galaxies Forming Stars? ApJ, 681(2):1035–1045, July 2008. doi: 10.1086/588212.

[240] V. Olivares, P. Salome, F. Combes, S. Hamer, P. Guillard, M. D. Lehnert, F. L. Polles, R. S. Beckmann, Y. Dubois, M. Donahue, A. Edge, A. C. Fabian, B. McNamara, T. Rose, H. R. Russell, G. Tremblay, A. Vantyghem, R. E. A. Canning, G. Ferland, B. Godard, S. Peirani, and G. Pineau des Forets. Ubiquitous cold and massive filaments in cool core clusters. A&A, 631:A22, November 2019. doi: 10.1051/0004-6361/201935350.

[241] Ewan O'Sullivan, Simona Giacintucci, Arif Babul, Somak Raychaudhury, Tiziana Venturi, Chris Bildfell, Andisheh Mahdavi, J. B. R. Oonk, Norman

Murray, Henk Hoekstra, and Megan Donahue. A Giant Metrewave Radio Telescope/Chandra view of IRAS 09104+4109: a type 2 QSO in a cooling flow. MNRAS, 424(4):2971–2993, August 2012. doi: 10.1111/j.1365-2966.2012.21459.x.

[242] E. K. Panagoulia, A. C. Fabian, and J. S. Sanders. A volume-limited sample of X-ray galaxy groups and clusters - I. Radial entropy and cooling time profiles. MNRAS, 438(3):2341–2354, March 2014. doi: 10.1093/mnras/stt2349.

[243] J. R. Peterson and A. C. Fabian. X-ray spectroscopy of cooling clusters. Phys. Rep., 427(1):1–39, April 2006. doi: 10.1016/j.physrep.2005.12.007.

[244] J. R. Peterson, F. B. S. Paerels, J. S. Kaastra, M. Arnaud, T. H. Reiprich, A. C. Fabian, R. F. Mushotzky, J. G. Jernigan, and I. Sakelliou. X-ray imaging-spectroscopy of Abell 1835. A&A, 365:L104–L109, January 2001. doi: 10.1051/0004-6361:20000021.

[245] R. Piffaretti, M. Arnaud, G. W. Pratt, E. Pointecouteau, and J. B. Melin. The MCXC: a meta-catalogue of x-ray detected clusters of galaxies. A&A, 534:A109, October 2011. doi: 10.1051/0004-6361/201015377.

[246] Annalisa Pillepich, Cristiano Porciani, and Thomas H. Reiprich. The X-ray cluster survey with eRosita: forecasts for cosmology, cluster physics and primordial non-Gaussianity. MNRAS, 422(1):44–69, May 2012. doi: 10.1111/j.1365-2966.2012.20443.x.

[247] Planck Collaboration and et al. Planck 2013 results. XXIX. The Planck catalogue of Sunyaev-Zeldovich sources. A&A, 571:A29, November 2014. doi: 10.1051/0004-6361/201321523.

[248] Planck Collaboration and et al. Planck 2015 results. XXVII. The second Planck catalogue of Sunyaev-Zeldovich sources. A&A, 594:A27, September 2016. doi: 10.1051/0004-6361/201525823.

[249] Planck Collaboration, N. Aghanim, Y. Akrami, M. Ashdown, J. Aumont, C. Baccigalupi, M. Ballardini, A. J. Banday, R. B. Barreiro, N. Bartolo, S. Basak, R. Battye, K. Benabed, J. P. Bernard, M. Bersanelli, P. Bielewicz, J. J. Bock, J. R. Bond, J. Borrill, F. R. Bouchet, F. Boulanger, M. Bucher, C. Burigana, R. C. Butler, E. Calabrese, J. F. Cardoso, J. Carron, A. Challinor, H. C. Chiang, J. Chluba, L. P. L. Colombo, C. Combet, D. Contreras, B. P. Crill, F. Cuttaia, P. de Bernardis, G. de Zotti, J. Delabrouille, J. M. Delouis, E. Di Valentino, J. M. Diego, O. Doré, M. Douspis, A. Ducout, X. Dupac, S. Dusini, G. Efstathiou, F. Elsner, T. A. Enßlin, H. K. Eriksen, Y. Fantaye, M. Farhang, J. Fergusson, R. Fernandez-Cobos, F. Finelli, F. Forastieri, M. Frailis, A. A. Fraisse, E. Franceschi, A. Frolov, S. Galeotta, S. Galli, K. Ganga, R. T. Génova-Santos, M. Gerbino, T. Ghosh, J. González-Nuevo, K. M. Górski, S. Gratton, A. Gruppuso, J. E. Gudmundsson, J. Hamann, W. Handley, F. K. Hansen, D. Herranz, S. R. Hildebrandt, E. Hivon, Z. Huang, A. H. Jaffe, W. C. Jones,

A. Karakci, E. Keihänen, R. Keskitalo, K. Kiiveri, J. Kim, T. S. Kisner, L. Knox, N. Krachmalnicoff, M. Kunz, H. Kurki-Suonio, G. Lagache, J. M. Lamarre, A. Lasenby, M. Lattanzi, C. R. Lawrence, M. Le Jeune, P. Lemos, J. Lesgourgues, F. Levrier, A. Lewis, M. Liguori, P. B. Lilje, M. Lilley, V. Lindholm, M. López-Caniego, P. M. Lubin, Y. Z. Ma, J. F. Macías-Pérez, G. Maggio, D. Maino, N. Mandolesi, A. Mangilli, A. Marcos-Caballero, M. Maris, P. G. Martin, M. Martinelli, E. Martínez-González, S. Matarrese, N. Mauri, J. D. McEwen, P. R. Meinhold, A. Melchiorri, A. Mennella, M. Migliaccio, M. Millea, S. Mitra, M. A. Miville-Deschênes, D. Molinari, L. Montier, G. Morgante, A. Moss, P. Natoli, H. U. Nørgaard-Nielsen, L. Pagano, D. Paoletti, B. Partridge, G. Patanchon, H. V. Peiris, F. Perrotta, V. Pettorino, F. Piacentini, L. Polastri, G. Polenta, J. L. Puget, J. P. Rachen, M. Reinecke, M. Remazeilles, A. Renzi, G. Rocha, C. Rosset, G. Roudier, J. A. Rubiño-Martín, B. Ruiz-Granados, L. Salvati, M. Sandri, M. Savelainen, D. Scott, E. P. S. Shellard, C. Sirignano, G. Sirri, L. D. Spencer, R. Sunyaev, A. S. Suur-Uski, J. A. Tauber, D. Tavagnacco, M. Tenti, L. Toffolatti, M. Tomasi, T. Trombetti, L. Valenziano, J. Valiviita, B. Van Tent, L. Vibert, P. Vielva, F. Villa, N. Vittorio, B. D. Wandelt, I. K. Wehus, M. White, S. D. M. White, A. Zacchei, and A. Zonca. Planck 2018 results. VI. Cosmological parameters. A&A, 641:A6, September 2020. doi: 10.1051/0004-6361/201833910.

[250] Gregory B. Poole, Arif Babul, Ian G. McCarthy, A. J. R. Sanderson, and Mark A. Fardal. The impact of mergers on relaxed X-ray clusters - III. Effects on compact cool cores. MNRAS, 391(3):1163–1175, December 2008. doi: 10.1111/j.1365-2966.2008.14003.x.

[251] Marc Postman, Lori M. Lubin, James E. Gunn, J. B. Oke, John G. Hoessel, Donald P. Schneider, and Jennifer A. Christensen. The Palomar Distant Clusters Survey. I. The Cluster Catalog. AJ, 111:615, February 1996. doi: 10.1086/117811.

[252] Deovrat Prasad, Prateek Sharma, Arif Babul, Gerard M. Voit, and Brian W. O'Shea. Cool-core cycles and Phoenix. MNRAS, 495(1):594–599, June 2020. doi: 10.1093/mnras/staa1247.

[253] P. Predehl, R. A. Sunyaev, W. Becker, H. Brunner, R. Burenin, A. Bykov, A. Cherepashchuk, N. Chugai, E. Churazov, V. Doroshenko, N. Eismont, M. Freyberg, M. Gilfanov, F. Haberl, I. Khabibullin, R. Krivonos, C. Maitra, P. Medvedev, A. Merloni, K. Nandra, V. Nazarov, M. Pavlinsky, G. Ponti, J. S. Sanders, M. Sasaki, S. Sazonov, A. W. Strong, and J. Wilms. Detection of large-scale X-ray bubbles in the Milky Way halo. Nature, 588(7837):227–231, January 2020. doi: 10.1038/s41586-020-2979-0.

[254] Peter Predehl, Robert Andritschke, Werner Becker, Walter Bornemann, Heinrich Bräuninger, Hermann Brunner, Thomas Boller, Vadim Burwitz, Wolfgang Burkert, Nicolas Clerc, Evgeniy Churazov, Diogo Coutinho, Konrad Dennerl,

Josef Eder, Valentin Emberger, Tanja Eraerds, Michael J. Freyberg, Peter Friedrich, Maria Fürmetz, Antonis Georgakakis, Christoph Grossberger, Frank Haberl, Olaf Hälker, Gisela Hartner, Günther Hasinger, Johannes Hoelzl, Heinrich Huber, Andreas von Kienlin, Walter Kink, Ingo Kreykenbohm, Georg Lamer, Ilya Lomakin, Igor Lapchov, Lorenzo Lovisari, Norbert Meidinger, Andrea Merloni, Benjamin Mican, Joseph Mohr, Siegfried Müller, Kirpal Nandra, Florian Pacaud, Mikhail N. Pavlinsky, Emanuele Perinati, Elmar Pfeffermann, Daniel Pietschner, Jonas Reiffers, Thomas Reiprich, Jan Robrade, Mara Salvato, Andrea E. Santangelo, Manami Sasaki, Hartmut Scheuerle, Christian Schmid, Jürgen Schmitt, Axel D. Schwope, Rashid Sunyaev, Christoph Tenzer, Lars Tiedemann, Weizong Xu, Valeri Yaroshenko, Sabine Walther, Michael Wille, Jörn Wilms, and Yu-Ying Zhang. eROSITA on SRG. In Tadayuki Takahashi, Jan-Willem A. den Herder, and Mark Bautz, editors, *Space Telescopes and Instrumentation 2014: Ultraviolet to Gamma Ray*, volume 9144 of *Society of Photo-Optical Instrumentation Engineers (SPIE) Conference Series*, page 91441T, July 2014. doi: 10.1117/12.2055426.

[255] Peter Predehl, Walter Bornemann, Heinrich Bräuninger, Hermann Brunner, Vadim Burwitz, Diogo Coutinho, Konrad Dennerl, Josef Eder, Peter Friedrich, Maria Fürmetz, Gisela Hartner, Andreas von Kienlin, Walter Kink, Norbert Meidinger, Benjamin Mican, Siegfried Müller, Kirpal Nandra, Elmar Pfeffermann, Christian Rohé, and Valeri Yaroshenko. eROSITA mated with SRG. In Jan-Willem A. den Herder, Shouleh Nikzad, and Kazuhiro Nakazawa, editors, *Space Telescopes and Instrumentation 2018: Ultraviolet to Gamma Ray*, volume 10699 of *Society of Photo-Optical Instrumentation Engineers (SPIE) Conference Series*, page 106995H, July 2018. doi: 10.1117/12.2315139.

[256] D. A. Rafferty, B. R. McNamara, P. E. J. Nulsen, and M. W. Wise. The Feedback-regulated Growth of Black Holes and Bulges through Gas Accretion and Starbursts in Cluster Central Dominant Galaxies. ApJ, 652(1):216–231, November 2006. doi: 10.1086/507672.

[257] D. A. Rafferty, B. R. McNamara, and P. E. J. Nulsen. The Regulation of Cooling and Star Formation in Luminous Galaxies by Active Galactic Nucleus Feedback and the Cooling-Time/Entropy Threshold for the Onset of Star Formation. ApJ, 687(2):899–918, November 2008. doi: 10.1086/591240.

[258] Alexandre Refregier and David Bacon. Shapelets - II. A method for weak lensing measurements. MNRAS, 338(1):48–56, January 2003. doi: 10.1046/j.1365-8711.2003.05902.x.

[259] Christopher S. Reynolds, Sebastian Heinz, and Mitchell C. Begelman. The hydrodynamics of dead radio galaxies. MNRAS, 332(2):271–282, May 2002. doi: 10.1046/j.1365-8711.2002.04724.x.

[260] E. Rizza, J. O. Burns, M. J. Ledlow, F. N. Owen, W. Voges, and M. Bliton. X-

ray observations of distant Abell clusters. MNRAS, 301(2):328–342, December 1998. doi: 10.1046/j.1365-8711.1998.01972.x.

[261] Daniel Rosa-González, Elena Terlevich, and Roberto Terlevich. An empirical calibration of star formation rate estimators. MNRAS, 332(2):283–295, May 2002. doi: 10.1046/j.1365-8711.2002.05285.x.

[262] R. Rosner and W. H. Tucker. On Magnetic Fields, Heating and Thermal Conduction in Halos, and the Suppression of Cooling Flows. ApJ, 338:761, March 1989. doi: 10.1086/167234.

[263] M. Rossetti, F. Gastaldello, D. Eckert, M. Della Torre, G. Pantiri, P. Cazzoletti, and S. Molendi. The cool-core state of Planck SZ-selected clusters versus X-ray-selected samples: evidence for cool-core bias. MNRAS, 468(2):1917–1930, June 2017. doi: 10.1093/mnras/stx493.

[264] Eduardo Rozo, Eli S. Rykoff, Benjamin P. Koester, Timothy McKay, Jiangang Hao, August Evrard, Risa H. Wechsler, Sarah Hansen, Erin Sheldon, David Johnston, Matthew Becker, James Annis, Lindsey Bleem, and Ryan Scranton. Improvement of the Richness Estimates of maxBCG Clusters. ApJ, 703(1): 601–613, September 2009. doi: 10.1088/0004-637X/703/1/601.

[265] A. Ruiz, G. Risaliti, E. Nardini, F. Panessa, and F. J. Carrera. Analysis of Spitzer-IRS spectra of hyperluminous infrared galaxies. A&A, 549:A125, January 2013. doi: 10.1051/0004-6361/201015257.

[266] F. Ruppin, M. McDonald, L. E. Bleem, S. W. Allen, B. A. Benson, M. Calzadilla, G. Khullar, and B. Floyd. Stability of Cool Cores During Galaxy Cluster Growth: A Joint *Chandra*/SPT Analysis of 67 Galaxy Clusters Along a Common Evolutionary Track Spanning 9 Gyr. *arXiv e-prints*, art. arXiv:2012.14669, December 2020.

[267] H. R. Russell, A. C. Fabian, J. S. Sanders, R. M. Johnstone, K. M. Blundell, W. N. Brandt, and C. S. Crawford. The X-ray luminous cluster underlying the bright radio-quiet quasar H1821+643. MNRAS, 402(3):1561–1579, March 2010. doi: 10.1111/j.1365-2966.2009.16027.x.

[268] H. R. Russell, B. R. McNamara, A. C. Edge, M. T. Hogan, R. A. Main, and A. N. Vantyghem. Radiative efficiency, variability and Bondi accretion on to massive black holes: the transition from radio AGN to quasars in brightest cluster galaxies. MNRAS, 432(1):530–553, June 2013. doi: 10.1093/mnras/stt490.

[269] H. R. Russell, M. McDonald, B. R. McNamara, A. C. Fabian, P. E. J. Nulsen, M. B. Bayliss, B. A. Benson, M. Brodwin, J. E. Carlstrom, A. C. Edge, J. Hlavacek-Larrondo, D. P. Marrone, C. L. Reichardt, and J. D.

Vieira. Alma Observations of Massive Molecular Gas Filaments Encasing Radio Bubbles in the Phoenix Cluster. ApJ, 836(1):130, February 2017. doi: 10.3847/1538-4357/836/1/130.

[270] E. S. Rykoff, B. P. Koester, E. Rozo, J. Annis, A. E. Evrard, S. M. Hansen, J. Hao, D. E. Johnston, T. A. McKay, and R. H. Wechsler. Robust Optical Richness Estimation with Reduced Scatter. ApJ, 746(2):178, February 2012. doi: 10.1088/0004-637X/746/2/178.

[271] E. S. Rykoff, E. Rozo, M. T. Busha, C. E. Cunha, A. Finoguenov, A. Evrard, J. Hao, B. P. Koester, A. Leauthaud, B. Nord, M. Pierre, R. Reddick, T. Sadibekova, E. S. Sheldon, and R. H. Wechsler. redMaPPer. I. Algorithm and SDSS DR8 Catalog. ApJ, 785(2):104, April 2014. doi: 10.1088/0004-637X/785/2/104.

[272] Edwin E. Salpeter. The Luminosity Function and Stellar Evolution. ApJ, 121: 161, January 1955. doi: 10.1086/145971.

[273] J. S. Sanders, A. C. Fabian, S. W. Allen, R. G. Morris, J. Graham, and R. M. Johnstone. Cool X-ray emitting gas in the core of the Centaurus cluster of galaxies. MNRAS, 385(3):1186–1200, April 2008. doi: 10.1111/j.1365-2966.2008.12952.x.

[274] Craig L. Sarazin. X-ray emission from clusters of galaxies. *Reviews of Modern Physics*, 58(1):1–115, January 1986. doi: 10.1103/RevModPhys.58.1.

[275] Craig L. Sarazin. *X-Ray Emission from Clusters of Galaxies*. Cambridge University Press, 2009.

[276] P. Schechter. An analytic expression for the luminosity function for galaxies. ApJ, 203:297–306, January 1976. doi: 10.1086/154079.

[277] Neelima Sehgal, Hy Trac, Viviana Acquaviva, Peter A. R. Ade, Paula Aguirre, Mandana Amiri, John W. Appel, L. Felipe Barrientos, Elia S. Battistelli, J. Richard Bond, Ben Brown, Bryce Burger, Jay Chervenak, Sudeep Das, Mark J. Devlin, Simon R. Dicker, W. Bertrand Doriese, Joanna Dunkley, Rolando Dünner, Thomas Essinger-Hileman, Ryan P. Fisher, Joseph W. Fowler, Amir Hajian, Mark Halpern, Matthew Hasselfield, Carlos Hernández-Monteagudo, Gene C. Hilton, Matt Hilton, Adam D. Hincks, Renée Hlozek, David Holtz, Kevin M. Huffenberger, David H. Hughes, John P. Hughes, Leopoldo Infante, Kent D. Irwin, Andrew Jones, Jean Baptiste Juin, Jeff Klein, Arthur Kosowsky, Judy M. Lau, Michele Limon, Yen-Ting Lin, Robert H. Lupton, Tobias A. Marriage, Danica Marsden, Krista Martocci, Phil Mauskopf, Felipe Menanteau, Kavilan Moodley, Harvey Moseley, Calvin B. Netterfield, Michael D. Niemack, Michael R. Nolta, Lyman A. Page, Lucas Parker, Bruce Partridge, Beth Reid, Blake D. Sherwin, Jon Sievers, David N. Spergel,

Suzanne T. Staggs, Daniel S. Swetz, Eric R. Switzer, Robert Thornton, Carole Tucker, Ryan Warne, Ed Wollack, and Yue Zhao. The Atacama Cosmology Telescope: Cosmology from Galaxy Clusters Detected via the Sunyaev-Zel'dovich Effect. ApJ, 732(1):44, May 2011. doi: 10.1088/0004-637X/732/1/44.

[278] Federico Sembolini, Gustavo Yepes, Marco De Petris, Stefan Gottlöber, Luca Lamagna, and Barbara Comis. The MUSIC of galaxy clusters - I. Baryon properties and scaling relations of the thermal Sunyaev-Zel'dovich effect. MNRAS, 429(1):323–343, February 2013. doi: 10.1093/mnras/sts339.

[279] I. Sevilla-Noarbe, B. Hoyle, M. J. Marchã, M. T. Soumagnac, K. Bechtol, A. Drlica-Wagner, F. Abdalla, J. Aleksić, C. Avestruz, E. Balbinot, M. Banerji, E. Bertin, C. Bonnett, R. Brunner, M. Carrasco-Kind, A. Choi, T. Giannantonio, E. Kim, O. Lahav, B. Moraes, B. Nord, A. J. Ross, E. S. Rykoff, B. Santiago, E. Sheldon, K. Wei, W. Wester, B. Yanny, T. Abbott, S. Allam, D. Brooks, A. Carnero-Rosell, J. Carretero, C. Cunha, L. da Costa, C. Davis, J. de Vicente, S. Desai, P. Doel, E. Fernandez, B. Flaugher, J. Frieman, J. Garcia-Bellido, E. Gaztanaga, D. Gruen, R. Gruendl, J. Gschwend, G. Gutierrez, D. L. Hollowood, K. Honscheid, D. James, T. Jeltema, D. Kirk, E. Krause, K. Kuehn, T. S. Li, M. Lima, M. A. G. Maia, M. March, R. G. McMahon, F. Menanteau, R. Miquel, R. L. C. Ogando, A. A. Plazas, E. Sanchez, V. Scarpine, R. Schindler, M. Schubnell, M. Smith, R. C. Smith, M. Soares-Santos, F. Sobreira, E. Suchyta, M. E. C. Swanson, G. Tarle, D. Thomas, D. L. Tucker, A. R. Walker, and DES Collaboration. Star-galaxy classification in the Dark Energy Survey Y1 data set. MNRAS, 481(4):5451–5469, December 2018. doi: 10.1093/mnras/sty2579.

[280] I. Sevilla-Noarbe, K. Bechtol, M. Carrasco Kind, A. Carnero Rosell, M. R. Becker, A. Drlica-Wagner, R. A. Gruendl, E. S. Rykoff, E. Sheldon, B. Yanny, A. Alarcon, S. Allam, A. Amon, A. Benoit-Lévy, G. M. Bernstein, E. Bertin, D. L. Burke, J. Carretero, A. Choi, H. T. Diehl, S. Everett, B. Flaugher, E. Gaztanaga, J. Gschwend, I. Harrison, W. G. Hartley, B. Hoyle, M. Jarvis, M. D. Johnson, R. Kessler, R. Kron, N. Kuropatkin, B. Leistedt, T. S. Li, F. Menanteau, E. Morganson, R. L. C. Ogando, A. Palmese, F. Paz-Chinchón, A. Pieres, C. Pond, M. Rodriguez-Monroy, J. Allyn Smith, K. M. Stringer, M. A. Troxel, D. L. Tucker, J. de Vicente, W. Wester, Y. Zhang, T. M. C. Abbott, M. Aguena, J. Annis, S. Avila, S. Bhargava, S. L. Bridle, D. Brooks, D. Brout, F. J. Castander, R. Cawthon, C. Chang, C. Conselice, M. Costanzi, M. Crocce, L. N. da Costa, M. E. S. Pereira, T. M. Davis, S. Desai, J. P. Dietrich, P. Doel, K. Eckert, A. E. Evrard, I. Ferrero, P. Fosalba, J. García-Bellido, D. W. Gerdes, T. Giannantonio, D. Gruen, G. Gutierrez, S. R. Hinton, D. L. Hollowood, K. Honscheid, E. M. Huff, D. Huterer, D. J. James, T. Jeltema, K. Kuehn, O. Lahav, C. Lidman, M. Lima, H. Lin, M. A. G. Maia, J. L. Marshall, P. Martini, P. Melchior, R. Miquel, J. J. Mohr, R. Morgan, E. Neilsen, A. A. Plazas, A. K. Romer, A. Roodman, E. Sanchez, V. Scarpine, M. Schubnell, S. Serrano,

M. Smith, E. Suchyta, G. Tarle, D. Thomas, C. To, T. N. Varga, R. H. Wechsler, J. Weller, R. D. Wilkinson, and DES Collaboration. Dark Energy Survey Year 3 Results: Photometric Data Set for Cosmology. ApJS, 254(2):24, June 2021. doi: 10.3847/1538-4365/abeb66.

[281] N. I. Shakura and R. A. Sunyaev. Reprint of 1973A&A....24..337S. Black holes in binary systems. Observational appearance. A&A, 500:33–51, June 1973.

[282] Keren Sharon, Michael D. Gladders, Jane R. Rigby, Eva Wuyts, Matthew B. Bayliss, Traci L. Johnson, Michael K. Florian, and Hakon Dahle. The Mass Distribution of the Strong Lensing Cluster SDSS J1531+3414. ApJ, 795(1):50, November 2014. doi: 10.1088/0004-637X/795/1/50.

[283] Aneta Siemiginowska, C. C. Cheung, Stephanie LaMassa, D. J. Burke, Thomas L. Aldcroft, Jill Bechtold, Martin Elvis, and D. M. Worrall. X-Ray Cluster Associated with the z = 1.063 CSS Quasar 3C 186: The Jet is Not Frustrated. ApJ, 632(1):110–121, October 2005. doi: 10.1086/432871.

[284] Aneta Siemiginowska, D. J. Burke, Thomas L. Aldcroft, D. M. Worrall, S. Allen, Jill Bechtold, Tracy Clarke, and C. C. Cheung. High-redshift X-ray Cooling-core Cluster Associated with the Luminous Radio-loud Quasar 3C 186. ApJ, 722(1):102–111, October 2010. doi: 10.1088/0004-637X/722/1/102.

[285] Joseph Silk and Martin J. Rees. Quasars and galaxy formation. A&A, 331: L1–L4, March 1998.

[286] J. D. Silverman, P. J. Green, W. A. Barkhouse, D. W. Kim, M. Kim, B. J. Wilkes, R. A. Cameron, G. Hasinger, B. T. Jannuzi, M. G. Smith, P. S. Smith, and H. Tananbaum. The Luminosity Function of X-Ray-selected Active Galactic Nuclei: Evolution of Supermassive Black Holes at High Redshift. ApJ, 679(1): 118–139, May 2008. doi: 10.1086/529572.

[287] J. D. Silverman, K. Kovač, C. Knobel, S. Lilly, M. Bolzonella, F. Lamareille, V. Mainieri, M. Brusa, N. Cappelluti, Y. Peng, G. Hasinger, G. Zamorani, M. Scodeggio, T. Contini, C. M. Carollo, K. Jahnke, J. P. Kneib, O. Le Fevre, S. Bardelli, A. Bongiorno, H. Brunner, K. Caputi, F. Civano, A. Comastri, G. Coppa, O. Cucciati, S. de la Torre, L. de Ravel, M. Elvis, A. Finoguenov, F. Fiore, P. Franzetti, B. Garilli, R. Gilli, R. Griffiths, A. Iovino, P. Kampczyk, A. Koekemoer, J. F. Le Borgne, V. Le Brun, C. Maier, M. Mignoli, R. Pello, E. Perez Montero, E. Ricciardelli, M. Tanaka, L. Tasca, L. Tresse, D. Vergani, C. Vignali, E. Zucca, D. Bottini, A. Cappi, P. Cassata, C. Marinoni, H. J. McCracken, P. Memeo, B. Meneux, P. Oesch, C. Porciani, and M. Salvato. The Environments of Active Galactic Nuclei within the zCOSMOS Density Field. ApJ, 695(1):171–182, April 2009. doi: 10.1088/0004-637X/695/1/171.

[288] J. Singal, J. George, and A. Gerber. The Mid-infrared Luminosity Evolution and Luminosity Function of Quasars with WISE and SDSS. ApJ, 831(1):60, November 2016. doi: 10.3847/0004-637X/831/1/60.

[289] M. F. Skrutskie, R. M. Cutri, R. Stiening, M. D. Weinberg, S. Schneider, J. M. Carpenter, C. Beichman, R. Capps, T. Chester, J. Elias, J. Huchra, J. Liebert, C. Lonsdale, D. G. Monet, S. Price, P. Seitzer, T. Jarrett, J. D. Kirkpatrick, J. E. Gizis, E. Howard, T. Evans, J. Fowler, L. Fullmer, R. Hurt, R. Light, E. L. Kopan, K. A. Marsh, H. L. McCallon, R. Tam, S. Van Dyk, and S. Wheelock. The Two Micron All Sky Survey (2MASS). AJ, 131(2):1163–1183, February 2006. doi: 10.1086/498708.

[290] G. F. Smoot, C. L. Bennett, A. Kogut, E. L. Wright, J. Aymon, N. W. Boggess, E. S. Cheng, G. de Amici, S. Gulkis, M. G. Hauser, G. Hinshaw, P. D. Jackson, M. Janssen, E. Kaita, T. Kelsall, P. Keegstra, C. Lineweaver, K. Loewenstein, P. Lubin, J. Mather, S. S. Meyer, S. H. Moseley, T. Murdock, L. Rokke, R. F. Silverberg, L. Tenorio, R. Weiss, and D. T. Wilkinson. Structure in the COBE Differential Microwave Radiometer First-Year Maps. ApJ, 396:L1, September 1992. doi: 10.1086/186504.

[291] Marcelle Soares-Santos, Reinaldo R. de Carvalho, James Annis, Roy R. Gal, Francesco La Barbera, Paulo A. A. Lopes, Risa H. Wechsler, Michael T. Busha, and Brian F. Gerke. The Voronoi Tessellation Cluster Finder in 2+1 Dimensions. ApJ, 727(1):45, January 2011. doi: 10.1088/0004-637X/727/1/45.

[292] Taweewat Somboonpanyakul, Michael McDonald, Henry W. Lin, Brian Stalder, and Antony Stark. The Clusters Hiding in Plain Sight (CHiPS) Survey: A First Discovery of a Massive Nearby Cluster around PKS 1353-341. ApJ, 863(2):122, August 2018. doi: 10.3847/1538-4357/aace55.

[293] Taweewat Somboonpanyakul, Michael McDonald, Matthew Bayliss, Mark Voit, Megan Donahue, Massimo Gaspari, Hakon Dahle, Emil Rivera-Thorsen, and Antony Stark. The Clusters Hiding in Plain Sight (CHiPS) Survey: CHIPS1911+4455, a Rapidly Cooling Core in a Merging Cluster. ApJ, 907 (1):L12, January 2021. doi: 10.3847/2041-8213/abd540.

[294] Taweewat Somboonpanyakul, Michael McDonald, Massimo Gaspari, Brian Stalder, and Antony A. Stark. The Clusters Hiding in Plain Sight (CHiPS) survey: Complete sample of extreme BCG clusters. *arXiv e-prints*, art. arXiv:2101.01730, January 2021.

[295] W. B. Sparks. Mergers, Cooling Flows, and Evaporation. ApJ, 399:66, November 1992. doi: 10.1086/171903.

[296] W. B. Sparks, F. Macchetto, and D. Golombek. Imaging Observations of Gas and Dust in NGC 4696 and Implications for Cooling Flow Models. ApJ, 345: 153, October 1989. doi: 10.1086/167890.

[297] D. N. Spergel, L. Verde, H. V. Peiris, E. Komatsu, M. R. Nolta, C. L. Bennett, M. Halpern, G. Hinshaw, N. Jarosik, A. Kogut, M. Limon, S. S. Meyer, L. Page, G. S. Tucker, J. L. Weiland, E. Wollack, and E. L. Wright. First-Year

Wilkinson Microwave Anisotropy Probe (WMAP) Observations: Determination of Cosmological Parameters. ApJS, 148(1):175–194, September 2003. doi: 10.1086/377226.

[298] Brian Stalder, Antony A. Stark, Stephen M. Amato, John Geary, Stephen A. Shectman, Christopher W. Stubbs, and Andrew Szentgyorgyi. PISCO: the Parallel Imager for Southern Cosmology Observations. In Suzanne K. Ramsay, Ian S. McLean, and Hideki Takami, editors, *Ground-based and Airborne Instrumentation for Astronomy V*, volume 9147 of *Society of Photo-Optical Instrumentation Engineers (SPIE) Conference Series*, page 91473Y, July 2014. doi: 10.1117/12.2054933.

[299] R. Stanek, E. Rasia, A. E. Evrard, F. Pearce, and L. Gazzola. Massive Halos in Millennium Gas Simulations: Multivariate Scaling Relations. ApJ, 715(2): 1508–1523, June 2010. doi: 10.1088/0004-637X/715/2/1508.

[300] S. A. Stanford, Anthony H. Gonzalez, Mark Brodwin, Daniel P. Gettings, Peter R. M. Eisenhardt, Daniel Stern, and Dominika Wylezalek. The Massive and Distant Clusters of WISE Survey. II. Initial Spectroscopic Confirmation of z ~1 Galaxy Clusters Selected from 10,000 deg^2. ApJS, 213(2):25, August 2014. doi: 10.1088/0067-0049/213/2/25.

[301] Daniel Stern, S. G. Djorgovski, R. A. Perley, Reinaldo R. de Carvalho, and J. V. Wall. Radio Properties of Z>4 Optically Selected Quasars. AJ, 119(4): 1526–1533, April 2000. doi: 10.1086/301316.

[302] Daniel Stern, Peter Eisenhardt, Varoujan Gorjian, Christopher S. Kochanek, Nelson Caldwell, Daniel Eisenstein, Mark Brodwin, Michael J. I. Brown, Richard Cool, Arjun Dey, Paul Green, Buell T. Jannuzi, Stephen S. Murray, Michael A. Pahre, and S. P. Willner. Mid-Infrared Selection of Active Galaxies. ApJ, 631(1):163–168, September 2005. doi: 10.1086/432523.

[303] Daniel Stern, Roberto J. Assef, Dominic J. Benford, Andrew Blain, Roc Cutri, Arjun Dey, Peter Eisenhardt, Roger L. Griffith, T. H. Jarrett, Sean Lake, Frank Masci, Sara Petty, S. A. Stanford, Chao-Wei Tsai, E. L. Wright, Lin Yan, Fiona Harrison, and Kristin Madsen. Mid-infrared Selection of Active Galactic Nuclei with the Wide-Field Infrared Survey Explorer. I. Characterizing WISE-selected Active Galactic Nuclei in COSMOS. ApJ, 753(1):30, July 2012. doi: 10.1088/0004-637X/753/1/30.

[304] A. Streblyanska, A. Aguado-Barahona, A. Ferragamo, R. Barrena, J. A. Rubiño-Martín, D. Tramonte, R. T. Genova-Santos, and H. Lietzen. Optical validation and characterization of Planck PSZ2 sources at the Canary Islands observatories. I. First year of LP15 observations. A&A, 628:A13, August 2019. doi: 10.1051/0004-6361/201935674.

[305] M. Sun. Every BCG with a Strong Radio Agn has an X-Ray Cool Core: Is the Cool Core-Noncool Core Dichotomy Too Simple? ApJ, 704(2):1586–1604, October 2009. doi: 10.1088/0004-637X/704/2/1586.

[306] R. A. Sunyaev and Ya. B. Zeldovich. Formation of Clusters of Galaxies; Protocluster Fragmentation and Intergalactic Gas Heating. A&A, 20:189, August 1972.

[307] Ralph S. Sutherland and M. A. Dopita. Cooling Functions for Low-Density Astrophysical Plasmas. ApJS, 88:253, September 1993. doi: 10.1086/191823.

[308] T. Szabo, E. Pierpaoli, F. Dong, A. Pipino, and J. Gunn. An Optical Catalog of Galaxy Clusters Obtained from an Adaptive Matched Filter Finder Applied to Sloan Digital Sky Survey Data Release 6. ApJ, 736(1):21, July 2011. doi: 10.1088/0004-637X/736/1/21.

[309] T. Tamura, J. S. Kaastra, J. R. Peterson, F. B. S. Paerels, J. P. D. Mittaz, S. P. Trudolyubov, G. Stewart, A. C. Fabian, R. F. Mushotzky, D. H. Lumb, and Y. Ikebe. X-ray spectroscopy of the cluster of galaxies Abell 1795 with XMM-Newton. A&A, 365:L87–L92, January 2001. doi: 10.1051/0004-6361:20000038.

[310] A. N. Taylor, S. Dye, T. J. Broadhurst, N. Benítez, and E. van Kampen. Gravitational Lens Magnification and the Mass of Abell 1689. ApJ, 501(2):539–553, July 1998. doi: 10.1086/305827.

[311] Karun Thanjavur, Jon Willis, and David Crampton. K2: A New Method for the Detection of Galaxy Clusters Based on Canada-France-Hawaii Telescope Legacy Survey Multicolor Images. ApJ, 706(1):571–591, November 2009. doi: 10.1088/0004-637X/706/1/571.

[312] Jeremy Tinker, Andrey V. Kravtsov, Anatoly Klypin, Kevork Abazajian, Michael Warren, Gustavo Yepes, Stefan Gottlöber, and Daniel E. Holz. Toward a Halo Mass Function for Precision Cosmology: The Limits of Universality. ApJ, 688(2):709–728, December 2008. doi: 10.1086/591439.

[313] J. L. Tonry, C. W. Stubbs, K. R. Lykke, P. Doherty, I. S. Shivvers, W. S. Burgett, K. C. Chambers, K. W. Hodapp, N. Kaiser, R. P. Kudritzki, E. A. Magnier, J. S. Morgan, P. A. Price, and R. J. Wainscoat. The Pan-STARRS1 Photometric System. ApJ, 750(2):99, May 2012. doi: 10.1088/0004-637X/750/2/99.

[314] G. R. Tremblay, C. P. O'Dea, S. A. Baum, R. Mittal, M. A. McDonald, F. Combes, Y. Li, B. R. McNamara, M. N. Bremer, T. E. Clarke, M. Donahue, A. C. Edge, A. C. Fabian, S. L. Hamer, M. T. Hogan, J. B. R. Oonk, A. C. Quillen, J. S. Sanders, P. Salomé, and G. M. Voit. Far-ultraviolet morphology of star-forming filaments in cool core brightest cluster galaxies. MNRAS, 451(4):3768–3800, August 2015. doi: 10.1093/mnras/stv1151.

[315] Joachim Truemper. ROSAT-A New Look at the X-ray Sky. *Science*, 260(5115): 1769–1771, June 1993. doi: 10.1126/science.260.5115.1769.

[316] W. Tucker, P. Blanco, S. Rappoport, L. David, D. Fabricant, E. E. Falco, W. Forman, A. Dressler, and M. Ramella. 1E 0657-56: A Contender for the Hottest Known Cluster of Galaxies. ApJ, 496(1):L5–L8, March 1998. doi: 10.1086/311234.

[317] Pieter G. van Dokkum. Cosmic-Ray Rejection by Laplacian Edge Detection. PASP, 113(789):1420–1427, November 2001. doi: 10.1086/323894.

[318] M. P. van Haarlem, C. S. Frenk, and S. D. M. White. Projection effects in cluster catalogues. MNRAS, 287(4):817–832, June 1997. doi: 10.1093/mnras/287.4.817.

[319] K. Vanderlinde, T. M. Crawford, T. de Haan, J. P. Dudley, L. Shaw, P. A. R. Ade, K. A. Aird, B. A. Benson, L. E. Bleem, M. Brodwin, J. E. Carlstrom, C. L. Chang, A. T. Crites, S. Desai, M. A. Dobbs, R. J. Foley, E. M. George, M. D. Gladders, N. R. Hall, N. W. Halverson, F. W. High, G. P. Holder, W. L. Holzapfel, J. D. Hrubes, M. Joy, R. Keisler, L. Knox, A. T. Lee, E. M. Leitch, A. Loehr, M. Lueker, D. P. Marrone, J. J. McMahon, J. Mehl, S. S. Meyer, J. J. Mohr, T. E. Montroy, C. C. Ngeow, S. Padin, T. Plagge, C. Pryke, C. L. Reichardt, A. Rest, J. Ruel, J. E. Ruhl, K. K. Schaffer, E. Shirokoff, J. Song, H. G. Spieler, B. Stalder, Z. Staniszewski, A. A. Stark, C. W. Stubbs, A. van Engelen, J. D. Vieira, R. Williamson, Y. Yang, O. Zahn, and A. Zenteno. Galaxy Clusters Selected with the Sunyaev-Zel'dovich Effect from 2008 South Pole Telescope Observations. ApJ, 722(2):1180–1196, October 2010. doi: 10.1088/0004-637X/722/2/1180.

[320] A. Vikhlinin, A. Kravtsov, W. Forman, C. Jones, M. Markevitch, S. S. Murray, and L. Van Speybroeck. Chandra Sample of Nearby Relaxed Galaxy Clusters: Mass, Gas Fraction, and Mass-Temperature Relation. ApJ, 640(2):691–709, April 2006. doi: 10.1086/500288.

[321] A. Vikhlinin, R. A. Burenin, H. Ebeling, W. R. Forman, A. Hornstrup, C. Jones, A. V. Kravtsov, S. S. Murray, D. Nagai, H. Quintana, and A. Voevodkin. Chandra Cluster Cosmology Project. II. Samples and X-Ray Data Reduction. ApJ, 692(2):1033–1059, February 2009. doi: 10.1088/0004-637X/692/2/1033.

[322] A. Vikhlinin, A. V. Kravtsov, R. A. Burenin, H. Ebeling, W. R. Forman, A. Hornstrup, C. Jones, S. S. Murray, D. Nagai, H. Quintana, and A. Voevodkin. Chandra Cluster Cosmology Project III: Cosmological Parameter Constraints. ApJ, 692(2):1060–1074, February 2009. doi: 10.1088/0004-637X/692/2/1060.

[323] W. Voges, B. Aschenbach, Th. Boller, H. Bräuninger, U. Briel, W. Burkert, K. Dennerl, J. Englhauser, R. Gruber, F. Haberl, G. Hartner, G. Hasinger, M. Kürster, E. Pfeffermann, W. Pietsch, P. Predehl, C. Rosso, J. H. M. M.

Schmitt, J. Trümper, and H. U. Zimmermann. The ROSAT all-sky survey bright source catalogue. A&A, 349:389–405, September 1999.

[324] Wolfgang Voges. The ROSAT All-Sky X-ray survey. Environment Observation and Climate Modelling Through International Space Projects, July 1992.

[325] G. M. Voit, M. Donahue, G. L. Bryan, and M. McDonald. Regulation of star formation in giant galaxies by precipitation, feedback and conduction. Nature, 519(7542):203–206, March 2015. doi: 10.1038/nature14167.

[326] G. Mark Voit. Tracing cosmic evolution with clusters of galaxies. *Reviews of Modern Physics*, 77(1):207–258, April 2005. doi: 10.1103/RevModPhys.77.207.

[327] G. Mark Voit. A Role for Turbulence in Circumgalactic Precipitation. ApJ, 868(2):102, December 2018. doi: 10.3847/1538-4357/aae8e2.

[328] G. Mark Voit and Megan Donahue. An Observationally Motivated Framework for AGN Heating of Cluster Cores. ApJ, 634(2):955–963, December 2005. doi: 10.1086/497063.

[329] G. Mark Voit, Greg Meece, Yuan Li, Brian W. O'Shea, Greg L. Bryan, and Megan Donahue. A Global Model for Circumgalactic and Cluster-core Precipitation. ApJ, 845(1):80, August 2017. doi: 10.3847/1538-4357/aa7d04.

[330] S. A. Walker, A. C. Fabian, H. R. Russell, and J. S. Sanders. The effect of the quasar H1821+643 on the surrounding intracluster medium: revealing the underlying cooling flow. MNRAS, 442(3):2809–2816, August 2014. doi: 10.1093/mnras/stu1067.

[331] Tracy M. A. Webb, Adam Muzzin, Allison Noble, Nina Bonaventura, James Geach, Yashar Hezaveh, Chris Lidman, Gillian Wilson, H. K. C. Yee, Jason Surace, and David Shupe. The Star Formation History of BCGs to z = 1.8 from the SpARCS/SWIRE Survey: Evidence for Significant In Situ Star Formation at High Redshift. ApJ, 814(2):96, December 2015. doi: 10.1088/0004-637X/814/2/96.

[332] Xiao-Qing Wen, Hong Wu, Chen Cao, and Xiao-Yang Xia. Mid-to-Far Infrared Spectral Energy Distribution of Galaxies in the Spitzer First Look Survey Field. Chinese J. Astron. Astrophys., 7(2):187–198, April 2007. doi: 10.1088/1009-9271/7/2/02.

[333] Z. L. Wen and J. L. Han. Dependence of the bright end of composite galaxy luminosity functions on cluster dynamical states. MNRAS, 448(1):2–8, March 2015. doi: 10.1093/mnras/stu2722.

[334] Z. L. Wen, J. L. Han, and F. S. Liu. A Catalog of 132,684 Clusters of Galaxies Identified from Sloan Digital Sky Survey III. ApJS, 199(2):34, April 2012. doi: 10.1088/0067-0049/199/2/34.

[335] Simon D. M. White, Julio F. Navarro, August E. Evrard, and Carlos S. Frenk. The baryon content of galaxy clusters: a challenge to cosmological orthodoxy. Nature, 366(6454):429–433, December 1993. doi: 10.1038/366429a0.

[336] R. Williamson, B. A. Benson, F. W. High, K. Vanderlinde, P. A. R. Ade, K. A. Aird, K. Andersson, R. Armstrong, M. L. N. Ashby, M. Bautz, G. Bazin, E. Bertin, L. E. Bleem, M. Bonamente, M. Brodwin, J. E. Carlstrom, C. L. Chang, S. C. Chapman, A. Clocchiatti, T. M. Crawford, A. T. Crites, T. de Haan, S. Desai, M. A. Dobbs, J. P. Dudley, G. G. Fazio, R. J. Foley, W. R. Forman, G. Garmire, E. M. George, M. D. Gladders, A. H. Gonzalez, N. W. Halverson, G. P. Holder, W. L. Holzapfel, S. Hoover, J. D. Hrubes, C. Jones, M. Joy, R. Keisler, L. Knox, A. T. Lee, E. M. Leitch, M. Lueker, D. Luong-Van, D. P. Marrone, J. J. McMahon, J. Mehl, S. S. Meyer, J. J. Mohr, T. E. Montroy, S. S. Murray, S. Padin, T. Plagge, C. Pryke, C. L. Reichardt, A. Rest, J. Ruel, J. E. Ruhl, B. R. Saliwanchik, A. Saro, K. K. Schaffer, L. Shaw, E. Shirokoff, J. Song, H. G. Spieler, B. Stalder, S. A. Stanford, Z. Staniszewski, A. A. Stark, K. Story, C. W. Stubbs, J. D. Vieira, A. Vikhlinin, and A. Zenteno. A Sunyaev-Zel'dovich-selected Sample of the Most Massive Galaxy Clusters in the 2500 deg^2 South Pole Telescope Survey. ApJ, 738(2):139, September 2011. doi: 10.1088/0004-637X/738/2/139.

[337] Edward L. Wright, Peter R. M. Eisenhardt, Amy K. Mainzer, Michael E. Ressler, Roc M. Cutri, Thomas Jarrett, J. Davy Kirkpatrick, Deborah Padgett, Robert S. McMillan, Michael Skrutskie, S. A. Stanford, Martin Cohen, Russell G. Walker, John C. Mather, David Leisawitz, III Gautier, Thomas N., Ian McLean, Dominic Benford, Carol J. Lonsdale, Andrew Blain, Bryan Mendez, William R. Irace, Valerie Duval, Fengchuan Liu, Don Royer, Ingolf Heinrichsen, Joan Howard, Mark Shannon, Martha Kendall, Amy L. Walsh, Mark Larsen, Joel G. Cardon, Scott Schick, Mark Schwalm, Mohamed Abid, Beth Fabinsky, Larry Naes, and Chao-Wei Tsai. The Wide-field Infrared Survey Explorer (WISE): Mission Description and Initial On-orbit Performance. AJ, 140(6): 1868–1881, December 2010. doi: 10.1088/0004-6256/140/6/1868.

[338] Xiang-Ping Wu, Tzihong Chiueh, Li-Zhi Fang, and Yan-Jie Xue. A comparison of different cluster mass estimates: consistency or discrepancy? MNRAS, 301 (3):861–871, December 1998. doi: 10.1046/j.1365-8711.1998.02055.x.

[339] Lilan Yang, Paolo Tozzi, Heng Yu, Elisabeta Lusso, Massimo Gaspari, Roberto Gilli, Emanuele Nardini, and Guido Risaliti. X-Ray Properties of AGN in Brightest Cluster Galaxies. I. A Systematic Study of the Chandra Archive in the $0.2 < z < 0.3$ and $0.55 < z < 0.75$ Redshift Range. ApJ, 859(1):65, May 2018. doi: 10.3847/1538-4357/aabfd7.

[340] Xiaohu Yang, H. J. Mo, Y. P. Jing, Frank C. van den Bosch, and YaoQuan Chu. Populating dark matter haloes with galaxies: comparing the 2dFGRS with mock galaxy redshift surveys. MNRAS, 350(4):1153–1173, June 2004. doi: 10.1111/j.1365-2966.2004.07744.x.

[341] Adi Zitrin, Felipe Menanteau, John P. Hughes, Dan Coe, L. Felipe Barrientos, Leopoldo Infante, and Rachel Mandelbaum. A Highly Elongated Prominent Lens at z = 0.87: First Strong-lensing Analysis of El Gordo. ApJ, 770(1):L15, June 2013. doi: 10.1088/2041-8205/770/1/L15.

[342] F. Zwicky. Die Rotverschiebung von extragalaktischen Nebeln. *Helvetica Physica Acta*, 6:110–127, January 1933.

[343] F. Zwicky. On the Masses of Nebulae and of Clusters of Nebulae. ApJ, 86:217, October 1937. doi: 10.1086/143864.

[344] F. Zwicky, E. Herzog, P. Wild, M. Karpowicz, and C. T. Kowal. *Catalogue of galaxies and of clusters of galaxies, Vol. I.* Pasadena: California Institute of Technology, 1961.

[345] Fritz Zwicky, E. Herzog, and P. Wild. *Catalogue of galaxies and of clusters of galaxies.* Pasadena: California Institute of Technology, 1968.